J.W. McPherson

Reliability Physics and Engineering

Time-To-Failure Modeling

Springer

Reliability Physics and Engineering

J.W. McPherson Ph.D

Reliability Physics and Engineering

Time-To-Failure Modeling

Springer

J.W. McPherson
IEEE Fellow
Texas Instruments Senior Fellow Emeritus

ISBN 978-1-4419-6347-5 e-ISBN 978-1-4419-6348-2
DOI 10.1007/978-1-4419-6348-2
Springer New York Dordrecht Heidelberg London

Library of Congress Control Number: 2010930979

To my family:
Victoria, Cameron, Brandi,
Austin and Gabrielle

Preface

All engineers could benefit from at least one course in *reliability physics and engineering*. It is very likely that, starting with your very first engineering position, you will be asked — how long is your newly developed device expected to last? This text was designed to help you to answer this fundamentally important question. All materials and devices are expected to degrade with time, so it is very natural to ask — how long will the product last?

The evidence for *material/device degradation* is apparently everywhere in nature. A fresh coating of paint on a house will eventually crack and peel. Doors in a new home can become stuck due to the shifting of the foundation. The new finish on an automobile will oxidize with time. The tight tolerances associated with finely meshed gears will deteriorate with time. Critical parameters associated with high-precision semiconductor devices (threshold voltages, drive currents, interconnect resistances, capacitor leakages, etc.) will degrade with time. In order to understand the lifetime of the material/device, it is important to understand the *reliability physics* (kinetics) for each of the potential failure mechanisms and then be able to develop the required *reliability engineering* methods that can be used to prevent, or at least minimize the occurrence of, device failure.

Reliability engineering is a fundamental part of all good *electrical and mechanical engineering* product designs. Since proper *materials selection* can also be a critically important reliability factor, *reliability engineering* is also very important to *materials scientists*. Reliability is distinguished from quality in that quality usually refers to time-zero compliance or conformance issues for the material/device. Reliability refers to the time-dependence of material/device degradation. All devices (electrical and/or mechanical) are known to degrade with time. *Measuring and modeling the degradation rate, the time-to-failure, and the failure rate* are the subjects of reliability engineering.

Many electrical and mechanical devices, perhaps due to performance and/or cost reasons, push their standard operating conditions (use conditions) very close to the intrinsic strength of the materials used in the design. Thus, it is not a question of whether the device will fail, but when. Reliability engineering methods permit the *electrical engineer*, armed with accelerated testing data, to claim with confidence that a newly designed integrated circuit will last at least 10 years under specified voltage and temperature operating conditions. Reliability engineering methods

permit the *mechanical engineer* to claim that the newly-designed engine will last for 180,000 miles at 3000 rpm with an oil change required every 6,000 miles. Reliability *engineering* methods enable the *materials scientist* to select a cost-effective material which can safely withstand a specified set of high-temperature and high-stress use conditions for more than 10 years.

This textbook provides the basics of reliability physics and engineering that are needed by *electrical engineers, mechanical engineers, biomedical engineers, materials scientists, and applied physicists* to help them to build better devices/products. The information contained within should help all fields of engineering to develop better methodologies for more: *reliable product designs, reliable materials selections, and reliable manufacturing processes* — all of which should help to improve product reliability. A mathematics level through differential equations is assumed. Also, a familiarity with the use of Excel spreadsheets is assumed. Any needed statistical training and tools are contained within the text. While device failure is a statistical process (thus making statistics important), the emphasis of this book is clearly on the physics of failure and developing the reliability engineering tools required for product improvements during *device design* and *device fabrication* phases.

Acknowledgments

I would like to thank the many excellent engineers that I had the pleasure of working with and learning from during my three- decade career with Texas Instruments. Also, I am very appreciative of the ideas developed during stimulating discussions with many colleagues in reliability physics and engineering within industry, universities and national laboratories. Will be forever grateful to Professors E.G. Purdom and P.A.M. Dirac for being outstanding role models during my earliest physics education.

Texas Instruments Senior Fellow Emeritus J.W. McPherson, Ph.D.
IEEE Fellow

Contents

Chapter 1
Introduction

It is very frustrating (and often very expensive) to buy a device only to have it to fail with time. However, all devices (from integrated circuits to automobile tires) are fabricated from materials that will tend to degrade with time. The *materials degradation* will continue until some critical device parameter can no longer meet the required specification for proper device functionality. At this point, one usually says: the device has failed. This failure could be due to an increase in capacitor leakage (in the case of the integrated circuits) or the inability of an automobile tire to hold proper pressure (blowout). Materials degradation and eventual *device failure* are the subjects of *reliability physics and engineering*. *Reliability physics* is normally associated with understanding the *kinetics* of failure mechanisms. *Reliability engineering* is usually associated with establishing: proper *design rules*, robust *materials selection* criteria, and good *manufacturing guidelines* for reliable device fabrication and use.

Device failure, be it either *electrical* or *mechanical*, can usually be attributed to the *degradation of a given material under stress*. The term stress, as used in this text, is very general and not restricted just to the more common meaning: mechanical stress. Capacitors can fail because of *dielectric breakdown* due to *electric-field stress*. Interconnects can fail because of resistance rises due to *electromigration-induced voiding* as a result of a high *current density stress*. Metal-oxide-silicon field-effect transistors (*MOSFETs*) can fail due to interface-state generation during a *voltage/field stress*. *Mechanical components* can fail because of creep due to a high *tensile stress*. Metal *corrosion* can occur because of high *humidity stress*. *Fatigued components* can occur due to *cyclical stress*. *Worn surfaces* can occur due to shearing *frictional stress*. *Rupture* can occur in components because of *crack propagation* due to *thermomechanical stress* during temperature cycling.

Stress, as used in this text, will refer to any *external agent* which is capable of causing a *degradation* to occur in the material properties such that the device can no longer function properly in its intended application. In the case of dielectrics, this could be the dielectric breakdown which occurs when an electric-field stress exceeds the dielectric strength of the material (e.g., for SiO_2 this is > 10 MV/cm). Or, in the case of metals, this might be the rupture which occurs when a mechanical

J.W. McPherson, *Reliability Physics and Engineering*,
DOI 10.1007/978-1-4419-6348-2_1,

stress is applied which exceeds the rupture strength of the metal (e.g., for aluminum interconnects this is > 600 MPa). However, even when a material is stored at a fixed level of stress less than the material's strength, the material will still degrade with time and device failure is eventually expected.

The observed *time-to-failure* (TF) will depend on the *temperature* and the magnitude of the applied *stress* relative to the breakdown strength of the material. The breakdown strength is usually defined as the level of stress at which the material is expected to fail instantaneously. [By instantaneous, it is meant that the time-to-failure is extremely short (few seconds) versus the time-to-failure (many years) when the material is stressed at 50% of this level.] To ensure that time-dependent failures are minimized during the expected lifetime of the product, generally, a good engineering design will comprehend the distribution of material strengths that is likely to result from normal processing/fabrication, and then keep the design level and application stress level well below these strength values by using some safety factor for increased reliability margin.

The *safety factor* approach is, however, only qualitative (relative to time-to-failure modeling) and is becoming increasing difficult to use for aggressive designs. For example, integrated circuits where device feature sizes continue to be aggressively scaled according to *Moore's Law* (a 0.7x reduction in feature size per technology node), the scaling has generally caused device current densities and electric fields to increase, forcing the normal use conditions to be ever closer to the breakdown strength of the materials. In addition, the temperature cycling of the assembled silicon chips generally leads to large thermo mechanical stresses due to the thermal-expansion mismatch of the dissimilar materials used in chip fabrication and in the assembly process.

Mechanical devices also tend to be designed aggressively because of higher performance and/or materials cost-reduction demands. This serves to push the normal operational conditions much closer to the *breakdown strength* of the materials. How close can the application stress be to the material's strength (commonly referred to as the reliability margin or design rule), in order to achieve many years of reliable device operation, depends on the degradation rate for the material/device. The stress and temperature dependence for this degradation rate is the subject of reliability physics and is normally studied through the use of accelerated testing.

Chapters 2-4 will concentrate on *material/device degradation* and the development of the critically important *time-to-failure models*. Since time-to-failure is a statistical process, an overview of the needed *statistical tools* is presented in Chapters 5 and 6. *Failure rate modeling* is presented in Chapter 7. The use of *accelerated testing* methods and the modeling of the *acceleration factors* are presented in Chapters 8 and 9, respectively. Important *ramp-to-failure testing* methods are introduced in Chapter 10. In Chapter 11, *time-to-failure models* are presented for selected failure mechanisms in *electrical engineering* applications. Likewise, in Chapter 12, time-to-failure models are presented for selected failure mechanisms in *mechanical engineering* applications. Chapter 13 describes how *dynamical*

(time-dependent) stresses can be converted into *static-value equivalents* for easy use with all the models developed. The book is concluded with Chapter 14 which focuses on the practical use of *reliability enhancement factors*, during initial product design and development, in order to increase the expected product lifetime and to reduce the expected device failure rate during customer use.

Chapter 2
Materials and Device Degradation

Degradation is seemingly fundamental to all things in nature. Often this is described as one of the consequences of the Second Law of Thermodynamics — *entropy (disorder) of isolated systems will tend to increase with time.*[1] The evidence for degradation is apparently everywhere in nature. A fresh coating of paint on a house will eventually crack and peel. The finish on a new automobile will oxidize with time. The tight tolerances associated with finely meshed gears will deteriorate with time. The critical parameters associated with precision semiconductor devices (threshold voltages, drive currents, interconnect resistances, capacitor leakage, etc.) will degrade with time. In order to understand the useful lifetime of the device, it is important to be able to model how critically important material/device parameters degrade with time.

2.1 Material/Device Parameter Degradation Modeling

Reliability concerns arise when some critically important material/device parameter (e.g., mechanical strength, capacitor leakage, transistor threshold voltage, brake-lining thickness, etc.) degrades with time. Let S represent a *critically important material/device parameter* and let us assume that S changes monotonically and relatively slowly over the lifetime of the material/device. A Taylor expansion about t=0, produces the Maclaurin Series:

$$S(t) = S_{t=0} + \left(\frac{\partial S}{\partial t}\right)_{t=0} t + \frac{1}{2}\left(\frac{\partial^2 S}{\partial t^2}\right)_{t=0} t^2 + \ldots \,. \tag{2.1}$$

It will be assumed that the higher order terms in the expansion can be approximated by simply introducing a power-law exponent m and writing the above expansion in a shortened form:

$$S = S_o\left[1 \pm A_o(t)^m\right], \tag{2.2}$$

[1] Regardless of how carefully crafted a material/device is at time zero, the material/device will degrade with time.

J.W. McPherson, *Reliability Physics and Engineering*,
DOI 10.1007/978-1-4419-6348-2_2,

where A_o is a material/device-dependent coefficient[2] and m is the power-law exponent. Both A_o and m are adjustable parameters that can be extracted from observed parameter-degradation data. For $+A_o$, the observed parameter S increases monotonically with time, whereas for $-A_o$ it decreases. Either an increase in a critical device parameter S (increase in threshold voltage of a semiconductor device, increase in leakage of a capacitor, increase in resistance of a conductor, etc.) or a decrease in critical parameter S value (decrease of pressure in a vessel, decrease of spacing between mechanical components, decrease in lubricating properties of a fluid, etc.) can eventually lead to device failure. Since *device failure* can result from either increase or decrease of some critically important material/device parameter S, both cases are discussed.

2.1.1 Material/Device Parameter Decreases With Time

Shown in Fig. 2.1 is the observed time dependence of the degradation for a critical device parameter S for three devices.[3]

Reduction in a critically important parameter S can be described by:

$$S = S_o[1 - A_o(t)^m]. \tag{2.3}$$

Taking the logarithm of both sides of Eq. (2.3) yields,

$$\ln(S^*) = m\ \ln(t) + \ln(A_o) \tag{2.4}$$

where:

$$S^* = 1 - \frac{S}{S_o} = \frac{S_o - S}{S_o}. \tag{2.5}$$

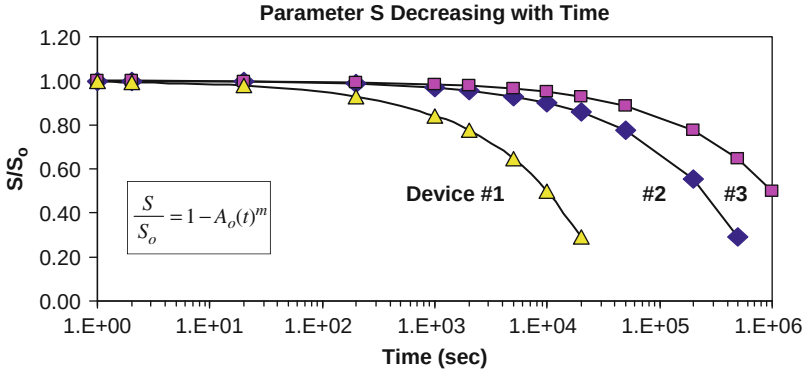

Fig. 2.1 Critical material/device parameter S is observed to reduce with time.

[2]Note that A_o must have the units of reciprocal-time to the m^{th} power.

[3]The term *device* is very general: any apparatus that serves some useful purpose.

Using Eq. (2.4), a logarithmic plot for the three devices shown in Fig. 2.1 is now re-plotted in Fig. 2.2. Note that the unknown parameters in Eq. (2.3) can now be easily extracted from such plots.

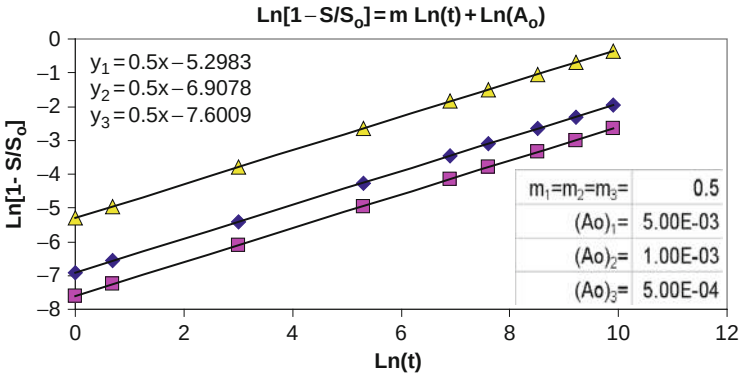

Fig. 2.2 Logarithmic plots reveal straight lines with equal slopes m (for the three devices) but each device has a different prefactor A_o[4].

Example Problem 2.1

The threshold voltage V_{th} for a semiconductor device was found to degrade with time t, as indicated by the data in the table below.

Time: t (hr)	V_{th}(Volts)
0	0.750
1	0.728
2	0.723
10	0.710

a) Find the power-law exponent m which best describes the degradation of the threshold voltage V_{th} data versus time.
b) Find the complete power-law equation which describes the shift in threshold voltage V_{th}.
c) Estimate the value expected for the threshold voltage after 100hrs.

[4] A_o is said to be materials/device dependent. A_o variation will result in a distribution of degradations for the devices, as discussed in Chapter 6.

Solution

a) Inspecting the data, one can see that the device parameter V_{th} is decreasing with time. Thus, power-law model, Eq. (2.3), is used:

$$V_{th} = (V_{th})_o[1 - A_o(t)^m].$$

Rearranging, one obtains:

$$\frac{(V_{th})_o - V_{th}}{(V_{th})_o} = A_o(t)^m.$$

Taking the logarithm of both sides of the above equation, one obtains:

$$\ln\left[\frac{(V_{th})_o - V_{th}}{(V_{th})_o}\right] = m\ \ln(t) + \ln(A_o).$$

Using the data in the above table, one can add useful columns to the table as shown below:

Time: t (hr)	V_{th}(Volts)	$\frac{(V_{th})_O - V_{th}}{(V_{th})_O}$	ln(t)	$\ln\left[\frac{(V_{th})_O - V_{th}}{(V_{th})_O}\right]$
0	0.750	0.000		
1	0.728	0.030	0	−3.51
2	0.723	0.036	0.693	−3.33
10	0.710	0.053	2.303	−2.93

Thus, plotting the values in the last two columns on the right of the table, one obtains:

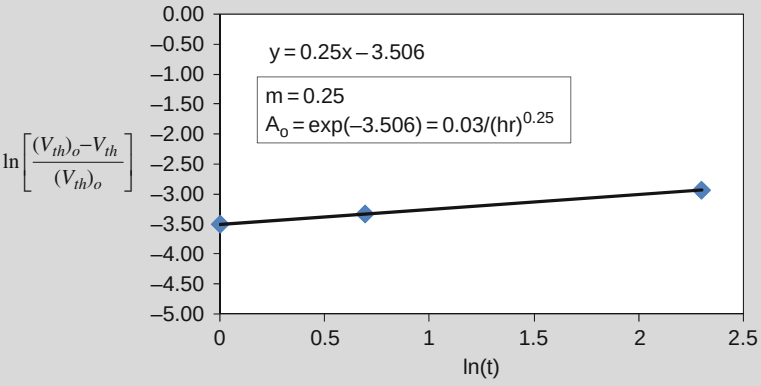

a) From the above plot, one can see that the slope (power-law exponent m) is given by: m=0.25.
b) Using Eq. (2.3), the threshold voltage V_{th} shift/degradation equation is given by:

$$V_{th} = (V_{th})_0(1 - A_0 t^m) = (0.75V)\left[1 - \frac{0.03}{(hr)^{0.25}}(t)^{0.25}\right].$$

c) The value of the threshold voltage V_{th}, after t=100hrs, is expected to be:

$$V_{th} = (0.75V)\left[1 - \frac{0.03}{(hr)^{0.25}}(100hr)^{0.25}\right] = 0.68V.$$

2.1.2 Material/Device Parameter Increases With Time

As previously mentioned, degradation is not always associated with a decrease in a critical parameter S.

Device failure can result from an increase in a critically important material/device parameter with the increase assumed to be described by:

$$S = S_o[1 + A_o(t)^m], \tag{2.6}$$

where A_o is again a material/device-dependent coefficient and m is the time-dependence exponent. Shown in Fig. 2.3 is the time dependence for the degradation of three devices due to the increase in magnitude of the critical parameter S.

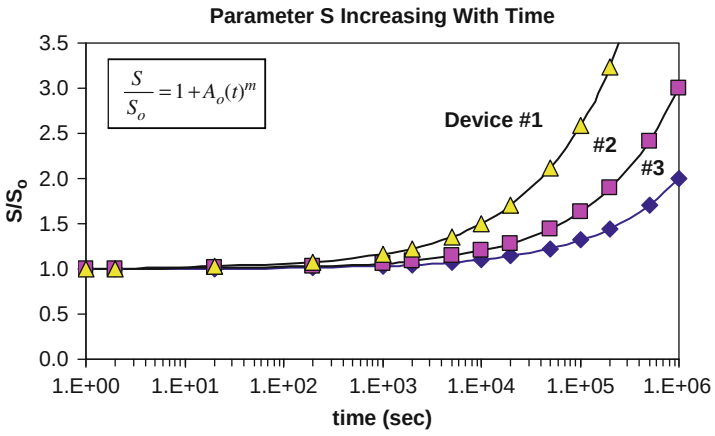

Fig. 2.3 Critical material/device parameter S is observed to degrade (increase) with time.

Taking the natural logarithm of both sides of Equation 2.6 yields,

$$\ln(S^*) = m\ \ln(t) + \ln(A_o), \tag{2.7}$$

where:

$$S^* = \frac{S}{S_o} - 1 = \frac{S - S_o}{S_o}. \tag{2.8}$$

Using Eq. (2.7), the logarithmic plots for the three devices, with increasing critical parameter S as shown in Fig. 2.3, are now re-plotted in Fig. 2.4. Note that the unknown parameters in Eq. (2.6) can be easily extracted from such plots.

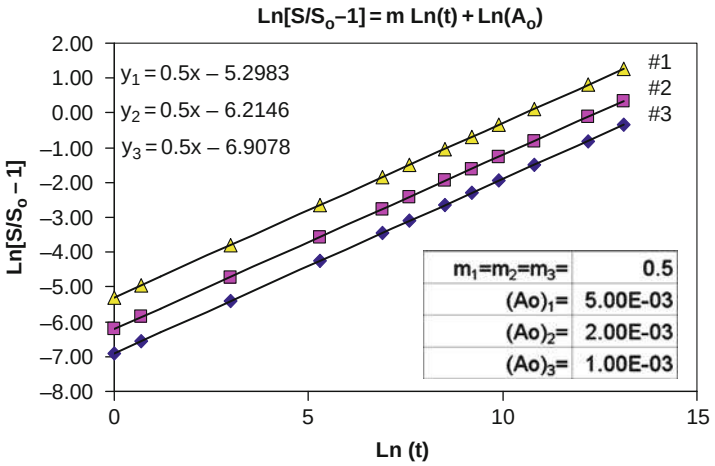

Fig. 2.4 Ln-Ln plots reveal straight lines with equal slopes m for the three devices, but each device has a different prefactor A_o.

Example Problem 2.2

During a fatigue study, *crack propagation* occurred in a metal component. The crack size was observed to increase with the number of cyclical stress cycles N_{cyc}. The crack-propagation data is shown below in the table.

# Cycles: N_{cyc}	Crack-Size: CS (μm)
0	1
100	2
200	9
300	28

a) Find the power-law exponent *m* which best describes the crack size CS growth versus number of cycles N_{cyc}.

b) Find the complete power-law equation which describes the crack size CS versus N_{cyc}.
c) What is the expected crack size CS after 500 cycles?

Solution

a) Inspecting the data, one can see that the crack size (CS) is increasing with time. Thus, power-law Eq. (2.6) is used:

$$CS = (CS)_o[1 + A_o(N_{cyc})^m].$$

Rearranging, one obtains:

$$\frac{CS - (CS)_o}{(CS)_o} = A_o(N_{cyc})^m.$$

Taking the logarithm of both sides of the above equation, one obtains:

$$\ln\left[\frac{CS - (CS)_o}{(CS)_o}\right] = m\ \ln(N_{cyc}) + \ln(A_o).$$

Using the data in the above table, one can add useful columns to the table as shown in the table below.

# Cycles: N_{cyc}	Crack-Size: CS (μm)	$\frac{CS-(CS)_o}{(CS)_o}$	$\ln(N_{cyc})$	$\ln\left[\frac{CS-(CS)_o}{(CS)_o}\right]$
0	1	0		
100	2	1	4.605	0.000
200	9	8	5.298	2.079
300	28	27	5.704	3.296

Plotting the values in the last two columns on the right of the above table, one obtains:

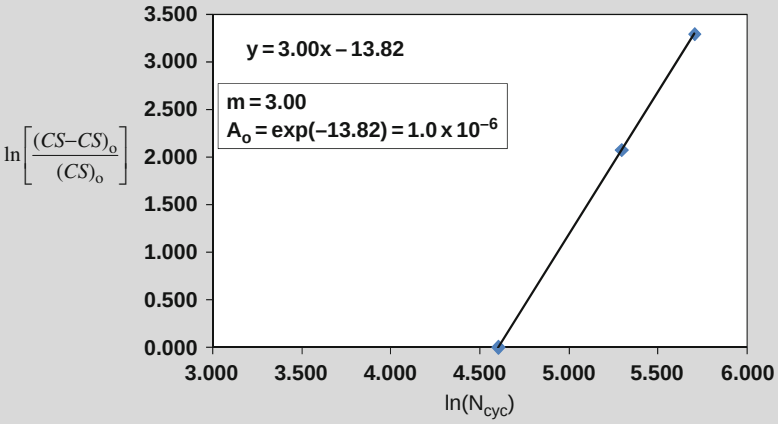

a) From the above plot, one can see that the slope (power-law exponent m) is given by: m=3.
b) The crack size CS increase, Eq. 2.6, is given by:

$$CS = (CS)_0[1 + A_0(N_{cyc})^m) = (1\mu m)\left[1 + \frac{1 \times 10^{-6}}{(cycle)^3}(N_{cyc})^3\right].$$

c) The value of the crack size CS after 500 cycles is expected to be:

$$CS = (1\mu m)\left[1 + \frac{1 \times 10^{-6}}{(cycle)^3}(500\ cycles)^3\right] = 126\mu m.$$

2.2 General Time-Dependent Degradation Models

There are many time-dependent forms for degradation. However, one of the following three forms is generally used: power-law, exponential, or logarithmic. These three forms were selected because they tend to occur rather frequently in nature. The power-law is clearly the more frequently used. If, however, a power-law model gives a rather poor fit to the degradation data, then perhaps the other two models should be investigated. The three degradation models are shown in Table 2.1, as well as how the model parameters can be easily extracted from the observed degradation data.

Table 2.1 Selected Time-Dependent Degradation Models.

Power-Law	$S = S_o[1 \pm A_o(t)^m]$	$Ln\left[\pm\frac{S}{S_o}\mp 1\right]$; Ln(A$_0$); m; 0; $Ln(t)$
Exponential	$S = S_o \exp(\pm A_o t)$	$Ln\left[\frac{S}{S_o}\right]$; $\pm A_o$; 0; t
Logarithmic	$S = S_o[1 \pm \ln(A_o t + 1)]$	$\exp\left[\pm\frac{S}{S_o}\mp 1\right]$; A_o; 1; 0; t

2.3 Degradation Rate Modeling

The power-law model is one of the most widely used forms for time-dependent degradation. For this reason, special attention is given to this model. For convenience of illustration, let us assume that the critical parameter S is decreasing with time and that A_o=1. Then Eq. (2.3) reduces to:

$$S^* = 1 - \frac{S}{S_o} = (t)^m. \tag{2.9}$$

In Figure 2.5 one can see the usefulness and flexibility of the power-law time-dependent model. Note that for m = 1, one will see the expected linear degradation relationship. For m < 1, one can see the tendency for the degradation to saturate for long times. However, for m > 1, the degradation increases strongly with time and with no evidence of saturation effects.

The degradation rate is better emphasized when the actual degradation rate R equation is used:

$$R = \frac{dS^*}{dt} = m(t)^{m-1}. \tag{2.10}$$

The degradation rate, for several values of m, is shown in Fig. 2.6. Note that when m=1, a constant degradation rate is expected. For m < 1, a decreasing degradation rate is expected. For m > 1, an increasing degradation rate is expected. For a decreasing degradation rate, there is at least some hope that the degradation may saturate before causing material/device failure. For a constant degradation rate, the time-to-failure is easily predicted. For an increasing degradation rate, the degradation is ever increasing, eventually leading to a catastrophic condition. Thus, of the three degradation rate conditions (decreasing, constant, increasing), each of which can produce failure, the increasing degradation rate is clearly the most worrisome.

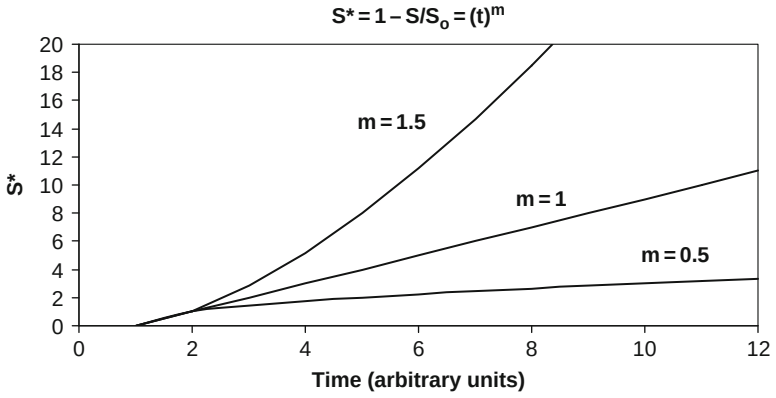

Fig. 2.5 Power-law time-dependent degradation model: a) for m = 1, b) m < 1, and for m > 1.

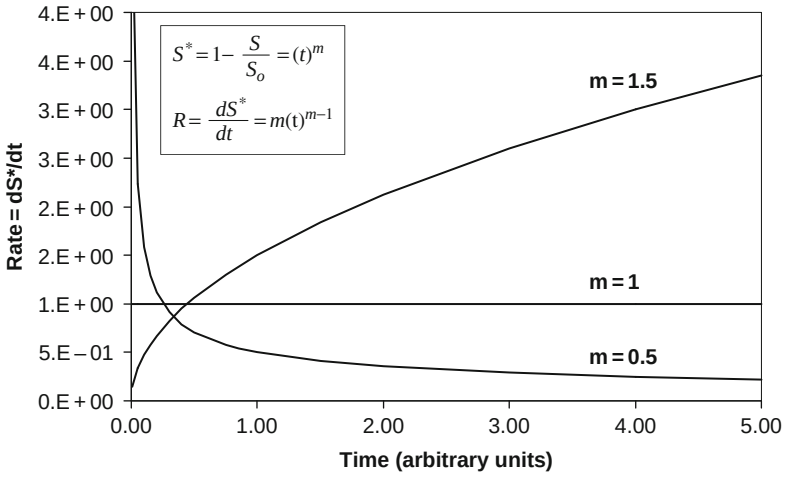

Fig. 2.6 Degradation rate as predicted by the power-law model: a) m = 1, b) m < 1, and c) m > 1. One can see that m = 1 produces a constant degradation rate. m < 1 produces a decreasing degradation rate. Whereas, m > 1 produces an increasing degradation rate.

Example Problem 2.3

a) In Example Problem 2.1, it was determined that the threshold-voltage parameter for a semiconductor device was degrading (decreasing) with time. Is the *degradation rate,* for the threshold-voltage parameter V_{th}, increasing or decreasing with time?
b) In Example Problem 2.2, it was determined that the crack-size parameter for a metal component was degrading (increasing) with the number of cyclical stress cycles. Is the *degradation rate*, for the crack size CS parameter, increasing or decreasing with the number of cycles?

Solution

a) It was determined, in Example Problem 2.1, that the threshold voltage V_{th} parameter was decreasing with time according to the equation:

$$V_{th} = (V_{th})_0(1 - A_0 t^m) = (0.75\,V)\left[1 - \frac{0.03}{(hr)^{0.25}}(t)^{0.25}\right].$$

Since the exponent for the degradation is m=0.25 (less than 1) then, according to Eq. (2.10), or Fig. 2.6, the *degradation rate* for the threshold-voltage parameter is decreasing with time.

b) It was determined in Example Problem 2.2 that the crack-size parameter was increasing with time according to the equation:

$$CS = (CS)_0[1 + A_0(N_{cyc})^m) = (1\mu m)\left[1 + \frac{1 \times 10^{-6}}{(cycle)^3}(N_{cyc})^3\right].$$

Since the exponent for the degradation is m=3 (greater than 1), then according to Eq. (2.10), or Fig. 2.6, the *degradation rate* (crack growth rate) is increasing (in fact, strongly increasing) with time.

2.4 Delays in the Start of Degradation

Sometimes materials/devices will be remarkably stable for a period of time t_0 and then show relatively rapid degradation with time. Examples of this include: a tire that holds stable pressure until a nail punctures the tire; the resistance of a metal conductor is stable until a void starts to form; the fuel efficiency of an engine until the fuel injector starts to clog; an air-conditioner compressor that works fine until a leak in the coolant system develops; etc. Sometimes, it can be extremely important to be able to identify precisely when the degradation started.[5]

If a time-delay t_0 exists, before the start of degradation for the important material/device parameter S, then one can write the degradation equation as:

$$\begin{array}{ll} S = S_0 & (for\ t \le t_0) \\ S = S_o[1 \pm A_0(t - t_0)^m] & (for\ t \ge t_0) \end{array}. \tag{2.11}$$

In the above equation, the + sign is used when S increases with time whereas the – sign is used when S decreases with time. Eq. (2.10) is very useful in determining the precise time that the instability started. The degradation rate R equation can be used to help pinpoint t_0, the time at which degradation actually started. Taking the derivative of Eq. (2.11) one obtains:

$$\begin{array}{ll} R_1 = \dfrac{dS}{dt} = 0 & (for\ t \le t_0) \\ R_2 = \dfrac{dS}{dt} = (\pm)\, mS_oA_0(t - t_0)^{m-1} & (for\ t \ge t_0) \end{array}. \tag{2.12}$$

Note that:

a) if $m>1$, then R_2 goes to zero at $t=t_0$;
b) if $m=1$, then R_2 is a constant; and
c) if $m<1$, then R_2 goes to infinity at $t=t_0$.

[5] If significant degradation (but not failure) started in the warranty period, does one have a claim? Sometimes, it can be very important to be able to identify the onset of degradation.

One can see from above equations that the rate/slope R of the degradation can be used to find the time delay t_0. If one plots the observed degradation rate R versus time t, then the time at which the rate R goes to zero, or R goes to infinity, is $t = t_0$. If R goes to zero, or infinity, at t=0, then t_0=0 and a time delay is not needed in the degradation equation. The power-law model with a time delay t_0, as well as other models, are shown in Table 2.2.

Table 2.2 Delayed Start (t_o) Degradation Models.

Power-Law $S = S_o[1 \pm A_o(t-t_o)^m]$	$Ln\left[\pm\frac{S}{S_o}\mp 1\right]$, $Ln(A_o)$, m, 0, t_o, $Ln(t-t_o)$
Exponential $S = S_o \exp[\pm A_o(t-t_o)]$	$Ln\left[\frac{S}{S_o}\right]$, $\pm A_o$, 0, t_o, $t-t_o$
Logarithmic $S = S_o\{1 \pm \ln[A_o(t-t_o)+1]\}$	$\exp\left[\pm\frac{S}{S_o}\mp 1\right]$, 1, A_o, 0, t_o, $t-t_o$

Example Problem 2.4

The fuel efficiency for a new auto remained very stable during the first 12 months of use. However, after about 1 year of use, a measureable degradation occurred in the efficiency (Eff) as shown in the below table.

Time (Mo)	Efficiency (MPG)	Time (Mo)	R=d(Eff)/dt (MPG/Mo)
0	22.00		
2	22.00		
4	22.00		
6	22.00		
8	22.00		
10	22.00		
12	22.00		
14	21.75	13	−0.1264
16	21.42	15	−0.1639
18	21.06	17	−0.1819
20	20.67	19	−0.1947
22	20.26	21	−0.2048
24	19.83	23	−0.2132

a) Pinpoint the time t_0 that the degradation actually started.
b) Determine the power-law equation which best fits the efficiency versus time for the full 24 months of use.

Solution

The observed degradation rate R is shown in the graph below.

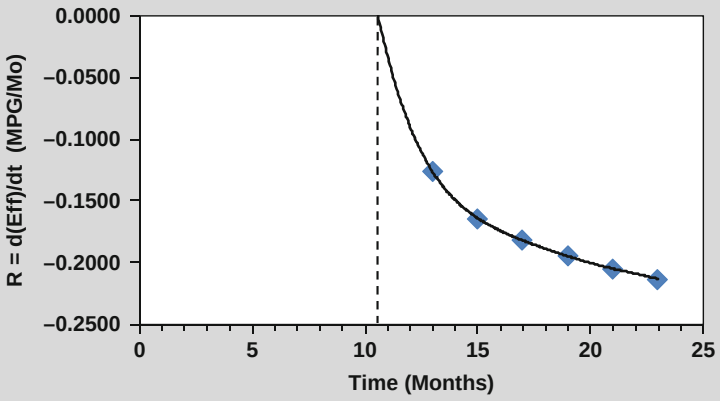

a) One can see from the above plot of degradation rate R versus time that degradation rate R goes to zero at $t = t_0 = 10.5$ Months.[6]
b) Now that the value of the time-delay t_0=10.5 Months has been determined, then one can proceed with finding the best fitting parameters (m,A_0) as follows:

$$Eff = (Eff)_o[1 - A_0(t - 10.5Mo)^m] \qquad (for\ t \geq 10.5Mo).$$

Rearranging and taking the logarithm of both sides, one obtains:

$$\ln\left[\frac{(Eff)_0 - Eff}{(Eff)_0}\right] = m\ \ln(t - 10.5) + \ln(A_0).$$

[6] Note that even though the degradation started at 10.5 months, the degradation at 12 months is so small that it went undetected by the measuring instrument.

The plot of the data is shown in the graph below.

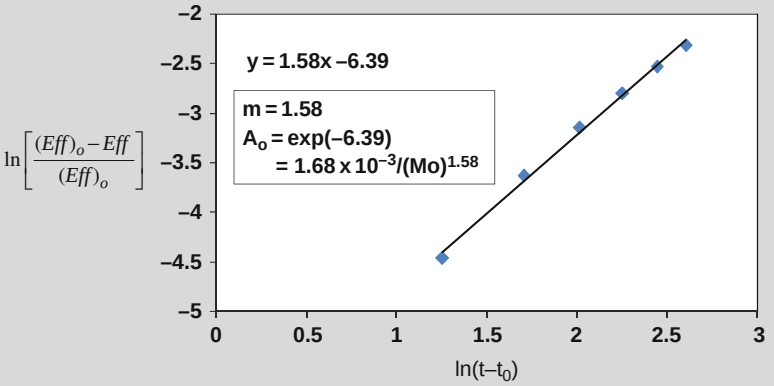

Therefore, the power-law equation, with time delay, that best-fits the fuel efficiency data is:

$$Eff = 22.0 \qquad (for\ t \leq 10.5Mo)$$

$$Eff = (22.0)\left[1 - \frac{1.68 \times 10^{-3}}{(Mo)^{1.58}}(t - 10.5Mo)^{1.58}\right] \qquad (for\ t \geq 10.5Mo).$$

The plot of the data, and the modeled fit to the data, are shown in the graph below.

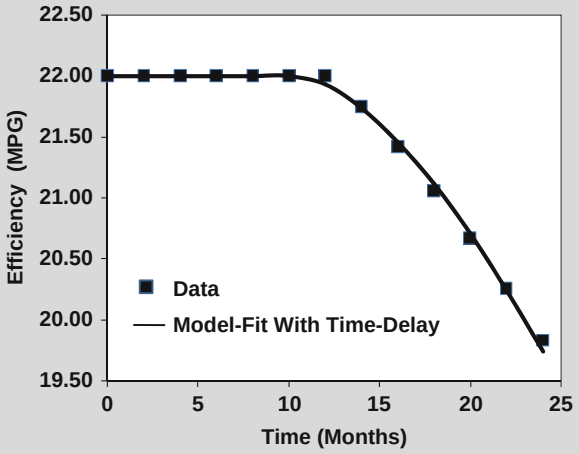

Example Problem 2.5

In semiconductor processing, yield (number of electrically good chips on a Si-wafer divided by the total number of chips on a wafer) is a key manufacturing parameter. The yield data is shown below for several weeks. Using the yield-degradation rate, pinpoint when the yield degradation started.

Time (Wk)	Yield (%)
1	68.2
2	67.2
3	68.2
4	67.2
5	68.2
6	67.1
7	65.0
8	64.0
9	60.0
10	55.5
11	53.0
12	48.5

Solution

To find the rate of yield degradation, additional columns are added to the table as shown below.

Time (Wk)	Yield (%)	Time (Wk)	R=d(Yield)/dt (%/Wk)
1	68.2		
2	67.2	1.5	−1.00
3	68.2	2.5	1.00
4	67.2	3.5	−1.00
5	68.2	4.5	1.00
6	67.1	5.5	−1.10
7	65.0	6.5	−2.10
8	64.0	7.5	−1.00
9	60.0	8.5	−4.00
10	55.5	9.5	−4.50
11	53.0	10.5	−2.50
12	48.5	11.5	−4.50

The plot of the yield-degradation rate is shown below.

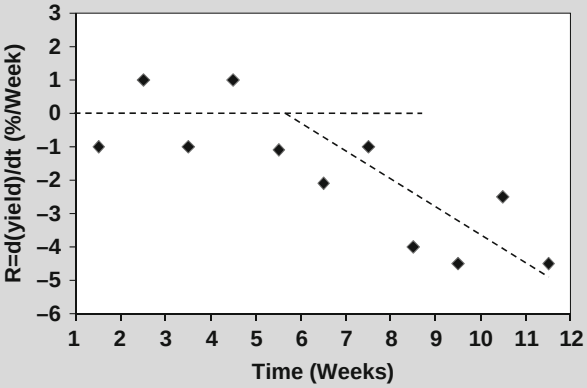

One can see that while the degradation rate shows fluctuation from week to week, the average degradation rate was nearly constant through the first five weeks. Between weeks 5 and 7, the average degradation rate changed with time. This helps to pinpoint the time that some process step(s) started to go out of control.

2.5 Competing Degradation Mechanisms

Competing mechanisms can also occur (one mechanism is driving an increase in the critical parameter S while the other mechanism is driving a reduction in S). This can be described by the equation:

$$S = S_o\left[1 + A_o(t)^{m_1}\right]\left[1 - B_o(t)^{m_2}\right], \tag{2.13}$$

where the first term on the right of the above equation is tending to increase the parameter S while the second term on the right is trying to decrease the parameter S. These mechanisms are competing and can produce either a maximum or minimum in the degradation, as illustrated in Fig. 2.7.

In Fig. 2.7, a maximum occurs in the critical parameter S/S_o due to the dominance of the *increasing mechanism* initially, then due to the dominance of *decreasing mechanism* during the later stages.[7] If the roles are reversed, the decreasing term

[7] An example of competing mechanism comes from the joining/bonding of dissimilar materials. During the bonding of dissimilar metals at high temperatures, interdiffusion of the two materials is usually required in order to establish good bonding. Initially, this interdiffusion of materials will cause an increase in bonding strength. However, often during the later stages of interdiffusion, the bond strength can start to weaken due to Kirkendall voiding.

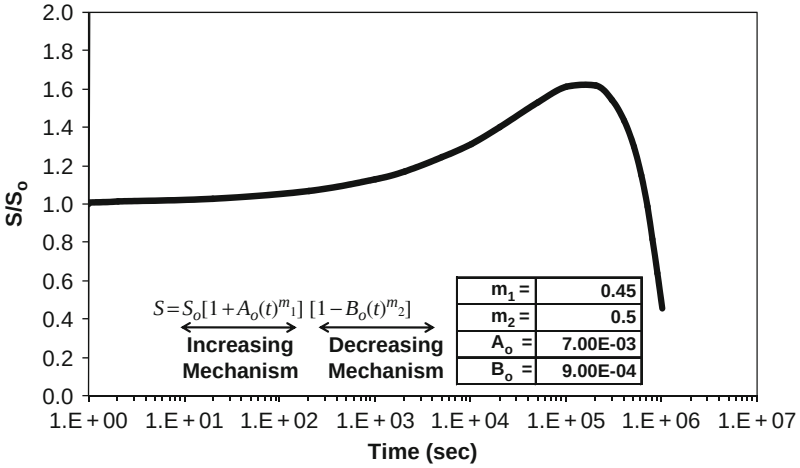

Fig. 2.7 Maximum or minimum in the degradation parameter S/S_o is generally indicative of competing mechanisms: one mechanism driving an increase in S and the other driving a decrease in S.

dominates initially, but the increasing term dominates during the later stages of parameter degradation, then a minimum will be observed.

Table 2.3 indicates a method that is sometimes useful in separating the problem into early stages of degradation versus the later stages of degradation. If the strengthening term dominates the early stages while the later stages are dominated by the weakening term, then the model parameters can easily be extracted.

Table 2.3 Model Parameter Extraction Method (Competing Mechanisms).

$$S = S_o\left[1 + A_o(t)^{m_1}\right]\left[1 - B_o(t)^{m_2}\right]$$

Limiting Conditions: Strengthening Term / Weakening Term

1. During Early Stages:

$$S \cong S_o\left[1 + A_o(t)^{m_1}\right]$$

$$\Rightarrow \ln\left(\frac{S}{S_o} - 1\right) = \ln(A_o) + m_1 \ln(t)$$

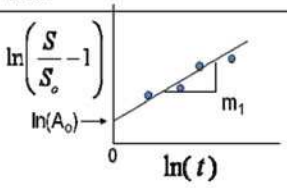

2. During Later Stages:

$$S \cong S_o'\left[1 - B_o(t)^{m_2}\right]$$

$$where: S_o' = S_o\left[1 + A_o(t_1)^{m_1}\right]$$

$$\Rightarrow \ln\left(1 - \frac{S}{S_o'}\right) = \ln(B_o) + m_2 \ln(t)$$

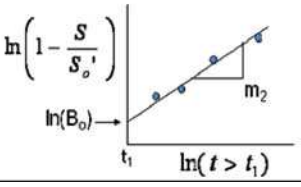

Problems

1. The threshold voltage V_{th} for a semicondutor device was observed to degrade with time. The degradation data is shown in the table.

Time (hr)	Vth (Volt)
0	0.40
1	0.42
10	0.44
100	0.48

   a) Find the power-law equation which best fits the threshold voltage V_{th} versus time data.
   b) What is the expected value of the threshold voltage V_{th} after 1000hrs?
   c) Is the *degradation rate* increasing or decreasing with time?

   Answers:

   a) $V_{th} = 0.40\,V\left[1 + \dfrac{0.05}{(hr)^{0.3}}\,(t)^{0.3}\right]$

   b) $V_{th}(t = 1000hr) = 0.56\,V$

   c) Since m=0.3(<1), then degradation rate is decreasing with time.

2. The pressure P in a tire was found to degrade with time according to the table shown.

Time (day)	P (lb/in^2)
0	32.00
1	30.72
2	30.06
3	29.53

   a) Find the power-law equation which best-fits the pressure P versus time data.
   b) What is the expected value of the pressure P after 10 days?
   c) Is the *degradation rate* for the pressure P increasing or decreasing with time?

   Answers:

   a) $P = 32(lb/in^2)\left[1 - \dfrac{0.04}{(day)^{0.6}}\,(t)^{0.6}\right]$

   b) $P(t = 10\,day) = 26.9\,lb/in^2$

   c) Since m=0.6(<1), then d*egradation rate* is decreasing with time.

3. As current flowed through a precision resistor, it was noted that the value of resistance R for the resistor degrades with time according to the data in the table.

Time (hr)	R (ohm)
0	10.00
1	10.02
5	10.22
10	10.63

   a) Find the power-law equation which best-fits the resistance R versus time.
   b) What is the expected value of the resistance R after 100 hrs?
   c) Is the *degradation rate* for the resistance R increasing or decreasing with time?

   Answers:

   a) $R = 10.00(ohm)\left[1 + \dfrac{0.002}{(hr)^{1.5}}\,(t)^{1.5}\right]$

   b) $R(t = 100hr) = 30.00ohm$

   c) Since m=1.5(>1), then d*egradation rate* is increasing with time.

4. A metal component was corroding/oxidizing with time. The metal-oxide thickness with time is shown in the table.

Time (yr)	Oxide Thickness T_{ox}(μm)
0	1.00
1	1.90
2	2.27
3	2.56

   a) Find the power-law equation which best-fits the oxide thickness T_{ox} versus time data.
   b) What is the expected value of the oxide thickness T_{ox} after 10 yrs?
   c) Is the *degradation rate* for the oxide thickness T_{ox} increasing or decreasing with time?

   Answers:

   a) $T_{ox} = 1.00(\mu m)\left[1 + \dfrac{0.9}{(yr)^{0.5}}\,(t)^{0.5}\right]$

   b) $T_{ox}(t = 10\,yr) = 3.85\mu m$

   c) Since m=0.5(<1), then d*egradation rate* is decreasing with time.

5. The prostate-specific antigen (PSA) test is routinely used to detect the possibility of prostate cancer. The absolute level of the PSA is expected to be < 4.0 ngm/ml, but the rate of change is also important. Below are the hypothetical PSA levels for a patient over a three year period. The absolute PSA level is less that 4.0 ngm/ml, but is the rate a concern?

   a) Find the power-law model which best-fits the increase in PSA versus time data.
   b) Is the increase in PSA occurring at an increasing or decreasing rate?

Time (yr)	PSA (ngm/ml)
0	1
1	1.1
2	1.4
3	1.9

Answers:

a) $PSA = (PSA)_0[1 + A_0(t)^m] = (1.0ngm/ml)\left[1 + \frac{0.1}{(yr)^2}(t)^2\right]$

b) Since m=2 (>1), the rate of increase for the PSA is very strong and should be noted to the physician.

6. For our nervous system to work properly, the nerve cell must be able to generate a potential difference of about 50 mV. This is done through the differential diffusion rates of sodium (Na-ions) and potassium (K-ions). The ratio of the Na to K in our blood is typically (Na/K)=31.93. If this ratio drops to 25.47, then health issues can sometimes occur.

Time (yr)	(Na/K) Ratio
0	31.93
1	31.61
2	31.51
3	31.43

   a) Find the power-law model which best-fits the reduction in (Na/K) ratio versus time data.
   b) Is the decrease of the (Na/K) ratio occurring at an increasing or decreasing rate?

Answers:

a) $\left(\frac{Na}{K}\right) = \left(\frac{Na}{K}\right)_0 (1 - A_0 t^m) = (31.93)\left[1 - \frac{0.01}{(yr)^{0.4}}(t)^{0.4}\right]$

b) Since m=0.4 (<1), the rate of reduction is decreasing with time.

7. The size of an inoperable brain tumor was monitored for three months preceding the use of an experimental drug and for three months post drug use. The data is shown below.

   a) What is the power-law equation that describes tumor growth prior to experimental drug use?
   b) What is the power-law equation that describes tumor growth versus time after experimental drug use?
   c) Take the ratio of the two growth rates to see if the experimental drug was effective at reducing the tumor growth rate.

Time (Mo)	Tumor Size: S (cm)
0	1.00
1	1.10
2	1.20
3	1.30
Drug Introduction	
3	1.30
4	1.43
5	1.48
6	1.52

Answers:

a) $S_{before\ drug} = (1.00\,cm)\left[1 + \dfrac{0.1}{(hr)}t\right] \qquad (t \leq 3Mo)$

b) $S_{after\ drug} = (1.30\,cm)\left[1 + \dfrac{0.1}{(hr)^{0.5}}(t - 3Mo)^{0.5}\right] \qquad (t \geq 3Mo)$

c) $\dfrac{R_{after}}{R_{before}} = \dfrac{dS_{after}/dt}{dS_{before}/dt} = \dfrac{0.65}{(t - 3Mo)^{0.5}} \qquad (t > 3Mo)$

Note that in the 4th month, after the drug was introduced, the tumor growth rate was 65% of what it would have been without the drug. In the 5th month, the tumor growth rate was 46% of what it would have been if no drug was introduced.

8. The pressure P of a toxic gas, in a very large storage vessel, was monitored every month during its 12 month storage and the results are shown below.

   a) Pinpoint the month that a leak started to occur, causing a gradual release of the gas.
   b) What is the power-law equation that best-fits the degradation data?
   c) Children, in a nearby school, had a mysterious illness in month 3. Could this have been due to the gas leak?

Time (Mo)	Pressure: P (atm)
0	5.0
1	5.0
2	5.0
3	5.0
4	5.0
5	5.0
6	5.0
7	5.0
8	4.9
9	4.7
10	4.4
11	4.0
12	3.5

Answers:

a) t_0=6.6 Months.

b) $P = 5.0\,atm \qquad (t \leq 6.6Months)$

$$P = 5.0\,atm\left[1 - \frac{1.03 \times 10^{-2}}{(Mo)^{2.0}}(t - 6.6Mo)^{2.0}\right](t \geq 6.6Months)$$

c) The gas leak did not start until month 6.6. The illness of the children at the local school occurred in month 3.

9. Nuclear decay from a radioactive material exhibited the decay characteristics:

$$\frac{N}{N_0} = \exp\left[-\left(\frac{6.93 \times 10^{-3}}{hr}\right)t\right].$$

a) Plot the exponential decay function through the first 100 hrs.
b) Find the best fitting power-law model to this exponential function through the first 100 hrs.
c) Plot both the exponential and the best fitting power-law model and compare the plots through 100 hrs.

Answer:

(b) $$\frac{N}{N_0} = 1 - \frac{0.00941}{(hr)^{0.871}}(t)^{0.871}$$

10. In semiconductor processing, yield (number of electrically good chips on a wafer divided by the total number of chips on a wafer) is a key manufacturing parameter. The yield data is shown below for several weeks. Using the yield-degradation rate, when did the yield start to degrade?

Time (Wk)	Yield (%)
1	52.1
2	52.6
3	52.7
4	51.6
5	52.2
6	51.7
7	52.2
8	51.9
9	51.3
10	50.4
11	49.2
12	47.7

Answer: Yield started to degrade between weeks 7 and 8.

11. Thermo-sonic Au ball-bonding to aluminum pads is a common attachment process for silicon chips. If these bonds are stored at high temperatures (>150°C), one can observe competing mechanisms: interdiffusion of the two elements tends to strengthen the bonds initially but Kirkendall voiding tends to weaken the bonds during longer storage times. The bond strength S data is shown versus the storage time at high temperature in the below table.

    Determine the degradation equation for the ball bonds shown.

Time (sec)	Bond Strength: S (gm-f)
0.00E+00	20.00
1.00E+00	20.01
1.00E+01	20.03
1.00E+02	20.10
1.00E+03	20.31
1.00E+04	20.90
1.00E+05	22.16
2.00E+05	22.47
4.00E+05	22.32
6.00E+05	21.75
8.00E+05	20.94
1.00E+06	20.00
2.00E+06	14.14
2.20E+06	12.83
2.30E+06	12.17
2.40E+06	11.49
2.50E+06	10.81
2.60E+06	10.12
2.70E+06	9.43
2.80E+06	8.73
3.00E+06	7.32
4.00E+06	0.00

Answer:

$$S = (20.00gm \bullet f)\left[1 + \frac{1 \times 10^{-3}}{(\text{sec})^{0.5}}(t)^{0.5}\right]\left[\left(1 - \frac{5 \times 10^{-4}}{(\text{sec})^{0.5}}(t)^{0.5}\right)\right]$$

12. A metal-oxide thickness T_{ox} was found to take a logarithmic growth functional form:

$$\frac{T_{ox}}{(T_{ox})_0} = 1 + \ln\left[\left(\frac{1 \times 10^{-2}}{hr}\right)t + 1\right]$$

a) Plot the logarithmic growth function through the first 100 hrs.
b) Find the best fitting power-law model to this logarithmic growth function through the first 100 hrs.
c) Plot both the logarithmic and the best fitting power-law model and compare the fits through the first 100 hrs.

Answer: (b) $\frac{T_{ox}}{(T_{ox})_0} = 1 + \frac{0.0138}{(hr)^{0.858}}t^{0.858}$

Chapter 3
From Material/Device Degradation to Time-To-Failure

In the previous chapter, it was suggested that material/device degradation will occur with time and that this continuing *degradation* will eventually cause *device failure*. Methods were presented in Chapter 2 which can be used for modeling the time-dependence of degradation. The question that we would like to address in this chapter is — *how does one go from the time-dependence of degradation to the time-to-failure for the device*? The time-to-failure equations are critically important, for device failure-mechanisms, and will be the focus of the remaining chapters in this book.

3.1 Time-To-Failure

Time-to-failure (*TF*) occurs when an important material/device parameter degrades to a point that the device can no longer function properly in its intended application. For an electronic device, this could be the time associated with a 10% reduction in circuit speed, relative to its initial (time-zero) value. For an automobile tire, this could be the time required for the tire tread to reach 10% of its original (time-zero) value.

In Chapter 2 it was learned that the degradation of an important material/device parameter S could be modeled with a power-law equation:

$$S = S_o \left[1 \pm A_o(t)^m\right]. \tag{3.1}$$

Plus sign (+) is used when the parameter S increases with time while the minus sign (−) is used when the parameter S decreases with time. Solving for time, one obtains:

$$t = \left[\frac{1}{\pm A_0}\left(\frac{S - S_0}{S_0}\right)\right]^{1/m}. \tag{3.2}$$

Time-to-failure ($t = TF$) occurs when the material/device parameter shifts by some critical amount such that the device no longer functions properly:

J.W. McPherson, *Reliability Physics and Engineering*,
DOI 10.1007/978-1-4419-6348-2_3,

$$TF = \left[\frac{1}{\pm A_0} \left(\frac{S - S_0}{S_0} \right)_{crit} \right]^{1/m}. \tag{3.3}$$

One can see, from Eq. (3.3), that the time-to-failure (*TF*) increases as the critical amount of allowed parameter degradation increases. Also, *TF* increases as the exponent *m* decreases. Note that *TF* goes to infinity as *m* goes to zero. Recall that $m = 0$ means that no degradation is occurring with time, thus TF goes to infinity.

Shown in Fig. 3.1 is a parameter S that is decreasing with time. Time-to-failure occurs when parameter reaches some critical level.

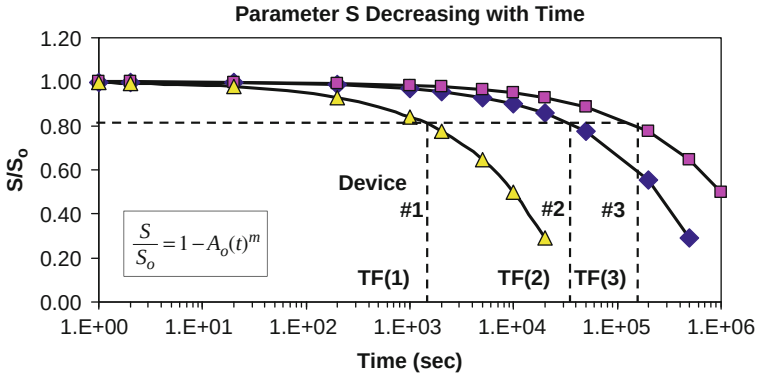

Fig. 3.1 Time-To-Failure depends on the amount of degradation that can be tolerated in some critically important material/device parameter S. Note that for a 20% decrease in the critically important material/device parameter S, ($S/S_o = 0.8$), the time-to-failure will be different for the three devices versus what it would be for 60% decrease.

Example Problem 3.1

In Example Problem 2.1, the important threshold V_{th} parameter for a semiconductor device was found to decrease/shift according to the power-law equation:

$$V_{th} = (V_{th})_0(1 - A_0 t^m) = (0.75\ V)\left[1 - \frac{0.03}{(hr)^{0.25}}(t)^{0.25}\right].$$

Assuming that the maximum threshold voltage V_{th} shift that one can tolerate is 20%, before device failure occurs, then what is the time-to-failure?

Solution

Since the threshold voltage V_{th} is an important decreasing device parameter, then Eq.(3.3) gives the time-to-failure:

$$TF = \left[\frac{1}{A_0}\left(\frac{(V_{th})_0 - V_{th}}{(V_{th})_0}\right)_{crit}\right]^{1/m}.$$

This equation becomes:

$$TF = \left[\frac{1}{0.03/(hr)^{0.25}}\left(\frac{(V_{th})_0 - 0.8(V_{th})_0}{(V_{th})_0}\right)_{crit}\right]^{1/0.25}$$
$$= \left[\frac{0.2}{0.03/(hr)^{0.25}}\right]^4$$
$$= 1975.3\ hrs.$$

In summary, it will take approximately 1975 hrs for this device parameter V_{th} to decrease/shift by 20% and to cause device failure.

Shown in Fig. 3.2 is an important material/device parameter S that is increasing with time. Time-to-failure occurs when the degradation reaches a critical level.

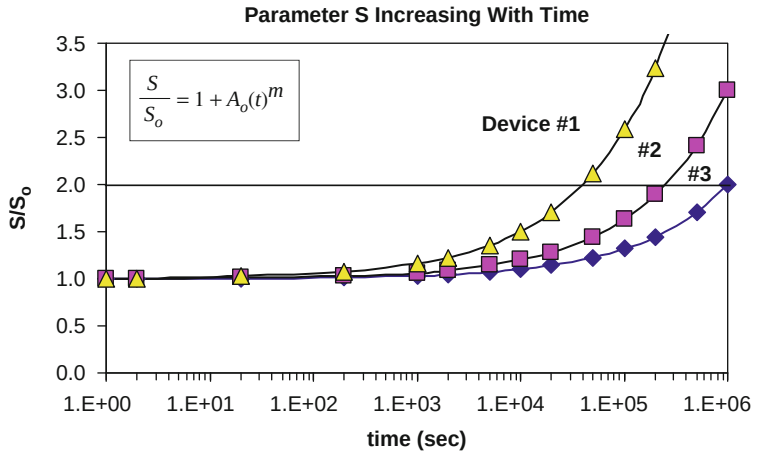

Fig. 3.2 Time-To-Failure depends on the amount of degradation that can be tolerated in some critically important material/device parameter S. Note that for a 100% increase in the critically important parameter S ($S/S_o = 2$) the time-to-failure will be different for the three devices versus what it would be for 50% increase in S, (S/S_o=1.5).

Example Problem 3.2

In Example Problem 2.2 the important reliability parameter was crack size (CS) and CS was found to increase with the number of cyclical-stressing cycles N_{cyc} according to the power-law equation:

$$CS = (CS)_0[1 + A_0(N_{cyc})^m] = (1\mu m)\left[1 + \frac{1 \times 10^{-6}}{(cycle)^3}(N_{cyc})^3\right].$$

Assuming that the maximum crack size can increase by 500 times its original value before the device fails, what is the expected number of cycles-to-failure?

Solution

Since the crack size (CS) was found to increase with the number of cyclical-stress cycles, then Eq.(3.3) gives the cycle-to-failure CTF:

$$CTF = \left[\frac{1}{A_0}\left(\frac{CS - (CS)_0}{(CS)_0}\right)_{crit}\right]^{1/m}.$$

This equation becomes:

$$\begin{aligned} CTF &= \left[\frac{1}{1 \times 10^{-6}/(cyc)^3}\left(\frac{500(CS)_0 - (CS)_0}{(CS)_0}\right)_{crit}\right]^{1/3} \\ &= \left[\frac{499}{1 \times 10^{-6}/(cyc)^3}\right]^{1/3} \\ &= 793.2\ cycles. \end{aligned}$$

In summary, it will take approximately 793 cycles of cyclical stress for the initial crack-size (1 μm) to propagate to a crack size of 500 μm and to cause failure.

3.2 Time-To-Failure Kinetics

In Chapter 2, we discussed the fact that the above degradation parameter A_0 is, in general, material/microstructure dependent and this can lead to *TF* values which are device-dependent (as illustrated in Fig. 3.1 and 3.2). However, there are also other very important properties of A_0 (such as its *stress* and *temperature* dependence) that we have not yet discussed.[1]

It is common experience that electrical devices tend to degrade faster as the voltage V and/or temperature T increases. In this case, the degradation parameter A_0 is not only a function of material variations but also a function of the applied *voltage*

[1] A more detailed discussion of degradation kinetics is found in Chapter 8.

and the use *temperature*: $A_0 = A_0(V, T)$. It is also common experience that mechanical devices tend to degrade faster as the mechanical stress σ and the temperature T increases. In this case, A_0 is not only a function of materials variations but also the applied mechanical stress σ and the use temperature T: $A_0 = A_0(\sigma, T)$.

Seldom are devices purely electrical or purely mechanical; they can be more accurately described as *electro-mechanical* devices. Therefore, for electro-mechanical devices, the relationship between *TF* and parameter S degradation is given by:

$$TF = \left[\frac{1}{\pm A_0(V, \sigma, T)} \left(\frac{S - S_0}{S_0} \right)_{crit} \right]^{1/m}. \tag{3.4}$$

Plus sign (+) is used for an increasing parameter S and minus sign (−) is used for a decreasing parameter S. One can see, from Eq. (3.4), that *TF* kinetics (voltage, stress, and temperature dependence) may not have a simple inverse relation with degradation kinetics contained in the degradation parameter $A_0(V, \sigma, T)$. In fact, only for the special case of $m = 1$(constant degradation rate), will *TF* have a simple inverse relationship with the degradation parameter $A_0(V, \sigma, T)$. Therefore, while a critical amount of *degradation* $(\Delta S/S_0)_{\text{crit}}$ is necessary to produce *device failure*, one should not expect the time-to-failure equation $TF(V, \sigma, T)$ to necessarily have a simple inverse relation with the degradation kinetics contained in $A_0(V, \sigma, T)$.

Problems

1. The threshold voltage V_{th} for a semicondutor device was found to degrade according to the power-law equation:

$$V_{th} = 0.40\, V \left[1 + \frac{0.05}{(hr)^{0.3}} (t)^{0.3} \right].$$

   Find the time required for threshold voltage to increase by 10%.

   Answer: Time required = 10.1 hrs

2. The pressure P in a tire was found to degrade according to the power-law equation:

$$P = 32(lb/in^2) \left[1 - \frac{0.04}{(day)^{0.6}} (t)^{0.6} \right].$$

   Find the time required for the pressure P to degrade to 16 lb/in^2.

   Answer: Time required = 67.3 days

3. A current flowing through a precision resistor causes the resistance R to rise according to the power-law equation:

$$R = 10.00(ohm)\left[1 + \frac{0.002}{(hr)^{1.5}}\,(t)^{1.5}\right].$$

Find the time required for the resistance to increase by 10%.

Answer: Time required =13.6 hrs

4. A metal component was corroding/oxidizing according to the power-law degradation:

$$T_{ox} = 1.00(\mu m)\left[1 + \frac{0.9}{(yr)^{0.5}}\,(t)^{0.5}\right].$$

Find the time required for the oxide-thickness to increase to 3 times its original thickness.

Answer: Time required = 4.9 yrs

5. The prostate-specific antigen (PSA) values for a certain patient were found to increase according to:

$$PSA = (1.0ngm/ml)\left[1 + \frac{0.1}{(yr)^2}(t)^2\right].$$

Find the time required for the PSA level to reach *4.0ngm/ml*.

Answer: Time required = 5.5 yrs

6. The ratio of the Na to K in a certain patient's blood was described by:

$$\left(\frac{Na}{K}\right) = \left(\frac{Na}{K}\right)_0 (1 - A_0 t^m) = (31.93)\left[1 - \frac{0.01}{(yr)^{0.4}}(t)^{0.4}\right].$$

Find the time required for the ratio to degrade to 30.00 .

Answer: Time required = 90 yrs

7. The size of an inoperable brain tumor was found to increase, according to the power-law equation:

$$S = (1.30\,cm)\left[1 + \frac{0.1}{(Mo)^{0.5}}(t)^{0.5}\right].$$

Find the time required for the tumor to grow in size to 1.6cm.

Answer: Time required = 5.3 Months

8. The pressure P of a gas in a vessel was found to degrade according to the power-law model:

$$P = 5.0\,atm \qquad (t \leq 6.6\,Months)$$

$$P = 5.0\,atm\left[1 - \frac{1.03 \times 10^{-2}}{(Mo)^{2.0}}(t - 6.6Mo)^{2.0}\right] \qquad (t \geq 6.6\ Months).$$

Find the time required for the pressure to reduce by 5% of its original value.

Answer: Time required = 8.8 Months

9. Bond strengths of thermo-sonic bonded Au balls to aluminum pads were found to degrade according to the equation:

$$S = (20.00gm - f)\left[1 + \frac{1 \times 10^{-3}}{(\text{sec})^{0.5}}(t)^{0.5}\right]\left[\left(1 - \frac{5 \times 10^{-4}}{(\text{sec})^{0.5}}(t)^{0.5}\right)\right].$$

Find the time required for the bond-strength to reduce to 50% of its original value.

Answer: Time required = 2.6×10^6 seconds

10. Nuclear decay from a radioactive material exhibited the decay characteristics:

a) $$\frac{N}{N_0} = \exp\left[-\left(\frac{6.93 \times 10^{-3}}{hr}\right)\ t\right].$$

The nuclear decay can be approximated by the power-law:

b) $$\frac{N}{N_0} = 1 - \frac{0.00941}{(hr)^{0.871}}(t)^{0.871}.$$

Using models (a) and (b), find the time required for the material to reduce to 50% of its original value.

Answers:

a) Exponential Model: Time required = 100 hrs
b) Power-Law Model: Time required = 96 hrs

11. A metal-oxide thickness T_{ox} was found to increase in a logarithmic manner according to:

a) $$\frac{T_{ox}}{(T_{ox})_0} = 1 + \ln\left[\left(\frac{1 \times 10^{-2}}{hr}\right)\ t + 1\right].$$

The growth can also be approximated by the power-law:

b) $$\frac{T_{ox}}{(T_{ox})_0} = 1 + \frac{0.0138}{(hr)^{0.858}}t^{0.858}.$$

Find the time required, using both models, for the oxide thickness to increase to 2 times its original value.

Answers:

a) Logarithmic Model: Time required = 172 hrs
b) Power-Law Model: Time required = 147 hrs

Chapter 4
Time-To-Failure Modeling

All materials tend to degrade, and will eventually fail, with time. For example, *metals* tend to *creep* and *fatigue*; *dielectrics* tend to *trap charge* and *breakdown*; *paint* tends to *crack* and *peel*; *polymers* tend to lose their *elasticity* and become more *brittle*, *teeth* tend to *decay* and *fracture*; etc. All devices (electrical, mechanical, electromechanical, biomechanical, bioelectrical, etc.) will tend to degrade with time and eventually fail. The rate of degradation and eventual time-to-failure will depend on the electrical, thermal, mechanical and chemical environments to which the device is exposed.

4.1 Flux-Divergence Impact on Time-To-Failure

In the case of metals, due to the extended nature of the valence-electron wave functions forming metallic bonds, the bonding of the atoms is relatively independent of the exact location of individual metal ions. This is the reason that metals tend to have ductile and malleable properties. Therefore, it is relatively easy for the metal ions to flow under the presence of an external force. While metal ion movement is necessary for failure, it is not sufficient. For a material to degrade, and eventually fail, a *flux divergence* in the particle transport is required as illustrated in Fig. 4.1.

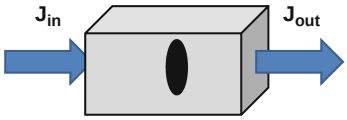

Fig. 4.1 Material degradation (voiding or accumulation of material is shown in darker region of volume V of interest) occurs due to a flux divergence. J_{in} represents the flux of particles into the volume V of interest and J_{out} represents the flux of particles out. The volume V of interest is bounded by a surface of area A. Flux divergence occurs if $J_{in} \neq J_{out}$.

By flux divergence, we mean that the flux of particles (number of particles per unit area per unit time) flowing into a region must be greater than or less than the flux of particles leaving the region. A region of voiding or accumulation is depicted

J.W. McPherson, *Reliability Physics and Engineering*,
DOI 10.1007/978-1-4419-6348-2_4,

in Fig. 4.1 and occurs because of a flux divergence in the particle transport process. This depiction could represent electromigration-induced voiding leading to an open circuit failure, a buildup of chlorine ions on a bond pad leading to corrosion failure, or the trapping of electrons or holes in a dielectric leading to dielectric breakdown. The flux divergence can be described by Fick's Second Law (which is a statement of the conservation of mass),

$$\vec{\nabla} \bullet \vec{J}(x,t) = -\frac{\partial \rho(x,t)}{\partial t}, \tag{4.1}$$

where *J(x,t)* represents the particle flux at the specified coordinates x (= x_1, x_2, x_3) and time t, and *ρ(x,t)* represents the density of such particles. Integrating both sides over the observation volume *V* and then using the divergence theorem,[1] one can express Eq. (4.1) in integral form,

$$\int \vec{J} \bullet d\vec{A} = -\frac{dN(t)}{dt}, \tag{4.2}$$

where *N* represents the total number of particles contained in the volume *V* of interest which is bounded by a closed surface of area *A*.

In analogy with reaction-rate theory, it is convenient to think of the voiding (or accumulation) in terms of a *reaction-rate* equation,

$$\frac{dN(t)}{dt} = -k(t)N(t), \tag{4.3}$$

where *k(t)* is the *reaction-rate constant* for failure. Comparing Eqs. (4.2) and (4.3), one obtains a relationship between the *reaction-rate constant* and the flux divergence,

$$k(t) = \frac{\int \vec{J}(x,t) \bullet d\vec{A}}{N(t)}. \tag{4.4}$$

In this text, the *reaction-rate constant,*[2] given by Eq. (4.4), will be referred to as a *degradation-rate constant*. One can see clearly that the degradation-rate constant is directly proportional to the *net flux* of particles crossing the *boundary area A enclosing the volume V of interest*. Thus, a flux divergence is needed to produce material degradation (and material degradation is needed to eventually cause device failure). Also, *k* can be either positive or negative depending on the details of the flux divergence; thus, Eq. (4.3) can be used to describe either accumulation or depletion of particles.

---

[1] The divergence theorem states that: $\int_V \vec{\nabla} \bullet \vec{J}\, dV = \int_A \vec{J} \bullet d\vec{A}$, where V is the volume of interest which is bounded by a surface of area A.

[2] The reaction-rate constant, in many cases, may not really be constant. It may, in general, be a function of time.

The general solution to Eq. (4.3) can be found by separating the variables and integrating,

$$\int_{N(0)}^{N(t)} \frac{dN}{N} = -\int_{0}^{t} k(t)dt, \tag{4.5}$$

giving:

$$\frac{N(t)}{N(0)} = \exp\left[-\int_{0}^{t} k(t)dt\right]. \tag{4.6}$$

Failure is expected at time $t{=}TF$, when the ratio $N(t = TF)/N(0)$ reaches some critical fraction f_{crit}. This gives:

$$f_{crit} = \frac{N(TF)}{N(0)} = \exp\left[-\frac{\int_{0}^{TF} k(t)dt}{\int_{0}^{TF} dt}\, TF\right]. \tag{4.7}$$

One will note that, in Eq. (4.7),[3] the time-averaged value of the degradation-rate constant $\langle k \rangle$ appears where:

$$\langle k \rangle = \frac{\int_{0}^{TF} k(t)dt}{\int_{0}^{TF} dt}. \tag{4.8}$$

Using Eqs. (4.4) and (4.8), and solving Eq. (4.7) for TF, one obtains the time-to-failure TF equation:

$$TF = \frac{\ln(1/f_{crit})}{\left\langle \frac{\int \vec{J}(x,\, t) \bullet d\vec{A}}{N(t)} \right\rangle}. \tag{4.9}$$

Remember that the brackets < >, in the above equation, represent the time-averaged value of the quantities enclosed. The above equation shows explicitly that a flux divergence in the particle transport is required to produce failure. The equation also shows that the impact of the flux divergence is somewhat mitigated by the number of atoms in failing volume. For example, with voiding-induced failure, if the

[3] We have inserted the identity: $TF = \int_{0}^{TF} dt$.

amount of flux divergence (net number of particles per sec leaving the volume) is constant, then one would expect that the time required for 10% of the atoms to leave the volume of interest would depend on the number of atoms in the volume. This is evident by the fact that a wider metal conductor tends to fail more slowly than a narrow one at the same stress level.[4] This is indeed the case for crack propagation. If the crack growth rate is constant (flux divergence is constant), then the time required for the crack to propagate through the material increases with its thickness.

For many failure mechanisms, the transport of material can be described as Fickian-like. Fickian transport considers both the drift and diffusion components for the atoms in the transport process:

$$J(x,t) = \mu\, \rho(x,t)F - D\frac{\partial \rho(x,t)}{\partial x}, \tag{4.10}$$

where: μ is the particle *mobility,* ρ is the *particle density, F* is the *driving force,* and D is the *diffusivity* for the moving particles. The first term on the right-hand side of Eq. (4.10) is referred to as the *drift component* while the second term is referred to as the *diffusion component*. The *mobility* μ is given by the *Einstein relation*:

$$\mu = \frac{D}{K_B T} = \frac{D_o \exp\left(-\frac{Q_{diffusion}}{K_B T}\right)}{K_B T}, \tag{4.11}$$

where $Q_{diffusion}$ is the activation energy for diffusion, T is the Kelvin temperature, and K_B is Boltzmann's constant (8.62×10^{-5} eV/K). D_o is the diffusion coefficient and, for a solid material, is given by,

$$D_o = \frac{\nu_o}{6}(r_o)^2, \tag{4.12}$$

where: ν_o is the vibration/interaction frequency ($\sim 10^{13}$/sec) and r_o is the mean atom spacing ($\sim$2Å) in the material. Equations (4.9) through (4.11) suggest that the time-to-failure (TF) should depend (exponentially) on temperature T and on the driving force F. The force F acting on an atom is, of course, derived from gradients: gradient in electrical potential, gradient in mechanical stress, gradient in chemical potential, etc.

[4] This is generally true for electromigration-induced failure in conductors. Wider metal leads, at the same current density stress, tend to last longer. An *apparent exception* seems to exist in aluminum where very narrow metal leads can last longer than wider metal leads during electromigration testing. With aluminum, a *bamboo-like grain-boundary microstructure* can develop when the metal width and thickness are comparable to the Al grain size. Here, however, the amount of flux divergence is no longer constant, but is reduced by the bamboo grain structure thus causing the narrow metal leads to last longer than the wider leads.

4.2 Stress Dependence and Activation Energy

It must be emphasized that even if we know the physics behind the driving force F, and the activation energy Q for the diffusion process, which should permit accurate modeling of the flux given by Eq. (4.10), seldom do we know the exact details of the flux divergence. The exact details of the flux divergence are often imbedded in the details of the materials microstructure. Thus, Eq. (4.9) is difficult to use when constructing a time-to-failure equation. For this reason, it is usually assumed that the flux divergence is related to the applied stress ξ through either a *power-law* or *exponential dependence*. Thus, the time-to-failure equation Eq. (4.9) is normally assumed to reduce to one of the two following forms:

$$TF = A_o(\xi)^{-n} \exp\left(\frac{Q}{K_B T}\right), \tag{4.13a}$$

or

$$TF = B_o \exp(-\gamma \bullet \xi)\ \exp\left(\frac{Q}{K_B T}\right). \tag{4.13b}$$

In the above equations, ξ is the generalized stress (the agent which produces material degradation and eventual device time-to-failure), n is the power-law exponent, γ is the exponential stress parameter, Q is the activation energy, and A_o and B_o are material/device dependent prefactors. The key reliability physics parameters are the time-to-failure kinetic values (n,γ,Q) and these are determined from actual time-to-failure data using the following equations:

$$n = -\left[\frac{\partial \ln TF}{\partial \ln \xi}\right]_T, \tag{4.14a}$$

or

$$\gamma = -\left[\frac{\partial \ln TF}{\partial \xi}\right]_T, \tag{4.14b}$$

and

$$Q = K_B \left[\frac{\partial \ln TF}{\partial (1/T)}\right]_\xi .^{5} \tag{4.15}$$

From the above equations, the power-law exponent n is determined from the partial derivative of the logarithm of time-to-failure *ln(TF)* with respect to the logarithm of the stress *ln(ξ)* while holding the temperature T constant. Thus, to determine n, one usually does a log-log plot of TF versus the stress variable ξ. The slope of the best fitting straight line is n. This is illustrated in Fig. 4.2. n is simply a power-law exponent and, as such, n is dimensionless.

[5] To properly use this equation, the temperature T must be expressed in Kelvin.

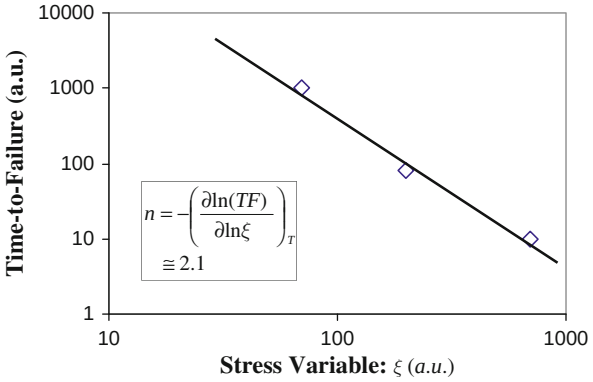

Fig. 4.2 Method is illustrated for determination of the power-law exponent n from time-to-failure data. n is dimensionless.

The exponential model parameter γ, according to Eq. (4.14b), is determined from the partial derivative of the logarithm of time-to-failure *ln(TF)* with respect to the stress ξ while holding the temperature *T* constant. Thus, to determine γ, one usually does a semi-log plot of TF versus the stress variable ξ. The slope of this best fitting straight line is γ. The units for γ must be in reciprocal stress units so that the product $\gamma\xi$ remains dimensionless. This is illustrated in Fig. 4.3.

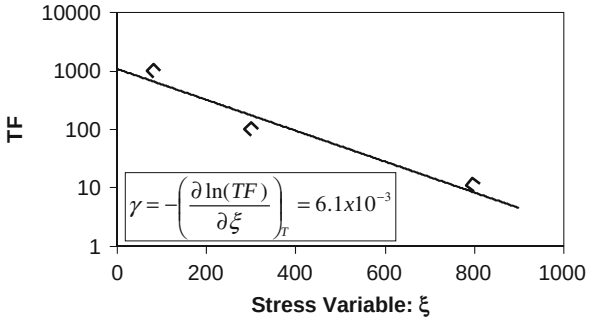

Fig. 4.3 Method is illustrated for determination of the exponential parameter γ from time-to-failure data. γ must be expressed in the units of reciprocal stress such that the product $\gamma\xi$ is dimensionless.

The activation energy *Q* is determined from the partial derivative of the logarithm of time-to-failure *ln(TF)* with respect to the inverse temperature (1/T) while holding the stress ξ constant. The temperature *T* must be expressed in Kelvin. Thus, to determine the activation energy *Q*, one usually does a semi-log plot of TF versus the inverse temperature (1/T). Boltzmann's constant (8.62×10^{-5}eV/K) times the

slope of this best fitting straight line is Q. In this text, the units for Q are normally expressed in electron volts (eV) [see Fig. (4.4)].

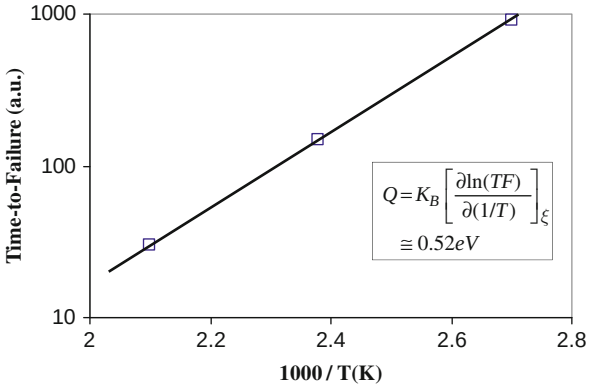

Fig. 4.4 Method is illustrated for determination of the activation energy Q, from time-to-failure data. In this text, Q will normally be expressed in the units of electron volts(eV). The temperature must be expressed in Kelvin.

In Figs. 4.2–4.4, we have illustrated how the time-to-failure kinetics are obtained directly from observed time-to-failure data. For these illustrations, the stress dependence for the time-to-failure could be described by a power-law model with exponent $n=2$ or with an exponential model with $\gamma = 6.1 \times 10^{-3}$ *(in units of reciprocal stress).* The temperature dependence was described as being Arrhenius-like with an activation energy of Q=0.52 (in units of eV). It should be emphasized that when determining the stress dependence n (or γ), using Eq. (4.14), the temperature must be held constant (either physically or mathematically). This can become an important issue if the applied stress (such as current density) actually heats the sample.[6] Therefore, one may wish to determine the activation energy first, using Eq. (4.15), with the stress level held fixed, and then use the activation energy Q to extrapolate to some fixed temperature condition as the stress is changed.

Example Problem 4.1

Metal rods were tested at a constant tensile stress level, and elevated temperature, until the metal rod failed due to creep. The tensile stress levels (in

[6]This can be a very important issue if the stress also tends to serve as a significant source of self-heating, e.g., Joule heating can raise the temperature of the conductor when the current density stress is increased in a metal stripe during electromigration testing. This temperature rise (with the level of current-density stress) must be taken into account when determining the failure kinetics.

Mega-Pascals) and the temperatures (in °C) for the test conditions are shown in the table below, as well as the time-to-failure data.

		Mechanical Tensile-Stress: σ		
T		600 MPa	700 MPa	800 MPa
E	500°C	–	29.9 hrs	–
M	550°C	18.5 hrs	10.0 hrs	5.8 hrs
P	600°C	–	3.8 hrs	–

a) Assuming a power-law time-to-failure model, what is the power-law exponent for the stress σ?
b) What is the activation energy Q determined from this test?

Solution

a) The stress dependence for the power-law time-to-failure model is given by Eq. (4.14a):

$$n = -\left[\frac{\partial \ln TF}{\partial \ln \sigma}\right]_T.$$

Thus, one needs to perform a ln(TF) versus ln(σ) plot (while holding the temperature T constant). As an equivalent approach, one can perform a TF versus σ plot, using a logarithmic scaling of both axes. This latter approach was chosen and the plot is shown below.

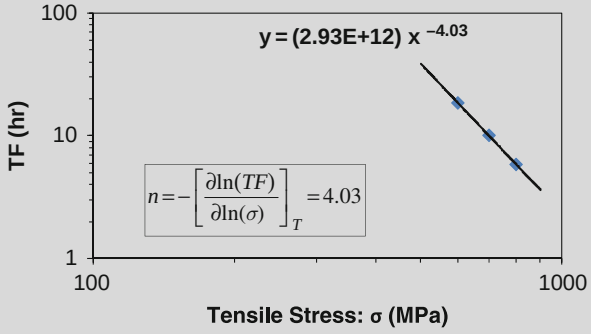

One can see from the above plot that the stress exponent for the power-law is n=4.

b) After converting the temperature from centigrade to Kelvin, the activation energy Q determination is shown in the plot below.[7]

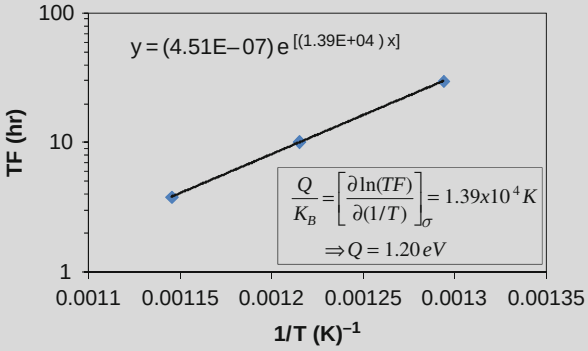

From the plot above we see that the activation is Q=1.2 eV.

4.3 Conservative Time-To-Failure Models

Since the time-to-failure TF models have adjustable parameters, it is likely that each of the time-to-failure TF models will fit, quite nicely, the accelerated time-to-failure data over a limited accelerated stress range. The stress-test range, however, is usually limited because of the time required to take TF data. At the lower stress levels, the test time could easily be years! Therefore, one usually has to model limited TF data, taken under higher stress conditions, and then hope that the model is still valid for extrapolations to much lower stress use conditions. Unless some overriding physics supports one model over the other, then one might want to select the more conservative model (the model which predicts the shortest time to failure). But *which model is more conservative*?

Shown in Table 4.1 is a set of accelerated stress data (in arbitrary units) with the corresponding time-to-failure TF (also in arbitrary units). We want to obtain the best fitting for each model to the accelerated data and then see which model is more conservative (which model produces the shortest time-to-failure when the models are used to predict time-to-failure at much lower levels of stress).

The time-to-failure TF data is plotted in Fig. 4.5. Both the exponential and power-law models tend to fit the actual accelerated data extremely well. However, even though both models tend to fit the accelerated data points extremely well, the two models give very different predictions for the time-to-failure (when the models are

[7]Remember that one must convert the temperature from Centigrade to Kelvin. The conversion equation is T(K) = T(°C) + 273.

Table 4.1 Arbitrary Accelerated Data.

Stress: ξ (arbitrary units)	TF (arbitrary units)
100	1.00
90	1.52
80	2.44
70	4.17

used to extrapolate to much lower values of stress). One can see easily that the *exponential model* gives a lower estimate of time-to-failure TF (at lower values of stress ξ) versus the *power-law model*. For this reason, we say that the *exponential model gives a more conservative estimate of time-to-failure versus the power-law model*. One should always remember that the exponential model is more conservative. This may be very important to remember in the case of very high-reliability applications, if there is little understanding of the exact physics of failure. An understanding of failure mechanisms, and their physics of failure, can often be very helpful in helping one to decide on which model to use.

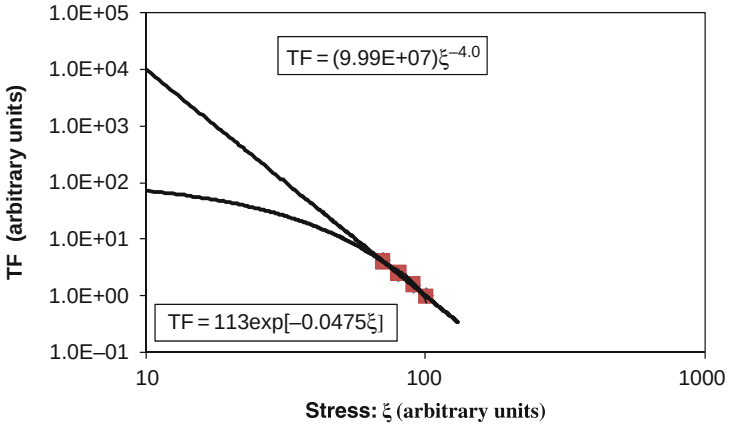

Fig. 4.5 The two time-to-failure TF models (exponential and power-law) were used to fit the accelerated stress data shown in Table 4.1. Note that the two models fit the accelerated TF data extremely well at the higher values of stress. At the lower stress levels, the two models generate dramatically different predictions. Note that the exponential model is more conservative (shorter time-to-failure prediction) at lower stress levels.

In summary, model selection would seem to be easy — just use the more conservative model, right? Well maybe, maybe not. There is the apparent reliability truism: *the customer never gets mad if the device lasts longer than you predict*. However, the *customer may get upset if you were too conservative*, during device design and development phases, *and your new device does not meet either the cost or performance expectations.* Therefore, there should always be an emphasis on

understanding the physics-of-failure so that you can possibly use a more physics-based model selection. Many physics-based models are presented, in Chapters 11 and 12, to aid you in your model selection. This will give you some degree of confidence in your model selection — knowing that a certain time-to-failure model is widely used for the failure mechanism of interest, and under what conditions the model is generally accepted to be valid.

4.4 Time-To-Failure Modeling Under High Stress

The breakdown strength ξ_{BD} of a material is defined as the level of stress at which the material is expected to fail *instantaneously*. Since the material breakdown generally involves atom movement, and atoms cannot move faster than the speed of light, *instantaneous* behavior is not really possible. By *instantaneous,* we will mean that the time-to-failure t_o at a stress level of ξ_{BD} is extremely short versus the time-to-failure *TF* at 50% of ξ_{BD}. For example, a device/material might be able to operate safely for years at 50% of ξ_{BD}, but could fail in milliseconds at ξ_{BD}. Usually ξ_{BD} is determined experimentally by ramping up the level of the stress ξ until ξ_{BD} is recorded. Ramp-to-failure testing and t_o determination is discussed in Chapter 10.

Since stressing close to ξ_{BD} is obviously in a very high stress region, a special form of Eq. (4.13b) is sometimes used. One can write Eq. (4.13b) as:

$$TF = B_0(T) \exp(-\gamma \xi). \tag{4.16}$$

By inserting an identity[8] and rewriting one obtains:

$$TF = t_o(T) \exp\left[\gamma(\xi_{BD} - \xi)\right], \tag{4.17}$$

where,

$$t_o(T) = B_o(T) \exp(-\gamma \xi_{BD}) = B_o \exp(-\gamma \xi_{BD}) \exp\left(\frac{Q_o}{K_B T}\right). \tag{4.18}$$

One will note that Eq. (4.17) is self-consistent in that: when $\xi = \xi_{BD}$ then $TF = t_o$, where t_o is the time-to-failure at breakdown. This will be very useful for interpreting ramp-to-failure test results (Chapter 10). It is also important to note that, experimentally, one finds that γ can be temperature dependent, and this temperature dependence has been expressed historically as:[9]

$$\gamma(T) = \gamma_0 + \frac{\gamma_1}{K_B T}. \tag{4.19}$$

[8] Identity is used: $\exp(-\gamma \xi_{BD}) \exp(\gamma \xi_{BD}) = 1$.

[9] In Problem 7, at the end of this chapter, it is shown that a stress dependent activation energy also develops if a Maclaurin Series expansion is used: $\gamma(T) = a_o + (a_1 K_B)T$.

Thus, if γ has the expected temperature dependence, as described by Eq. (4.19), then Eq. (4.13b) can be written as:

$$TF = t_o \exp\left[\gamma_o \left(\xi_{BD} - \xi\right)\right] \exp\left(\frac{Q - \gamma_1 \xi}{K_B T}\right), \tag{4.20}$$

where $Q = Q_o + \gamma_1 \xi_{BD}$. Note that Eq. (4.20) suggests that, under very high stress conditions (very close to the breakdown strength of the material), the effective activation energy $Q_{eff} = Q - \gamma_1 \xi$ may show a reduction with stress if $\gamma_1 \neq 0$.[10] A stress dependent activation energy is widely reported for time-dependent dielectric breakdown TDDB (under high electric-field stress conditions) and for creep-rate studies for metals (under high mechanical stress conditions at high temperatures). Thus, one should consider the possibility of a stress dependent activation energy when doing extremely high-stress time-to-failure testing. The physics behind this stress dependent activation energy is discussed in detail in Chapter 8.

Problems

1. If a *constant flux divergence* exists, and is given by:

$$\int \vec{J} \bullet d\vec{A} = R = \frac{100,000 \; Billion \;\; atoms}{\text{sec}},$$

find the time required for 50% of the atoms to flow out of 1 cm^3 of aluminum. Hint:

$$N_{atoms} = \frac{(density)_{Al}\,(Volume)_{Al}}{(atomic\ weight)_{Al}} = \frac{\left(2.7 gm/cm^3\right)\left(1\ cm^3\right)}{(27.0 gm)/(6.02 \times 10^{23}\ atoms)}$$
$$= 6.0 \times 10^{22} atoms$$

   Answer: 9.5yrs

2. If the *reaction-rate constant* k shows a monotonic time dependence, then Chapter 2 suggests that one can approximate the time dependence with:

$$k(t) = k_0\left[1 \pm a_0 t^m\right],$$

where the plus (+) sign is used for an increasing reaction rate constant and a minus (−) sign for a decreasing reaction rate constant. Using Eq. (4.3), show that the time-to-failure TF is given by the transcendental equation:

[10] The occurrence of a stress-dependent activation energy (for high level of stress) is discussed in detail in Chapter 10.

$$TF = \frac{\ln\left[N_0/N(t=TF)\right]}{k_0\left[1 \pm a_0 \frac{(TF)^m}{m+1}\right]}.$$

3. Electromigration (EM) testing of Cu produced the following table of time-to-failure results:

Electromigration Time-To-Failure Data			
	1×10^6 (A/cm^2)	2×10^6 (A/cm^2)	3×10^6 (A/cm^2)
280°C	–	20.3 hr	–
300°C	20 hr	10 hr	6.7 hr
320°C	–	5 hr	–

   a) Find the power-law exponent n for the current density.
   b) Find the activation energy Q for this failure mechanism.

   Answers: a) $n = 1$ b) $Q = 1.0$ eV

4. Corrosion testing of a metal produced the following table of time-to-failure results:

Corrosion Time-To-Failure Data			
	60% RH	70% RH	80% RH
25°C	–	824 hr	–
50°C	332 hr	100 hr	30 hr
75°C	–	16.4 hr	–

   a) Find the exponential-dependence parameter γ for the humidity.
   b) Find the activation energy for this failure mechanism.

   Answers: a) $\gamma = 0.12\ (\%\text{RH})^{-1}$ b) $Q = 0.7$ eV

5. Testing for surface-inversion/mobile-ions in ICs produced the following time-to-failure results:

Mobile-Ions Time-To-Failure Data			
	3 V	6 V	9 V
60°C	–	67.70 hr	–
70°C	40 hr	20 hr	13.30 hr
80°C	–	6.33 hr	–

a) Find the power-law exponent n which describes the voltage dependence.
b) Find the activation energy Q for this failure mechanism.

Answers: a) $n = 1$ b) $Q = 1.2$ eV

6. Testing for channel hot-carriers in n-type MOSFETs produced the following time-to-failure results.

Hot-Carrier Injection Time-To-Failure Data

	5 μA/μm	15 μA/μm	25 μA/μm
25°C	–	5.65 hr	–
50°C	324 hr	12 hr	2.60 hr
75°C	–	22.90 hr	–

a) Find the power-law exponent n which describes the substrate current dependence.
b) Find the activation energy Q for this failure mechanism.

Answers: a) $n = 3$ b) $Q = -0.25\ eV$

7. Using Eq. (4.13.b) for time-to-failure, and assuming that the temperature dependence of γ can be expressed by the Maclaurin Series:

$$\gamma(T) \cong a_o + (a_1 K_B)T,$$

show that a stress-dependent activation energy develops of the form:

$$Q_{eff} = Q - a_1(K_B T)^2\, \xi\,.$$

References

McPherson, J.: *Stress Dependent Activation Energy*, IEEE International Reliability Physics Symposium Proceedings, 12(1986).

McPherson, J. and E. Ogawa: *Reliability Physics and Engineering*. In: **Handbook of Semiconductor Manufacturing Technology, 2nd Edition**, CRC Press 30-1(2008).

Chapter 5
Gaussian Statistics — An Overview

The *Gaussian distribution* (*normal* or *bell-shaped distribution*) is a widely used statistical distribution and it is generally used as the foundation for statistical quality control. Simply measuring the time-zero values of a parameter (resistor values, mechanical tolerances, children heights, class grades on a test, etc.) can result in a distribution of values which can be described by a normal distribution.

5.1 Normal Distribution

The normal distribution *f(x)* shown in Fig. 5.1 is defined by the equation:

$$f(x) = \frac{1}{\sigma\sqrt{2\pi}} \exp\left\{-\left[\frac{x - x_{50}}{\sigma\sqrt{2}}\right]^2\right\}. \tag{5.1}$$

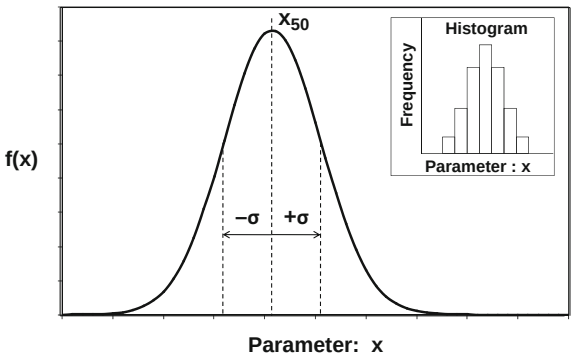

Fig. 5.1 Gaussian (or normal) distribution is illustrated. x_{50} is the mean=mode=median. 68.3% of observations are between (+/−)σ, 95.5% of observations are between (+/−)2σ and 99.7% of observations are between (+/−)3σ.

J.W. McPherson, *Reliability Physics and Engineering*,
DOI 10.1007/978-1-4419-6348-2_5, © Springer Science+Business Media, LLC 2010

For the normal distribution (since it is symmetrical), x_{50} represents the mean = mode = median. In order to be consistent with later chapters in this book, x_{50}[1] will be referred to as the median (50% of the values are below the median value and 50% are above). σ is the standard deviation[2] (represents the spread in the data) and can be approximated by $\sigma = x_{50} - x_{16}$, where x_{16} represents the value and where 16%[3] of the observations are below this value. Once x_{50} and σ are determined from the data, then the full distribution is described by Eq. (5.1).

x_{50} and σ can be determined from a plot of the cumulative fraction F(x):

$$F(x) = \int_0^x f(x)dx. \tag{5.2}$$

The cumulative (cum) fraction F integral in Eq. (5.2) must be numerically evaluated and is given by:

$$\begin{aligned} F(x) &= \frac{1}{2} erfc\left(\frac{x_{50} - x}{\sigma\sqrt{2}}\right) \qquad (for\ x \le x_{50}) \\ and & \\ F(x) &= 1 - \frac{1}{2} erfc\left(\frac{x - x_{50}}{\sigma\sqrt{2}}\right) \quad (for\ x \ge x_{50}) \end{aligned}, \tag{5.3}$$

where the *erfc* stands for the *error function complement*. Some often used values for the *erfc* are shown in Table 5.1. In the past, such tables were widely used by engineers. Now, however, *ERFC* is a standard *Excel Function* so any arbitrary value is readily available to the engineer.

Shown below (Table 5.2) is an example of a suggested method for data collection that can be used for relatively easy statistical analysis. In this example, 25 measurements were taken on the shear strength (in units of gm-f)[4] of Au ball-bonds to aluminum pads on semiconductor chips. These 25 observed measurements (data points) were then ranked from smallest to largest value. In order to insure that all 25 data points can be used when plotting the data, an unbiased estimate is used for the cumulative fraction failed F.[5] An unbiased estimate used for F in this text is:

---

[1] Mean can be estimated: $x_{50} = \sum_{i=1}^{N} x_i/N$, where N is the sample size.

[2] Standard deviation can be estimated: $\sigma = \left[\sum_{i=1}^{N} (x_i - x_{50})^2/(N-1)\right]^{1/2}$.

[3] A more precise value is 15.87%.

[4] One gm-f equals 9.8×10^{-3} Newton.

[5] A cumulative probability of exactly F=1 cannot be plotted. Therefore, in order to ensure that all 25 data points can be plotted, then an *unbiased estimate* of the cum F is needed. In reliability physics and engineering, Eq. (5.4) is generally used.

Table 5.1 Error Function Complement (*erfc*).

y	erfc(y)	y	erfc(y)
0	1.0000	1	0.1573
0.1	0.8875	1.1	0.1198
0.2	0.7773	1.2	0.0897
0.3	0.6714	1.3	0.0660
0.4	0.5716	1.4	0.0477
0.5	0.4795	1.5	0.0339
0.6	0.3961	1.6	0.0237
0.7	0.3222	1.7	0.0162
0.8	0.2579	1.8	0.0109
0.9	0.2031	1.9	0.0072
1	0.1573	2.0	0.0047

$$F = \frac{Observation\ \#\ -\ 0.3}{Sample\ Size\ +\ 0.4}, \tag{5.4}$$

where *observation #* is the cumulative number of observations.

The cum fraction F is very useful in that it permits relatively easy plotting of the statistical data and relatively easy parameter (x_{50}, σ) extraction from the data.

In Table 5.2, the Z-value is the number of standard deviations associated with a given cum fraction F and can found from standard lookup tables such as the ones below, or can be easily generated with an EXCEL spreadsheet: to go from Z to F, use the EXCEL function F=NORMSDIST(Z); to go from F to Z, use the EXCEL function: Z=NORMSINV(F).

The plot of the data (from Table 5.2) is shown in Fig. 5.2, as well as the extracted best fitting normal distribution parameters (x_{50}, σ). Using these best fitting normal-distribution parameters (x_{50},σ), shown in Fig. 5.2, the resulting normal distribution is shown Fig. 5.3.

In general, once the normal distribution parameters (x_{50}, σ) are determined, then any other fraction F can be found using the equation:

$$x_F = x_{50} - z_F\sigma. \tag{5.5}$$

The following relations are so frequently used that they are highlighted here:

$$x_{16\%} = x_{50} - 1\sigma; \quad x_{1\%} = x_{50} - 2.33\sigma; \quad x_{0.13\%} = x_{50} - 3\sigma. \tag{5.6}$$

5.2 Probability Density Function

The normal distribution, as defined by Eq. (5.1), is a normalized distribution (which means that the total area under the curve is equal to unity). Thus, f(x) can be thought of as a probability density function such that f(x)dx is the probability of finding a

Table 5.2 Statistical Data for Bond Shear Strengths.

Statistical Data Collection and Analysis Method				
Sample Size	Observation	Ranked Data	Unbiased Estimate of Cum Fraction*	Normal Distribution
25	#	Shear Strength (gm-f)	F	Z-Value
	1	17.07	0.028	−1.918
	2	17.11	0.067	−1.499
	3	18.02	0.106	−1.246
	4	18.20	0.146	−1.055
	5	18.50	0.185	−0.896
	6	18.61	0.224	−0.757
	7	18.70	0.264	−0.632
	8	18.72	0.303	−0.515
	9	18.79	0.343	−0.406
	10	18.96	0.382	−0.301
	11	19.20	0.421	−0.199
	12	19.34	0.461	−0.099
	13	19.42	0.500	0.000
	14	19.44	0.539	0.099
	15	19.46	0.579	0.199
	16	19.55	0.618	0.301
	17	19.61	0.657	0.406
	18	19.75	0.697	0.515
	19	19.81	0.736	0.632
	20	19.88	0.776	0.757
	21	19.96	0.815	0.896
	22	19.98	0.854	1.055
	23	20.03	0.894	1.246
	24	20.25	0.933	1.499
	25	20.26	0.972	1.918

*Unbiased Estimate: F = (Observation # −0.3) / (Sample Size + 0.4)

value between x and x+dx, as illustrated in Fig. 5.4. The probability of finding a value in the range, between x_1 and x_2, is then given by:

$$P(x_1 \text{ to } x_2) = \int_{x_1}^{x_2} f(x)dx = F(x_2) - F(x_1). \tag{5.7}$$

Table 5.3. Conversion Tables for F to Z and Z to F.

From Cum F to Z-Values		From Z-Values to Cum F	
Cum	Standard Deviations (Z-values)	Standard Deviations	Cum F
F	NORMSINV(F)	Z-Value	NORMSDIST(Z)
0.001	−3.090232306	−3.0	0.0013
0.01	−2.326347874	−2.5	0.0062
0.1	−1.281551566	−2.0	0.0228
0.2	−0.841621234	−1.5	0.0668
0.3	−0.524400513	−1.0	0.1587
0.4	−0.253347103	−0.5	0.3085
0.5	−1.39214E-16	0.0	0.5000
0.6	0.253347103	0.5	0.6915
0.7	0.524400513	1.0	0.8413
0.8	0.841621234	1.5	0.9332
0.9	1.281551566	2.0	0.9772
0.95	1.644853627	2.5	0.9938
0.99	2.326347874	3.0	0.9987
0.999	3.090232306		

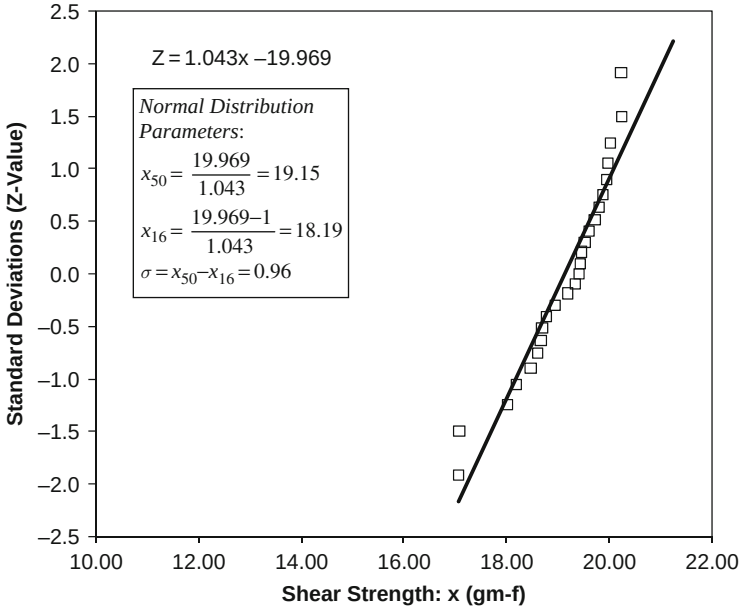

Fig. 5.2 Normal distribution plotting for data found in Table 5.2.

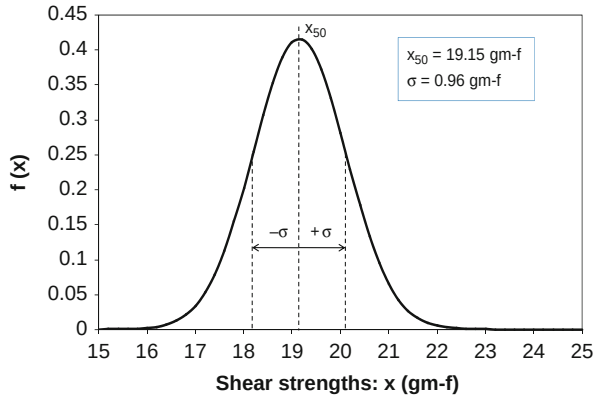

Fig. 5.3 Shear strengths (from Table 5.2) presented as a normal distribution.

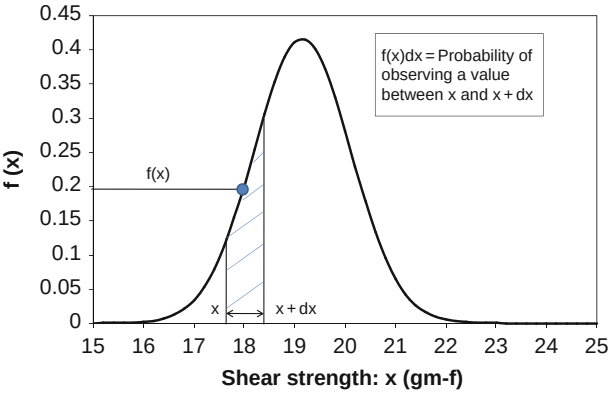

Fig. 5.4 f(x)dx represents the probability of observing a value of shear strength between x and x+dx.

Example Problem 5.1

From Fig. 5.3, normal distribution characteristic parameters that describe the ball-bond shear strengths are:

$$x_{50} = 19.15\ gm - f$$
$$and$$
$$\sigma = 0.96\ gm - f.$$

Find the probability that, if one does a single measurement of the shear strength of the ball bonds, a value between 18.0 and 19.0 gm-f will be obtained.

Solution

$$P(18.0\ to\ 19.0) = \int_{18.0}^{19.0} f(x)dx = F(19.0) - F(18.0)$$

The cum fail fractions are given by:

$$F(19.0) = \tfrac{1}{2} erfc\left(\tfrac{19.15-19.0}{0.96\sqrt{2}}\right) = 0.438$$
$$and$$
$$F(18.0) = \tfrac{1}{2} erfc\left(\tfrac{19.15-18.0}{0.96\sqrt{2}}\right) = 0.115$$

This gives:

$$P(18.0\ to\ 19.0) = F(19.0) - F(18.0) = 0.438 - 0.115 = 0.323$$

Therefore, the probability of a single bond-shear measurement producing a value between 18.0 and 19.0 gm-f is 0.323 (or 32.3%).

5.3 Statistical Process Control

Suppose that one knows (maybe from previous experience) that the lower reliable bond strength is 15.5 gm-f (an under-bonding condition). Likewise, when the time-zero bond strength exceeds 24.5 gm-f (an over-bonding condition), the bond is also unreliable. A very natural question to ask is—how does one statistically characterize the bonding process and is this process under control for reliable use? To answer the above questions, *capability* parameters *Cp* and *Cpk* are used.

Cp and *Cpk* are defined quantities:

$$Cp = \frac{(Upper\ Spec\ Limit) - (Lower\ Spec\ Limit)}{6\sigma} \tag{5.8}$$

and

$$Cpk = Cpl = \frac{(x_{50} - Lower\ Spec)}{3\sigma} \tag{5.9a}$$

or

$$Cpk = Cpu = \frac{(Upper\ Spec - x_{50})}{3\sigma}. \tag{5.9b}$$

The value of *Cpk* is stated based on whether Eq. (5.9a) or Eq. (5.9b) produces a smaller value. For a perfectly *centered* process, note that $Cpk = Cpl = Cpu = Cp$.

Example Problem 5.2

For the ball-bonding process illustrated in Fig. 5.3, with (x_{50}=19.15gm-f, σ=0.96), what is the *capability* (*Cp*) for this process and how well is it centered (*Cpk*)? Assume that the lower permitted level is 15.5 gm-f and the upper permitted level is 24.5 gm-f.

Solution

The process *capability* is given by:

$$Cp = \frac{(24.5 - 15.5)gm - f}{6(0.96)gm - f} = 1.56.$$

The centering for the process is given by:

$$Cpk = Cpu = \frac{(24.5 - 19.15)\ gm - f}{3(0.96)gm - f} = 1.86$$

or

$$Cpk = Cpl = \frac{(19.15 - 15.5)\ gm - f}{3(0.96)gm - f} = 1.27.$$

Therefore, *Cpk* is 1.27 (note that the smaller of the two Cpk values is used). Cpk is non-symmetrical (since *Cpl* is not equal to *Cpu*), and is dominated by the lower-end specification.

Example Problem 5.3

From the previous example problem, it was determined that *Cpk*=1.27 and was dominated by the lower-end of the distribution relative to the specification (spec). (a) What fraction of the bonds has the potential for reliability problems occurring at the lower-end of the spec? (b) Fraction of bonds above the upper-end spec?

Solution

(a) One will need to find the number of standard deviations (*Z-value*) that corresponds to the lower-end spec. From Fig. 5.2 one obtains:

$$Z = \left(\frac{1.043}{gm - f}\right) x - 19.969.$$

With the lower-end spec at x = 15.5gm-f, this gives: Z = −3.803.
Using the EXCEL NORMSDIST function, one obtains:

$$\text{F} = \text{NORMSDIST}(-3.803) = 7.15 \times 10^{-5}.$$

Therefore, the fraction of bonds at reliability risk due to the lower-end spec is 71.5 ppm (parts per million) or 0.00715% of the bonds.

(b) One needs to find the number of standard deviations (Z-value) at the upper-end specification. Again, using:

$$Z = \left(\frac{1.043}{gm - f}\right) x - 19.969,$$

with the upper-end spec of x=24.5gm-f, one obtains: Z=5.585.
Using the EXCEL NORMSDIST function, one obtains:

$$\text{F} = \text{NORMSDIST}(5.585) = 0.9999999883.$$

Therefore, the fraction of the bonds at reliability risk due to the upper-end spec is 1−F where:
$1 - F = 1 - 0.9999999883 = 11.7 \times 10^{-9}$ or 11.7 parts per billion (ppb).

Problems

1. O-rings (from a manufacturing line) were randomly selected for diameter measurements. The 25 measurements are shown in the below table (all measurements are in mm). Find the Normal Distribution parameters: median diameter size (x_{50}) and the standard deviation σ.

181.4	173.0	172.2	173.5	180.5
187.8	178.6	170.7	179.5	186.5
171.1	180.0	183.4	177.3	187.0
176.7	186.1	182.5	174.2	188.7
184.0	185.6	190.0	175.4	189.5

Answers: x_{50}= 181.6 mm σ = 6.8 mm

2. For the O-ring manufacturing process in Problem 1 (x_{50}=181.6 mm, σ=6.8 mm), find the capability parameters: *Cp* and *Cpk*. Assume that the upper spec limit is 215 mm and the lower spec limit is 155 mm.

   Answers: $Cp = 1.47$ $Cpk = 1.30$

3. The breakdown-strength distribution for capacitor dielectrics had a median value of $(E_{bd})_{50}$ =10.50 MV/cm and a σ=1.8 MV/cm.

   a) Find the fraction of caps with a breakdown ≤ 8MV/cm.
   b) Find the fraction of caps with a breakdown ≥ 12 MV/cm.

   Answers: a) 0.082 b) 0.202

4. The rupture-strength distribution of water pipes had a median value of $(\text{Rupture-Stress})_{50}$ =900 MPa and a σ=120 MPa.

   a) Find the fraction of pipes with a rupture stress of ≤ 600 MPa.
   b) Find the fraction of pipes with a rupture stress of ≥ 1300 MPa.

   Answers: a) 6.21×10^{-3}= 6210 ppm b) 4.29×10^{-4} = 429 ppm

5. Resistors have a resistance-value distribution with a median value of $(R)_{50}$ =189 ohm and a σ=3.5 ohm.

   a) Find the fraction of resistors with a resistance value of ≤160 ohms.
   b) Find the fraction of resistors with a resistance value of ≥200 ohms.

   Answers: a) 5.55×10^{-7} = 0.555 ppm b) 8.37×10^{-4} = 837 ppm

6. A group of patients had a heart-rate distribution with a median value $(HR)_{50}$=60 beats/min and a σ=2 beats/min.

   a) Find the fraction of patients with a heart rate of ≤ 50 beats/min.
   b) Find the fraction of patients with a heart rate of ≥ 70 beats/min.

   Answers: a) 2.87×10^{-7} = 0.287 ppm b) 2.87×10^{-7} = 0.287 ppm

7. Using the breakdown-strength distribution, defined in Problem 3, what are the process capability parameters: *Cp* and *Cpk*? Assume an upper-level limit of 12MV/cm and a lower-level limit of 8 MV/cm.

   Answers: *Cp = 0.37* *Cpk = 0.28*

8. For the rupture-strength distribution, defined in Problem 4, what are the process capability parameters: *Cp* and *Cpk* ? Assume an upper-level limit of 1300Mpa and a lower-level limit of 800 MPa.

   Answers: $Cp = 0.97$ $Cpk = 0.83$

9. For the resistor distribution, defined in Problem 5, what are the process capability parameters: *Cp* and *Cpk* ? Assume an upper-level limit of 200 ohm and a lower-level limit of 160 ohm.

   Answers: $Cp = 1.90 \quad Cpk = 1.05$

10. For the heart-rate distribution, defined in Problem 6, what are the capability parameters: *Cp* and *Cpk* for this group of patients? Assume an upper-level limit of 70 beats/min and a lower-level limit of 50 beats/min.

    Answers: $Cp = 1.67 \quad Cpk = 1.67$

References

Ash, C.: **The Probability Tutoring Book**, IEEE Press, (1993).
Bowker, A. and G. Lieberman: **Engineering Statistics**, Prentice-Hall Publishing, (1972).
Dixon, W. and F. Massey: **Introduction to Statistical Analysis**, McGraw-Hill Book Co., (1957).
Fowler, J., L. Cohen and P. Jarvis: **Practical Statistics for Field Biology**, John Wiley & Sons, (1998).
Larsen, R.: **Engineering with EXCEL**, 2nd Ed., Pearson/Prentice Hall Publishing, (2005).
Miller, I. and J. Freund: **Probability and Statistics for Engineers**, Prentice Hall Publishing, (1977).

Chapter 6
Time-To-Failure Statistics

When nearly identically processed materials/devices are placed under the same set of stress conditions, they will not fail exactly at the same time. An explanation for this occurrence is that slight differences can exist in the materials microstructure, even for materials/devices processed nearly identically. This means that not only are we interested in time-to-failure but, more precisely, we are interested in the distribution of times-to-failure. Once the distribution of times-to-failure is established, then one can construct a probability density function f(t) which will permit one to calculate the probability of observing a failure in any arbitrary time interval between t and t + dt, as illustrated in Figure 6.1.

Historically, two probability density functions have been widely used to describe material/device failures: *lognormal* and *Weibull distributions*. Due to their importance in reliability physics and engineering, each distribution will be discussed in some detail. The possibility of having to use *multimodal distributions* or *mixed multiple failure distributions* to describe your time-to-failure data is also presented.

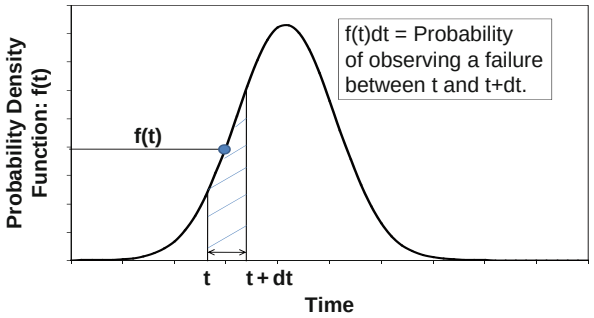

Fig. 6.1 Probability density function f(t) for failure. f(t)dt represents the probability of finding a device failure between t and t+dt.

J.W. McPherson, *Reliability Physics and Engineering*,
DOI 10.1007/978-1-4419-6348-2_6, © Springer Science+Business Media, LLC 2010

6.1 Lognormal Probability Density Function

The lognormal distribution is based on the normal distribution, except that failures are assumed to be logarithmically distributed in time, rather than linearly distributed in time. The use of the lognormal distribution has been very popular for describing time-to-failure for devices where the degradation mechanism is fairly general/extensive in nature and not restricted to simply a very localized/microscopic region of the material. Examples of failure mechanisms where the use of the lognormal distribution has gained popularity include: electromigration-induced failure, corrosion-induced failure, wear-induced failure, creep-induced failure, and fatigue-induced failure. These are discussed in Chapters 11 and 12.

The lognormal probability density function is defined by:

$$f(t) = \frac{1}{\sigma t\sqrt{2\pi}} \exp\left\{-\left[\frac{\ln(t) - \ln(t_{50})}{\sigma\sqrt{2}}\right]^2\right\} \tag{6.1}$$

where t_{50} is the median time-to-failure and σ is the logarithmic standard deviation.[1] σ is usually approximated by $\sigma = \ln(t_{50}) - \ln(t_{16}) = \ln(t_{50}/t_{16})$ where t_{16} represents the time-to-failure for 16% of the units. The cumulative failure probability F for the lognormal distribution is given by:

$$\begin{aligned} F(t) &= \frac{1}{2} erfc\left(\frac{\ln(t_{50}) - \ln(t)}{\sigma\sqrt{2}}\right) \qquad (for\ t \le t_{50}) \\ F(t) &= 1 - \frac{1}{2} erfc\left(\frac{\ln(t) - \ln(t_{50})}{\sigma\sqrt{2}}\right) \qquad (for\ t \ge t_{50}) \end{aligned} \tag{6.2}$$

A systematic approach to collecting cumulative fraction F failure data for statistical analysis is shown in Table 6.1.

The cumulative time-to-failure data (from Table 6.1) is shown in Fig. 6.2 with lognormal probability scaling. One can see from Fig. 6.2 that if normal probability scaling versus ln(t) is used, a best fitting straight line develops whereby both t_{50} and t_{16} can be read directly from the plot. However, this requires a special scaling, as illustrated in Fig. 6.2, for the cumulative fraction of devices failed. As discussed in Chapter 5 for the normal distribution, an alternative method to this type of representation of the lognormal distribution is to simply use the number of logarithmic standard deviations represented by the *Z-values*. Recall that *Z=1* represents

[1] Note that the lognormal distribution has the same general form as does the normal distribution in Chapter 5. The major differences are: (1) the natural logarithm of time ln(t) is used rather simply the time t; and (2) σ now represents the logarithmic standard deviation $\sigma = \ln(t_{50}/t_{16})$. Also, the (1/t) in the prefactor of the lognormal distribution is needed to ensure that f(t)dt will continue to represent the probability of failure. This is due to the fact that dln(t) = (1/t)dt.

Table 6.1 Method for Collection of Cumulative Fraction Failure Data.

Sampe Size = 132				
Time (hrs)	Number of New Failures Recorded at Each Time Interval	Cum # Failures	Raw Cum Fraction	Unbiased* Cum Fraction F
500	3	3	0.02	0.02
1000	27	30	0.23	0.22
1500	37	67	0.51	0.50
2000	29	96	0.73	0.72

*Unbiased Estimate of F = (Cum # Failures − 0.3)/ (Sample Size + 0.4)

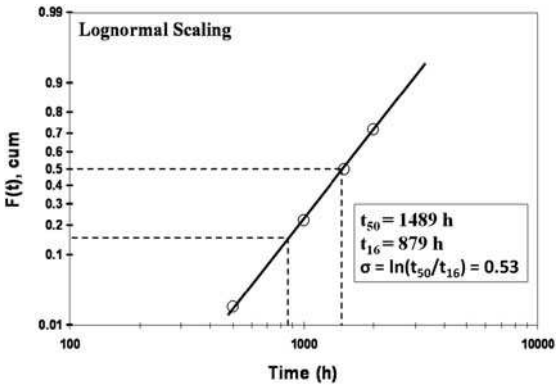

Fig. 6.2 Lognormal plotting of cumulative data from Table 6.1.

one logarithmic standard deviation $\sigma=\ln(t_{50}/t_{16})$, *Z=2* represents two logarithmic standard deviations, etc. Also recall from Chapter 5, the conversion of cumulative fraction failed *F* to a *Z-value*, and vice-versa, can be easily done using EXCEL functions: *Z=NORMSINV(F)* and *F=NORMSDIST(Z)*, respectively. Conversions, from F to Z and from Z to F, are shown in Table 6.2.

The *Z-values* in the table above represent logarithmic standard deviations. Thus, using Z values, the data is replotted in Fig. 6.3.

In general, once the lognormal parameters (t_{50},σ) are determined then any other cum fraction F can be obtained using the equation:

$$t_{F\%} = t_{50} \exp[Z_F \bullet \sigma]. \tag{6.3}$$

The following relations are so frequently used for the lognormal distribution that they are highlighted here:

$$t_{16\%} = \frac{t_{50}}{\exp(1\sigma)}; \qquad t_{1\%} = \frac{t_{50}}{\exp(2.33\sigma)}; \qquad t_{0.13\%} = \frac{t_{50}}{\exp(3\sigma)}. \tag{6.4}$$

Table 6.2 Lognormal Conversion Tables for F to Z and Z to F.

F	Z-Value	Z-Value	F
0.001	−3.0902	−3.50	0.00023
0.010	−2.3263	−3.00	0.00135
0.100	−1.2816	−2.50	0.00621
0.150	−1.0364	−2.00	0.02275
0.200	−0.8416	−1.50	0.06681
0.250	−0.6745	−1.25	0.10565
0.300	−0.5244	−1.00	0.15866
0.350	−0.3853	−0.75	0.22663
0.400	−0.2533	−0.50	0.30854
0.450	−0.1257	−0.25	0.40129
0.500	0.0000	0.00	0.50000
0.550	0.1257	0.25	0.59871
0.600	0.2533	0.50	0.69146
0.650	0.3853	0.75	0.77337
0.700	0.5244	1.00	0.84134
0.750	0.6745	1.25	0.89435
0.800	0.8416	1.50	0.93319
0.850	1.0364	2.00	0.97725
0.900	1.2816	2.50	0.99379
0.950	1.6449	3.00	0.99865
0.990	2.3263	3.50	0.99977
0.999	3.0902		

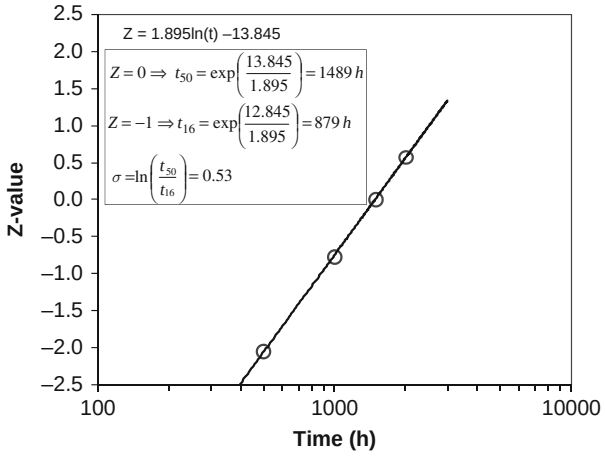

Fig. 6.3 Alternative method for performing a lognormal plot of the time-to-failure data found in Table 6.1. Note that the figure here differs from the normal distribution in that a logarithmic scaling is used for the time axis. t_{50} is extracted from the best fitting linear equation by setting the Z-value $= 0$. t_{16} is obtained by setting the Z-value $= -1$. σ is calculated using $\sigma = \ln(t_{50}/t_{16})$.

6.2 Weibull Probability Density Function

The Weibull distribution is a *weakest-link* type distribution. By using the term *weakest link*, one means that the failure of the whole (for example a chain) is dominated by the degradation rate for the weakest element (one of the links). The Weibull distribution is very popular when plotting semiconductor failure mechanisms such as time-dependent dielectric breakdown (TDDB) where the entire capacitor fails when a very localized region of the capacitor fails. The Weibull distribution tends to fit TDDB data extremely well because one small localized region (usually called a percolation region/path) of the dielectric will tend to degrade more rapidly than the other regions of the dielectric. Thus, the failure of the whole (capacitor) tends to be dominated by the degradation of this weakest link (very localized/microscopic region within the dielectric). The Weibull distribution is also very useful for system reliability where the entire system fails when one of the constituent components fails.

The Weibull probability density function is defined by

$$f(t) = \left(\frac{\beta}{\alpha}\right)\left(\frac{t}{\alpha}\right)^{\beta-1} \exp\left[-\left(\frac{t}{\alpha}\right)^{\beta}\right], \tag{6.5}$$

where α is referred to as the characteristic time-to-failure and β is referred to as the *shape* (or *dispersion* or *Weibull slope*) parameter.

Unlike the lognormal distribution (where the cumulative failure probability F(t) must be obtained by numerical methods represented by the error function), an analytical expression can be found for the cumulative Weibull failure probability function,

$$F(t) = \int_0^t f(t)dt = 1 - \exp\left[-\left(\frac{t}{\alpha}\right)^{\beta}\right]. \tag{6.6}$$

Rearranging Eq. (6.6) and taking the appropriate logarithms, one obtains:

$$\ln\left[-\ln(1-F)\right] = \beta[\ln(t/\alpha)]\,. \tag{6.7}$$

One can see that when F=0.63212, the left-hand side of Eq. (6.7) goes to zero. It tells us that the characteristic time α is the time for 63.212% of the devices to fail. Generally, one simply approximates this and writes the Weibull characteristic time as: $\alpha = t_{63}$. Solving for the Weibull slope β in Eq. (6.7), one obtains:

$$\beta = \frac{\ln\left[-\ln(1-F)\right]}{\ln(t/t_{63})}.^{2} \tag{6.8}$$

[2]Note that any cumulative fraction F, and its corresponding failure time, may be used in Eq. (6.8) to determine the Weibull slope. The author's preference is to use F=0.1 and t_{10}. However, this is only a preference, not a requirement.

Using the time-to-failure data shown in Table 6.1, a Weibull plot of the data is shown in Fig. 6.4 using a special Weibull probability scaling. The determination of the *characteristic time* t_{63} and *Weibull slope* β, which give the best fitting to the time-to-failure data, are shown. One can see that the Weibull distribution gives a reasonably good fitting to the data. The Weibull parameters that give the best fitting to the data are: a characteristic time of t_{63}=1738 hours and a slope of β=3.02.

An alternative method for performing the Weibull plotting is through the use of *Weibits*. The conversion of cumulative fraction failed *F* into *Weibits* is given by: Weibit = ln[−ln(1−F)]. Table 6.3 shows a few selected conversions.

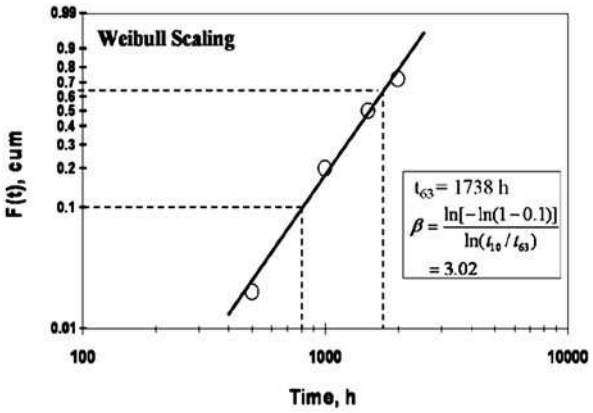

Fig. 6.4 Weibull probability plotting is shown for data in TABLE 6.1.

Table 6.3 Conversions from F to *Weibits* and *Weibits* to F.

Cum F	Weibits Ln(−Ln(1−F)]	Weibits Ln[−Ln(1−F)]	Cum F
0.001	−6.90725507	−3.0	0.048568007
0.01	−4.60014923	−2.5	0.078806345
0.1	−2.25036733	−2.0	0.126576982
0.2	−1.49993999	−1.5	0.199989287
0.3	−1.03093043	−1.0	0.307799372
0.4	−0.67172699	−0.5	0.454760788
0.5	−0.36651292	0.0	0.632120559
0.6	−0.08742157	0.5	0.807704354
0.7	0.185626759	1.0	0.934011964
0.8	0.475884995	1.5	0.988685714
0.9	0.834032445	2.0	0.999382021
0.95	1.0971887	2.5	0.999994881
0.99	1.527179626	3.0	0.999999998
0.999	1.932644734		

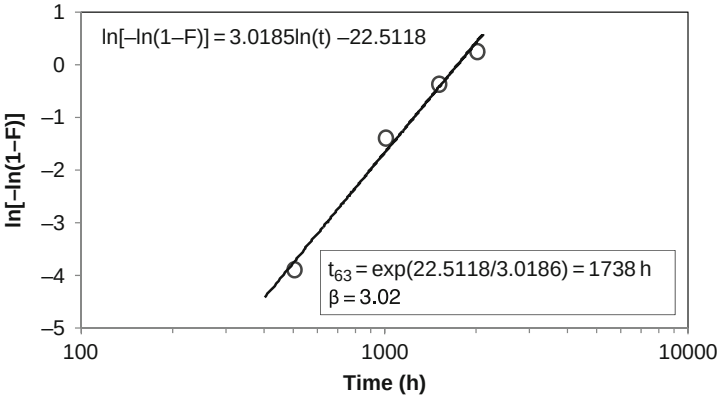

Fig. 6.5 Weibull distribution plotting in terms of Weibits (Weibit = ln[−ln(1−F)]). Note that a Weibit = 0, produces t_{63}. The slope of the best linear fitting is β.

The new Weibull plot of the time-to-failure data, found in Table 6.1, is shown in Fig. 6.5.

One should always keep in mind, when working with such Weibull plots, that best fitting a Weibit = 0 (using the best fitting line) corresponds to t_{63}. The slope of this best fitting line is the Weibull slope β. Once the Weibull distribution parameters (t_{63},β) are established, then any other cum fraction can be found using:

$$t_{F\%} = t_{63} \exp\left\{\frac{1}{\beta} \ln\left[-\ln(1-F)\right]\right\}. \tag{6.9}$$

Some often used values for the Weibull distribution are highlighted here:

$$t_{10\%} = \frac{t_{63}}{\exp\left[\frac{2.25}{\beta}\right]}; \quad t_{1\%} = \frac{t_{63}}{\exp\left[\frac{4.60}{\beta}\right]}; \quad t_{0.1\%} = \frac{t_{63}}{\exp\left[\frac{6.91}{\beta}\right]}. \tag{6.10}$$

6.3 Multimodal Distributions

Generally a multimodal failure distribution has more than one failure mechanism present in the single set of time-to-failure data. Sometimes this can be easily detected in the time-to-failure data because the failure mechanisms are slightly separated in time. Often, however, the mechanisms are mixed (occurring during the same time intervals).

6.3.1 Multimodal Distribution (Separated In Time)

When taking time-to-failure data sometimes more than one failure mechanism/mode can be active during a single reliability test. In semiconductor devices, one might have electromigration, TDDB, and hot-carrier injection (HCI) failures occurring during the same high-temperature operating life test. In mechanical systems, one might have wear, fatigue and corrosion-induced failures occurring during the same test. Multimodal time-to-failure data is shown in Table 6.4.

Evidence for more than one failure mechanism being active during a single reliability test can sometimes be detected as *points of inflection* in the lognormal and/or Weibull plots. In Table 6.4, time-to-failure data is shown. When this time-to-failure data is plotted in a single lognormal plot[3] (as shown in Fig. 6.6), at least three failure mechanisms/modes (A, B, and C) are indicated in Fig. 6.6 by the two indicated *points of inflection.*

As one can see from Fig. 6.6, Mechanism A is responsible for about 22% of the total failures. Mechanism B is responsible for about 40% of the total failures and

Table 6.4 Multimodal Time-To-Failure Data.

Rank F	Time-To-Failure hrs	Normal Distribution Z-value NORMSINV(F)
0.01	7	−2.326
0.05	12	−1.645
0.10	15	−1.282
0.15	20	−1.036
0.20	23	−0.842
0.25	100	−0.674
0.30	105	−0.524
0.35	110	−0.385
0.40	120	−0.253
0.45	130	−0.126
0.50	140	0.000
0.55	150	0.126
0.60	160	0.253
0.65	500	0.385
0.70	520	0.524
0.75	530	0.674
0.80	550	0.842
0.85	570	1.036
0.90	590	1.282
0.95	610	1.645

[3] A lognormal distribution was used here but a Weibull distribution could have been used and would show similar results.

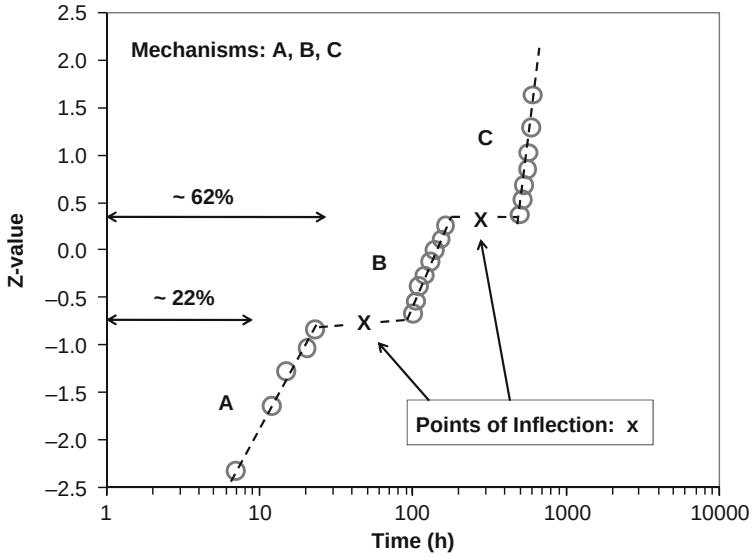

Fig. 6.6 Two inflection points are evident in this single lognormal plot. The two inflection points suggest the possibility of three failure mechanisms (A,B,C) existing in this single set of time-to-failure data.

mechanism C represents about 38% of the total number of failures. Many times we would like to estimate what distribution A (alone) would look like, or B (alone) or C (alone).

The estimated contribution of each of the mechanisms is given by:

Mechanism A

$$F_A = \frac{Rank(F)}{0.22} \tag{6.11}$$

Mechanism B

$$F_B = \frac{Rank(F) - 0.22}{0.62 - 0.22} \tag{6.12}$$

Mechanism C

$$F_C = \frac{Rank(F) - 0.62}{1 - 0.62}\,. \tag{6.13}$$

In Table 6.5, the three separate mechanisms are now shown.

Shown in Fig. 6.7 are the individual distributions (t_{50}, σ) for each mechanism.

Table 6.5 Separation of Mechanisms For Distribution Plotting.

Rank F	Adjusted by point of Inflection F_A = [Rank F]/0.22	Adjusted by points of Inflection F_B = [Rank F − 0.22]/(0.62−0.22)	Adjusted by point of Inflection F_C = [Rank F − 0.62]/(1−0.62)	Time-To-Failure hrs	Normal Distribution Z-value NORMSINV(F)
0.01	0.05			7	−1.691
0.05	0.23			12	−0.748
0.1	0.45			15	−0.114
0.15	0.68			20	0.473
0.2	0.91			23	1.335
0.25		0.08		100	−1.440
0.3		0.20		105	0.842
0.35		0.33		110	−0.454
0.4		0.45		120	−0.126
0.45		0.58		130	0.189
0.5		0.70		140	0.524
0.55		0.83		150	0.935
0.6		0.95		160	1.645
0.65			0.08	500	−1.412
0.7			0.21	520	−0.805
0.75			0.34	530	−0.407
0.8			0.47	550	−0.066
0.85			0.61	570	0.267
0.9			0.74	590	0.634
0.95			0.87	610	1.119

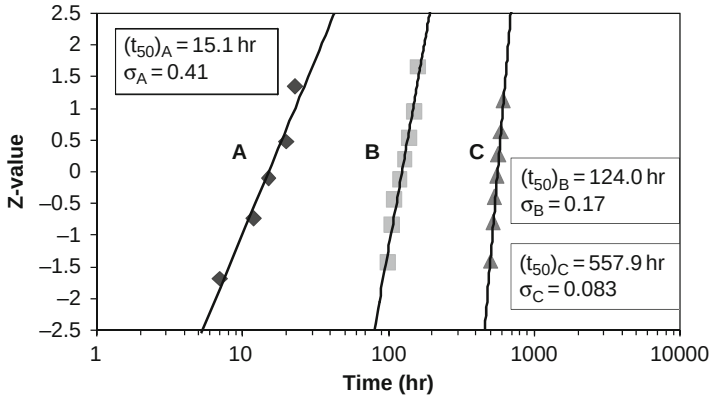

Fig. 6.7 The three mechanisms, shown in Fig. 6.6, are now separated with the individual t_{50} and σ values determined for each.

6.3.2 Mixed Multiple Failure Mechanisms

Sometimes multiple failure mechanisms are occurring in a single set of time-to-failure data but with no obvious *points of inflection* to help separate the mechanisms. In this case a *Kaplan-Meiers* type of decoupling method is useful for separating the mechanisms. The method is illustrated below.

Time-to-failure data is shown in Table 6.6. Suppose that, through electrical or physical failure analysis, one can identify that the failures are a mixture of two failure mechanisms: type A and type B. The questions that we would like to answer are: 1) w*hat would the failure distribution look like if only mechanism A was active;* and 2) w*hat would the failure distribution look like if only mechanism B was active?*

The cum fraction F_A calculation for A-type failures alone is complicated by the fact that the B-type failures are occurring during the same time intervals, and vice versa. For this reason, one will find it more useful to work with the survivor probability $(1-F_A)$ rather than the cum failure probability F_A. One must take into account

Table 6.6 Mixed Multiple Failure Mechanisms.

Sample Size (SS)=100			
Read Points (hrs)	Cum F	Mechanism A (Cum # fails)	Mechanism B (Cum # fails)
0	0	0	0
500	0.02	0	2
1000	0.22	5	17
1500	0.50	12	38
2000	0.72	20	52

that both failure mechanisms are occurring during the same intervals and when B-failures occur they are taking away from the effective sample size for A, and vice versa.

One can take advantage of the fact that the probability $(1-F)_{i+1}$ of surviving the $i^{th}+1$ time interval must be equal to the probability $(1-F)_i$ of surviving the previous i^{th} time interval times the probability of surviving the present time interval. For example:

$$(1-F_A)_{i+1} = (1-F_A)_i \left(\frac{SS - (Cum\ \#\ for\ A)_{i+1} - (Cum\ \#\ for\ B)_{i+1}}{SS - (Cum\ \#\ for\ B)_{i+1}} \right) \quad (6.14)$$

and

$$(1-F_B)_{i+1} = (1-F_B)_i \left(\frac{SS - (Cum\ \#\ for\ A)_{i+1} - (Cum\ \#\ for\ B)_{i+1}}{SS - (Cum\ \#\ for\ A)_{i+1}} \right). \quad (6.15)$$

In the above equations, SS is the beginning sample size (at time zero) and Cum # represents the cumulative number of failures for each mechanism (A or B) at the indicated time interval. Shown in Table 6.7 is an example of how to use the above equations to generate the individual cumulative failure distributions for mechanisms A and B separately. Figure 6.8 shows the individual Weibull plots[4] of the failure mechanisms for A and B, along with their characteristic Weibull parameters (t_{63},β).

Shown in Fig. 6.8 are the Weibull plots of F_A and F_B for the separated mechanisms A and B, respectively, for the data taken from Table 6.7.

From Fig. 6.8, one can see that that the characteristic times (t_{63}) are different for the two failure mechanisms as well as their Weibull slopes (β).

Table 6.7 Decoupling of Mixed Multiple Failure Mechanisms.

Sample Size (SS)=100							
Read Points (hrs)	Cum F	Mechanism A (Cum # fails)	Mechanism B (Cum # fails)	$1-F_A$	$1-F_B$	F_A	F_B
0	0	0	0	1	1	0	0
500	0.02	0	2	1.00	0.98	0	0.02
1000	0.22	5	17	0.94	0.80	0.06	0.20
1500	0.50	12	38	0.76	0.46	0.24	0.54
2000	0.72	20	52	0.44	0.16	0.56	0.84

[4] A lognormal distribution could also have been used and would produce similar results.

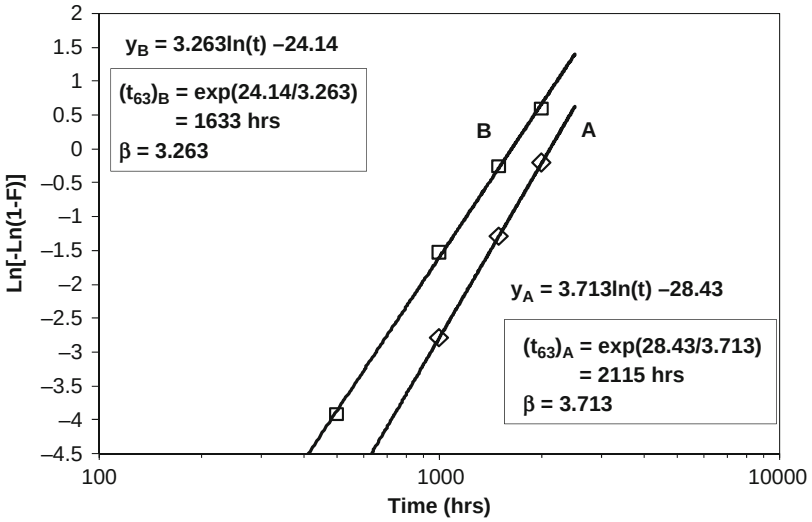

Fig. 6.8 Separation of Mixed Multiple Failure Mechanisms is illustrated. The characteristic Weibull parameters are given for each mechanism.

Problems

1. Time-to-rupture data (from a creep study) was shown for steel rods that were held at a fixed level of stress at very high temperatures until rupture occurred. The time-to-failure data is shown in hours.

44.0	43.3	49.0	36.0	70.8
50.3	45.2	47.4	36.3	68.3
65.6	51.4	43.2	39.4	70.7
54.5	58.3	42.5	52.2	56.5
41.1	60.2	42.7	63.6	40.0

   Find the lognormal distribution that gives the best fitting to the data. What are the values of the median time-to-failure (t_{50}) and logarithmic standard deviation (σ)?

   Answers: $t_{50} = 49.8$ hrs, $\sigma = \ln(t_{50}/t_{16}) = 0.22$

2. Given the lognormal distribution (t_{50}=49.8 hrs, σ= 0.22) from Problem 1,

   a) What is the expected time for 0.1% of the steel rods to rupture?
   b) What is the expected time for 99.9% of the steel rods to rupture?

   Answers: a) $t_{0.1\%} = 25.2$ hrs b) $t_{99.9\%} = 98.3$ hrs

3. Given the lognormal distribution (t_{50}=49.8 hrs, σ= 0.22) from Problem 1, what fraction of failures occur between 35 and 55 hrs?

   Answer: 0.620

4. Using the time-to-rupture data in problem 1, find the Weibull distribution that gives the best fitting to the data. What are the values for t_{63} and the Weibull slope β?

   Answer: $t_{63} = 55.2$ hrs, $\beta = 5.4$

5. Given the Weibull distribution (t_{63}=55.2 hrs, β= 5.4) from Problem 3,

   a) What is the expected time for 0.1% of the steel rods to rupture?
   b) What is the expected time for 99.9% of the steel rods to rupture?

   Answers: a) $t_{0.1\%} = 15.4$ hrs b) $t_{99.9\%} = 79.0$ hrs

6. Given the Weibull distribution ($t_{63} = 55.2$ hrs, $\beta = 5.4$) from Problem 3, what fraction of the failures occurred between 35 and 55 hrs?

   Answer: 0.543

7. Using the normal distribution in Chapter 5, fit the data shown in Table 6.1.

   a) What are the values of t_{50} and sigma for the normal distribution?
   b) Compare your normal fit to the lognormal-fit shown in Fig. 6.3. Which distribution gives the better fitting, normal or lognormal?

   Answers:

   a) t_{50} =1573 hrs, $\sigma = 576$ hrs
   b) Lognormal distribution gives a better fitting to this data set.

8. The following time-to failure data was collected and found to have two failure mechanisms in the time-to-failure data.

Cum Fraction F	Time-To-Failure (Hr)
0.05	16
0.09	20
0.15	25
0.22	30
0.3	35
0.38	42
0.45	104
0.51	110
0.63	118
0.68	127
0.75	135
0.82	143
0.87	150
0.9	155

   a) Perform a lognormal-plot of the above data.
   b) Find the point-of-inflection which separates the two mechanisms.

c) Replot the data for the two mechanisms.
d) What are the (t_{50},σ) values for the two mechanisms?

Answers:

b) Point of inflection: F = 0.49
d) Mechanism A: t_{50} = 30.6 hrs, σ = 0.48
Mechanism B: t_{50} = 133.1 hrs, σ = 0.18

9. Using the time-to failure data (shown in the table in Problem 8):

a) Perform a Weibull plot of the above data.
b) Find the point of inflection which separates the two mechanisms.
c) Re-plot the data for the two mechanisms.
d) What are the (t_{50},σ) values for the two mechanisms?

Answers:

b) Point of inflection: F = 0.42.
d) Mechanism A: t_{63} = 32.3 hr, β= 2.99
Mechanism B: t_{63} = 139.6 hr, β = 6.29

References

Dhillon, B. and C. Singh: **Engineering Reliability**, John Wiley & Sons, (1981).
McPherson, J.: *Reliability Physics*. In: **Handbook of Semiconductor Manufacturing Technology**, Marcel Dekker, 959 (2000).
Miller, I. and J. Freund: **Probability and Statistics for Engineers** *2nd Ed.*, Prentice Hall, (1977).
Nelson, W.: **Accelerated Testing**, John Wiley and Sons, (1990).

Chapter 7
Failure Rate Modeling

For a collection of devices, it is critically important to be able to understand the expected *failure rate* for the devices. For the supplier of such devices, the expected failure rate will be an important indicator of future warranty liability. For the customer, the expected failure rate will be an important indicator of future satisfaction. For *mission-critical*[1] applications, it is of paramount importance for one to know that the expected failure rate will be extremely low.

7.1 Device Failure Rate

The *survivor failure rate* for a collection of devices is of great reliability importance. The failure-rate equation, by which the devices are expected to fail, is given by:

$$\frac{dM}{dt} = -\lambda(t)\, M(t). \tag{7.1}$$

M(t) represents the number of survivors at any time *t*, and $\lambda(t)$ represents the *instantaneous survivor failure* rate. One can write

$$\mathrm{M(t)} = \mathrm{M(0)}\,[1 - \mathrm{F(t)}], \tag{7.2}$$

where *M(0)* is the number of devices at time zero and *F(t)* is the cumulative failure probability as previously discussed in Chapter 6. Using the equations above, the *instantaneous survivor failure rate* $\lambda(t)$ is given by:

[1]The use of the expression *mission critical* came into vogue for space applications. In space applications, device repair or replacement is very difficult, if not impossible. Therefore, it is imperative that such devices have extremely low failure rates. However, today, life-support implantable devices are widely used. If one of these devices is part of your life-support system, there is little doubt that you would describe this as a *mission-critical* application.

J.W. McPherson, *Reliability Physics and Engineering*,
DOI 10.1007/978-1-4419-6348-2_7,

$$\lambda(t) = -\frac{1}{M(t)}\frac{dM}{dt} = -\frac{1}{M(0)[1-F(t)]}\left[-M(0)\frac{dF}{dt}\right] = \frac{f(t)}{1-F(t)}, \tag{7.3}$$

where f(t) is the probability density function (from Chapter 6).

7.2 Average Failure Rate

Separating the variables and integrating, the solution to Eq. (7.1) can be written as:[2]

$$\int_0^t \frac{dM}{M(t)} = -\int_0^t \lambda(t)dt = -t\left(\frac{\int_0^t \lambda(t)dt}{\int_0^t dt}\right) = -\langle\lambda\rangle t, \tag{7.4}$$

where $\langle\lambda\rangle$ is the time-averaged failure rate. The solution to Eq. (7.4) becomes:

$$\mathrm{M(t)} = \mathrm{M(0)exp[-} < \lambda > \mathrm{t]}. \tag{7.5}$$

Even though the failure rate $\lambda(t)$ is, in general, a function of time, the *average failure rate* $< \lambda >$ over some interval 0 to t can often be useful and requires closer attention:

$$\begin{aligned} < \lambda > &= \frac{\int_0^t \lambda(t)\,dt}{\int_0^t dt} = \frac{1}{t}\int_0^t \frac{f(t)}{1-F(t)}\,dt \\ &= \frac{1}{t}\int_0^t \frac{dF(t)/dt}{1-F(t)}\,dt = \frac{1}{t}\int_0^t \frac{dF}{1-F(t)} \\ &= \frac{1}{t}\ln\left[\frac{1}{1-F(t)}\right]. \end{aligned} \tag{7.6}$$

Eq. (7.6) can be approximated for small cum fraction F by,

$$\langle\lambda\rangle \cong \frac{F(t)}{t}. \tag{7.7}$$

[2]The identity $1 = t/\int_0^t dt$ is used in Eq. (7.4).

Remember that $< \lambda >$ represents the average failure rate over the interval 0 to t. Therefore, during reliability testing, the average failure rate is usually estimated by:

$$\langle \lambda \rangle = \frac{Cum\,\#\,Failures}{Total\,\#\,Device - Hrs} = \frac{F \bullet SS}{SS \bullet (\#\,Test\ Hrs)} = \frac{F}{\#\,Test\ Hrs}. \tag{7.8}$$

In the equation above, SS is the sample size. The unit of failure rate is the *FIT* (failure in time) and represents 1 failure per billion device-hrs ($1-FIT$ = 1failure/10^9 dev−hr = 10^{-9} fails/dev−hr = 10^{-9}/hr).[3] While the instantaneous failure rate is obviously more precise, the average failure rate can often be useful, especially for very complex/multi-component systems and when estimating cum fraction *F*.

7.2.1 Lognormal Average Failure Rate

The average failure rate, using the lognormal cumulative failure distribution *F(t)* from Chapter 6, becomes:

$$\begin{aligned}
\langle \lambda \rangle_{\log\ normal} &= \frac{1}{t} \ln \left[\frac{1}{1 - F(t)} \right] \\
&= \frac{1}{t} \ln \left[\frac{1}{1 - \frac{1}{2} erfc \left(\frac{\ln(t_{50}) - \ln(t)}{\sigma \sqrt{2}} \right)} \right] (for\ t \le t_{50}) \\
&= \frac{1}{t} \ln \left[\frac{1}{\frac{1}{2} erfc \left(\frac{\ln(t) - \ln(t_{50})}{\sigma \sqrt{2}} \right)} \right] (for\ t \ge t_{50}).
\end{aligned} \tag{7.9}$$

7.2.2 Weibull Average Failure Rate

The average failure rate, using the Weibull cumulative failure distribution F(t) from Chapter 6, is given by:

[3] In order to be consistent with Eq. (7.1), the true unit of failure rate λ must be in reciprocal time. Often the pseudo units (failures and devices) are introduced for emphasis and to facilitate a little *bookkeeping*. However, the true units of the FIT are: 1 FIT = 10^{-9}/hr.

$$\langle\lambda\rangle_{Weibull} = \frac{1}{t}\ln\left[\frac{1}{1-F(t)}\right] = \frac{1}{t}\ln\left[\frac{1}{\exp\left[-\left(\frac{t}{t_{63}}\right)^{\beta}\right]}\right] \tag{7.10}$$
$$= \frac{1}{t}\left(\frac{t}{t_{63}}\right)^{\beta}.$$

Example Problem 7.1

The observed average failure rate for a collection of devices was found to be : $<\lambda> = \lambda_0 = 1000$ FITs. If one starts with 50,000 devices at time zero, how many devices are expected to fail after 1 year? [Note: 1 yr = 8760hrs]

Solution

$M(t) = M_0 \exp(-\lambda_0 t)$

$\Rightarrow$

$$M(t = 8760hrs) = (50,000\ devices)\exp\left[-(1000FITs)\left(\frac{10^{-9}/hr}{1\ FIT}\right)(8760hrs)\right]$$
$$= 49564.$$

$\#\ Failures = M_0 - M(t = 8760hrs) = 50,000 - 49564 = 436.$

Example Problem 7.2

Suppose that one has a system which is made up of 1000 components, with the components having an average failure rate of 100 fits. What would be the mean (average) time between failures for such a system?

Solution

$$Average\ System\ Failure\ Rate = (1000\ devices) \bullet (100\ FITs)$$
$$= (1000 devices) \bullet \left(\frac{100\, failures}{10^9\ device \bullet hr}\right)$$
$$= \frac{1\, failure}{10^4\ hours}.$$

Since 10^4 hrs =1.14yrs, then one would expect this system to fail (on average) once every 1.14 yr. This represents the mean-time-between-failures (MTBF) and is a very important reliability parameter. MTBF describes, on average, the level of reliability problems that can be expected for such a system.

7.3 Instantaneous Failure Rate

The instantaneous survivor failure rate is generally of greater value to the reliability engineer than simply the average failure rate.[4] Both the lognormal and Weibull instantaneous failure rates are discussed in detail.

7.3.1 Lognormal Instantaneous Failure Rate

Using Eq. (7.3), with f(t) and F(t) found in Eq. (6.1) and Eq. (6.2), respectively, then the lognormal instantaneous failure rate becomes:

$$\lambda(t) = \frac{\dfrac{1}{\sigma\ t\ \sqrt{2\pi}}\ \exp\left\{-\left[\dfrac{\ln(t)-\ln(t_{50})}{\sigma\sqrt{2}}\right]^2\right\}}{1-\dfrac{1}{2}erfc\left(\dfrac{\ln(t_{50})-\ln(t)}{\sigma\sqrt{2}}\right)} \quad (for\ \ t \le t_{50})$$

and

$$\lambda(t) = \frac{\dfrac{1}{\sigma\ t\ \sqrt{2\pi}}\ \exp\left\{-\left[\dfrac{\ln(t)-\ln(t_{50})}{\sigma\sqrt{2}}\right]^2\right\}}{\dfrac{1}{2}erfc\left(\dfrac{\ln(t)-\ln(t_{50})}{\sigma\sqrt{2}}\right)} \quad (for\ \ t \ge t_{50}). \tag{7.11}$$

7.3.2 Weibull Instantaneous Failure Rate

Using Eq. (7.3), and *f(t)* and *F(t)* found in Eq. (6.5) and Eq. (6.6), respectively, then the Weibull instantaneous failure rate takes on a relatively simple form:

$$\lambda(t) = \left(\frac{\beta}{t_{63}}\right)\left(\frac{t}{t_{63}}\right)^{\beta-1}. \tag{7.12}$$

[4] A common-experience analogy is perhaps useful — the instantaneous speed that you drive is usually far more important than your average speed. Speeding tickets are normally issued based on instantaneous speed, not average speed!

The Weibull failure rate is widely used because it describes *weakest link* type failure mechanisms very well. Also, another reason for its popularity is that its form is relatively simple, versus the lognormal failure rate, Eq. (7.11). Note that for $\beta = 1$, the failure rate is a constant (independent of time). It will be shown, in example problem 7.3, that the Weibull failure rate decreases when $\beta < 1$, increases when $\beta > 1$, and is constant for $\beta = 1$.

Example Problem 7.3

In a reliability test, it was found that the characteristic Weibull lifetime was $t_{63} = 87{,}600$ hrs. Determine the Weibull instantaneous failure rate curve for: β=0.5, β=1.0 and β=1.5.

Solution

Shown below is the failure rate $\lambda(t)$ in FITs, given by Eq. (7.12). In Fig. 7.1a below, the failure rate is shown with a linear scaling of the time. In Fig. 7.1b, the failure rate is shown with a logarithmic scaling of the time. These figures indicate that for β=0.5, the failure rate decreases with time. For β=1.0, the failure rate is constant. For β=1.5, the failure rate increases with time.

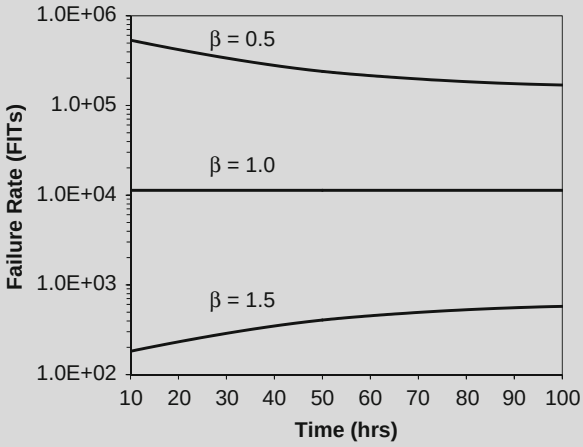

Fig. 7.1a Failure rate is observed to decrease with time for $\beta < 1$, failure rate is constant for β=1, and failure rate is observed to increase for $\beta > 1$. Linear time-scaling is shown.

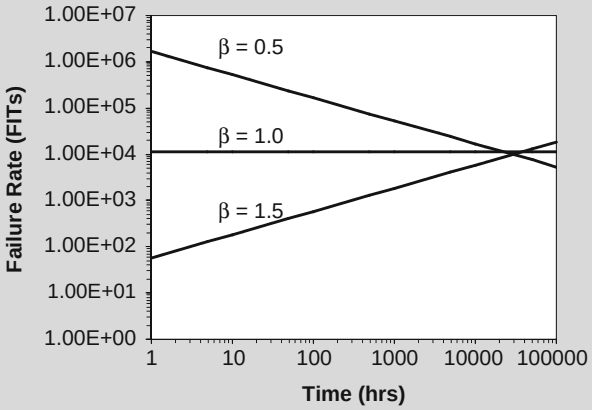

Fig. 7.1b Failure rate is observed to decrease with time for $\beta < 1$, failure rate is constant for $\beta=1$, and failure rate is observed to increase for $\beta > 1$. Logarithmic time-scaling is shown.

7.4 Bathtub Curve

The failure-rate curve for devices (either electrical or mechanical) generally takes the form shown in Fig. 7.2. From its obvious shape, this reliability curve is commonly referred to as the *bathtub curve* for reliability. There are three distinct reliability regions associated with this curve and these are highlighted in (Fig. 7.2). First, during the early stages of device use, the failure rate is relatively high and this region is referred to as the early failure rate (EFR) region. The failures occurring in the EFR region are generally due to rather gross defects. Second, after the initial high EFR portion of the curve, a much lower and stable failure rate region occurs

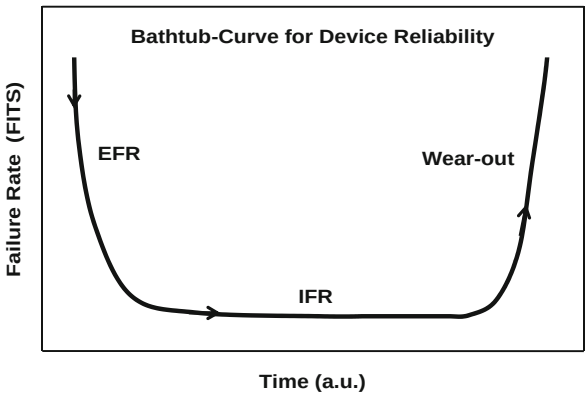

Fig. 7.2 Bathtub reliability curve is used to describe device failure-rate characteristics for nearly all devices.

and this region is referred to as the intrinsic failure rate (IFR) region. The IFR fails can be due to very small defects in the materials. After the IFR region, one usually has a region of rapid turn-up in the failure rate which is referred to as the wear-out region. The wear-out region is driven by normal material/device degradation, as discussed in Chapter 2. This wear-out region is strongly dependent of the level of stress and temperature, as discussed in Chapter 4.

The old reliability *joke* among air travelers — if you are either scheduled for the maiden flight on a new airliner or scheduled for a trip on an airliner that has been in service for more than 25 years, then *you may want to reconsider your travel plans*! In the former case, one worries about EFR and in the later case one worries about wear out. If you are told that the plane is about 10 years old, with outstanding reliability and service record, then you should be at the bottom of the bathtub curve (lowest failure rate) — so *sit back and enjoy the flight*!

Depressing as the subject may be, the bathtub curve also describes the mortality rate for humans. The death rate for newborns is relatively high during the first few hours of life because of birth defects in critically important organs (heart, lungs, kidneys, brain, etc.). This is the early failure rate (EFR) portion of the curve for humans[5] and helps to explain why doctors generally have more apprehension/anxiety during the first 24 hrs of a newborn's life. After this initial period, the level of concern tends to reduce with time and drops rather sharply after 1-day, 1-week, 1-month, etc. After a year or so, the mortality rate tends to flatten (bottom of bathtub curve) and the mortality rate is at its lowest value (*sweet part of the reliability curve*). Unfortunately, however, after about 70+ years of use, your components (organs) start wearing out and the system (your body) starts to fail.

7.5 Failure Rate for Electronic Devices

The early failure rate (EFR) portion of the reliability curve for electronic devices can be very similar to that shown in Fig. 7.2. This EFR region, for integrated circuits, is dominated by manufacturing defects (materials with extremely low breakdown strengths) and shows a rather sharp reduction in failure rate with time. This EFR region (higher failure-rate region) can last for a year or more at normal operating voltage and temperature conditions: (V_{op}, T_{op}). This can be a reliability headache (very expensive) for the supplier because the warranty period is generally one year. To avoid the supplier headaches, from irate customers having initially very high failure rates, the supplier may sometimes choose to exercise the devices for a period of time (to eliminate the defective devices) before sending the product to their customers. This period of time, in which the devices are exercised to eliminate the defective devices, is often called *burn-in*.

The IFR region still contains some relatively small defects (which tend to reduce the breakdown strength of the materials). The failure rate that is observed at the

[5]This is why the EFR region is also referred to as *infant mortality*.

bottom of the bathtub curve is nearly constant and is due primarily to those intrinsic weaknesses (intermediate breakdown strengths) found in a population of otherwise good devices. This portion of the curve is referred to as the intrinsic failure-rate (IFR) region.

Finally, if the devices are operated long enough, they will eventually start to fail even though the material strengths may be excellent; this region is referred to as the wear-out region. The wear-out region is correlated with the materials-type selection, design rules used, and the use conditions.

In order to reduce the high failure rate during the EFR period, burn-in is sometimes needed; but, one year of burn-in at nominal operating conditions (V_{op}, T_{op}) is not practical. If, however, one increases the normal operating conditions to (V_{stress}, T_{stress}), then one can accelerate the time-to-failure process for these defective devices. Hopefully, under the accelerated conditions, the defective devices will fail much more rapidly (hours, minutes, or even seconds) versus the one year period of normal conditions. This all depends on the acceleration factor (subject of Chapters 8 and 9).

One also has to be careful that the accelerated burn-in process does not significantly weaken the good devices. It is assumed that the design and materials used in the good devices are such that these devices have many years of reliable operation; therefore, losing one year of lifetime is rather insignificant. Again, this all depends on the acceleration factor used for the burn-in process.

Example Problem 7.4

The reliability of 5,000 devices was monitored during a 10 year period. The failures are shown below.

Table 7.1 Observed Failure Data for 5,000 Devices.

Sample Size=	5,000														
Time (yr)	0.1	0.2	0.3	0.4	0.5	1	2	3	4	5	6	7	8	9	10
Number of Fails	15	1	0	0	0	1	2	2	2	2	2	2	5	15	25

a) Construct the failure rate curve (*bathtub curve*).
b) How long should the devices have been *burned-in* so that the shipped product had a failure rate of < 100 fits?
c) If *wear out* is defined as the time for the failure rate to exceed 100 fits, when did this product start to wear out?

Solution

a) The failure data, provided in this problem, is first re-organized in Table 7.2 below for relatively easy data analysis. Shown in Fig. 7.3 is

the cumulative fraction failed F for the complete data set. The EFR, IFR and Wear-Out regions are also indicated. The EFR region is treated as an independent failure rate contributor with the cum fraction F_{EFR} calculated using the entire sample size of 5000 (see Table 7.2). The IFR region is also treated as an independent failure rate contributor but uses a reduced sample size of 4984. The wear-out region is also treated as an independent failure rate contributor, but with a further reduced sample size of 4971. The total failure rate will be a sum of these independent contributors to the failure rate.

Table 7.2 Failure Data Reorganized (from Table 7.1).

				$(SS)_{EFR}$		$(SS)_{IFR}$		$(SS)_{wearout}$	
				= SS		= SS − 16		= SS − 16 − 13	
SS=	5000			5000	EFR	4984	IFR	4971	Wearout
Time (yr)	# FAILS	F	ln[−ln(1−F)	F_{EFR}	ln[−ln(1−F_{EFR})]	F_{IFR}	ln[−ln(1−F_{IFR})]	$F_{Wearout}$	ln[−ln(1−$F_{Wearout}$)]
0.1	15	0.0030	−5.8076	0.0030	−5.8076				
0.2	1	0.0032	−5.7430	0.0032	−5.7430				
0.3	0	0.0032	−5.7430						
0.4	0	0.0032	−5.7430						
0.5	0	0.0032	−5.7430						
1	1	0.0034	−5.6823			0.0002	−8.5139		
2	2	0.0038	−5.5709			0.0006	−7.4151		
3	2	0.0042	−5.4706			0.0010	−6.9040		
4	2	0.0046	−5.3794			0.0014	−6.5674		
5	2	0.0050	−5.2958			0.0018	−6.3159		
6	2	0.0054	−5.2187			0.0022	−6.1150		
7	2	0.0058	−5.1470			0.0026	−5.9477		
8	5	0.0068	−4.9874					0.0010	−6.9014
9	15	0.0098	−4.6205					0.0040	−5.5136
10	25	0.0148	−4.2057					0.0091	−4.7002

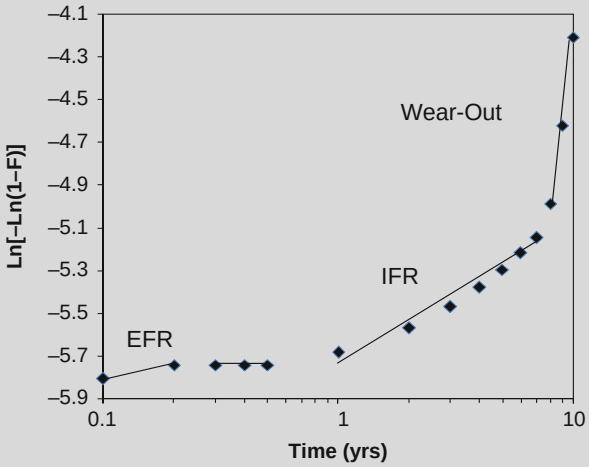

Fig. 7.3 Weibull plot of cum fraction failed F versus time for failure data shown in Table 7.2. The EFR, IFR and Wear-Out regions are indicated.

The characteristic Weibull parameters (t_{63},β), which best describe each of the independent regions (EFR, IFR, Wear-Out), are shown in Fig. 7.4. From these characteristic values, and using the Weibull failure rate Eq. (7.12), the constructed bathtub curve is shown in Fig. 7.5

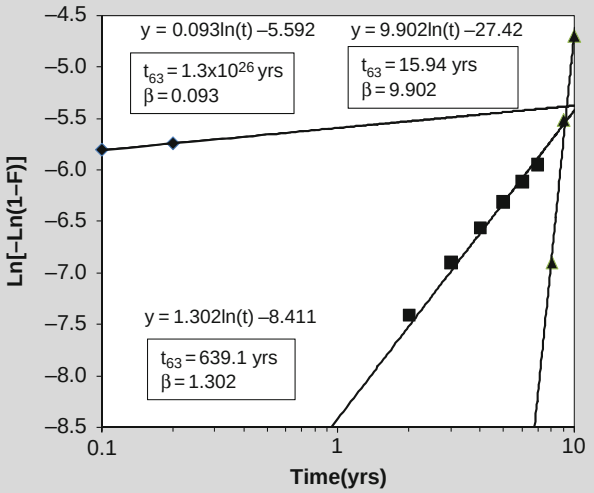

Fig. 7.4 Individual Weibull plots for the independent failure rate contributors: EFR, IFR and Wear-Out regions. Characteristic Weibull parameters (t_{63},β) for each independent region are shown.

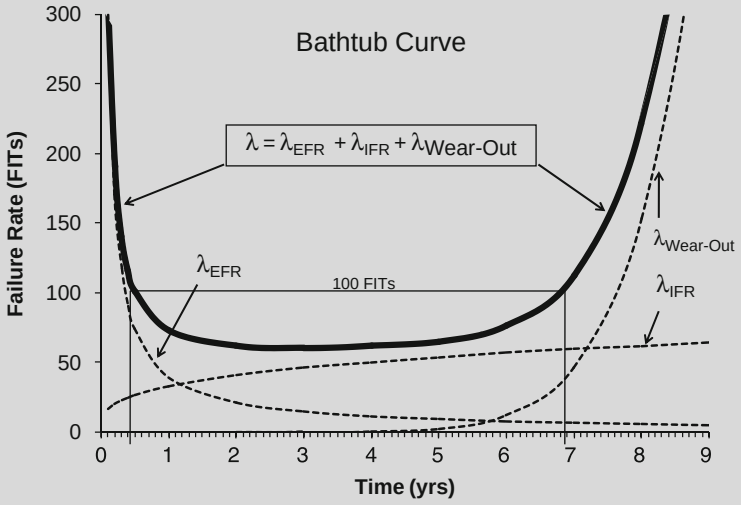

Fig. 7.5 Bathtub reliability curve is created when the independent failure rate contributors are added: EFR + IFR + Wear-Out.

b) Using the above bathtub curve (Fig. 7.5) one can see that the device/product should be burned-in for at least 0.5 years, if the goal is to ship product with a failure rate of < 100 FITs.
c) One can see, from Fig. 7.5, that the failure rate again exceeds 100 FITs after 6.9 years of use and thus defines the start of wear-out.

It must be noted that it is probably unrealistic to burn-in devices for 0.5yrs (6 months) before being shipped; thus, accelerated methods have to be developed which will accelerate this burn-in time. Normally this acceleration is achieved through the use of elevated voltages, elevated mechanical stresses, and/or elevated temperature. This will be discussed in more detail in Chapters 8 and 9.

Problems

1. For certain implantable medical devices, the median time-to-failure is $t_{50} = 87600$ hrs (10 yrs) and a logarithmic standard deviation of σ=0.7. Assuming a lognormal distribution:

   a) What is the instantaneous failure rate at 8 years?
   b) What is the average failure rate after 8 years?
   c) What fraction of the devices is expected to fail after 8 years?

   Answers:

   a) $\lambda_{@\ t=70080\ hrs} = 1.24 \times 10^{-5}/hr$
   b) $<\lambda>_{after\ 780080} = 6.71 \times 10^{-6}/hr$
   c) $F = 0.375$

2. A certain collection of capacitors has a Weibull time-to-failure distribution with a characteristic time-to-failure of t_{63}=100,000 hrs and a Weibull slope of $\beta = 1.2$.

   a) What is the instantaneous failure rate at 9 years?
   b) What is the average failure rate after 9 years?
   c) What fraction of the capacitors is expected to fail after 9 years?

   Answers:

   a) $\lambda_{@\ t=78840\ hrs} = 1.14 \times 10^{-5}/hr$
   b) $<\lambda>_{after\ 78840\ hrs} = 9.54 \times 10^{-6}/hr$
   c) $F = 0.528$

3. For a mechanical component, fatigue data indicates that the median cycle-to-failure is $(CTF)_{50} = 26000$ cycles and a logarithmic standard deviation of σ=1.2. Assuming a lognormal distribution:

   a) What is the instantaneous failure rate at 18000 cycles?
   b) What is the average failure rate after 18000 cycles?
   c) What fraction of the components is expected to fail after 18000 cycles?

   Answers:

   a) $\lambda_{@\ 18000\ \text{cycles}} = 2.84 \times 10^{-5}$/cycle
   b) $<\lambda>_{after\ 18000\ cycles} = 2.65 \times 10^{-5}$/cycle
   c) F = 0.380

4. Certain mechanical components are found to corrode and can be described by a lognormal time-to-failure distribution with a characteristic time-to-failure of t_{50}=50,500 hrs and a $\sigma = 1.2$.

   a) What is the instantaneous failure rate at 40,000 hrs?
   b) What is the average failure rate after 40,000 hrs?
   c) What fraction of the components is expected to fail after 40,000 hrs?

   Answers:

   a) $\lambda_{@\ t=40000\ \text{hrs}} = 1.41 \times 10^{-5}$/hr
   b) $<\lambda>_{after\ 40000\ hrs} = 1.37 \times 10^{-5}$/hr
   c) F = 0.423

5. Certain integrated circuits are found to fail, due to channel hot-carrier injection, and can be described by Weibull time-to-failure distribution with a characteristic time-to-failure of t_{63}=75,000 hrs and a Weibull slope of $\beta = 2.0$.

   a) What is the instantaneous failure rate at 60,000 hrs?
   b) What is the average failure rate after 60,000 hrs?
   c) What fraction of the circuits is expected to fail after 60,000 hrs?

   Answers:

   a) $\lambda_{@\ t=60000\ \text{hrs}} = 2.13 \times 10^{-5}$/hr
   b) $<\lambda>_{after\ 60000\ hrs} = 1.07 \times 10^{-5}$/hr
   c) F = 0.473

6. Certain automobile tires are found to wear out according to a lognormal wear-out distribution with characteristic parameters: $(\text{wear-out})_{50}$=38,000 miles with a $\sigma = 0.6$.

   a) What is the instantaneous wear-out rate at 32,000 miles?
   b) What is the average wear-out rate after 32,000 miles?
   c) What fraction of the tires is expected to wear out after 32,000 miles?

Answers:

a) $\lambda_{@\ 32000\ \text{miles}} = 3.25 \times 10^{-5}/\text{mile}$
b) $<\lambda>_{after\ 32000\ miles} = 1.53 \times 10^{-5}/\text{mile}$
c) $F = 0.388$

7. Certain hinges on doors are found to fail according to a Weibull distribution with the parameters: $(\text{number of closures})_{63} = 25000$ with a Weibull slope of $\beta = 0.5$.

a) What is the instantaneous failure rate at 18,000 closures?
b) What is the average failure rate after 18,000 closures?
c) What fraction of hinges is expected to fail after 18,000 closures?

Answers:

a) $\lambda_{@18000\ closures} = 2.36 \times 10^{-5}/\text{closure}$
b) $<\lambda>_{after\ 18000\ closures} = 4.71 \times 10^{-5}/\text{closure}$
c) $F = 0.572$

8. Crowns, from a certain dental supply company, are found to fail according to a Weibull distribution with the parameters: $t_{63} = 15.0$ years and a Weibull slope of $\beta = 1.0$.

a) What is the instantaneous failure rate at 12 yrs?
b) What is the average failure rate after 12 yrs?
c) What fraction of crowns is expected to fail after 12 yrs?

Answers:

a) $\lambda_{@\ t=\ 12\ yrs} = 6.67 \times 10^{-2}/\text{yr}$
b) $<\lambda>_{after\ 12\ yrs} = 6.67 \times 10^{-2}/\text{yr}$
c) $F = 0.551$

9. Certain cell phones can start to fail after a number of drops. (Note: dropped phones not dropped calls.) The failures in a certain test are found to be described well by a Weibull distribution with the parameters: $(\text{number of drops})_{63} = 88$ drops and Weibull slope of $\beta = 0.6$.

a) What is the instantaneous failure rate at 50 drops?
b) What is the average failure rate after 50 drops?
c) What fraction of phones is expected to fail after 50 drops?

Answers:

a) $\lambda_{@\ 50\ \text{drops}} = 8.55 \times 10^{-3}/\text{drop}$
b) $<\lambda>_{after\ 50\ drops} = 1.42 \times 10^{-2}/\text{drop}$
c) $F = 0.510$

10. Temperature-cycling of bi-metallic layers was found to produce delamination-type failures conforming to a lognormal distribution with parameters: median cycle-to-failure of (cycles-to-failure)$_{50} = 1600$ cycles and $\sigma = 0.9$.

    a) What is the instantaneous failure rate at 1300 cycles?
    b) What is the average failure rate after 1300 cycles?
    c) What fraction of components is expected to fail after 1300 cycles?

    Answers:

    a) $\lambda_{@\ 1300\ \text{cycles}} = 5.62 \times 10^{-4}$/cycle
    b) $<\lambda>_{after\ 1300\ cycles} = 4.04 \times 10^{-4}$/cycle
    c) $F = 0.409$

References

McPherson, J: *Accelerated Testing*. In: **Electronic Materials Handbook**, **Vol. 1 Packaging**, ASM International, 887 (1989).

Miller, I. and J. Freund: **Probability and Statistics for Engineers**, **2nd**. **Ed**. Prentice-Hall, (1977).

Thomas, T. and P. Lawler: *Statistical Methods for Reliability Prediction*. In: **Electronic Materials Handbook**, **Vol. 1 Packaging**, ASM International, 895 (1989).

Chapter 8
Accelerated Degradation

Generally, materials/devices exist in *metastable* states. These states are referred to as being *metastable* because they are only *apparently stable*. Metastable states will change/degrade with time. The rate of degradation of the materials (and eventual time-to-failure for the device) can be accelerated by an elevated *stress* (e.g., *mechanical stress, electrical stress, electrochemical stress*, etc.) and/or elevated *temperature*.

By *accelerating the degradation rate,* one means: accelerating the normal degradation process through the use of elevated stress and/or temperature. Accelerated testing is intended to shorten the normal time-to-failure process (which could take years), without changing the physics of failure. The objective of accelerated testing is to understand the *stress* and *temperature dependence* (*kinetics*) of failure mechanisms so that reliability estimations and reliability improvements can be made through: better design rules, better materials selection criteria, and/or better process control. Also, reliability improvements can be made through: defect reduction, burn-in, intrinsic failure-rate reduction, and wear-out prevention.

8.1 Metastable States

Materials/devices/systems often appear to be in very stable states. However, they are simply captured in momentary *metastable* states. *Metastable* means that the existing state/configuration is only *apparently stable* in that it can undergo transformation, with time, to a more stable state (state with lower *free energy*). For example, a pebble on the edge of a cliff appears to be very stable until a slight push is given to the pebble. Note, however, that an input of energy was required to bring about a change in the metastable state.

Perhaps it is instructive to work through a simple example, one that is common to all of our experiences, to better illustrate the driving force for all materials/devices to reach the lowest free-energy state available. Shown in Fig. 8.1 is a rectangular block that is momentarily captured in a *metastable vertical state* with potential energy U_1. Since $U_2 - U_1$ is negative, if an energy input of ΔU^* is supplied (for example, by simply shaking or bumping the supporting table) then a potential energy reduction

J.W. McPherson, *Reliability Physics and Engineering*,
DOI 10.1007/978-1-4419-6348-2_8,

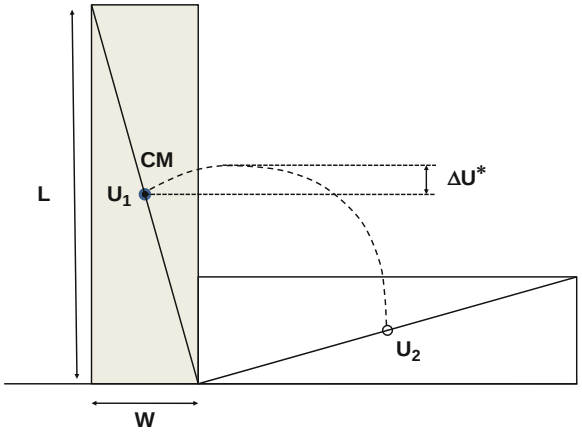

Fig. 8.1 Rectangular block is momentarily captured in the vertical position with potential energy U_1. This vertical position is a metastable state for the block's center of mass (CM) because a lower potential energy state (U_2) is available for the center of mass. The driving force for a change of state is that U_2 must be of lower potential energy than U_1. However, an input of work energy (by an amount of ΔU^*) is required to activate the change of state.

driving force exists for the block's center of mass (CM) to go from *vertical state* (with potential energy U_1) to *horizontal state* (with lower potential energy U_2).

The driving force (ΔU) for the transformation of the block, from the vertical to the horizontal position, is given by:

$$\Delta U = U_2 - U_1 = -\frac{Mg}{2}(L - W)\,. \tag{8.1}$$

The input work energy ΔU^* required to activate the transformation process is given by:

$$\Delta U^* = \frac{mg}{2}\left(\sqrt{L^2 + W^2} - L\right). \tag{8.2}$$

One can see, from the above equations, that when the height of the block L increases relative to the width W, the block becomes less stable in the vertical state (ΔU becomes more negative) and the input energy ΔU^* required to produce the block transformation (from vertical to horizontal state) also reduces.

In the simple example shown in Fig. 8.1, only gravitation potential energy was considered to be important. The required energy input needed to produce a block transformation (from the vertical to the horizontal state) was in the form of work (something must shake or bump the supporting table). However, we will discuss thermodynamic systems where the required energy input for transformation can be in the form of heat and/or work. Reduction in the *Gibbs Potential* (or *Gibbs Free Energy*) ΔG will serve as the driving force (as opposed to simply the gravitation potential energy ΔU used for the block transformation analysis).

8.2 Impact of Temperature on Degradation Rate

It is common experience that devices (automobile tires, valve springs, shock absorbers, computers, TVs, cell phones, iPods, etc.) generally degrade faster at higher temperatures. Shown below, in Fig. 8.2, is a free energy description of why things generally tend to degrade faster at higher temperatures.[1]

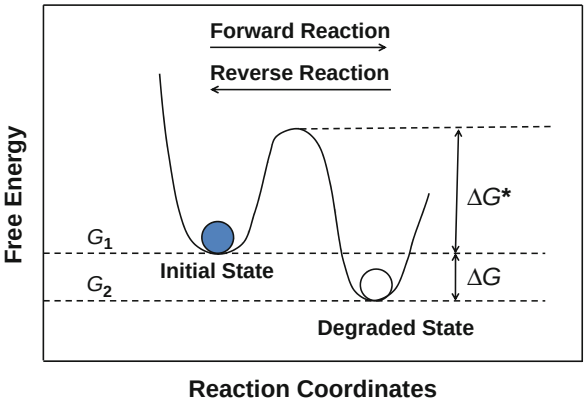

Fig. 8.2 Free energy description of material/device degradation is illustrated. The initial state is metastable because the degraded state has a lower free energy. The relative stability of the initial metastable state is impacted by the activation energy ΔG^* needed to go from the initial metastable state to the degraded state. The degradation rate is generally controlled by the Boltzmann probability.

Initially (at time-zero) one can see from Fig. 8.2 that the material/device is only *apparently* in a stable state, with a Gibbs free energy of G_1. However, one knows from experience that the material/device will degrade with time, moving toward the degraded state G_2. The *driving force* for the degradation is a difference in the *free energy*. This implies that $G_2 - G_1$ must be negative for the degradation process to proceed. To avoid any ambiguities with sign convention, in all of the equations which follow in this chapter, we have used the absolute value: $\Delta G = |G_2 - G_1|$ in the rate equations. It will be understood that the free energy of the degraded state G_2 must be lower than the initial state G_1 for the degradation reaction to proceed. Therefore, the larger ΔG, the stronger is the driving force for degradation.

While the driving force for degradation is a free energy difference ΔG between the initial state and the degraded state, the rate of the degradation reaction is limited by the activation energy ΔG^*. Generally heat and/or work is required to overcome this activation energy barrier. In analogy with chemical reaction rates, one can think of the degradation rate in terms of a degradation rate constant k. The idea of a degradation rate constant was first introduced in Chapter 4. The forward (or degradation) reaction rate $k_{forward}$ (Fig. 8.2) is given by:

[1] A few exceptions to this general degradation rule exist. Very shallow charge-traps in MOSFETs can sometimes be filled more efficiently at lower temperatures. This will be discussed more in detail when the hot carrier injection (HCI) failure mechanism is discussed in Chapter 10.

$$k_{forward} = k_0 \exp\left[-\frac{\Delta G^*}{K_B T}\right], \tag{8.3}$$

where K_B is Boltzmann's constant and T is the temperature in Kelvin.[2] The reverse (or recovery) reaction rate is controlled by:

$$k_{reverse} = k_0 \exp\left[-\frac{(\Delta G + \Delta G^*)}{K_B T}\right]. \tag{8.4}$$

Thus, the net degradation reaction rate for the material/device is given by $k_{net} = k_{forward} - k_{reverse}$:

$$k_{net} = k_0 \exp\left[-\frac{\Delta G^*}{K_B T}\right]\left\{1 - \exp\left[-\frac{\Delta G}{K_B T}\right]\right\}. \tag{8.5}$$

One can see that the driving force, for the net degradation rate, is ΔG. If $\Delta G = 0$, then the net degradation reaction rate is zero regardless of the activation energy ΔG^*. In the event the degraded state has a lower free energy than the initial state ($\Delta G \neq 0$), then the activation energy ΔG^* becomes critically important in retarding the degradation reaction. In fact, when $\Delta G >> K_B T$, then the reverse reaction rate becomes negligible and Eq. (8.5) reduces simply to:

$$k_{net} = k_0 \exp\left[-\frac{\Delta G^*}{K_B T}\right]. \tag{8.6}$$

From Eq. (8.6) one can see that the activation energy can be extracted from the observed degradation rate using:

$$\Delta G^* = -K_B \left[\frac{\partial \ln(k_{net})}{\partial(1/T)}\right]. \tag{8.7}$$

8.3 Free Energy of Activation

Reaction rates are often expressed in terms of a free energy difference (ΔG) and free energy of activation (ΔG^*) ; or, enthalpy difference (ΔH) and enthalpy of activation (ΔH^*) ; or, internal energy difference (ΔU) and internal energy of activation (ΔU^*). This usage can sometimes be confusing — which of these thermodynamic descriptions should be used? This book has chosen to use the Gibbs free energy

[2] Eq. (8.3) represents the Boltzmann probability that atoms in the initial state will obtain the necessary energy to go over the barrier to the degraded state. It is possible that the atoms can tunnel through the barrier, but the tunneling probability is very small except for the very lightest of elements such as hydrogen. For other elements, the Boltzmann probability is usually much greater than the tunneling probability. Boltzmann's constant is 8.62×10^{-5}eV/K .

approach since it is quite general. The conditions for which it is acceptable to use the enthalpy approach or the internal energy approach, are now discussed.

Changes in Gibbs free energy ΔG can be written as:

$$\Delta G = \Delta H - T\Delta S, \tag{8.8}$$

where G is the Gibbs free energy, H is the enthalpy, T is the temperature (K), and S is the entropy. Similarly, the free energy of activation can be written as:

$$\Delta G^* = \Delta H^* - T\Delta S^*. \tag{8.9}$$

For a reaction in the forward direction [see Fig. 8.2], one obtains:

$$\begin{aligned} k_{forward} &= k_o \exp\left[-\frac{\Delta G^*}{K_B T}\right] = k_0 \exp\left[-\left(\frac{\Delta H^* - T\Delta S^*}{K_B T}\right)\right] \\ &= k_0 \exp\left(\frac{\Delta S^*}{K_B}\right) \exp\left(-\frac{\Delta H^*}{K_B T}\right) \\ &= k_1 \exp\left(-\frac{\Delta H^*}{K_B T}\right). \end{aligned} \tag{8.10}$$

Therefore, in the forward direction, it makes little/no difference whether one uses the free energy of activation ΔG^* or the enthalpy of activation ΔH^*. The only difference is a prefactor change. Similar results occur for a reaction in the reverse direction. One obtains:

$$\begin{aligned} k_{reverse} &= k_0 \exp\left[-\frac{(\Delta G + \Delta G^*)}{K_B T}\right] \\ &= k_o \exp\left[\frac{\Delta S + \Delta S^*}{K_B}\right] \exp\left[-\left(\frac{\Delta H + \Delta H^*}{K_B T}\right)\right] \\ &= k_2 \exp\left[-\left(\frac{\Delta H + \Delta H^*}{K_B T}\right)\right]. \end{aligned} \tag{8.11}$$

Thus, the net reaction rate ($k_{net} = k_{forward} - k_{reverse}$) becomes:

$$\begin{aligned} k_{net} &= k_0 \exp\left[-\frac{\Delta G^*}{K_B T}\right] \left\{1 - \exp\left[-\frac{\Delta G}{K_B T}\right]\right\} \\ &= k_0 \exp\left[\frac{\Delta S^*}{K_B}\right] \exp\left[-\frac{\Delta H^*}{K_B T}\right] \left\{1 - \exp\left[\frac{\Delta S}{K_B}\right] \exp\left[-\frac{\Delta H}{K_B T}\right]\right\} \\ &= k_1 \exp\left[-\frac{\Delta H^*}{K_B T}\right] \left\{1 - k_2 \exp\left[-\frac{\Delta H}{K_B T}\right]\right\}. \end{aligned} \tag{8.12}$$

Thus, for degradation reactions strongly favored in the forward direction the net reaction rate constant becomes:

$$k_{net} = k_1 \exp\left[-\frac{\Delta H^*}{K_B T}\right]. \tag{8.13}$$

One can see that the only significant difference between Eq. (8.6) and Eq. (8.13) is in the prefactor. Thus, for reactions that are strongly favored in the forward direction, one can safely use either the free energy of activation ΔG^* or the enthalpy of activation ΔH^*.

Also, since

$$\Delta H = \Delta U + p\Delta V, \tag{8.14}$$

then, if little/no change occurs in the solid's volume during the degradation, the $p\Delta V$ term is often ignored and one uses the approximation for solids: $\Delta H \cong \Delta U$ and $\Delta H^* \cong \Delta U^*$.

8.4 Impact of Stress and Temperature on Degradation Rate

Let us now consider the impact of applying a *stress* ξ to the material/device and investigate its impact on the degradation rate. Remember, the stress ξ can be general in nature (can be mechanical stress, electrical stress, chemical stress, etc.) and represents any external agent which can enhance/accelerate the degradation rate.

8.4.1 Real Versus Virtual Stresses

If one applies a stress to a material and it produces a time-to-failure distribution which is strongly dependent on the material dimensions, then the stress will be referred to as a *virtual stress*. If one applies a stress to a material and it produces a time-to-failure distribution that is approximately independent of the material dimensions, then it will be referred to as a *real stress*. A few examples of *real* versus *virtual* stresses are given below.

Current I flowing through a conductor may eventually cause electromigration-induced failure, but the observed time-to-failure(TF) is strongly dependent on the cross-sectional area A of the conductor. However, if one uses current density J *(= I/Area)* instead of current I, then the TF depends only on the magnitude of J and is approximately independent of the cross-sectional area of the conductor. In this case, one would describe J as a *real stress* and I as a *virtual stress*.

In dielectrics, if one *ramps* the voltage to breakdown and records the breakdown voltage V_{bd}, one finds that V_{bd} is strongly dependent on the dielectric thickness $t_{dielectric}$. However, if electric field $E(= V/t_{dielectric})$ is used instead of voltage V, then one finds that the breakdown field E_{bd} is approximately independent of dielectric

thickness. In this case, one would describe E as a *real stress* and V as a *virtual stress*.

In mechanical devices, if one applies a large tensile force F to a member, the member may eventually fail with time due to creep but the time-to-failure is strongly dependent on the cross-sectional area A of the member. However, if tensile stress σ $(= F/A)$ is used instead of force F, then the time-to-failure TF depends only on the magnitude of the stress σ and TF is approximately independent of the material dimensions. Thus, σ will be referred to as a *real stress* and the force F as a *virtual stress*.

Real stresses are generally preferred when reporting time-to-failure data because it is much more likely that someone else will be able to reproduce your time-to-failure results. Time-to-failure results using virtual stresses are very difficult to reproduce unless someone uses exactly the same material dimensions. As an additional reminder; generally, if it is a real stress, tables can be found listing a breakdown strength for the material (the stress level at which nearly instantaneous time-to-failure can be expected). For example: the rupture strength for steel is a mechanical stress level of $\sigma_{rupture} \approx 2GPa$; the dielectric breakdown strength of SiO_2 dielectric is electric field of $E_{BD} \approx 10\,MV/cm$; and the fusing current density of aluminum is $J_{Fuse} \approx 20\ MA/cm^2$. Tables listing virtual stresses [breakdown force for mechanical systems, or breakdown voltage for dielectrics, or breakdown current for conductors] are of relatively little value (because the value changes with material dimensions) and therefore generally cannot be found in tables. In this text, when we refer to *stress* it is implied that it is a *real stress* unless otherwise stated.

8.4.2 Impact of Stress on Materials/Devices

The external stress ξ can increase the degradation rate by lowering the activation energy ΔG^* and/or by increasing the free energy difference ΔG of the degraded state relative to the initial metastable state. It will be assumed that the impact of stress on the free energy of activation ΔG^* and the free energy difference ΔG can be represented by a Maclaurin Series:

$$\begin{aligned} \Delta G^* &\cong \left(\Delta G^*\right)_{\xi=0} + \left[\frac{\partial(\Delta G^*)}{\partial \xi}\right]_{\xi=0} \xi \\ &= \Delta G_0^* - a\xi, \end{aligned} \tag{8.15}$$

and

$$\begin{aligned} \Delta G &\cong (\Delta G)_{\xi=0} + \left[\frac{\partial(\Delta G)}{\partial \xi}\right]_{\xi=0} \xi \\ &= \Delta G_0 + b\xi. \end{aligned} \tag{8.16}$$

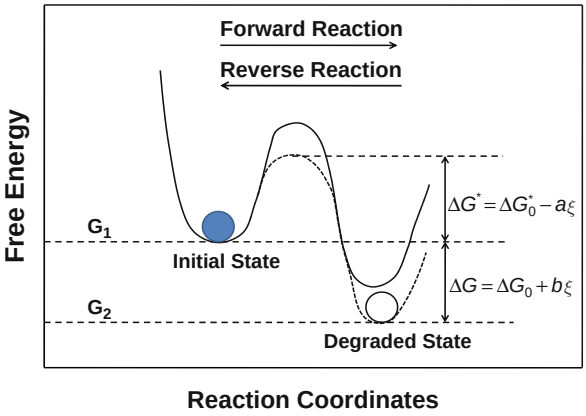

Fig. 8.3 Free energy impact when a stress ξ is applied to a material/device. The stress ξ can have at least two impacts on the free energy: (1) the stress can make the initial metastable state even more unstable by increasing the free energy difference ΔG between the initial and degraded states and (2) the stress can lower the activation energy ΔG^* which would accelerate the degradation rate.

The parameters a and b in Eqs. (8.15) and (8.16) will have to be determined from actual stress-induced degradation data.[3] The expected impact of stress ξ on the free energy is illustrated in Fig. 8.3.

Using Eq. (8.5), along with Eqs. (8.15) and (8.16), the net reaction rate for material/device degradation becomes:

$$k_{net} = k_0 \exp\left[-\frac{(\Delta G_0^* - a\xi)}{K_B T}\right]\left\{1 - \exp\left[-\frac{(\Delta G_0 + b\xi)}{K_B T}\right]\right\}. \tag{8.17}$$

Let us now consider a special case of Eq. (8.17). Suppose that ΔG is very small and can be neglected. Eq. (8.17) becomes:

$$\begin{aligned} k_{net} &= k_0 \exp\left[-\frac{(\Delta G_0^* - a\xi)}{K_B T}\right]\left\{1 - \exp\left[-\frac{(b\xi)}{K_B T}\right]\right\} \\ &= k_0 \exp\left[-\frac{(\Delta G_0^* - a\xi)}{K_B T}\right] 2\exp\left[-\frac{b\xi}{2K_B T}\right] \sinh\left[\frac{b\xi}{2K_B T}\right] \\ &= 2k_0 \sinh\left[\frac{b\xi}{2K_B T}\right] \exp\left\{-\frac{[\Delta G_0^* - (a - b/2)\xi]}{K_B T}\right\}. \end{aligned} \tag{8.18}$$

Note also that if $b\xi >> 2K_BT$, then due to the properties of the hyperbolic *sinh(x)* function[4] one obtains:

[3] Our hypotheses are: (1) the stress ξ will serve to lower the activation energy [a will be positive as written] and (2) the stress may also serve to increase the free energy difference between the initial state and the degraded state [b will be positive as written]. The actual degradation rate data will tell us if our hypotheses are correct.

[4] *sinh(x)* $\sim x$ for small x and *sinh(x)* $\sim$ *exp(x)/ 2* for large x.

$$k_{net} = \left(\frac{k_0 b}{K_B T}\right) \xi \exp\left\{-\frac{\Delta G_0^*}{K_B T}\right\} \qquad (for\ low\ stress) \tag{8.19}$$

and

$$k_{net} = k_0 \exp\left\{-\frac{\left[\Delta G_0^* - a\xi\right]}{K_B T}\right\} \qquad (for\ high\ stress). \tag{8.20}$$

One can see, from the net degradation reaction rate (in the low-stress region), that the stress ξ has no impact on reducing the activation energy ΔG_0^*. The degradation reaction rate is driven purely by increasing the free energy separation ΔG of the degraded state from initial metastable state. Thus, ΔG is impacted by the stress ξ but the activation energy ΔG^* is not.[5]

Let us take a closer look at the net degradation rate constant under high stress, Eq. (8.20). If the free-energy difference ΔG (from the initial metasable state and the degrade state) is not large, then under high stress conditions what drives the net reaction rate is simply a reduction in free energy of activation ΔG_0^* Also, if a is temperature dependent and has a simple temperature-dependence of the form:[6]

$$a \;=\; a_o \;+\; (a_1 K_B)\, T, \tag{8.21}$$

then the net degradation rate constant K_{net} under high stress becomes:

$$k_{net} = k_0 \exp\left[a_1 \xi\right] \exp\left\{-\frac{\left(\Delta G_0^* - a_0 \xi\right)}{K_B T}\right\} \quad (for\ high\ stress). \tag{8.22}$$

One can see that under high stress, the degradation rate constant under high stress is exponentially dependent on the stress ξ. Also, one can see that under high stress conditions, the effective activation energy for the degradation rate constant can be stress dependent.

Since the net degradation rate depends linearly on the stress ξ at low fields and exponentially dependent on the stress ξ at very high fields, then it might be reasonable to expect a power-law dependence $(\xi)^n$ at intermediate values of stress. The power-law model that is often used for degradation rates:

$$k_{net} = k_0'' \xi^n \exp\left\{-\frac{\Delta G^*}{K_B T}\right\}. \tag{8.23}$$

The best fitting degradation rate model parameters $(n, \Delta G^*)$ are extracted from degradation rate data using:

---

[5]Note that since it was assumed that the free energy difference between the initial state and the degraded state was zero, when $\xi = 0$, then the net degradation rate at low stress levels goes to zero when b is zero.

[6]A Maclaurin Series expansion is carried out (keeping only the first term).

$$n = \left[\frac{\partial \ln(k_{net})}{\partial \ln(\xi)}\right]_{T=constant} \tag{8.24}$$

and

$$\Delta G^* = -K_B \left[\frac{\partial \ln(k_{net})}{\partial (1/T)}\right]_{\xi=constant}. \tag{8.25}$$

8.5 Accelerated Degradation Rates

Acceleration of the degradation rate occurs when we increase the stress variable ξ and/or the temperature T. One can compare the degradation rate under a set of operating conditions (ξ_{op}, T_{op}) versus another set of stress conditions (ξ_{stress}, T_{stress}) by using the acceleration factor AF for degradation. AF for degradation rate is defined as:

$$AF = \frac{k_{net}(\xi_{stress}, T_{stress})}{k_{net}(\xi_{op}, T_{op})}. \tag{8.26}$$

Using Eq. (8.26), in conjunction with Eqs. (8.19) and (8.22), one obtains:

$$AF = \left(\frac{T_{op}}{T_{stress}}\right)\left(\frac{\xi_{stress}}{\xi_{op}}\right)\exp\left[-\left(\frac{\Delta G^*}{K_B}\right)\left(\frac{1}{T_{stress}} - \frac{1}{T_{op}}\right)\right] \text{(for low stress)} \tag{8.27a}$$

or

$$AF = \exp\left[a_1(\xi_{stress} - \xi_{op})\right]\exp\left\{\frac{(\Delta G_0^* - a_o\xi_{op})}{K_B T_{op}} - \frac{(\Delta G_0^* - a_o\xi_{stress})}{K_B T_{stress}}\right\}. \quad \text{(for high stress)} \tag{8.27b}$$

Since T must be expressed in Kelvin, the (T_{op}/T_{stress}) term in Equation (8.27a) is usually relatively small compared to the temperature dependence in the exponential term. Often any temperature dependence in the pre-factor is simply ignored when determining the acceleration factor. Note that the activation energy in Eq. (8.27b), since it depends on stress, is no longer of the simple Arrhenius type.

Also, to help bridge the gap between low and high-stress conditions, the power-law model, Eq. 8.23, is often used giving:

$$AF = \left(\frac{\xi_{stress}}{\xi_{op}}\right)^n \exp\left[-\left(\frac{\Delta G^*}{K_B}\right)\left(\frac{1}{T_{stress}} - \frac{1}{T_{op}}\right)\right]. \tag{8.28}$$

Example Problem 8.1

Suppose that the critical parameter for a certain device is observed to degrade two times faster when the temperature is simply elevated from 25°C to 35°C. What is the activation energy associated with this degradation process?

Solution

Must first convert °C to Kelvin:

$$25°\text{C} = (25 + 273)\text{K} = 298\text{K}$$
$$35°\text{C} = (35 + 273)\text{K} = 308\text{K}.$$

Using Eq. (8.28):

$$AF = 2 = \exp\left[-\left(\frac{\Delta G^*}{K_B}\right)\left(\frac{1}{T_{stress}} - \frac{1}{T_{op}}\right)\right]$$

$$\Rightarrow \Delta G^* = K_B \frac{\ln(2)}{\left(\frac{1}{T_{op}} - \frac{1}{T_{stress}}\right)}$$

$$= (8.62 \times 10^{-5} eV/K) \frac{\ln(2)}{\left(\frac{1}{298\,K} - \frac{1}{308\,K}\right)}$$

$$= 0.55\,eV.$$

Example Problem 8.2

During a constant temperature accelerated test, it was noted that a critical device parameter degradation rate increased by six times as the electric field was doubled. Using the power-law model, what is the field-dependence exponent n for the observed degradation?

Solution

Using Eq. (8.28):

$$AF = 6 = \left(\frac{E_{stress}}{E_{op}}\right)^n$$

$$\Rightarrow n = \frac{\ln(6)}{\ln\left(\frac{V_{stress}}{V_{op}}\right)}$$

$$= \ln(6)/\ln(2)$$

$$= 2.58.$$

Problems

1. The corrosion rate for a metal component doubles from 75 to 85°C. What is the activation energy Q associated with this corrosion rate?

   Answer: $Q = 0.74$ eV

2. The threshold voltage V_{th} degradation rate for a MOSFET device actually decreases by 40% from 25 to 50°C. What is the apparent activation energy Q associated with this degradation rate?

   Answer: $Q = -0.17$ eV

3. The wear rate for an automobile tire was found to occur 50% faster during the summer months (35°C) than during the winter months (15°C). What is the apparent/effective activation energy Q for this wear-rate increase during the summer months?

   Answer: $Q = 0.16$ eV

4. The creep rate for a metal was found to double when the temperature was elevated from 500 to 525°C. What is the activation energy Q?

   Answer: $Q = 1.47$ eV

5. The resistance degradation rate for a metal resistor, with current flowing, quadruples when the temperature increases from 250 to 300°C. What is the activation energy Q?

   Answers: $Q = 0.72$ eV

6. The tires, on a certain trailer, were found to wear out 89% faster when carrying a weight of 3 W than when the trailer was empty (weight of 1 W). Find the power-law exponent n that describes the wear rate for the tires versus the weight carried.

   Answer: $n = 0.58$

7. The creep rate for a metal was found to increase by 15 times when the tensile stress increased by a factor of 2. Find the power-law exponent n that describes creep-rate dependence on tensile stress.

   Answer: $n = 3.91$

8. Paint on a house was found to degrade 4 times faster (on the south side of the house which gets 3x more sun than does the west side of the house. Find the power-law exponent n that describes the degradation rate with sun exposure.

   Answer: $n = 1.26$

9. The operational frequency of a semiconductor device was found to degrade at a rate 4 times faster when the operational voltage was increased 10%. Find the power-law exponent n that describes the degradation rate versus voltage.

   Answer: $n = 14.5$

10. The degradation rate for the resistance of a conductor increases by 4x when the current is doubled. Find the power-law exponent n that describes the degradation rate versus current density.

    Answer: $n = 2$.

References

Barret, C., et al.: **The Principles of Engineering Materials**, Prentice Hall, (1973).

McPherson, J.: *Stress Dependent Activation Energy,* IEEE International Reliability Physics Symposium Proceedings, 12 (1986).

McPherson, J., *Accelerated Testing*. In: **Electronic Materials Handbook**, **Vol. 1 Packaging**, ASM International, 887 (1989).

McPherson, J.: *Accelerated Testing and VLSI Failure Mechanisms*, Tutorial, IEEE International Symposium on Physical and Failure Analysis of Integrated Circuits, (1989).

Chapter 9
Acceleration Factor Modeling

In reliability physics and engineering, the development and use of the *acceleration factor* is fundamentally important to the theory of accelerated testing. The acceleration factor permits one to take time-to-failure data very rapidly under *accelerated stress conditions*, and then to be able to extrapolate the accelerated time-to-failure results (into the future) for a given set of *operational conditions*.[1] Since experimental determination of the acceleration factor could actually take many years, the acceleration factor must be modeled using the time-to-failure (*TF*) models introduced in Chapter 4. Since the acceleration factor must be modeled, it brings up another important question — *how does one build some conservatism into the models without being too conservative*?

9.1 Acceleration Factor

The acceleration factor *AF* is defined as the ratio of the expected time-to-failure under *normal operating conditions* to the time-to-failure under some set of *accelerated stress conditions*,

$$AF = \frac{(TF)_{operation}}{(TF)_{stress}}. \tag{9.1}$$

Since the *TF* under *normal operation* may take many years to occur, then experimental determination of the acceleration factor *AF* (from *stress conditions* to *normal operating conditions*) is usually impractical. However, if one has proper time-to-failure models (developed under accelerated conditions) then one can use these TF-models to model the acceleration factor.

Two important time-to-failure (*TF*) models were presented in Chapter 4, the *power-law* and *exponential models*, and are reproduced here:

[1] Note: for the reliability engineer, this is very exciting because the acceleration factor permits one to effectively take a *crystal-ball* look into the future as to what will happen!

J.W. McPherson, *Reliability Physics and Engineering*,
DOI 10.1007/978-1-4419-6348-2_9,

Power-Law TF Model

$$TF = A_o\ (\xi)^{-n}\ \exp\left(\frac{Q}{K_B T}\right), \tag{9.2a}$$

and

Exponential TF Model

$$TF = B_o\ \exp(-\gamma \bullet \xi)\ \exp\left(\frac{Q}{K_B T}\right). \tag{9.2b}$$

In the above *TF* questions, the prefactor coefficients (A_o, B_o) will vary from device-to-device because the parameters are strongly fabrication/process-dependent.[2] This is the reason why the time-to-failure *TF* will actually be a distribution of times-to-failure. The Weibull and lognormal time-to-failure distributions were discussed in Chapter 6.

Using the time-to-failure models (Eq. 9.2) along with Eq. (9.1), one obtains for the power-law acceleration factor,

$$AF = \left(\frac{\xi_{stress}}{\xi_{op}}\right)^n \bullet \exp\left[\frac{Q}{K_B}\left(\frac{1}{T_{op}} - \frac{1}{T_{stress}}\right)\right]. \tag{9.3a}$$

Likewise, for the exponential model one obtains:

$$AF = \exp\left[\gamma(\xi_{stress} - \xi_{op})\right] \bullet \exp\left[\frac{Q}{K_B}\left(\frac{1}{T_{op}} - \frac{1}{T_{stress}}\right)\right]. \tag{9.3b}$$

It is very important to note that the *acceleration factor* is *very special*, in that the acceleration factor *AF* is independent of the materials/process dependent coefficients (A_o, B_o). This means that even though the time-to-failure *TF* must be expressed as a distribution of times-to-failure (because of device-to-device variation), the acceleration factor *AF* is unique. *AF* depends only on the physics-of-failure kinetics (n, γ, Q) and not on device-to-device variation (A_o, B_o).

As discussed in Chapter 4, the kinetic values (n, γ, Q) are determined through accelerated testing and are given by the equations:

$$n = -\left[\frac{\partial \ln TF}{\partial \ln \xi}\right]_T, \tag{9.4a}$$

$$\gamma = -\left[\frac{\partial \ln TF}{\partial \xi}\right]_T, \tag{9.4b}$$

[2]Time-to-failure for materials/devices is strongly process dependent. Small micro-structural differences in the material can lead to device-to-device variations producing different times-to-failure.

and

$$Q = K_B \left[\frac{\partial \ln TF}{\partial (1/T)} \right]_{\xi} . \tag{9.4c}$$

Given the kinetic values (n,γ,Q) from accelerated data[3], one can then easily model the acceleration factor without having to wait the many years which would otherwise be required to actually measure the acceleration factor.

It cannot be emphasized too strongly: it is extremely important that the device-dependent/materials-dependent/process-dependent prefactors, A_o and B_o, which appear so prominently in the time-to-failure equations, do not appear in the equations for the acceleration factor. This means that the *acceleration factor* depends only on the *physics of failure* (*kinetics*) and not *on device-to-device variation.*[4] Thus, for a single failure mechanism, all parts of the time-to-failure distribution should be accelerated by the same amount.

The modeled acceleration factor, Eq. (9.3), permits one to go from a time-to-failure distribution taken under accelerated test conditions to a projected time-to-failure distribution under normal operating conditions. The transformations from stress conditions to operating conditions, for the lognormal and Weibull distributions, are given by:

Lognormal

$$(t_{50})_{op} = AF \bullet (t_{50})_{stress} \tag{9.5}$$

and

$$(\sigma)_{op} = (\sigma)_{stress} \tag{9.6}$$

Weibull

$$(t_{63})_{op} = AF \bullet (t_{63})_{stress} \tag{9.7}$$

and

$$(\beta)_{op} = (\beta)_{stress} . \tag{9.8}$$

[3]Kinetic values are given in Chapters 11 and 12 for various failure mechanisms. Also, kinetic values (n,γ,Q) for various failure mechanisms can be found in reference materials, e.g., the IEEE International Reliability Physics Symposium Proceedings.

[4]The fact that the acceleration factor depends only on the kinetics of failure (n,γ,Q) and not on device-to-device variation (due to slight materials/process differences) is very important. This means that, for a single failure mechanism, all devices of the time-to-failure distribution should be accelerated by the same amount.

Note that while the characteristic time-to-failure for each distribution has been transformed using the acceleration factor, it has been assumed that the dispersion parameter (σ,β) for each distribution does not change with stress. The requirement that the dispersion parameter does not change with stress will serve as the definition for *uniform acceleration*: uniform acceleration tends to accelerate the entire time-to-failure distribution uniformly such that the dispersion/slope-parameters (σ,β) for the distributions do not change with the level of stress. One should always take enough accelerated data to establish the set of stress conditions under which the acceleration is uniform. A change in slope of the time-to-failure distribution, with stress level, may indicate a change in physics could be occurring.[5] The goal of accelerated testing is to accelerate the physics without changing the physics of failure!

Accelerated testing is fundamental to integrated circuit reliability improvements because: 1) the defects (materials with low breakdown strengths) in a population of otherwise good devices can be eliminated with a short duration accelerated stress (burn-in); 2) the intrinsic failures can be accelerated with stress/temperature (on a sampling basis) so that the intrinsic failure rate for a population of good devices can be determined; and, 3) the time for wear out (TF for the main distribution of devices) can be projected from stress conditions to a specified set of operating conditions.

9.2 Power-Law Versus Exponential Acceleration

It is prudent to ask the question: for the same set of time-to-failure data which can be fitted nearly equally well by either the *power-law* or the *exponential* time-to-failure model, which model gives a more conservative (smaller) time-to-failure value? Also, which model gives a more conservative (smaller) acceleration factor? Generally, unless one is aware of some overriding physics to support one model over the other, then it may be advisable to use the model with the more conservative acceleration factor. Example Problem 9.1 will be used to illustrate that when the same time-to-failure data set is used, the exponential model (versus the power-law model) produces a smaller time-to-failure and a smaller acceleration factor when the data is extrapolated from stress conditions to use conditions. For this reason, the exponential model is usually referred to as a more *conservative model*. This can be very important when one is unsure which model is more valid.

[5] An example of the physics of failure changing can be easily found from electromigration-induced failure in aluminum metallizations (discussed in Chapter 11). At relatively low temperatures, the Al-ion transport is dominated by grain-boundary diffusion with activation energy Q_{gb}. At much higher temperatures, the transport is dominated by bulk (within-grain or lattice) diffusion with activation energy Q_{bulk}, where: $Q_{bulk} > Q_{gb}$.

Example Problem 9.1

During constant temperature accelerated testing, time-to-failure data was collected and the data is shown in Fig. 9.1. The units of the stress are in arbitrary units (a.u.). The TF data could be fit rather nicely by a power-law model ξ^{-n} (with an exponent of n=4) or with an exponential model $\exp(-\gamma\xi)$ (with γ=0.0475 in units reciprocal stress). However, one can see that the extrapolated time-to-failure results from stress conditions (ξ=100 a.u.) to use conditions (ξ=10 a.u.) are quite different for the two models. The exponential model predicts a much shorter time-to-failure for use conditions (ξ=10 a.u.).

Determine:

a) Using the power-law model, what is the acceleration factor for a stress condition of ξ_{stress}=100 a.u. to a use condition of ξ_{use}=10 a.u.
b) Using the exponential model, what is the acceleration factor for a stress condition of ξ_{stress}=100 a.u. to a use condition of ξ_{use}=10 a.u.
c) Which is the more conservative model, the exponential ξ-model or the power-law model?

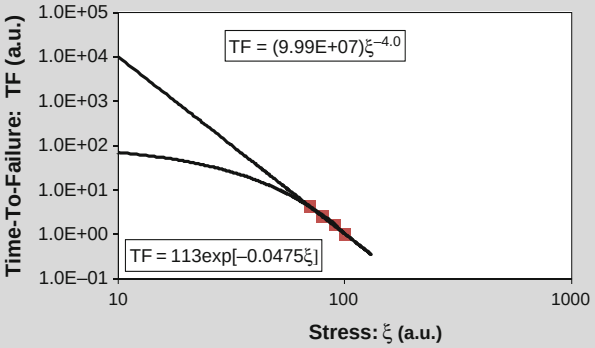

Fig. 9.1 Accelerated time-to-failure data is shown fitted using both a power-law model and an exponential model. Either model can fit the accelerated data quite well, but the two models give quite different predictions as to the time-to-failure when the results are extrapolated to much lower values of the stress. The time-to-failure TF and stress ξ are in arbitrary units (a.u.).

Solution

a) Power-Law Model:

$$AF = \left(\frac{\xi_{stress}}{\xi_{op}}\right)^{n} = \left(\frac{100}{10}\right)^{4} = 10,000.$$

b) Exponential Model

$$AF = \exp\left[\gamma(\xi_{stress} - \xi_{op})\right] = \exp\left[(0.0475)(100 - 10)\right] = 71.9.$$

c) For the same time-to-failure data set, the exponential model is more conservative than the power-law model. By conservative, one means that the exponential model produces a smaller time-to-failure and a smaller acceleration factor when we extrapolate from accelerated conditions to use conditions.

9.3 Cautions Associated with Accelerated Testing

There are at least two very important cautions associated with accelerated testing. First, the acceleration should only accelerate the failure physics — it should not change the failure physics. A simple story will perhaps serve as a reminder of this important caution. If one goes to a local farm and gathers some fresh fertilized chicken eggs, places them in an oven at 40°C and waits approximately 21 days, then one will likely obtain some very lively baby chicks. A highly accelerated testing approach would be to place the eggs in boiling water (100°C) and wait for only 7 minutes. However, this particular accelerated approach produces hard-boiled eggs — not the intended lively chicks. It's *painfully obvious* that we did more than simply accelerate the physics, the acceleration was too great and we changed the physics!

Second, the acceleration must be uniform — the acceleration must accelerate all parts of the Weibull (or lognormal) distribution the same. In Fig. 9.2, an example of uniform acceleration is shown. In Fig. 9.3, an example of nonuniform acceleration is shown (Weibull slopes are very different).

Note that for non-uniform acceleration, as illustrated in Fig. 9.3, there is no unique acceleration factor for the testing because the Weibull slopes β are very different.

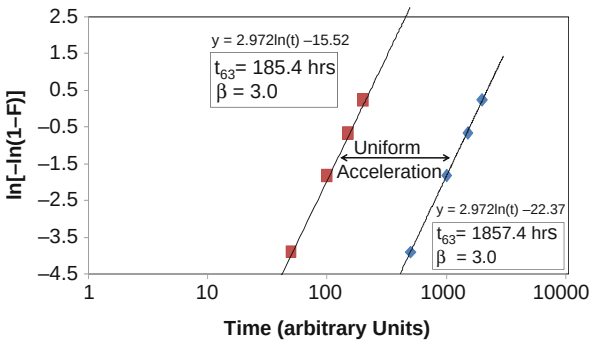

Fig. 9.2 Example is shown of uniform acceleration. Note that the Weibull slopes β are the same.

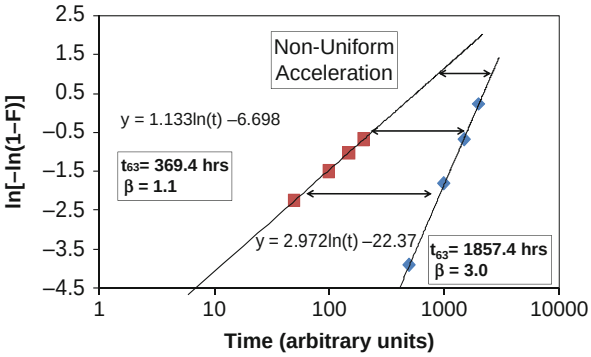

Fig. 9.3 Example is shown of non-uniform acceleration. Note that the Weibull slopes β are significantly different.

9.4 Conservative Acceleration Factors

Often, one is required to construct/model an acceleration factor which is well outside the region where actual stress data is available. Under these conditions, one might want to use a more conservative approach to acceleration factor construction. In this more conservative acceleration factor modeling approach, one can use the experimentally determined kinetics (n,Q) over the region where stress data is actually available, and then use more conservative kinetics (n_c, Q_c) outside the region where data is not available.

For a power-law time-to-failure model, the conservative acceleration factor becomes:

$$AF = \left(\frac{\xi_{stress}}{\xi_c}\right)^n \bullet \left(\frac{\xi_c}{\xi_{op}}\right)^{n_c} \bullet \exp\left[\frac{Q}{K_B}\left(\frac{1}{T_c} - \frac{1}{T_{stress}}\right)\right] \bullet \exp\left[\frac{Q_c}{K_B}\left(\frac{1}{T_{op}} - \frac{1}{T_c}\right)\right]. \tag{9.9}$$

In the equation above, (ξ_c, T_c) are the conservative limits on the stress and temperature. For values above (ξ_c, T_c), data is available showing that the kinetics (n,Q) are valid. Below (ξ_c, T_c), where little/no data is available, it may be advisable to use more conservative values for the kinetics (n_c, Q_c). Generally, the more conservative values are: $n_c < n$ and $Q_c < Q$.

Also, one can easily develop a similar conservative acceleration factor for the exponential time-to-failure model:

$$AF = \exp\left[\gamma(\xi_{stress} - \xi_c)\right] \bullet \exp\left[\gamma_c(\xi_c - \xi_{op})\right] \bullet \exp\left[\frac{Q}{K_B}\left(\frac{1}{T_c} - \frac{1}{T_{stress}}\right)\right] \bullet \exp\left[\frac{Q_c}{K_B}\left(\frac{1}{T_{op}} - \frac{1}{T_c}\right)\right]. \tag{9.10}$$

Generally, the more conservative values are: $\gamma_c < \gamma$ and $Q_c < Q$.

The reason that a conservative value for the acceleration factor is sometimes used — *a customer never gets mad if the device lasts longer than you predict*! However, a time-to-failure prediction that is too conservative generally results in over-design or performance limitations, both of which impact the cost/sale of the designed device.

Example Problem 9.2

In a constant temperature accelerated test, accelerated TF data was taken under highly accelerated conditions where the accelerated stress conditions ranged from ξ =1000 to 100 arbitrary units (a.u.). A power-law fit with n=2 served to describe very well the *TF* data over this accelerated stress range.

Determine the acceleration factor over the entire stress range from ξ = 1000a.u. to 10a.u:

(a) when using no conservatism and
(b) when using conservatism.

Solution

(a) Using no conservatism means that one would assume a power-law dependence n=2 (observed during accelerated testing over the stress range of 1000 a.u. to 100 a.u.) and assume that the power-law exponent n=2 continues to hold from 100 a.u. to 10 a.u. (clearly outside the range were one has accelerated data). Under these assumptions, Eq. (9.3a) gives:

$$AF = \left(\frac{\xi_{stress}}{\xi_{op}}\right)^{n} = \left(\frac{1000}{10}\right)^{2} = 10,000.$$

(b) A more conservative approach would be to assume that n=2 holds over the accelerated data range (1000 a.u. to 100 a.u.) and then perhaps assume something more conservative (e.g., n=1) from 100 a.u. to 10 a.u. (which is outside the range where one actually has accelerated data). Equation (9.9) gives:

$$AF = \left(\frac{\xi_{stress}}{\xi_{c}}\right)^{n} \bullet \left(\frac{\xi_{c}}{\xi_{op}}\right)^{n_c} = \left(\frac{1000}{100}\right)^{2} \bullet \left(\frac{100}{10}\right)^{1} = 1,000.$$

Problems

1. During accelerated *electromigration (EM)* time-to-failure testing of an aluminum-alloy at current density of $J = 2 \times 10^6$ A/cm^2 and a temperature of

150°, a lognormal distribution was obtained with the parameters: t_{50}=400hrs and a σ=0.5. Assuming a current density power-law exponent of n=2 an activation energy of Q=0.75 eV (and negligible Joule/self-heating):

a) What is the acceleration factor from stress conditions to use conditions ($J_{use} = 0.5 \times 10^6$ A/cm^2, $T_{use} = 105$°C)?
b) What is the expected time-to-failure for 1% of the devices during use conditions?

Answers: a) AF = 185 b) TF(1%) = 2.6 yrs

2. During accelerated *creep* time-to-failure testing of a metal-alloy at tensile stress level of σ=800 MPa and a temperature of 800°C, a lognormal distribution was obtained with the parameters: t_{50}=250hrs and a σ=0.8. Assuming a creep power-law exponent of n=4 and activation energy of Q=1.3 eV:

a) What is the acceleration factor from stress conditions to use conditions ($\sigma_{use} = 500$ MPa, $T_{use} = 500$°C)?
b) What is the expected time-to-failure for 1% of the devices during use conditions?

Answers: a) AF = 1532 b) TF(1%) = 6.8 yrs

3. During accelerated *fatigue* cycle-to-failure testing of a metal-alloy with a stress range of $\Delta\sigma$=400 MPa and a temperature of 25°C, a lognormal distribution was obtained with the parameters: $(CTF)_{50}$=2500cycles and a σ=0.7. Assuming a fatigue power-law exponent of n=4:

a) What is the acceleration factor from stress conditions to use conditions ($\Delta\sigma_{use} = 200$MPa, $T_{use} = 25°C$)?
b) What is the expected cycles-to-failure for 1% of the devices during use conditions?

Answers: a) AF = 16 b) TF(1%) = 7829 cycles

4. During accelerated *time-dependent dielectric breakdown* (*TDDB*) testing of a silica-based dielectric, at an electric field of E=10MV/cm and a temperature of 105°C, a Weibull distribution was obtained with the parameters: t_{63}=1.5hrs and a β=1.4. Assuming an exponential model with a field acceleration of γ=4.0 cm/MV:

a) What is the acceleration factor from stress conditions to use conditions ($E_{use} = 5$ MV/cm, $T_{use} = 105$°C)?
b) What is the expected time-to-failure for 1% of the devices during use conditions?

Answers: a) AF = 4.850×10^8 b) TF = 3107 yrs

5. During accelerated *corrosion* time-to-failure testing at 90% relative humidity (RH) and temperature of 121°, a lognormal distribution was obtained with

the parameters: t_{50}=1500hrs and a σ=0.7. Assuming an exponential time-to-failure model with a humidity acceleration parameter of $\gamma = [0.12]/\%RH$ and activation energy of 0.75 eV:

a) What is the acceleration factor from stress conditions to use conditions ($(\%RH)_{use} = 65\%$, $T_{use} = 85°C$)?
b) What is the expected time-to-failure for 1% of the devices during use conditions?

Answers: a) AF = 185 b) TF = 6.2 yrs

6. During *mobile-ions* time-to-failure testing of MOSFET isolation devices at 7.5 V and 150°C, a Weibull distribution was obtained with the parameters: t_{63}=1200hrs and a β=1.6. Assuming a power-law time-to-failure model with n=1 and activation energy of 1.0 eV:

a) What is the acceleration factor from stress conditions to use conditions ($V_{use} = 5.0V$, $T_{use} = 85°C$)?
b) What is the expected time-to-failure for 1% of the devices during use conditions?

Answers: a) AF = 218 b) TF(1%) = 1.7 yrs

7. For the accelerated *EM* data given in Problem 1, perform a more conservative time-to-failure analysis by using n=2 from $J = 2.0 \times 10^6$ to $1.0 \times 10^6 A/cm^2$ and n=1.5 below $1.0 \times 10^6 A/cm^2$.

a) What is the acceleration factor from stress conditions to use conditions ($J_{use} = 0.5 \times 10^6$ A/cm^2, $T_{use} = 105°C$)?
b) What is the expected time-to-failure for 1% of the devices during use conditions?

Answers: a) AF = 131 b) TF(1%) = 1.9 yrs

8. For the accelerated *creep* data given in Problem 2, perform a more conservative time-to-failure analysis by using n=4 from σ=800 to 600 MPa and n=3 below 600 MPa.

a) What is the acceleration factor from stress conditions to use conditions ($\sigma = 500$ MPa, $T_{use} = 500°C$)?
b) What is the expected time-to-failure for 1% of the devices during use conditions?

Answers: a) AF = 1279 b) TF(1%) = 5.7 yrs

9. For the accelerated *fatigue* data given in Problem 3, perform a more conservative time-to-failure analysis by using n=4 from Δσ=400 to 300 MPa and n=3 below Δσ =300 MPa.

a) What is the acceleration factor from stress conditions to use conditions ($\Delta\sigma = 200$ MPa, $T_{use} = 25°C$)?

b) What is the expected cycles-to-failure for 1% of the devices during use conditions?

Answers: a) AF = 10.7 b) TF(1%) = 5226 cycles

10. For the accelerated *TDDB* data given in Problem 4, perform a more conservative time-to-failure analysis by using γ=4 cm/MV from E=10MV/cm to 7 MV/cm and γ=3.5 cm/MV below 7 MV/cm.

a) What is the acceleration factor from stress conditions to use conditions (E_{use} = 5 MV/cm, T_{use} = 105°C)?
b) What is the expected time-to-failure for 1% of the devices during use conditions?

Answers: a) AF = 1.79×10^8 b) TF(1%) = 1150 yrs

11. For the accelerated *corrosion* data given in Problem 5, perform a more conservative time-to-failure analysis by using γ=[0.12]/%RH from 90%RH to 80%RH and γ=[0.1]/%RH below 80%RH.

a) What is the acceleration factor from stress conditions to use conditions ($\%RH_{use}$ = 65%, T_{use} = 85°C)?
b) What is the expected time-to-failure for 1% of the devices during use conditions?

Answers: a) AF = 137 b) TF = 4.6 yrs

12. For the *mobile-ions* time-to-failure data given in Problem 6, perform a more conservative time-to-failure analysis by using Q=1.0 eV from T=150°C to 100°C and Q = 0.75 eV below 100°C.

a) What is the acceleration factor from stress conditions to use conditions (V_{use} = 5.0V, T_{use} = 85°C)?
b) What is the expected time-to-failure for 1% of the devices during use conditions?

Answers: a) AF = 158 b) TF = 0.52 yrs

References

McPherson, J.: *Accelerated Testing*. In: **Electronic Materials Handbook**, **Vol. 1 Packaging**, ASM International, 887 (1989).

McPherson, J.: *Reliability Physics.* In: **Handbook of Semiconductor Manufacturing Technology**, **2nd Ed.**, Marcel Dekker, 959 (2000).

McPherson, J.: *Reliability Physics and Engineering*. In: **Handbook of Semiconductor Manufacturing Technology**, 2 CRC Press, 30-1 (2008).

Chapter 10
Ramp-to-Failure Testing

Engineers are constantly confronted with *time* issues. Applying a constant stress and waiting for failure can be very time consuming. Thus, it is only natural to ask the question — *does a rapid time-zero test exist that can be used on a routine sampling basis to monitor the reliability of the materials/devices?* The answer to this question is often *yes* and it is called the *ramp-to-failure* test. While the test is destructive in nature (one has to sacrifice materials/devices), it is generally much more rapid than conventional constant-stress time-to-failure tests. The relative quickness of the test also enables the gathering of more data and thus the gathering of better statistics.

10.1 Ramp-to-Failure Testing

Let us suppose that rather than applying a constant stress ξ and waiting for failure, we induce failure simply by ramping up the stress level $\xi(t)$ with time until the device fails. During the ramp testing, one carefully records the level of stress at failure/breakdown ξ_{bd} and the total time from start of stress to breakdown $t_{bd.}$ An example of linear ramp-to-failure/breakdown test is shown in Fig. 10.1.

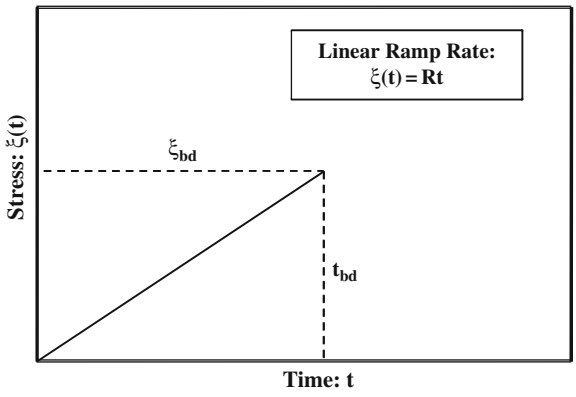

Fig. 10.1 Stress $\xi(t)$ is ramped with time in a linear manner until the material/device fails. The level of stress at failure/breakdown is recorded to be ξ_{bd}. The total time of the ramp to breakdown is t_{bd}. $R(= d\xi/dt)$ is a constant ramp rate.

J.W. McPherson, *Reliability Physics and Engineering*,
DOI 10.1007/978-1-4419-6348-2_10, © Springer Science+Business Media, LLC 2010

From this ramp-to-breakdown test, it can be easily seen that t_{bd} is not the length of time that the material actually experiences the stress level of ξ_{bd}. The time t_{bd} is the total observation time, and as such, comprehends the time that the material/device spent at the lower stress levels of the ramp as well as at time spent at ξ_{bd}. Therefore, the effective time t_{eff} actually spent at the breakdown strength ξ_{bd} will be lower than t_{bd}. One can use the acceleration factor to equate a differential element of *effective stress time* dt_{eff} with a differential element of *observed time dt*:

$$dt_{eff} = AF_{\xi(t),\,\xi_{bd}}\, dt. \tag{10.1}$$

Integrating both sides of the above equation to determine the effective time spent at ξ_{bd} for the entire ramp-to-breakdown test, one obtains:

$$t_{eff} = \int_0^{t_{bd}} AF_{\xi(t),\,\xi_{bd}}\, dt. \tag{10.2}$$

10.2 Linear Ramp Rate

Let us determine the effective time t_{eff} spent at ξ_{bd} during the linear ramp of $\xi(t)$, as illustrated in Fig 10.1, where:

$$\xi(t) = Rt. \tag{10.3}$$

Ramping the stress with a constant ramp rate $R(=d\xi/dt)$ means that that $t_{bd} = \xi_{bd}/R$.

10.2.1 Linear Ramp with Exponential Acceleration

Let us suppose that the acceleration factor in Eq. (10.2) is in the form of an exponential acceleration factor. From Chapter 9, one obtains:

$$AF_{\xi(t),\,\xi_{bd}} = \exp\left\{\gamma\left[\xi(t) - \xi_{bd}\right]\right\}. \tag{10.4}$$

Eq. (10.2) now becomes:

$$t_{eff} = \int_0^{\xi_{bd}/R} \exp\left[\gamma(Rt - \xi_{bd})\right] dt$$

$$
\begin{aligned}
&= \exp\left[-\gamma \xi_{bd}\right] \int_0^{\xi_{bd}/R} \exp\left[\gamma R t\right] dt \\
&= \exp\left[-\gamma \xi_{bd}\right] \left[\frac{1}{\gamma R}\right] \left[\exp(\gamma \xi_{bd}) - 1\right] \\
&= \left[\frac{1}{\gamma R}\right] \left[1 - \exp(-\gamma \xi_{bd})\right].
\end{aligned}
\tag{10.5}
$$

Therefore, for an exponential acceleration factor, the linear ramp produces an effective time t_{eff} spent at the breakdown strength ξ_{bd}:

$$
t_{eff} = \left[\frac{1}{\gamma R}\right] \left[1 - \exp(-\gamma \xi_{bd})\right] \cong \frac{1}{\gamma R}, \tag{10.6}
$$

where it is assumed in Eq. (10.6) that $\gamma \xi_{bd}$ is large enough that the exponential term is much smaller than 1. The fact that one has an expression for the effective time t_{eff} spent at the breakdown level ξ_{bd} is very important. Coupled with the appropriate acceleration factor, t_{eff} permits us to extrapolate from a breakdown value ξ_{bd} to a time-to-failure. The usefulness of t_{eff} is illustrated in the next example problem.

Example Problem 10.1

To make sure that capacitors will last an expected lifetime (10 yrs at 105°C), capacitors were randomly selected and then ramp-to-failure tested using a ramp rate of $R = dE/dt =$ 1MV/cm/sec at 105°C. During ramp testing, it was determined that the weakest device had a breakdown strength of $E_{bd} =$ 10.5MV/cm. Assuming an exponential acceleration factor with $\gamma =$ 4.0cm/MV, determine the expected time-to-failure at an operational field of 5MV/cm.

Solution

Since γE_{bd} is large, then $\exp[-\gamma E_{bd}] << 1$ and the effective time-to-failure at E_{bd} is given by:

$$
t_{eff} \cong \frac{1}{\gamma R} = \frac{1}{(4.0\, cm/MV)(1 MV/cm/\,\mathrm{sec})} = 0.25\,\mathrm{sec}\,.
$$

Therefore, if the capacitors last 0.25sec at E_{bd}=10.5 MV/cm (and at 105°C), then at a constant stress of E=5.0MV/cm (and at 105°C) they would be expected to last:

$$TF_{E=5MV/cm} = AF_{E_{bd}=10.5MV/cm,\ E=5MV/cm} \bullet (0.25\ \text{sec})$$
$$= \exp\left[(4.0\,cm/MV)(10.5-5)MV/cm\right] \bullet (0.25\ \text{sec})$$
$$= 8.96 \times 10^8\ \text{sec}\left(\frac{1hr}{3600\ \text{sec}}\right)\left(\frac{1\,yr}{8760hr}\right)$$
$$= 28yrs.$$

Therefore, based on the sampling results using the linear-ramp breakdown test, the capacitors should safely meet the 10-year lifetime requirement.

10.2.2 Linear Ramp with Power-Law Acceleration

Let us suppose that the acceleration factor in Eq. (10.2) is in the form of a power-law acceleration factor:

$$AF_{\xi(t),\,\xi_{bd}} = \left\{ \begin{array}{ll} 0 & [for\ \xi(t) \le \xi_{yield}] \\ \left[\dfrac{\xi(t)-\xi_{yield}}{\xi_{bd}-\xi_{yield}}\right]^n & [for\ \xi(t) \ge \xi_{yield}] \end{array} \right\}. \tag{10.7}$$

For reasons which will be established in Chapter 12, where *mechanical stress* is discussed in detail, an additional term has been inserted in Eq. (10.7) called the yield stress ξ_{yield}. Below ξ_{yield}, the stress $\xi(t)$ is expected to produce no damage to the material/device and thus the acceleration factor, as expressed by Eq. (10.7), is assumed equal to zero when the stress $\xi(t)$ is below ξ_{yield}.[1] Since a given material may or may not have a yield stress, then one must always question its existence. Using Eq. (10.7), Eq. (10.2) now becomes:

$$t_{eff} = \int_0^{\xi_{bd}/R} AF_{\xi(t),\xi_{bd}}\,dt$$
$$= \int_{\xi_{yield}/R}^{\xi_{bd}/R} \left[\frac{\xi(t)-\xi_{yield}}{\xi_{bd}-\xi_{yield}}\right]^n dt$$
$$= \left[\frac{1}{(\xi_{bd}-\xi_{yield}}\right]^n \int_{\xi_{yield}/R}^{\xi_{bd}/R} [Rt-\xi_{yield}]^{\,n}\,dt$$

[1] One should always question the existence of a yield stress ξ_{yield}. Some materials have a yield stress, some do not. Even if a material has a reported yield point, a slight crack/defect existing in the material may have an adverse impact on the yield point. The stress riser at the crack-tip/defect may produce a local stress in the material well above the yield stress. Degradation would now be expected even though the average stress may be below ξ_{yield}.

$$= \left[\frac{1}{\xi_{bd} - \xi_{yield}}\right]^{n} \left[\frac{(\xi_{bd} - \xi_{yield})^{n+1}}{R(n+1)}\right]$$
$$= \frac{1}{n+1}\left[\frac{\xi_{bd} - \xi_{yield}}{R}\right]. \tag{10.8}$$

Therefore, for a power-law acceleration factor, the linear-ramp test produces an effective time t_{eff} at the breakdown strength ξ_{bd} of:

$$t_{eff} = \frac{1}{n+1}\left[\frac{\xi_{bd} - \xi_{yield}}{R}\right]. \tag{10.9}$$

Example Problem 10.2

During the inspection of turbine blades, it was noted that small cracks existed at the base of the turbine blades. A potential reliability issue can develop if the cracks propagate during use and produce failure under the normal tensile-stress conditions of rotation. A random selection of these turbine blades was tested using a linear ramp-to-failure test. The linear ramp rate used for the tensile stress was $R = d\sigma/dt = 10$MPa/min and the testing was done at the expected use temperature of 850°C. The weakest turbine blade found during the ramp testing was $\sigma_{rupture} = 200$MPa. Assuming that the use-condition tensile stress is 10 MPa, find the expected time-to-failure. Assume that a power-law model is appropriate with a stress dependence exponent of n=4 and, because of stress risers (discussed in Chapter 12) at the crack tips, σ_{yield} is negligibly small.

Solution

For the weakest turbine blade ($\sigma_{rupture} = 200$MPa) found during the linear ramp stress testing, the time-to-failure under this ramp testing was:

$$TF_{@200\,MPa} = \frac{1}{n+1}\left[\frac{\xi_{bd}}{R}\right] = \frac{1}{4+1}\left[\frac{200\,MPa}{10\,MPa/\,\text{min}}\right] = 4\ \text{min}.$$

The expected time-to-failure at the use condition of 10 MPa would be:

$$TF_{@\sigma=10\,MPa} = AF_{\sigma_{rupture}=200\,MPa,\sigma=10\,MPa} \bullet (4\,\text{min})$$
$$= \left[\frac{200\,MPa}{10\,MPa}\right]^{4} (4\,\text{min})$$
$$= 6.40 \times 10^{5}\ \text{min}$$
$$= 6.40 \times 10^{5}\ \text{min}\left(\frac{1hr}{60\,\text{min}}\right)\left(\frac{1\,yr}{8760hr}\right)$$
$$= 1.2yrs.$$

10.3 Breakdown/Rupture Distributions

The breakdowns/ruptures that are determined using the ramp-to-breakdown method may not be described well by the normal distribution (which is a symmetrical distribution). This occurs because the breakdowns/ruptures at the high end of the distribution are generally relatively tightly grouped. This is because the breakdowns/ruptures are limited, on the high end of the distribution, by the fundamental strength of the material. However, at the lower end of the distribution, the breakdowns/ruptures are generally more widely spread due to defects existing in the materials. For this reason, the Weibull distribution is often used to describe the inherent non-symmetrical breakdown/rupture data. This is illustrated in Fig. 10.2.

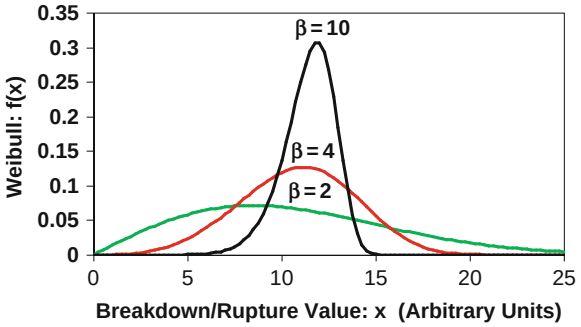

Fig. 10.2 The breakdown/rupture values, obtained from ramped-to-breakdown testing, can often be described by a Weibull distribution. Note that the Weibull distribution can be non-symmetrical, favoring the lower breakdown values. This tends to more accurately reflect actual breakdown/rupture data. The actual shape is a sensitive function of the Weibull slope β.

The Weibull probability density function $f(\xi_{bd})$ for the breakdown/rupture values is given by:

$$f(\xi_{bd}) = \left[\frac{\beta}{(\xi_{bd})_{63}}\right]\left[\frac{\xi_{bd}}{(\xi_{bd})_{63}}\right]^{\beta-1} \exp\left[-\left(\frac{\xi_{bd}}{(\xi_{bd})_{63}}\right)^{\beta}\right], \tag{10.10}$$

where $(\xi_{bd})_{63}$ is the characteristic Weibull value and β is the Weibull slope, with the method for determination given in Chapter 6. The cumulative Weibull probability function is given by:

$$F(\xi_{bd}) = \int_0^{\xi_{bd}} f(\xi_{bd})\, d\xi_{bd} = 1 - \exp\left[-\left(\frac{\xi_{bd}}{(\xi_{bd})_{63}}\right)^{\beta}\right]. \tag{10.11}$$

Example Problem 10.3

During ramp-to-rupture testing of metal rods, the following rupture values were obtained:

637 MPa	573 MPa	712 MPa	614 Mpa	552 Mpa
527 MPa	593 Mpa	666 Mpa	497 Mpa	453 Mpa

a) Find the Weibull parameters that give the best fitting to the rupture data.
b) Plot the Weibull probability density function.

Solution

a) The Weibull *best fitting* parameters are given by:

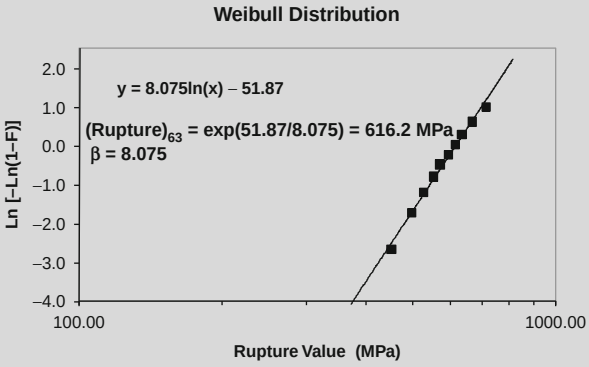

The Weibull parameters that produce the best fitting to the rupture data are: $(\text{Rupture})_{63}$=616 MPa and $\beta = 8.1$.

b) The Weibull probability density function is shown below. Note that the distribution is asymmetrical and tends to favor the lower part of the rupture distribution. The lower-value ruptures tend to occur more frequently because of defects in the materials.

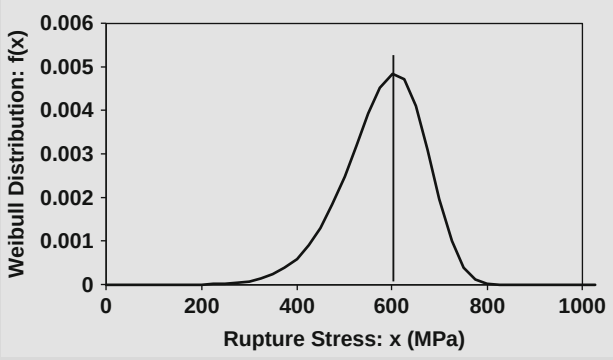

10.4 Cautions For Ramp-To-Failure Testing

One should note that the ramp-to-failure testing method can potentially be very fast. However, always remember the story of the *lively chicks versus the hard-boiled eggs* in Section 9.3. One should confirm that the linear ramp test is only accelerating the physics of failure, not changing the physics of failure. To help insure that you are accelerating the right activation energy mechanism, always try to do the ramp test at the expected material/device operating temperature T_{op}. Also, make the ramp rate as slow[2] as test time will permit. One should always take some constant-stress time-to-failure data points, just to confirm that the time-to-failure projections from the ramp stress test are correct. Finally, some stresses, such as a current density stress in a conductor, can produce severe Joule/self-heating as the current-density stress is ramped. Thus, in a ramp test using current density, one might be investigating *fusing physics* as opposed to the intended *electromigration physics*. However, many of the stresses of interest (mechanical stress, electric-field stress, electrochemical stress, etc.) may not produce significant self-heating. As you build your confidence in the ramp-to-failure test method (assuming that the results from the ramp test closely match those of a constant-stress time-to-failure test), then the majority of your future testing may be the ramp-to-failure method of testing.

10.5 Transforming Breakdown/Rupture Distributions into Constant-Stress Time-To-Failure Distributions

Shown in Fig. 10.3 is the breakdown/rupture ξ_{bd} distribution that was obtained from a linear ramp-to-failure test. The question is, *how does one transform these breakdown/rupture values into an expected constant-stress ξ_{op} time-to-failure distribution?*

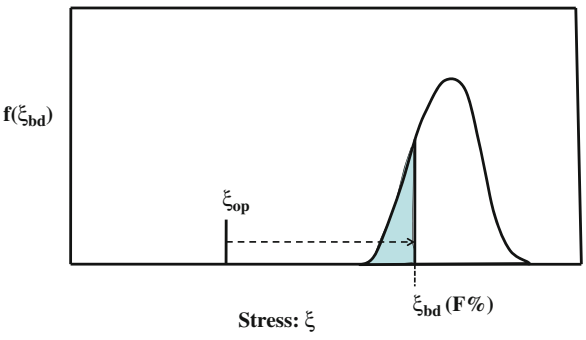

Fig. 10.3 Distribution $f(\xi_{bd})$ of breakdown/rupture strengths as determined from a linear ramp-to-failure test. $\xi_{bd}(F\%)$ represents the breakdown strength for a cumulative fraction F of the devices. ξ_{op} represents the expected constant-stress operational value.

[2]Generally, the slower the ramp rate, the closer the ramp test results will match actual constant-stress time-to-failure results.

The time-to-failure for a cumulative fraction F of the breakdown strengths is given by:

$$TF(F\%) = AF_{\xi_{bd}(F\%),\,\xi_{op}} \bullet t_{eff}, \tag{10.12}$$

where t_{eff} is the effective time-to-failure at ξ_{bd} during the ramp testing.

10.5.1 Transforming Breakdown/Rupture Distribution to Time-To-Failure Distribution Using Exponential Acceleration

One would like to find the transformation equation for converting a breakdown/rupture distribution into a time-to-failure distribution when one has exponential acceleration. Using Eq. (10.6) and Eq. (10.12) with the exponential acceleration factor,

$$AF_{\xi_{bd}(F\%),\xi_{op}} = \exp\left\{\gamma\ \left[\xi_{bd}(F\%) - \xi_{op}\right]\right\}, \tag{10.13}$$

gives:

$$TF(F\%) = \left(\frac{1}{\gamma R}\right)\exp\left\{\gamma\ \left[\xi_{bd}(F\%) - \xi_{op}\right]\right\}. \tag{10.14}$$

In Eq. (10.14), γ is the exponential acceleration parameter, $R(= d\xi/dt)$ is the linear ramp rate, $F\%$ is the percentage of devices that have a breakdown/rupture strength $\leq \xi_{bd}(F\%)$, and ξ_{op} is the expected constant-stress operational value.

10.5.2 Transforming Breakdown/Rupture Distribution to Time-To-Failure Distribution Using Power-Law Acceleration

One would like to find the transformation equation for converting a breakdown/rupture distribution into a time-to-failure distribution when one has power-law acceleration. Using Eq. (10.9) and Eq. (10.12), with the power-law acceleration factor,

$$AF_{\xi_{bd}(F\%),\xi_{op}} = \left[\frac{\xi_{bd}(F\%) - \xi_{yield}}{\xi_{op} - \xi_{yield}}\right]^{n}, \tag{10.15}$$

gives:

$$TF(F\%) = \frac{1}{n+1}\left[\frac{\xi_{op} - \xi_{yield}}{R}\right]\left[\frac{\xi_{bd}(F\%) - \xi_{yield}}{\xi_{op} - \xi_{yield}}\right]^{n+1}. \tag{10.16}$$

In Eq. (10.16), n is the power-law exponent for the acceleration, $R(= d\xi/dt)$ is the linear ramp rate, $F\%$ is the percentage of devices that have a breakdown/rupture strength $\leq \xi_{bd}(F\%)$, and ξ_{op} is the expected constant-stress operational value. If the material exhibits a yield stress, ξ_{yield}, it is also included in Eq. (10.16).

10.6 Constant-Stress Lognormal Time-To-Failure Distributions from Ramp Breakdown/Rupture Data

As discussed in Chapter 6, the lognormal time-to-failure distribution is fully defined when the characteristic parameters ($t_{50,}$ σ) are determined.

10.6.1 Exponential Acceleration

Given that the time-to-failure for exponential acceleration can be expressed by

$$TF(F\%) = \left(\frac{1}{\gamma R}\right) \exp\left\{ \gamma \left[\xi_{bd}(F\%) - \xi_{op}\right] \right\}, \tag{10.17}$$

the characteristic parameters for the lognormal distribution are given by:

$$TF(50\%) = \left(\frac{1}{\gamma R}\right) \exp\left\{ \gamma \left[\xi_{bd}(50\%) - \xi_{op}\right] \right\} \tag{10.18}$$

and

$$\sigma_{\log normal} = \ln\left[\frac{TF(50\%)}{TF(16\%)}\right] = \gamma \left[\xi_{bd}(50\%) - \xi_{bd}(16\%)\right]. \tag{10.19}$$

Example Problem 10.4

Assuming exponential acceleration with acceleration parameter γ, show that if the breakdown/rupture strengths are normally distributed then the expected time-to-failure results will be lognormally distributed.

Solution

From Eq. (10.19) one obtains:

$$\begin{aligned}\sigma_{\log normal} &= \ln\left[\frac{TF(50\%)}{TF(16\%)}\right] = \gamma \left[\xi_{bd}(50\%) - \xi_{bd}(16\%)\right] \\ &= \gamma \sigma_{normal}.\end{aligned}$$

Therefore, assuming exponential acceleration with acceleration parameter γ, if the breakdown strengths are normally distributed with standard deviation of σ_{normal}, the time-to-failure will be lognormally distributed with logarithmic standard deviation $\sigma_{lognormal} = \gamma\sigma_{normal}$.

10.6.2 Power-Law Acceleration

Given that the time-to-failure for power-law acceleration is given by

$$TF(F\%) = \frac{1}{n+1}\left[\frac{\xi_{op} - \xi_{yield}}{R}\right]\left[\frac{\xi_{bd}(F\%) - \xi_{yield}}{\xi_{op} - \xi_{yield}}\right]^{n+1}, \tag{10.20}$$

the characteristic parameters for the lognormal distribution are given by:

$$TF(50\%) = \frac{1}{n+1}\left[\frac{\xi_{op} - \xi_{yield}}{R}\right]\left[\frac{\xi_{bd}(50\%) - \xi_{yield}}{\xi_{op} - \xi_{yield}}\right]^{n+1} \tag{10.21}$$

and

$$\sigma = \ln\left[\frac{TF(50\%)}{TF(16\%)}\right] = (n+1)\ln\left[\frac{\xi_{bd}(50\%) - \xi_{yield}}{\xi_{bd}(16\%) - \xi_{yield}}\right]. \tag{10.22}$$

10.7 Constant-Stress Weibull Time-To-Failure Distributions from Ramp Breakdown/Rupture Data

As discussed in Chapter 6, the Weibull time-to-failure distribution is fully defined when the characteristic parameters (t_{63},β) are determined.

10.7.1 Exponential Acceleration

Given that the time-to-failure for exponential acceleration is given by

$$TF(F\%) = \left(\frac{1}{\gamma R}\right)\exp\left\{\ \gamma\ \left[\xi_{bd}(F\%) - \xi_{op}\right]\right\}, \tag{10.23}$$

the characteristic Weibull distribution parameters (t_{63},β) are given by:

$$TF(63\%) = \left(\frac{1}{\gamma R}\right)\exp\left\{\ \gamma\ \left[\xi_{bd}(63\%) - \xi_{op}\right]\right\}, \tag{10.24}$$

and

$$\beta = \frac{\ln[-\ln(1-F)]}{\gamma\,[\xi_{bd}(F\%) - \xi_{bd}(63\%)]}.\ ^{3} \tag{10.25}$$

10.7.2 Power-Law Acceleration

Given that the time-to-failure for power-law acceleration is given by

$$TF(F\%) = \frac{1}{n+1}\left[\frac{\xi_{op} - \xi_{yield}}{R}\right]\left[\frac{\xi_{bd}(F\%) - \xi_{yield}}{\xi_{op} - \xi_{yield}}\right]^{n+1}, \tag{10.26}$$

the characteristic parameters of the Weibull distribution are obtained by:

$$TF(63\%) = \frac{1}{n+1}\left[\frac{\xi_{op} - \xi_{yield}}{R}\right]\left[\frac{\xi_{bd}(63\%) - \xi_{yield}}{\xi_{op} - \xi_{yield}}\right]^{n+1} \tag{10.27}$$

and

$$\beta = \frac{\ln[-\ln(1-F)]}{(n+1)\ln\left[\dfrac{\xi_{bd}(F\%) - \xi_{yield}}{\xi(63\%) - \xi_{yield}}\right]},\ ^{4} \tag{10.28}$$

where n is the power-law exponent and R (=dξ/dt) is the constant ramp rate used to determine the breakdown strength ξ_{bd}.

Example Problem 10.5

During the ramp-breakdown testing of capacitors(caps) at 105°C with a ramp rate of R=1MV/cm/sec, it was determined that 10% of the caps break down at a field of ≤ 10.5MV/cm and 63% of the caps at ≤ 11MV/cm. If the devices are operated at a constant stress of 5MV/cm, what are the expected Weibull time-to-failure distribution parameters t_{63} and β?

1. Assume an exponential acceleration, with γ=4 cm/MV.
2. Assume a power-law acceleration, with n=42 and ξ_{yield}=0.

[3] Reminder — any cum fraction F can be used to determine β provided that the corresponding ξ_{bd}(F%) is also used. If one chooses to use F = 0.1, then $\beta = 2.25/\{\gamma[\xi_{bd}(63\%) - \xi_{bd}(10\%)]\}$.

[4] If one uses F=0.1 then $\beta = 2.25/\{(n+1)\ln[\xi_{bd}(63\%)/\xi_{bd}(10\%)]\}$.

Solution

1. For exponential acceleration, at 105°C, Eq. (10.23) gives:

$$TF(63\%) = \left(\frac{1}{\gamma R}\right) \exp\left\{\gamma\left[\xi_{bd}(63\%) - \xi_{op}\right]\right\}$$

$$= \left(\frac{1}{(4.0 cm/MV)(1 MV/cm/\sec)}\right) \bullet$$

$$\exp\left\{(4.0\, cm/MV)(11 MV/cm - 5 MV/cm)\right\}$$

$$= 6.62 \times 10^9 \sec \left(\frac{1 hr}{3600 \sec}\right)\left(\frac{1\, yr}{8760 hr}\right)$$

$$= 210 yrs.$$

The expected Weibull slope β from Eq. (10.25) is:

$$\beta = \frac{\ln[-\ln(1-F)]}{\gamma\left[\xi_{bd}(F\%) - \xi_{bd}(63\%)\right]}$$

$$= \frac{\ln[-\ln(1-0.1)]}{(4.0\, cm/MV)[10 MV/cm - 10.5 MV/cm]}$$

$$= 1.13.$$

2. For power-law acceleration at 105°C and no yield point, Eq. (10.26) gives:

$$TF(63\%) = \frac{1}{n+1}\left[\frac{\xi_{op}}{R}\right]\left[\frac{\xi_{bd}(63\%)}{\xi_{op}}\right]^{n+1}$$

$$= \frac{1}{43}\left[\frac{5 MV/cm}{1 MV/cm/\sec}\right]\left[\frac{11 MV/cm}{5 MV/cm}\right]^{43}$$

$$= 6.16 \times 10^{13} \sec \left[\frac{1 hr}{3600 \sec}\right]\left[\frac{1\, yr}{8760 hr}\right]$$

$$= 1.95 \times 10^6 yrs.$$

The expected Weibull slope β is given by Eq. (10.28):

$$\beta = \frac{\ln[-\ln(1-F)]}{(n+1)\ln\left[\frac{\xi_{bd}(F\%)}{\xi_{bd}(63\%)}\right]}$$

$$= \frac{\ln[-\ln(1-0.1)]}{(42+1)\ln\left[\frac{10.5MV/cm}{11MV/cm}\right]}$$

$$= 1.12.$$

Problems

1. Capacitor dielectrics were randomly selected and ramp-to-breakdown tested at 105°C, using a linear ramp rate of $R = dE/dt = 0.5$MV/cm/sec. During ramp-to-breakdown testing, it was determined that the breakdown distribution could be approximated by a normal distribution with: $(E_{bd})_{50} = 12$MV/cm and σ=1.0MV/cm. Determine the expected time-to-failure for 1% of the capacitors at an operational field of 5MV/cm at 105°C. Assume an exponential acceleration factor with $\gamma = 4.0$ cm/MV.

   Answer: TF(1%) = 2.1 yrs

2. Turbine blades were randomly selected and ramped-to-rupture at 700°C using a tensile stress with a linear ramp rate of $R = d\sigma_{stress}/dt = 5$MPa/min. During ramp-to-rupture testing, it was determined that the rupture distribution could be approximated by a normal distribution with: $(\sigma_{rupture})_{50} = 250$MPa with a σ =25 MPa. Determine the expected time-to-failure for 1% of the turbine blades at an operational tensile stress of 15 MPa at 700°C. Assume a power-law acceleration factor with n=4.0 and (because of small cracks) no yield point.

   Answer: TF(1%) = 0.4 yrs

3. Analyze Problem 1 except this time, assume a power-law acceleration with n = 40.

   Answer: TF(1%) = 4297 yrs

4. Analyze Problem 2, except this time assume an exponential acceleration with $\gamma = 0.06$/MPa.

   Answer: TF(1%) = 0.3 yrs

5. Steel pipes were randomly selected for pressurizing-to-rupture testing. Using a linear ramp rate of R=dP/dt=5kpsi/min, the rupture data tended to obey a Weibull distribution with $(P_{rupture})_{63} = 200$kpsi and a Weibull slope of β=10. Determine the expected time-to-failure for 1% of the pipes at an operational pressure of 5kpsi. Assume that the stress in the cylindrical pipes is directly proportional to the pressure and assume a power-law acceleration factor with an exponent of n=4 and (because of small cracks) no yield point.

   Answer: TF(1%) = 15.6 yrs

6. Suspension cables were randomly selected for tensile stressing-to-rupture testing. Using a linear ramp rate of $R=d\sigma_{Tensile}/dt=$ 4kpsi/min, the rupture data tended to obey a Weibull distribution with $(\sigma_{rupture})_{63} = 250$kpsi and a Weibull slope of β=12. Determine the expected time-to-failure for 1% of the cables at an operational pressure of 2kpsi. Assume a power-law acceleration factor with an exponent of n=4 and (because of small defects) no yield point.

   Answer: TF(1%) = 854 yrs

7. With no yield point, Equation (10.16) reduces to:

$$TF(F\%) = \frac{1}{n+1}\left[\frac{\xi_{op}}{R}\right]\left[\frac{\xi_{bd}(F\%)}{\xi_{op}}\right]^{n+1},$$

which is valid when the stress ξ is linearly ramped at a constant rate R (R=dξ/dt=constant) until failure occurs. Show that, if the stress is proportional to the power-law of some other parameter S,

$$\xi = C_o S^m,$$

then the time-to-failure equation becomes:

$$TF(F\%) = \frac{1}{n+1}\left[\frac{S_{op}^m}{R_1}\right]\left[\frac{S_{bd}(F\%)}{S_{op}}\right]^{m(n+1)},$$

where the ramp rate R_1 is given by:

$$R_1 = mS^{m-1}\left(\frac{dS}{dt}\right) = constant.$$

8. Using the results from Problem 7, metal storm shutters with small cracks were randomly selected for storm testing. The shutters were tested in a wind tunnel by ramping the wind speed S until the shutters failed. The stress σ in the shutters, due to the wind, is proportional to the square of the wind speed: $\sigma = C_o S^2$. Using a constant ramp rate of $R_1=2S(dS/dt)=10$ $(mph)^2$/min, the failure data tended to obey a Weibull distribution with $(S)_{63}=100$mph and a Weibull slope of β=10. Determine the expected time-to-failure for 1% of the shutters with a nominal

constant wind speed of 25 mph.[5] Assume a power-law acceleration factor of at least n=6, and because of the small cracks, no yield point.

Answer: TF(1%) = 7.2 yrs

References

Anolick, E. and G. Nelson: *Low-Field Time-Dependent Dielectric Breakdown*, IEEE International Reliability Symposium Proceedings, 8 (1979).

Berman, A.: *Time-Zero Dielectric Breakdown by a Ramp Method,* IEEE International Reliability Symposium Proceedings, 204 (1981).

McPherson, J.: *Stress-Dependent Activation Energy*, IEEE International Reliability Symposium Proceedings, 12 (1986).

[5] Actually, the wind speed is usually gusting (time-dependent).Chapter 13 describes how one can convert dynamical conditions to an effective static condition.

Chapter 11
Time-To-Failure Models for Selected Failure Mechanisms in Integrated Circuits

Advanced integrated circuits (*ICs*) are very complex, both in terms of their design and in their usage of many dissimilar materials (semiconductors, insulators, metals, plastic molding compounds, etc.). For cost reductions per device and improved performance, scaling of device geometries has played a critically important role in the success of semiconductors. This scaling—where device geometries are generally reduced by 0.7x for each new technology node and tend to conform to Moore's Law[1]—has caused the electric fields in the materials to rise (bringing the materials ever closer to their breakdown strength) and current densities in the metallization to rise causing electromigration (EM) concerns. The higher electric fields can accelerate reliability issues such as: time-dependent dielectric breakdown (TDDB), hot-carrier injection (HCI), and negative-bias temperature instability (NBTI). In addition, the use of dissimilar materials in a chip and in the assembly process produces a number of thermal expansion mismatches which can drive large thermomechanical stresses. These thermomechanical stresses can result in failure mechanisms such as stress migration (SM), creep, fatigue, cracking, delaminating interfaces, etc.

11.1 Electromigration (EM)

Electromigration (EM) has historically been a significant reliability concern for both Al-based and Cu-based metallizations. As illustrated in Fig. 11.1, due to the *momentum exchange* between the current carrying electrons and the host metal lattice, metal ions can drift under the influence of the *electron wind*. The force F exerted on a metal ion due to the electron wind is directly proportional to the electron current density $J^{(e)}$,

$$F = \rho_0 z^* e J^{(e)}, \tag{11.1}$$

where ρ_0 is the resistivity of the metal, and z^*e is the effective metal-ion charge.

[1] Moore's Law, attributed to Gordon Moore, states that the transistor density on ICs tends to double every 18–24 months.

J.W. McPherson, *Reliability Physics and Engineering*,
DOI 10.1007/978-1-4419-6348-2_11,

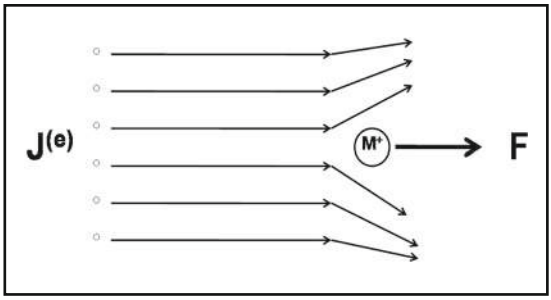

Fig. 11.1 For high electron current densities $J^{(e)}$, the electron wind (collisions of the electrons with the metal ions in the lattice) serves to exert a force F on the metal ion which is large enough to cause the metal ion M^+ to drift from the cathode toward the anode. Generally, this metal-ion movement is along grain boundaries in Al-alloys and along interfaces with copper.

Eventually, due to a flux divergence[2] (caused by gradients in microstructure, temperature, stress, impurities, etc.), vacancies[3] will start to cluster; the cluster can grow into a void; and finally the void growth will continue until the conductor reaches a resistive or open-circuit condition. This can be an important failure mechanism for ICs where the current densities in the metal stripes/leads can easily approach and even exceed a mega-amp per square centimeter (MA/cm^2). Shown in Fig. 11.2 is a metal conductor which was stressed at 2MA/cm^2 and at 150°C for a few hundred hours. Note the severe EM-induced voiding which has occurred in this test line/lead/stripe.

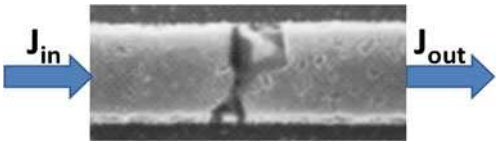

Fig. 11.2 Electromigration-induced transport (and eventual flux divergence) has produced severe voiding in the Al metal lead shown. The voiding will cause a resistance rise in the metal line/stripe/lead, eventually impacting device functionality. In the case shown here, the metal-ion flux is $J_{out} > J_{in}$, thus voiding occurs.

For Al-alloys, the metal-ion transport is primarily along grain boundaries (for temperatures $T < T_{melt}/2$).[4] Two idealized regular/uniform grain structures are

[2]Recall from Chapter 4 that a flux divergence represents the *net flow* of material into or out of a region of interest. A flux divergence can result in the accumulation or depletion of metal ions in the region of interest. Microstructure differences, such as grain size differences, can result in flux divergences.

[3]Vacancy is simply a vacant lattice site. A vacancy represents free space (a missing atom) and, as such, a clustering of vacancies can result in void formation. A discussion of vacancies can be found in Chapter 12.

[4]Grain boundary (or interface) transport generally dominates for $T < 0.5T_{melt}$, where T_{melt} is the melting temperature of the metal (expressed in Kelvin). Bulk (within grain or lattice) transport can dominate for $T > 0.5T_{melt}$. The activation energy for grain boundary transport Q_{gb} is roughly half that of bulk transport Q_{bulk}.

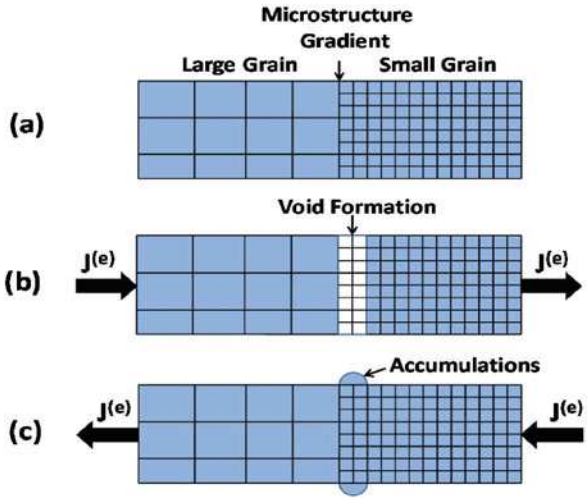

Fig. 11.3 Electromigration-induced transport is primarily along grain boundaries in polycrystalline Al-alloy conductors. a) Two regions of uniform grain structure are illustrated. b) Electron flow $J^{(e)}$ from left to right can serve to produce a void in the metal due to the flux divergence at the microstructure-gradient. c) Electron flow from right to left can produce an accumulation of metal due to the flux divergence at the microstructure gradient. The dominant electromigration-transport mechanism for Cu can be along the Cu/barrier interfaces.

illustrated in Fig. 11.3.[5] The transport of metal ions due to the *electron wind*, coupled with a flux divergence due to a microstructure gradient, as illustrated in Fig. 11.3, can cause either *voiding or accumulations* to occur. The *void nucleation-phase* generally has little/no impact on the electrical resistance rise in the metal stripe. The *void growth-phase*, however, can cause local current-crowding and a rise in resistance for the metal stripe.

If the metallization is actually an Al-alloy/barrier-metal laminate, then the resistance rise may show a time delay t_0 and then a gradual rise as illustrated in Fig. 11.4. This gradual rise in resistance, of course, assumes that the barrier metal is electromigration resistant. Some commonly used electromigration resistant *barriers* in integrated circuit applications include: TiW, TiN, and TaN. Without a barrier layer present to participate in *shunting* the current, the rise in resistance for the Al-alloy can be very abrupt for EM-induced damage. The use of barriers is illustrated in Fig. 11.5.

For pure copper metallization, the dominant diffusion path during EM testing is generally along interfaces, rather than along grain boundaries as in Al-alloys. Unlike aluminum, which forms a strongly bonded Al-oxide layer (Al_2O_3) on its surface, Cu-oxide is relatively poorly bonded to the Cu surface (refer to Fig. 12.44). This can

[5] Grain sizes are not really as regular/uniform as illustrated in Fig. 11.3. Grain sizes are generally lognormally distributed.

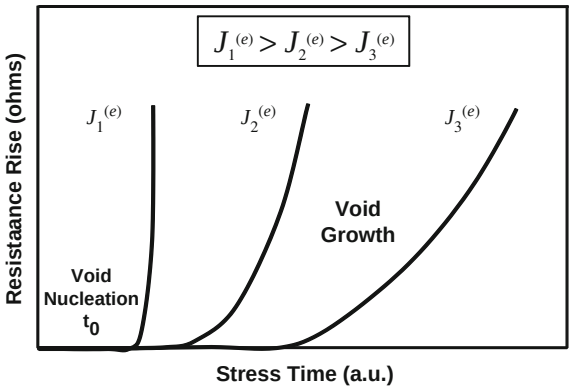

Fig. 11.4 Electromigration-induced resistance rise in layered metal stripes (e.g., Al-Cu/TiN) shows little/no resistance rise initially for a time t_0 and then a gradual rise in resistance. The TiN layer serves as an electromigration-resistant shunting layer to prevent catastrophic resistance rises (open-circuit conditions).

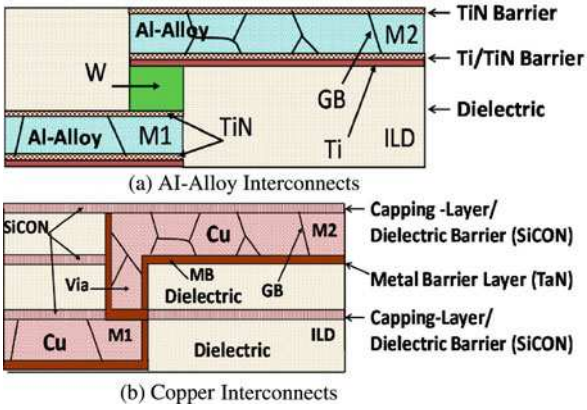

Fig. 11.5 (a) Al-alloy interconnect system for ICs. Grain-boundary(GB) transport in Al-alloy usually dominates EM performance. Flux-divergence/voiding is often associated with the W-plug via. (b) Copper interconnect system for ICs. Interfacial transport associated with the Cu/barrier interfaces usually dominates the EM performance. Flux-divergence/voiding is often associated with the via.

provide a high mobility interface for the Cu-ion transport. In order to reduce Cu-ion mobility along such interfaces, the Cu should be tightly bounded by well adhering barrier layers. Normally, the bottom and sidewalls of the Cu lead are bounded by a TiN or TaN barrier while the top of the Cu lead has a dielectric barrier such as SiN, SiCOH or SiCON. During EM transport, the Cu-ions will select one or more of the weak interfaces. (See Fig. 11.6 for typical failing locations.)

While differences in the materials properties between Cu and Al can dominate the mass transport mechanism, Cu metallization is also distinguished from Al because it is fabricated differently using the so-called *damascene* or *dual-damascene* process flow (refer to Fig. 11.5b). Damascene processes are used, rather than the physical/sputter-deposition and subtractive-etch processes used to make Al-alloy interconnects, because of better filling characteristics and because of difficulties with developing plasma etches for the Cu metallization.

In the damascene process flow, trenches are first etched into a dielectric layer (where the metallization will eventually go) and then the trenches are lined with a metal barrier material (such as Ta-based metallization) and a thin, *physically*

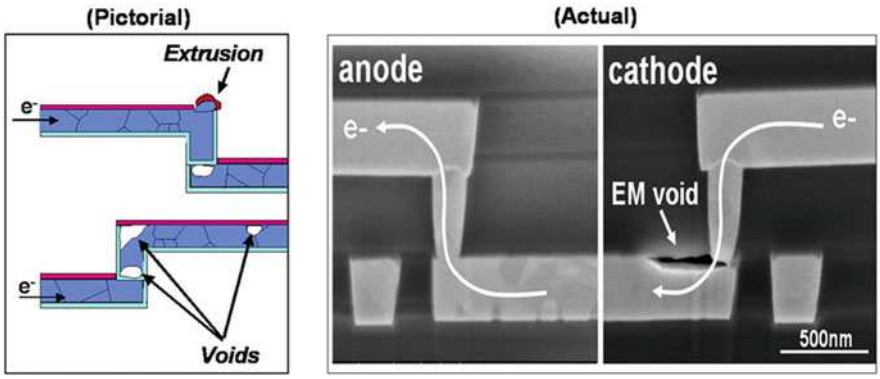

Fig. 11.6 Shown is a pictorial (on the left) of where EM-induced damage might be expected in Cu interconnects. Shown on right is the actual EM-induced voiding.

vapor-deposited Cu seed-layer. This trench feature is then filled with Cu metallization using an *electroplating process (EP)*. This is followed by *chemical mechanical polishing (CMP)* and subsequent cleans to define the interconnect geometry. Next, the Cu is capped by a sealing barrier layer, usually a dielectric barrier material.

In the *dual-damascene* process, the *via* openings are also formed in addition to the trench such that *via* and trench are not separated by a metal barrier as would be the case for single damascene interconnects. In dual-damascene Cu, a flux barrier (due to the use of a barrier) is present at the bottom of *via*.[6] This somewhat complicated interconnect architecture, utilizing dielectric and metal barriers with different interface properties, exhibits a number of flux divergence locations not seen in Al-metallization. For electron flow up into a via (up-direction EM), a flux divergence is located at the top corner of the trench. For *down-direction EM*, the flux divergence location is along the top surface of the lower metal trench where the metal barrier of the via and the dielectric cap (on the lower metal trench) meet. The voiding volumes necessary to cause severe resistance rises are also somewhat different for the two cases, leading to the general observation that *down-direction EM* failures occur somewhat faster than *up-direction EM*.[7] Additionally, defects present within a via may lead to premature EM failure (*early or weak-mode failure*) for an up-direction interconnect.

The presence of weak interfaces in Cu metallization, due to the fact that Cu does not form a strongly adhering native oxide, means that optimization of interfacial adhesion strength between Cu and the capping layer is critically important. Studies have shown that improvements in interfacial adhesion strength will improve EM performance. Also, when the interfacial adhesion is extremely good, as the case with

[6] *Via* is the term used to describe the physical/electrical connection of an upper level of metal to a lower level of metal through a dielectric layer.

[7] *Up* (into via) or *down* (into via) refers to the electron-flow direction.

Co-cladding of the Cu, the EM performance improves dramatically and the Cu EM performance can then be primarily limited by bulk diffusion, with a corresponding increase in activation energy Q.

Since electromigration transport is a mass conserving process then, in addition to the voiding problems, accumulations of the transported metal ions will also occur thus increasing the mechanical stress in the metallization and surrounding dielectrics. This localized buildup of stress in the metallization will serve to generate a *backflow* of metal ions (the *Blech effect*). For shorter leads (generally a few tens of microns) the *Blech effect* can be so strong that the backflow of metal ions will cancel the drift component[8] and electromigration-induced failure can be retarded. However, the buildup of mechanical stress in the metal lead is also accompanied by a buildup of opposing mechanical stress in the surrounding dielectrics which can cause potential fracturing of the surrounding dielectrics. Fracture of the surrounding dielectrics can facilitate the shorting of the test lead to the adjacent metal leads. For advanced Cu metallizations, which require low-k dielectrics that are relatively mechanically weak, this potential shorting failure-mechanism may need to be considered.

The model generally used to describe EM time-to-failure takes the form

$$TF = A_0(J^{(e)} - J^{(e)}_{crit})^{-n} \exp\left(\frac{Q}{K_B T}\right), \tag{11.2}$$

where:

- A_0 is a process/material-dependent coefficient. This coefficient can vary from device to device and is the reason that the time-to-failure TF is actually a distribution of times-to-failure. The device-to-device variation (A_0 variation) can be as subtle as slight microstructure differences in the metallization. A lognormal TF distribution is generally used for EM failure mechanisms.
- $J^{(e)}$ is the electron current density. $J^{(e)}$ must be greater than $J^{(e)}_{crit}$ to produce failure.
- $J^{(e)}_{crit}$ is a critical (threshold) current density which must be exceeded before significant EM damage is expected. $J^{(e)}{}_{crit}$ can be determined from the Blech length equation: $(J^{(e)} \bullet L)_{crit} = A_{Blech}$. For aluminum alloys, $A_{Blech} \cong 6000$ A/cm. For Cu, $A_{Blech} \cong 1000$ to 4000 A/cm, depending on the mechanical strength of the surrounding dielectrics and barrier materials. If the test stripe length is > 250 μm, then $J^{(e)}_{crit}$ is typically small compared to the normal EM stressing current density of > 1 MA/cm^2. For this reason, $J^{(e)}_{crit}$ is often ignored. However, the Blech effect may be an important design consideration for very short conductor lengths.

[8] Drift and diffusion (backflow) mechanisms were discussed in Chapter 6. If the backflow pressure (created by the accumulation of material) starts to cancel the drift-induced pressure, then *net* material flow ceases.

n is the current density exponent. $n = 2$ is normally used for aluminum-alloys and $n = 1$ for Cu.

Q is the activation energy. $Q = 0.5 - 0.6$ eV is generally used for Al and Al-Si, $Q = 0.7 - 0.9$ eV is used for Al-Cu alloys, and $Q = 1.0$ eV for pure Cu.

For Al-alloys, time-to-failure will generally show a metal-width dependence, with the worst case (smallest time-to-failure) occurring for metal widths approximately 2 times the mean grain size.[9] As for copper, the worst-case EM performance generally occurs with the most narrow metal widths.

Example Problem 11.1

Find the Blech length when a current density of $J^{(e)} = 1 \times 10^6 \text{A/cm}^2$ is flowing through an aluminum alloy conductor.

Solution

For aluminum alloys, the Blech relation becomes:

$$\left(J^{(e)} \bullet L\right)_{crit} \leq 6000\, A/cm$$

$$\Rightarrow L_{crit} \leq \frac{6000\, A/cm}{1 \times 10^6\, A/cm^2} = 6.0 \times 10^{-3} cm = 60 \mu m.$$

In summary, for a current density of 1×10^6 A/cm^2 flowing through an aluminum-alloy conductor, the electromigration-induced damage should be relatively small for conductors of length less than 60 um. This assumes, of course, that the conductor is adequately constrained by the covering dielectric layer(s) so that the *backflow stresses* can develop fully and thus retard the void growth. If the voiding is in the form of a very thin slit-like void, the back-flow stress may not be strong enough to prevent EM failure. For this reason the most conservative design approach is to assume that $J_{crit} = 0$.

Example Problem 11.2

Under typical Al-alloy electromigration testing conditions, the stress current densities are $J^{(e)}_{stress} \sim 1 \times 10^6 \text{A/cm}^2$ and the length of test structures is L $\sim$1000 μm. Under these stress conditions, show that $J^{(e)}_{crit}$ is much smaller than $J^{(e)}_{stress}$ and therefore can be safely neglected during electromigration testing.

Solution

The Blech relation gives for Al-alloys:

$$\left(J^{(e)} \bullet L\right)_{crit} \leq 6000\, A/cm$$

[9] For Al-alloys, stripe widths of approximately 3 μm are typically used for EM testing.

$$\Rightarrow J_{crit}^{(e)} \leq \frac{6000\,A/cm}{1000\mu m} \bullet \left(\frac{1\mu m}{10^{-4}cm}\right) = 6 \times 10^4\,A/cm^2.$$

Therefore, typically during electromigration testing, $J_{crit}^{(e)} << J_{stress}^{(e)} \sim 10^6$ A/cm^2 and can usually be safely neglected. Since the Blech constant A_{Blech} for Cu (1000–4000 A/cm) is typically smaller than for Al-alloys, then $J_{crit}^{(e)}$ is usually smaller for Cu versus Al-alloys.

Example Problem 11.3

Under accelerated electromigration testing of an Al-alloy, at a current density of $J_{stress} = 2 \times 10^6$ A/cm^2 and at a metal temperature of $T_{stress} = 200°C$, the EM data was found to be fitted well by a lognormal distribution with median time-to-failure of $t_{50} = 200$ hrs and a logarithmic standard deviation of $\sigma = 0.5$. Assuming an activation energy of $Q = 0.8$ eV and a current density exponent of $n = 2$, what is the maximum design current density J_{design} to produce fewer than 0.13% failures in 10 yrs at 105°C ?

Solution

Recall from Chapter 9 that:

$$AF = \frac{(TF)_{operation}}{(TF)_{stress}} = \left[\frac{J_{stress}}{J_{design}}\right]^2 \exp\left\{\frac{Q}{K_B}\left(\frac{1}{T_{design}} - \frac{1}{T_{stress}}\right)\right\}.$$

During stress, the time-to-fail for 0.13% of the devices (lognormal distribution from Chapter 6) is:

$$(TF_{0.13\%})_{stress} = \frac{t_{50}}{\exp(3\sigma)} = \frac{200hrs}{\exp[(3)(0.5)]} = 44.63hrs.$$

To last 10 yrs at 105°C, one will need an acceleration factor of:

$$AF = \frac{10yrs}{44.63hrs} = \frac{87600hrs}{44.63hrs} = 1962.8.$$

Solving the first equation above for J_{design}, one obtains:

$$J_{design} = J_{stress}\sqrt{\frac{\exp\left\{\frac{Q}{K_B}\left(\frac{1}{T_{design}} - \frac{1}{T_{stress}}\right)\right\}}{AF}}$$

$$= 2 \times 10^6 \frac{A}{cm^2} \sqrt{\frac{\exp\left\{\frac{0.8\,eV}{8.62 \times 10^{-5} eV/K}\left(\frac{1}{(105+273)K} - \frac{1}{(200+273)K}\right)\right\}}{1962.8}}$$

$$= 5.3 \times 10^5 \frac{A}{cm^2}\,.$$

In summary, based on the stated EM data and the planned use conditions for this metallization, the design current density should be restricted to approximately $J_{design} \leq 5.3 \times 10^5$ A/cm^2.

EM data is normally collected under DC conditions whereas the circuit operation is AC. This means that a method is needed to transform AC current densities into DC EM equivalents for design rule checking. For unipolar-current waveforms, $J^{(e)}$ can be taken as the average current density $< J^{(e)} >$. For bipolar current waveforms, a *sweepback* recovery action can take place and the effective current density $J^{(e)}$ has been described by $J^{(e)} = < J_+^{(e)} > - \mathrm{r} < J_-^{(e)} >$, where $< J_+^{(e)} >$ is the average of the positive polarity pulses and $< J_-^{(e)} >$ is the average of the negative polarity pulses.[10] The recovery coefficient r has a reported value of at least 0.7. While bipolar waveforms permit much more allowed current density to flow for EM reasons, one needs to be careful with Joule heating and limit Jrms.

Electromigration associated with vias must be investigated separately because they show characteristics which are different from single leads fed by bonding pads. For example, vias can show different degradation rates depending on electron current flow direction [upper level of metal (M2) to lower level of metal (M1) may be quite different versus M1 to M2]. Also, the degradation rate is strongly dependent on via structure (barrier layer, capping layer, and via etching), via number, layout, and a reservoir effect[11] can be present.

For Al-alloy stripes, terminated by bonding pads and having no barrier metallization, the total time-to-failure is dominated by nucleation and n is observed to be equal to 2 (which is commonly referred to as the Black equation).[12] However, for Al-alloy stripes with barrier metal and terminated by tungsten plugs, one may see both an incubation (nucleation) period dominated by n=2 and a resistance rise (drift period) dominated by n=1 (as illustrated in Fig. 11.4). Also, under high current

[10] It is assumed here that the average of the positive pulses is greater than the average of the negative pulses.

[11] Tabs (extra metal extensions) at the cathode-end connection (acting as a reservoir/source of additional metal ions) can slow down the voiding rate and thus can improve the time-to-failure.

[12] Jim Black was the first to propose a current density exponent of n=2 for electromigration in Al-alloys, without barrier layers, where the void-nucleation phase tends to dominate the time-to-failure. However, n=2 is not valid for all metal systems, e.g., n=1 is used for Cu metallization.

density test conditions, unaccounted for Joule heating can produce apparent current density exponents much greater than n=2. Similar observations hold for Cu metallization, where a mixture of void nucleation and void growth contributions is often simultaneously present; however, the trend appears to be weighted more towards growth-controlled EM and n=1 is generally used for Cu. In summary, one may need to be a little cautious (as described in Chapter 8) when extrapolating highly accelerated data to the expected operating conditions.

IC metallization must be used to make contact to shallow (<0.25um) n+ and p+ junctions in CMOS technologies. Being able to build stable/reliable contacts necessitates that a barrier metal be used between the interconnect metal and the shallow junction. Some common barrier metals often used are TiW, TiN and TaN. During contact electromigration transport, the dominant diffusing species which causes contact failure is reported to be silicon from the contact region. In addition to the barrier type being important, silicided junctions can also be important relative to retarding the transport process.

Eq. (11.2) can also be used to describe IC contacts (metal to silicon or silicide) failure due to electromigration. Here, however, the diffusing species which leads to failure is generally the silicon. Contact electromigration failure occurs when a *buildup* of silicon occurs in the contact window (assuming that silicon is in the aluminum-alloy metallization initially) leading to resistive contact formation; or, an erosion of silicon from the contact window can lead to junction leakage and failure. Since the current crowding can be severe in a shallow contact, the actual current density is non-uniform over the contact window and may be very difficult to specify. For this reason, normally the contact area is incorporated into the process-dependent prefactor A_o and the time-to-failure equation is usually written as:

$$TF = A_o\, I^{-n} \exp\left(\frac{Q}{K_B T}\right), \tag{11.3}$$

where, I is the current flowing into or out of the contact window during EM testing.[13] For aluminum-alloy to silicon contacts, the reported values of activation energy are generally in the range 0.8–0.9 eV. For silicided ($TiSi_2$, $TaSi_2$) contacts the values are higher 1.1–1.5 eV. Due to the extreme localized nature of the self heating during contact stressing, the values for n have been reported to be as low as 1 and as high as 11.[14]

[13]The current I, as used here, is a *virtual stress* (discussed in Section 8.4) because TF depends strongly on the dimensions of the contact. The use of a *real stress*, such as current density J(=I/Area), would normally be preferred. However, due to current crowding effects in the small contact window, the current density is very non-uniform and difficult to describe. For this reason, the virtual stress current I is used.

[14]Joule (or self) heating can be an important issue for contacts. Even though the ambient temperature may be held constant, the actual contact temperature can vary greatly with the current level applied. If the self heating is not properly accounted for, then very high *apparent n* values are obtained.

11.2 Stress Migration (SM)

Mechanical stress-related failures are very important for IC devices. When a metal is placed under a mechanical stress which exceeds its yield point, the metal will undergo *plastic deformation* with time.[15] This time-dependent phenomenon is described by metallurgists as *creep*. The creep will continue until the stress level is brought below the yield point or until the metal fails. This metal failure mechanism is especially important for ICs where one is confronted with: on-chip aluminum-alloy or copper metallization, gold ball-bonds and wires, iron-alloy or copper lead-frames, solder joints, etc.

Stress migration in ICs is the term used to describe the flow of metal atoms under the influence of mechanical stress. Generally this failure mechanism is driven by creep (under a fixed-strain condition) and, as such, it is a stress-relief mechanism for the metallization on the chip.[16] This stress-relief mechanism (resulting in void formation in the IC metallization) will generally continue until the mechanical stress in the metallization is relieved below its yield point (as discussed in Chapter 12).

11.2.1 SM in Aluminum Interconnects

Actually, mass flow occurs due to stress gradients in the material, not simply due to the applied stress in the material. Usually the stress gradients are assumed to be proportional to the applied mechanical stress σ. The source of this stress σ can be intrinsic and/or thermomechanical stress.

Relatively little permanent atom movement occurs until the stress σ exceeds the yield point of the metallization. The flux of the moving metal atoms is primarily along grain boundaries as illustrated in Fig. 11.7, but may also occur within a grain if the metal lead is very narrow and the grain structure can be considered *bamboo-like*.[17]

The inevitable flux divergence associated with the metal movement can cause notching and voiding to occur in IC metal leads/stripes (see Fig. 11.8).[18] The resistance rise associated with the void formation can cause electrical failures. The time-to-failure (TF) due to creep is described by

$$TF = A_o \, \sigma^{-n} \, Exp\left(\frac{Q}{K_B T}\right), \tag{11.4}$$

[15] This is normally referred to as *plastic* (versus *elastic*) deformation. Elastic deformations tend to produce no damage to the material while plastic deformations tend to cause some amount of permanent change to the material.

[16] Generally, metals will tend to flow in order to relieve the stress in the material. Unfortunately, such mass flow can result in notching/voiding in the metal.

[17] Grain boundaries which are nearly perpendicular to the metal stripe length.

[18] As discussed in Chapter 12, the strain energy reduction/release is greater than the energy increase associated with the creation of new surfaces.

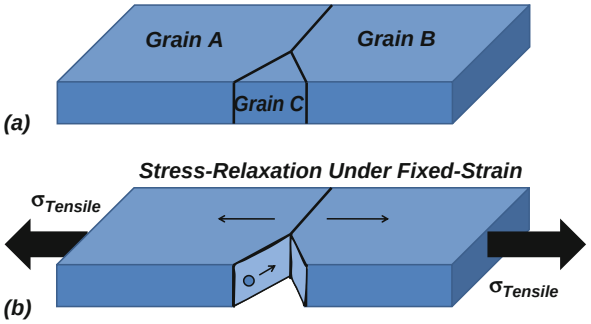

Fig. 11.7 Mechanical stress-gradients can cause metal atoms to flow (creep) in an effort to relieve the stress energy. The small grain C, with high specific-energy grain boundaries as illustrated in (a), may be absorbed by grains A and B to facilitate the stress relaxation shown in (b). As for Cu, the dominant diffusion paths may be along Cu/barrier interfaces.

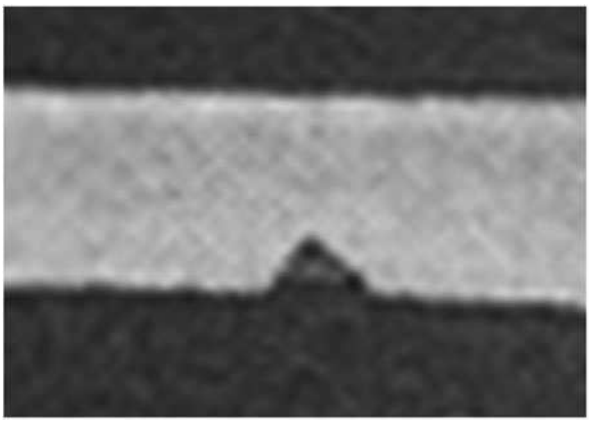

Fig. 11.8 Stress migration has served to produce notching/voiding in the Al-alloy metal lead shown.

where:

σ is the tensile stress in the metal for a constant strain;[19]
n is the stress migration exponent. $n = 2-4$ for soft metals such as aluminum and copper, $n = 4-6$ for mild steels, and $n = 6-9$ for very strong/hardened metals; and
Q is the activation energy. Q ≈ 0.6 – 0.8 eV for grain-boundary diffusion in aluminum, Q ≈ 1 eV for within-grain (bamboo-like) diffusion in aluminum.

[19]The metallization on a chip is constrained (fixed strain) due to the hard dielectrics surrounding the metallization. The creep, in this case, is a stress-relaxation mechanism under fixed strain which can lead to void formation.

For *on-chip* metallization, the dominant mechanical stress is generated by thermal-expansion mismatch of the metal and the constraining surrounding materials. For this reason, the stress is referred to as *thermomechanical stress* and σ is proportional to the change in temperature, i.e.

$$\sigma \propto \Delta T. \tag{11.5}$$

Therefore, if the metal creep is caused by thermomechanical stress, then the time-to-failure, Eq. (11.4), can be expressed by:[20]

$$TF = A_o\,(T_0 - T)^{-n}\,Exp\left(\frac{Q}{K_B T}\right) \tag{11.6}$$

where:

T_0 is defined as the stress-free temperature for the metal.[21]

The role of stress and stress relaxation is very important in the nucleation and growth of voids in aluminum-alloy interconnects. Cu doping in the aluminum is somewhat effective in suppressing grain-boundary diffusion, but is much less effective if the grain size is large compared to line width. In these *bamboo-like* leads, one observes *slit-like void* formation due to intra-grain diffusion.

To test for SM, typically long (> 1000 μm) and narrow stripes (< 2 μm width) are stored at temperatures in the range 150–200°C for 1–2 Khr and then electrically tested for resistance increases (or reduction in breakdown currents).[22] The SM baking temperature should be carefully selected because, as predicted from Eq. (11.6), there is a maximum in the creep rate (as illustrated in Fig. 11.9). This generally occurs in the 150–200°C range and serves to drive a minimum in the time-to-failure Eq. (11.6). This maximum in the creep rate occurs (because of competing mechanisms as discussed in Chapter 2) due to the high stress (but low mobility) at lower temperatures, and low stress (but high mobility) at high temperatures. Because the mechanical stress is temperature dependent, a straightforward determination of the diffusion activation energy is somewhat difficult to obtain. Generally, Q∼0.5–0.6 eV is used for grain-boundary diffusion and ∼1 eV for single-grain/bulk-diffusion.

The use of refractory metal barriers or layered metallization has tended to greatly reduce the impact of the damage caused by slit-like void formation in bamboo leads.

---

[20]This equation is usually referred to as the *McPherson and Dunn Model* for stress migration in interconnects.

[21]The prefactor ($T_0 - T$), in Eq. 11.6, can be expressed in °C or K, since this is a difference of two temperatures. However, the temperature in the exponential term must be expressed in K.

[22]The breakdown current is determined by ramping the current to breakdown. If the metal stripe has a notch/void in it, then the breakdown current should be lower.

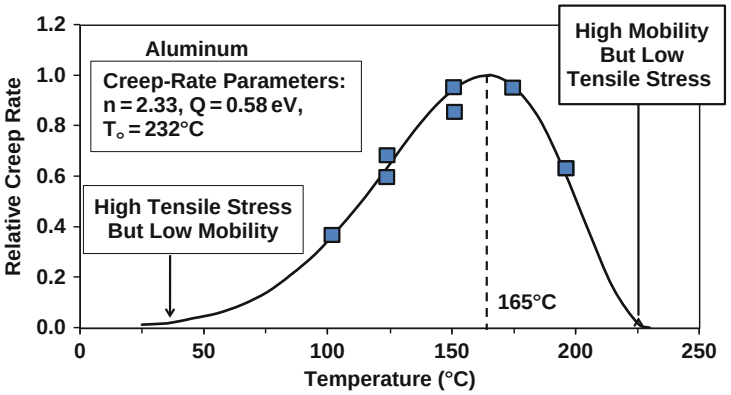

Fig. 11.9 Stress migration induced creep/voiding rate has a maximum at a critical temperature (which is generally in the 150–200°C range for Al-alloys). This maximum in the creep/voiding rate occurs because of the low mobility (but high stress) at lower temperatures and low stress (but high mobility) at elevated temperatures.

This is because the refractory metal layer tends to serve as a redundant conductor, shunting the current and reducing the electrical resistance rise when a SM-induced void forms.

11.2.2 SM in Cu Interconnects

Stress migration in Cu metallization (see Fig. 11.10) is also a concern, despite an expectation that Cu's generally superior EM capabilities would translate to significantly improved stress migration performance.

Similar to a comparison between Al and Cu EM, as it pertains to its use in advanced IC technology, the contrasting fabrication methods used for Cu versus Al generate pronounced differences in the type of stress migration issues that are found in the different metallizations. A basic difference between Cu and Al lies with their different melting points: 1083°C versus 660°C, respectively. Normal processing temperatures during integrated circuit fabrication can be as high as 400°C, which is a substantial fraction of the melting temperature of Al but to a lesser degree for Cu. Hence, the processing of Al metallization can lead to grains that are large and well-formed within interconnect wiring (so-called *bamboo* structure for narrow metal leads)—but similar processing temperatures do not greatly alter the microstructure of Cu after it has reached a certain level of stability. Therefore, the grain structure within Cu interconnect wiring is much more varied, both grain size-wise and texture-wise. Electroplated Cu also greatly impacts the evolved microstructure such that narrow lines remain small grained whereas wider lines develop larger grains.

Like Al stripes, Cu stripes can show evidence of SM-induced voiding; however, because of the presence of a somewhat redundant metal barrier and the lack of sufficient bamboo character to the Cu grains, its general impact on reliability may not

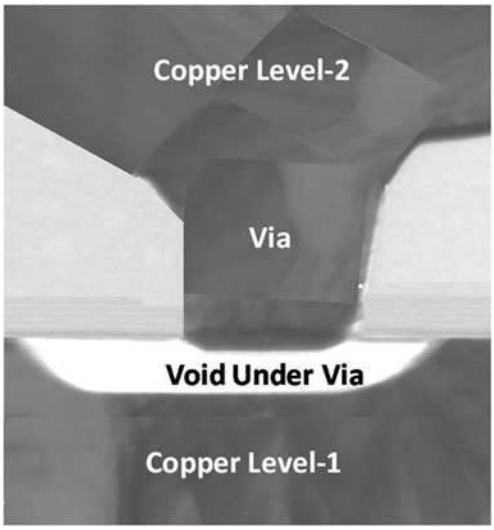

Fig. 11.10 Stress-induced voiding under a single via in a copper interconnect system. Wide Cu lines are servicing the via.

be quite as strong. However, when a void forms under or within *vias*,[23] as shown in Fig. 11.10 and illustrated in Fig. 11.11, the reliability impact can be substantial, especially when the via is an electrically *weak link* along the interconnect path. This via-voiding impact is felt most severely when wide leads are placed over and/or under single vias.[24] As indicated by the voiding illustrated in Fig. 11.11, once a void is nucleated, an ample supply of vacancies can be provided within wide Cu leads to enlarge the void, within the via or under a via, and enable very resistive or open-circuit formation.

Void growth continues until the local stress is relaxed below its yield point. Baking (or annealing) data is shown in Fig. 11.12 for single vias to wide Cu-lead test structures. The Cu-via baking data, similar to aluminum metallization previously discussed [refer to Fig. (11.9)], shows that a maximum occurs in via failure rate (creep rate). The critical temperature (150–200°C) at which the maximum occurs is roughly independent of the resistance rise used to define TF.

The resistance-rise data in Fig. 11.12 is indicative of the voiding/creep rate. Thus, fitting the stress-migration data in Fig. 11.12, using the McPherson and Dunn creep/voiding rate model, one obtains:

[23] On a chip, there can be several levels of metallization, stacked on top of one another with a layer of dielectric in between metal levels. The *via* is an electrical connection, through the dielectric layer(s), from an upper metal level to a lower metal level.

[24] The voiding is a stress-relief mechanism as discussed in Chapter 12. Void growth occurs because of vacancy flow due to stress gradients. More vacancies are available in wide Cu-leads versus narrow ones.

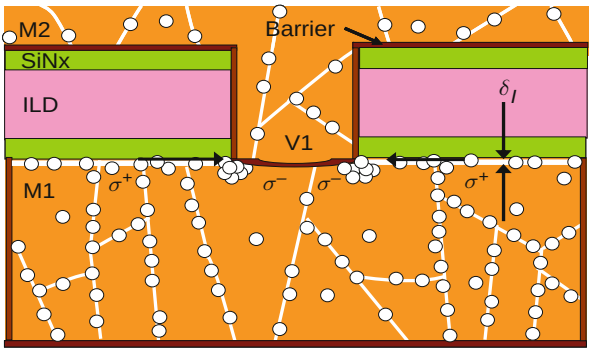

Fig. 11.11 Due to the fact that at least some of the plated Cu annealing during processing is done while the Cu is fully constrained by the barrier layers and dielectric layers, the Cu metallization becomes super-saturated with vacancies along grain boundaries and interfaces. These vacancies can move under presence of stress gradients and generally flow from tensile regions to compressive regions. Voiding under/within via is a stress-relief mechanism.

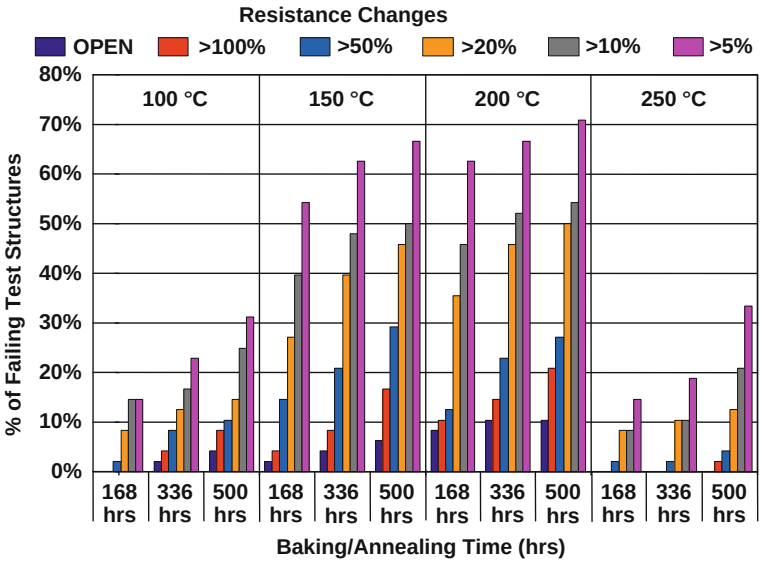

Fig. 11.12 Baking/annealing data is shown for single-via to wide Cu-lead test structures. These stress migration results show that a maximum occurs in voiding rate (creep rate) at a critical temperature in the range between 150 and 200°C. This critical temperature is independent of the resistance rise failure criteria used.

$$Creep\ (Voiding)\ Rate = B_o\ (T_o - T)^n\ \exp\left[-\frac{Q}{K_B T}\right], \tag{11.7}$$

where: stress exponent n = 3.2, an activation energy of Q = 0.74 eV, and a stress free temperature for the Cu of T_o = 270°C. The maximum in the creep/voiding rate occurs at a temperature close to T_{crit} = 190°C. The fitting is shown in Fig. 11.13.

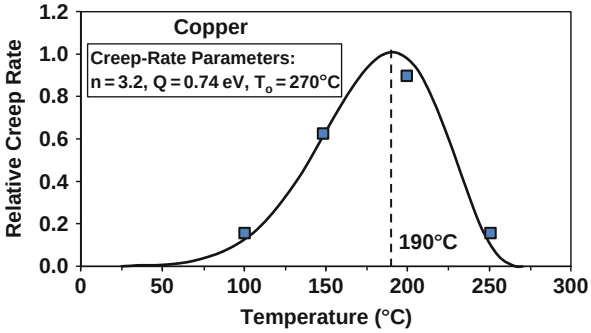

Fig. 11.13 Fitting of the relative creep-rate data (extracted from Fig. 11.12) produces the kinetic parameters: stress dependence exponent of n = 3.2, an activation energy of Q=0.74eV and a stress free temperature of 290°C. The maximum in the creep/voiding rate occurs at: T_{crit} = 190°C.

Example Problem 11.4

Show that if the creep rate [Eq. (11.7)] has a maximum in it, then the three kinetic parameters (n, Q, T_o) are not independent and must obey the equation:

$$Q = nK_B\left(\frac{T_{crit}^2}{T_o - T}\right).$$

Also show that the best fitting parameters (shown in Fig. 11.13) do indeed satisfy this equation.

Solution

One can easily show that if $R(T)$ has a maximum at $T = T_{crit}$, then ln[$R(T)$] also has a maximum at $T = T_{crit}$.

Proof

For a maximum to exist in R(T) *then it is necessary that:*

$$\left(\frac{dR}{dT}\right)_{T=T_{crit}} = 0.$$

*If we investigate ln[*R(T)*], one obtains:*

$$\left(\frac{d\ln[R(T)]}{dT}\right)_{T=T_{crit}} = \left[\frac{1}{R}\left(\frac{dR}{dT}\right)\right]_{T=T_{crit}} = \frac{1}{R(T_{crit})}\left(\frac{dR}{dT}\right)_{T=Tcrit} = 0.$$

Therefore, if R(T) has a maximum in the function at $T = T_{crit}$, then $\ln[R(T)]$ will also have a maximum at $T = T_{crit}$. Taking the natural logarithm of both sides of the Eq. (11.7), one obtains:

$$\ln[R] \;=\; \ln(B_o) \;+\; n\ln\left(T_o - T\right) \;-\; \frac{Q}{KT}.$$

Taking the derivative, and evaluating at $T = T_{crit}$, one obtains:

$$\left(\frac{d\ln[R(T)]}{dT}\right)_{T=T_{crit}} \;=\; 0 \;=\; -\frac{n}{T_0 - T_{crit}} \;+\; \frac{Q}{K_B T_{crit}^2},$$

giving

$$Q = nK_B\left(\frac{T_{crit}^2}{T_o - T_{crit}}\right).$$

Finally, we check to see if the best fitting parameters, shown in Fig. 11.13, actually satisfy this equation:

$$Q = nK_B\left(\frac{T_{crit}^2}{T_o - T_{crit}}\right) = 3.2(8.62\times 10^{-5} eV/K)\left(\frac{[(190+273)K]^2}{(270+273)K - (190+273)K}\right)$$
$$= 0.74\, eV$$

This activation energy agrees well with the best fitting activation energy Q = 0.74 eV shown in Fig. 11.13.

11.3 Corrosion

Corrosion failures can occur when ICs are exposed to moisture and contaminants. IC corrosion failures are usually classified as one of two broad groups: *bonding-pad corrosion* or *internal-chip corrosion*. The *bonding pad* is a rather large piece of on-chip metallization on the order of 50 μm × 50 μm. These bonding pads, historically, have provided the metallization contact surface for eventual Au or Cu-wire ball bonding (refer to Figs, 11.14, 11.20 and 11.21). This wire bonding permits electrical connection of the chip to the outside world. Bonding-pad corrosion

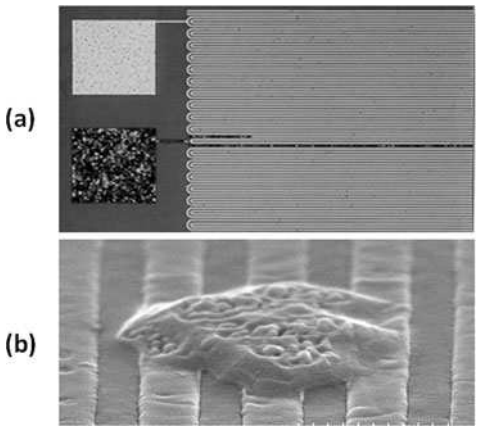

Fig. 11.14 (a) Corrosion of aluminum bonding pads can occur if chlorides and moisture are present. Grounded (Vss) pads are especially sensitive to corrosion. (b) Exposed Cu stripes can corrode during processing in the time window between post-CMP Cu-clean and cap-layer dielectric deposition. The volume of the corrosion product, usually $Cu(OH)_2$, can be much larger than the volume of Cu consumed.

can occur during die processing and/or post *assembly*[25]. Bonding pads that are connected/grounded to the silicon substrate [see Fig. 11.14(a)] are especially sensitive to corrosion. Bonding pad corrosion is usually more common (than internal chip corrosion) simply because the die-level passivation (often either silicon nitride or oxynitride) does not cover the bonding-pad metallization. Furthermore, any residual chlorides from aluminum and/or protective overcoat etching, plus moisture, can cause Al corrosion.[26]

Internal corrosion (internal to the chip, away from the bonding pads) can also occur if some weakness or damage exists in the die passivation layer which could permit moisture and contaminants (e.g., chlorides) to reach the exposed metallization. The internal corrosion can cause electrical discontinuities at localized regions of die.

Corrosion can be generally described in terms of a *corrosion cell*.[27] The corrosion cell must have four key components in order for corrosion to occur: an *anode* (a region for the *oxidation reaction* to occur), a *cathode* (a region for the

[25] *Assembly* describes the process used to encapsulate a silicon chip into plastic packaging with electrical connections to the outside world. This process includes: silicon chips are first separated from the wafer (usually by sawing), chips are then attached to a lead frame, the lead frame is then molded in plastic, and finally the leads are trimmed and formed.

[26] If Al corrosion occurs in a liquid state, the corrosion may have the appearance of simply missing aluminum. If Al corrosion occurs in humidity/moisture, the corrosion product (usually aluminum hydroxide) can be expansive in size and will appear to be black, under an optical microscope, due to its very rough/cracked texture. The volume of the corrosion product, usually $Al(OH)_3$, can be much larger than the volume of Al consumed.

[27] The corrosion cell is discussed in more detail in Chapter 12.

reduction reaction to occur), an *electrolyte* (through which the ions can diffuse), and a *conductor* to provide a pathway for the electron flow from the oxidation region to the reduction region. An example of *wet corrosion* is shown in Fig. 11.15. Metal corrosion (oxidation) can occur if there is an imperfection in the *native oxide* covering the metallization.

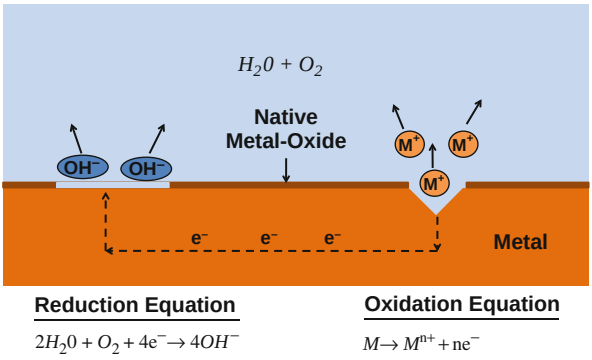

Fig. 11.15 Wet corrosion generally occurs with low activation energy because of the very high mobility of the diffusing ions in water. The ions must be able to diffuse away from the anode/cathode region for the corrosion cell to continue to work. In water, this diffusion process is relatively easy.

Generally, Al forms a good self-passivating oxide and it is much less corrosive than Cu, even though the *Galvanic Series*[28] would suggest just the opposite. However, if chlorides and moisture are present, then the Al_2O_3 native oxide protecting the Al can be quickly reduced. Once the native oxide is reduced, exposing a highly reactive virgin metal surface, the corrosion can proceed rapidly.

In order for the corrosion to continue at a rapid rate, the ions must be able to diffuse rapidly to and from the regions of oxidation/reduction.[29] This can occur most easily in liquids because the activation energy for diffusion in a liquid is generally very low ~0.3 eV. However, for *dry* or *ambient* corrosion [see Fig. 11.16] the activation energy for diffusion is generally higher and the corrosion rate is very dependent on the percentage relative humidity (%RH). In fact, the surface mobility on oxide has been found to be exponentially dependent on %RH over a rather wide range of %RH. With the surface mobility limited by the %RH, as illustrated in Fig. 11.16, then the time-to-failure is expected to be limited by the humidity. Also, an expansive corrosion product $M(OH)_n$ can develop.

During IC wafer processing, Cu-ions (which are produced during oxidation at some location in the circuit) can diffuse away from this region of oxidation and then may *plate out* again at other locations in the circuit. In Fig. 11.17, we show a Cu-via

[28] The Galvanic Series is discussed in Chapter 12.

[29] If the ions cannot diffuse away from the region of oxidation/reduction, then a rise in electrical potential will retard the corrosion potential.

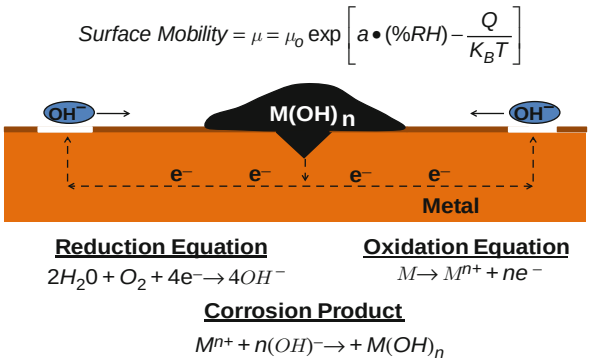

Fig. 11.16 Ambient corrosion has a very strong humidity-dependence and an expansive corrosion product $M(OH)_n$ can develop. The percentage relative humidity (%RH) has a great impact on surface/interface mobility. The ions have to be able to diffuse from the anode/cathode regions for the corrosion cell to work. Otherwise, the buildup of localized ions will create an electrical potential that will tend to offset the chemical corrosion potential.

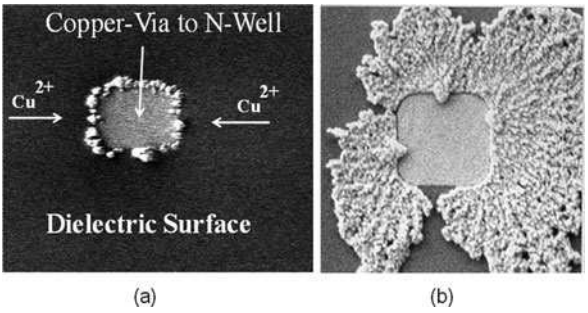

Fig. 11.17 Generally, immediately after chemical-mechanical polishing (CMP) of the plated Cu on a wafer, the exposed Cu is susceptible to oxidation. The oxidation of the Cu (in other parts of the circuit not shown) serves to free Cu-ions which can then diffuse across the dielectric surface. (a) If a grounded node (such as the Cu-via to an N-well connection shown above) can be found, then a reduction/re-plating of the Cu-ions can occur resulting in the unwanted Cu-nodules, as are shown in early stages in (a). The later stages are shown in (b).

(Cu-via contacted to a W-plug) to n-well. Since this is, in effect, a grounded Cu-via, any free Cu-ions on the surface of the dielectric can diffuse and plate out by reduction at these grounded locations: $Cu^{2+} + 2e \rightarrow Cu$. One can see in Fig. 11.17(a) the Cu-plated nodules at the perimeter of the grounded Cu via and how this region will continue to grow with time as shown in Fig. 11.17b. This is quite interesting. It should be emphasized that the Cu, which was originally electrochemically plated and chemically-mechanically polished, is now being re-plated by a secondary oxidation and reduction reaction.

The relative corrosion activities for Copper and Aluminum are shown in Fig. 11.18 as a function of applied voltage. The strong native oxide (Al_2O_3) on aluminum serves as a self-passivation layer and the corrosion activity for Al is relatively

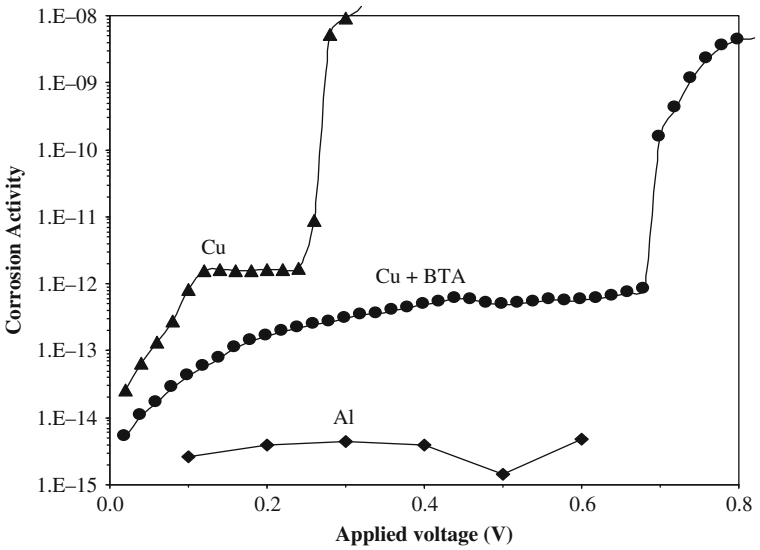

Fig. 11.18 Corrosion activity is shown as a function of applied voltage. The corrosion activity of the Cu is much higher than Al. The corrosion activity of the Cu can be reduced by adding thin protective layers such as BTA during processing.

low and is nearly independent of the applied voltage (from 0 to 0.8 V). However, the native oxide (Cu_xO_x) on copper is of relatively poor quality and does not protect the exposed copper—and a higher *corrosion activity*[30] is observed. In order to reduce the corrosion activity of the exposed Cu, corrosion inhibitors are generally used. BTA (benzotriazole:$C_6H_5N_3$) is a commonly used corrosion inhibitor which is added during chemical mechanical polishing (CMP) of the Cu to reduce post-CMP corrosion. The BTA serves to reduce the corrosion activity of the Cu to manageable levels during processing. However, even with the use of corrosion inhibitors, it is good practice to establish a tight processing *time window* between CMP processing of the Cu and dielectric barrier deposition in order to minimize corrosion.

To monitor the corrosion susceptibility of packaged chips, the industry generally uses one or more of three standard corrosion tests. These three tests have been widely used to accelerate potential IC corrosion failure mechanisms: biased 85°C and 85%RH, autoclave (121°C and 100%RH), and highly accelerated stress test (HAST) conditions (typically biased, 130°C and 85%RH). To extrapolate packaged-chips corrosion results, under highly accelerated conditions to use conditions, at least three models have been used.

[30]Corrosion activity was measured by monitoring the resistance-rise versus time, for a metal stripe when the test structure was stored in an ammonium-chloride solution.

11.3.1 Exponential Reciprocal-Humidity Model

The time-to-failure equation for IC failure due to corrosion is

$$TF = A_o \exp\left(\frac{b}{RH}\right) \exp\left(\frac{Q}{K_B T}\right), \tag{11.8}$$

where:

A_0 is a process/material dependent parameter and serves to produce a distribution of times-to-failure (Weibull or lognormal distributions),
b is the reciprocal humidity dependence parameter (approximately equal to ~300 %),
RH is the relative humidity expressed as a %[31], and
Q is the activation energy (approximately equal to 0.3 eV for phosphoric acid induced corrosion of aluminum and generally consistent with wet corrosion.[32]

This model was developed when phosphosilicate glass (PSG) was used for interconnect dielectric and/or passivation.[33] Too much phosphorus (> 8%) in the glass and the phosphorus would precipitate onto the glass surface and along its interfaces. With the addition of moisture, this would cause phosphoric acid to form which would attack the metallization.

11.3.2 Power-Law Humidity Model

The time-to-failure equation for IC failure due to corrosion is

$$TF = A_o \ (RH)^{-n} \exp\left(\frac{Q}{K_B T}\right), \tag{11.9}$$

where:

n is the power-law exponent and equal to 2.7,
RH= % relative humidity, and
Q is the activation energy and equal to 0.7–0.8 eV for chloride-induced corrosion of aluminum.

[31] 100% relative humidity represents saturated water vapor.

[32] This low value of activation energy (0.3 eV) is typical for wet corrosion mechanisms where the mobility of the diffusing ions is good. Due to a very high concentration of phosphorus in the PSG, liquid droplets of phosphoric acid can develop under humid conditions.

[33] The phosphorus in the glass is very useful in gettering unwanted sodium ions. The Na-ions, if present, can induce a surface-inversion failure mechanism. The surface-inversion failure mechanism is discussed in Section 11.6.

This model was developed for chloride-induced corrosion in plastic-packaged chips. Chlorine-based dry etches are generally used for the aluminum-alloy metallizations. If excessive amounts of chlorides are left on the die after post-etch cleanups, corrosion can occur with the addition of moisture.

11.3.3 Exponential Humidity Model

The time-to-failure equation for integrated circuit failure due to corrosion is

$$TF = A_o \exp(-a \bullet RH) \exp\left(\frac{Q}{K_B T}\right), \tag{11.10}$$

where:

a is the humidity acceleration parameter and is equal to 0.10–0.15 $(\%\text{RH})^{-1}$,
RH is the % relative humidity, and
Q is the activation energy and is equal to 0.7–0.8 eV for chloride-induced corrosion of aluminum in plastic packages.

This corrosion model was developed when it was shown that, over a wide range of humidity (20–80%), the surface conductivity is exponentially dependent on the humidity, as shown in Fig. 11.19.

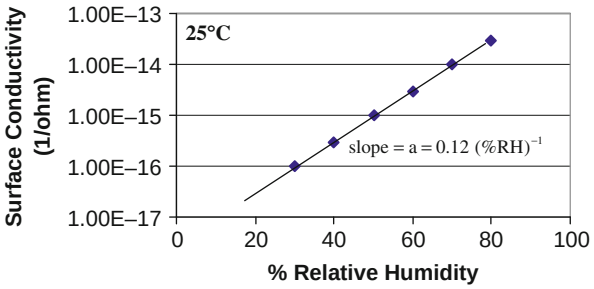

Fig. 11.19 The surface conductivity for SiO_2 over a wide range of humidity was observed to be exponentially dependent on the % relative humidity. An exponential acceleration parameter of $a = 0.12\ (\%\ RH)^{-1}$ was observed.

There seems to be reasonably good consensus that the proper activation energy for chloride-induced aluminum corrosion is in the 0.7–0.8 eV range. There is not a consensus for the humidity dependence. A comparison of the three models for the same data set tended to show some preference for the exponential model with a ~0.10–0.15 $(\%\text{RH})^{-1}$. However, the power-law model is a widely used corrosion model in the IC industry for plastic-package chips.

Example Problem 11.5

For an ambient relative humidity of 40% in a wafer fab, it was established that the longest corrosion-free time (time window) that a Cu metallization could be exposed to the ambient conditions was 4 hrs. If the humidity due to a clogged filter increases the relative humidity from 40 to 50%RH, what would the new time window be?

Solution

$$AF = \frac{(TF)_{40\%RH}}{(TF)_{50\%RH}} = \exp\left[a \bullet (50\%RH - 40\%RH)\right]$$

Assuming that $a = 0.12(\%\mathrm{RH})^{-1}$, then

$$AF = \exp\left[0.12(\%RH)^{-1}\,(50\%RH - 40\%RH)\right] = 3.32$$

Therefore, the time window becomes:

$$(TF)_{50\%RH} = \frac{(TF)_{40\%RH}}{AF} = \frac{4hrs}{3.32} = 1.2hrs.$$

In summary, by the humidity going from 40 to 50% RH, the safe (corrosion free) processing time window for the metallization reduced from 4hrs to 1.2hrs.

11.4 Thermal-Cycling/Fatigue Issues

Each time that assembled Si-chips are powered up and down, the assembled chips undergo a *thermal cycle*. Thermal cycling can induce important *fatigue*[34] failure mechanism for fully assembled chips. As shown in Fig. 11.20, the thermal expansion mismatch of the diverse materials used on the chip and during assembly can result in significant thermomechanical stresses. These thermomechanical stresses, and the cyclical nature of the power up and power down of the devices, can generate fatigue failures. For example, the lifted bonding ball shown in Fig. 11.21 resulted from thermomechanical stress during temperature cycling. The thermomechanical stress (generated by the thermal expansion coefficient mismatch of the: plastic molding compound, gold bonding ball, Au-Al intermetallics, Al pad, and silicon chip)

[34]Fatigue failure can result from cyclical stresses as discussed in Chapter 12.

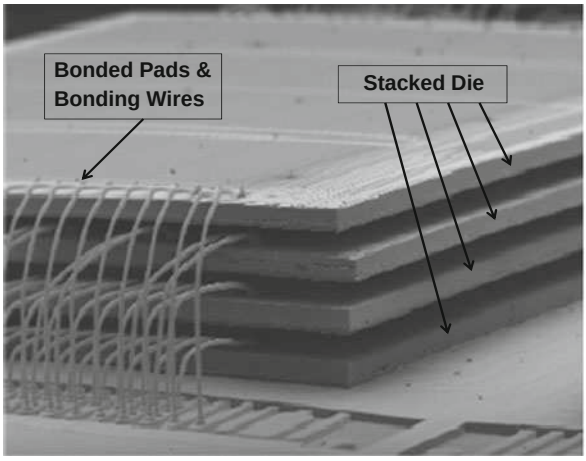

Fig. 11.20 Shown is a multiple-die stack with the on-die bonding pads, ball bonds to these pads and the ball wires. The individual die/chips are separated by adhesives. This ensemble of stacked-die will be eventually encapsulated in plastic for handling. Thus, the thermal expansion mismatch of dissimilar materials is ever-present during temperature cycling of the assembled die.

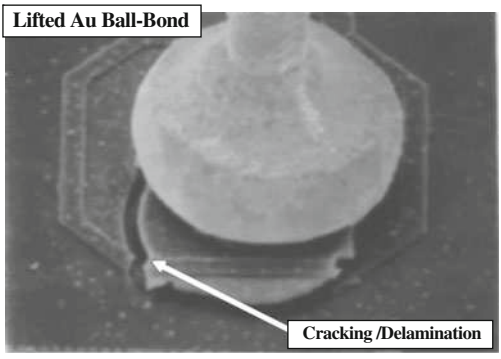

Fig. 11.21 Au ball-bond, originally bonded to an aluminum bonding pad on the die, has become detached during temperature cycling. The facture under the ball-bond is clearly evident in the micrograph.

served to weaken the bond during thermal cycling and eventually led to failure of the ball-bond attachment.

Thermal cycling of a device will naturally occur each time the assembled chips undergo a normal power-up and power-down cycle. Such thermal cycles can induce a cyclical thermomechanical stress that tends to degrade the materials, and may cause a host of potential failure modes: dielectric/thin-film cracking, lifted ball-bonds, fractured/broken bond wires, solder fatigue, cracked die, etc.

The thermomechanical stresses during thermal cycling can be very large due to the large thermal expansion mismatch that exists between the silicon, on-chip dielectrics and metallization, leadframe, and the plastic molding compound used for chip encapsulation. Thus, to accelerate thermal cycling failure mechanisms, the assembled chip(s) may be accelerated by using temperature cycling ranges outside the normal range of operation and then recording the number-of-cycles-to-failure. Some commonly used accelerated temperature cycling ranges for ICs include: $-65°C/150°C$, $-40°C/140°C$, and $0°C/125°C$.

As for modeling, one can assume that each thermal cycle generates plastic deformation which serves to damage the materials, as illustrated in Fig. 11.22. For ductile materials, low-cycle fatigue data is described rather well by the Coffin-Manson model:[35]

$$CTF = A_o \left(\Delta\varepsilon_p\right)^{-s}, \tag{11.11}$$

where:

CTF is the number of cycles-to-failure,
$\Delta\varepsilon_p$ is the plastic strain range[36], and
s is an empirically determined exponent.

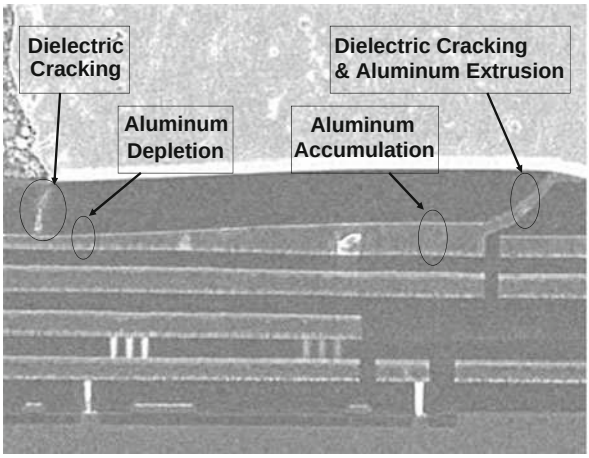

Fig. 11.22 Thermomechanical stresses during temperature cycling can cause plastic deformation and fatigue damage to on-chip metallization and their interfaces. Temperature cycling can also accelerate crack propagation in more brittle dielectric materials. The aluminum (in top layer metal) has shifted from left to right during temperature cycling. The accumulation of Al became so great that the surrounding dielectric cracked, thus permitting an Al extrusion to occur.

Low-cycle fatigue usually refers to stress conditions that only require a few hundred (or few thousand) cycles to produce failure. High-cycle fatigue usually refers to stress conditions which may require hundreds of thousands of cycles to produce failure.

During a temperature cycle, not all of the entire temperature range ΔT may be inducing plastic deformation. If a portion of this range ΔT_0 is actually in the elastic

[35] Coffin-Manson model is discussed in more detail in Chapter 12.

[36] The plastic strain range is outside the normal elastic region. Damage is occurring to the material in the plastic range.

range, then this should be subtracted and one can write a modified Coffin-Manson equation as:

$$\Delta\varepsilon_p \propto (\Delta T - \Delta T_o)^{\beta}. \tag{11.12}$$

Thus, for temperature cycling, the Coffin-Manson equation becomes:

$$CTF = A_o (\Delta T - \Delta T_o)^{-q}, \tag{11.13}$$

where q is an empirically-determined exponent. If the elastic range (ΔT_0) is much smaller than the entire temperature cycle range (ΔT), then it may be dropped without significant error being introduced. However, one should always question the assumption as to whether (ΔT_0) is an insignificant part of total thermomechanical stress range (ΔT).

As illustrated in Fig. 11.23, fatigue can also occur in brittle materials due to crack propagation.

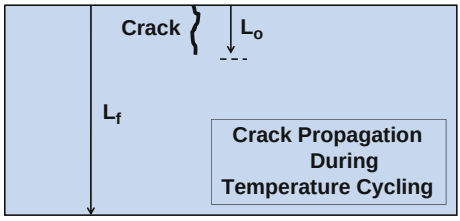

Fig. 11.23 Thermomechanical stress, during temperature cycling, can cause crack propagation (fatigue damage) for brittle materials and their interfaces.

Normally there are three distinct phases to brittle material failure: a crack-initiation phase (which usually exists at time zero), a crack growth phase (which tends to dominate the number of cycles to failure), and a catastrophic failure phase which is typically of relatively short duration.[37] Since the crack growth phase is of greatest duration (dominates the number of cycles to failure), the modeling effort is usually focussed on this phase. Experimentally one finds that the crack growth rate (increase in crack length per cycle) is dependent on the length of the existing crack and on the applied cyclical stress so, one can write:

$$\frac{dL}{dN} = C(\sigma_a)^m L^n, \tag{11.14}$$

where L is the crack length, N is the number of cycles, σ_a is the applied cyclical stress, m and n are empirically determined exponents. Separating the variables and integrating gives:

[37] Additional information on crack propagation can be found in Chapter 12.

$$CTF = \left[\frac{1}{C}\right]\left[\int_{L_o}^{L_f} \frac{dL}{L^n}\right](\sigma_a)^{-m} = B_o(\sigma_a)^{-m}. \tag{11.15}$$

In the previous equation, it is clear that B_o is a function of crack size (the initial crack size L_o and how large a crack is needed to produce failure L_f). Since B_o will vary from device to device, B_o causes CTF to actually become a cycles-to-failure distribution with either the lognormal or Weibull distribution preferred to describe the statistical data.

Since the cyclical stress is assumed to be thermomechanical, $\sigma_a \propto \Delta T$, then cycles-to-failure becomes:

$$CTF = A_o(\Delta T)^{-q}, \tag{11.16}$$

which is very similar to Eq. 11.13 for ductile materials. Thus, while the Coffin-Manson model was originally developed for ductile materials (metals), it has also been successfully applied to brittle materials with the appropriate selection of exponents as summarized in Table 11.1.

Table 11.1 Temperature-Cycling Exponents.

Material	Temp-Cycle Exponent
Soft Metals (Solder, Aluminum, etc.)	q=1–3
Hard Metals / Intermetallics	q=3–6
Brittle Materials (Dielectrics)	q=6–9

In summary, temperature cycling failures for integrated circuits can be described reasonably well by the modified Coffin-Manson equation. The equation works rather well even for brittle materials, where failure is dominated by crack growth rather than simple plastic deformation (which was assumed in the development of the original Coffin-Manson equation).

Example Problem 11.16

During a temperature cycling stress test of packaged die/chips, it was determined that the units were able to pass 500 cycles of temperature cycling from −65°C to 150°C but started to fail at 600 cycles. Failure analysis indicated that the failure mechanism was lifted ball-bonds due to fractured intermetallics (intermetallic region between the Au-ball and the Aluminum bonding pad). Assuming that the full thermomechanical stress range of −65°C to 150°C is in the plastic-deformation region for the intermetallic, and a cycling exponent of n=4, estimate how long the parts should survive for use conditions of 0 to 85°C.

Solution

Assuming that the entire thermomechanical stress range is in the plastic-deformation region for the intermetallic layer and that the temperature cycling exponent is n=4 for intermetallics, then the acceleration factor becomes:

$$AF = \frac{(CTF)_{0-85°C}}{(CTF)_{-65-150°C}} = \left[\frac{(\Delta T)_{-65-150°C}}{(\Delta T)_{0-85°C}}\right]^4 = \left[\frac{150°C-(-65°C)}{85°C-0°C}\right]^4 = 40.9.$$

Therefore, the cycles-to-failure CTF, for 0–85°C, becomes:

$$(CTF)_{0-85°C} = AF \bullet (CTF)_{-65-150°C} = (40.9) \bullet (500cyc) = 20,450cyc.$$

Assuming that the device is temperature cycled from 0 to 85°C, on average 4 times a day, then the time-to-failure TF becomes:

$$TF = \frac{20,450cyc}{4cyc/day} \bullet \left(\frac{24hr}{1\,day}\right) \bullet \left(\frac{1\,yr}{8760hr}\right) = 14\,yr.$$

11.5 Time-Dependent Dielectric Breakdown (TDDB)

Due to the very high operating electric fields in the gate dielectric of MOSFET devices, time-dependent dielectric breakdown (TDDB) can be an important IC failure mechanism. Usually after a relatively long period of degradation (bond-breakage/trap-creation) as illustrated in Fig. 11.24(a), the dielectric eventually undergoes breakdown (a catastrophic thermal runaway condition due to severe current flow). This localized current density and associated severe Joule heating can result in a conductive filament forming in the dielectric shorting the *poly*[38] gate to the substrate (thus shorting anode and cathode) in the MOSFET device [see Fig. 11.24(b)].

Historically, there are two TDDB models which have been widely used to describe the time-dependent dielectric breakdown failure mechanism in oxides. One model is field-driven (E-Model) while the other is current-driven (1/E - Model).

[38]Poly is short for polycrystalline silicon. Doped-poly has been a common electrode material for MOSFETs for many years. Advanced ICs may use metal gate-electrodes.

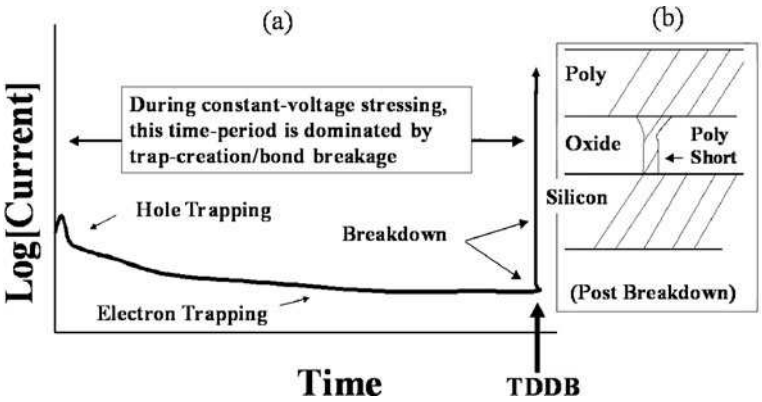

Fig. 11.24 a) Dielectric degradation occurs due to broken-bonds/trap-creation in the dielectric material and at the SiO_2/Si interface. b) The trapping of the holes initially and then followed by electron trapping continues up to the point of catastrophic breakdown whereby the localized Joule heating produces a melt-filament shorting the poly-gate and silicon-substrate. In very thin dielectrics (<10 nm), the pre-breakdown leakage may show a stress-induced leakage current increase prior to breakdown of the dielectric. Also, hyper-thin dielectrics (<4 nm) can show soft-breakdown characteristics.

11.5.1 Exponential E-Model

In the thermochemical *E-Model*,[39] the cause of low-field (< 10MV/cm) and high temperature TDDB is due to field-enhanced thermal bond-breakage. In this model, the field serves to stretch polar molecular bonds thus making them weaker and more susceptible to breakage by standard *Boltzmann (thermal) processes*. Since the field reduces the activation energy required to break a bond then the degradation rate is expected to increase exponentially with field.

Time-to-failure occurs when a localized density of broken bonds (or percolation sites) becomes sufficiently high to cause a conductive path to form from anode to cathode.

The time-to-failure equation, which is the inverse of degradation rate, decreases exponentially with field,

$$TF = A_o \exp(-\gamma E_{ox}) \exp\left(\frac{Q}{K_B T}\right), \tag{11.17}$$

where :

γ is the field-acceleration parameter,

[39]The E-Model was originally introduced as an empirical model and was later given a theoretical thermochemical foundation.

E_{ox} is the electric field in the oxide and is given by the voltage dropped V_{ox}[40] across the dielectric divided by the oxide thickness t_{ox},
Q is the activation energy (enthalpy of activation), and
A_o is a process/material dependent coefficient that varies from device to device and causes TF to acturally become a times-to-failure distribution, usually a Weibull distribution.

Many investigations have shown that γ is temperature dependent and that it can be described rather well by a simple 1/T dependence:

$$\gamma(T) = \left[\frac{\partial \ln(TF)}{\partial E}\right]_T = \frac{p_{eff}}{K_B T}. \tag{11.18}$$

The effective dipole moment p_{eff} is related to the amount of polar bonding in the molecule and is given by:

$$p_{eff}(m, n) = (z^* e)\, r_0\, \eta(m, n)^{-1} \left(\frac{2+k}{3}\right), \tag{11.19}$$

where: z^* is the effective charge transferred from the silicon-ion to its four oxygen-ion bonding neighbors [z^*=4(0.6)=2.4], r_o is the equilibrium bonding distance [r_o=1.7 Å], η is related purely to the bonding parameters in the Mie-Gruneisen bonding potential [$\eta(9, 1)^{-1}$=1.67][41], and the dielectric constant for SiO_2 is 3.9 [giving (2+k)/3 =1.97]. Thus, for the (9,1) bonding potential one obtains a value of $p_{eff} = 13.4$eÅ. If the bonding is less ionic and more covalent, then $\eta(9, 2)^{-1} = 0.93$ and produces a $p_{eff} = 7.5$eÅ .

p_{eff} is generally found to be from TDDB data in the range of 7–14eÅ[42] for SiO_2, but can be much larger for higher dielectric-constant k materials (as indicated by Eq. (11.19). The *1/T* dependence for γ, as given by Eq. (11.18), serves to drive an observed/effective activation energy that is field dependent. Using Eqs. (4.15, 11.17, 11.18), one obtains an effective activation energy which reduces linearly with the electric field,

$$Q_{eff} = Q - p_{eff}\, E_{ox}, \tag{11.20}$$

where:

Q_{eff} is the effective activation energy (eV) and
Q is the activation energy for Si-O bond breakage in absence of external electric field.

[40]For MOS-type capacitors on silicon, when stressing in accumulation: $V_{ox} \cong V_{applied} - 1V$. Whereas, when stressing in inversion: $V_{ox} \cong V_{applied}$.

[41]The values for η(m, n) can be found in Chapter 12.

[42]This range is consistent with effective dipole moments: $p_{eff}(9, 2)$ to $p_{eff}(9, 1)$.

The observed value of γ may not necessarily be temperature dependent if several types of disturbed bonding states are present and participating in the dielectric degradation process under high-field and/or high-temperature TDDB testing. Generally, however, for silica-based dielectrics with thicknesses > 40 Å and tested at 105°C, one generally finds that $\gamma \sim 4.0$ cm/MV and Q ~1.8 eV are observed during TDDB testing. Thus, if TDDB testing is done at 10MV/cm or greater, then according to Eq. (11.20) the expected activation energy is: $Q_{eff} \leq 1.8\,eV - (13e\overset{\circ}{A})(10\,MV/cm) = 0.5\,eV$. Thus, when TDDB testing is done at fields above 10MV/cm, the observed activation energy will generally be $\leq 0.5\,eV$. When TDDB testing is done at fields lower than 10MV/cm, the observed activation energy is generally greater > 0.5 eV.

11.5.2 Exponential 1/E - Model

In the *1/E* Model for TDDB (even at low fields) damage is assumed to be due to current flow through the dielectric due to Fowler-Nordheim (F-N) conduction. Electrons, which are F-N injected from the cathode into the conduction band of SiO_2, are accelerated toward the anode. As the electrons are accelerated through the dielectric, because of impact ionization, some damage to the dielectric might be expected. Also, when these accelerated electrons finally reach the anode, hot holes can be produced which may tunnel back into the dielectric causing damage (hot-hole anode-injection model). Since both the electrons (from the cathode) and the hot holes (from the anode) are the result of F-N conduction, then the time-to-failure is expected to show an exponential dependence on the reciprocal of the electric field, 1/E,

$$TF = \tau_o(T) Exp\left[\frac{G(T)}{E_{ox}}\right], \tag{11.21}$$

where:

$\tau_o(T)$ a temperature dependent prefactor, and
$G(T)$ is a temperature dependent field acceleration parameter for the 1/E Model .

The temperature dependence of G has been expressed as a 1/T power-series expansion given by,

$$G = \left[\frac{\partial \ln(TF)}{\partial(1/E)}\right]_T = G_o\left[1 + \left(\frac{\delta}{K_B}\right)\left(\frac{1}{T} - \frac{1}{300\,K}\right)\right], \tag{11.22}$$

where:

$$\delta = \left(\frac{K_B}{G_o}\right)\left[\frac{dG}{d(1/T)}\right]_{300\,K}, \tag{11.23}$$

and where the derivative is evaluated at 300 K. At room temperature, G_o ~ 350 MV/cm and δ ~0.017 eV. τ_o(T) is usually also represented as 1/T expansion,

$$\tau_o(T) = \tau_o Exp\left[\left(\frac{-Q}{K_B}\right)\left(\frac{1}{T} - \frac{1}{300\,K}\right)\right], \tag{11.24}$$

where: $\tau_o \sim 1 \times 10^{-11}$ sec and Q ~0.3 eV.

11.5.3 Power-Law Voltage V-Model

For SiO_2 dielectrics which are hyper-thin (< 40 Å), a power-law voltage model has been proposed for TDDB of the form:

$$TF = B_o(T)[V]^{-n}. \tag{11.25}$$

As we have discussed before, normally one prefers to use a *real stress* such as electric-field E (where time-to-failure TF, for a fixed field E, is approximately independent of the thickness of the dielectric). But, *V* as used here is a *virtual stress* (since time-to-failure TF at a fixed voltage *V* depends strongly on dielectric thickness). However, the argument has been made that for ballistic transport (no scattering or energy loss in these hyper-thin dielectric films) the amount of energy which is actually delivered to the anode is simply $(e) \times (V)$.

For hyper-thin oxide films, the observed exponent is generally in the range: n=40–48.

11.5.4 Exponential $\sqrt{E}$-Model

Current-induced dielectric degradation and TF models assume that the degradation is due to current flow through the dielectric. For high quality SiO_2, the dominant current flow is nearly always Fowler-Nordheim conduction and thus the damage is assumed to follow a 1/E Model. However, for other dielectrics, or even poor quality SiO_2 dielectrics (such as low-k interconnect dielectrics), the conduction mechanism may be Poole-Frenkel or Schottky conduction. Thus, based on current-induced degradation, one might expect a TF model of the form,

$$TF = C_o(T)\exp\left[-\alpha\sqrt{E}\right], \tag{11.26}$$

where the root-field acceleration parameter α is given by:

$$\alpha = -\left[\frac{\partial \ln(TF)}{\partial\sqrt{E}}\right]_T. \tag{11.27}$$

11.5.5 Which TDDB Model to Use?

Since the physics of each of the TDDB models seems to be quite different, then it is only natural to ask the question — *which model should one use?* That is probably too difficult of a question to try to answer in this text, because there seems to be no universal agreement (the physical arguments for each model seem to be reasonable). However, one can certainly ask the question — *what is the relative ranking of the models in terms of their conservatism*? This question does have an answer and it is illustrated in Fig. 11.25. When the models are used to fit the same set of accelerated TDDB data, the E-Model gives a shorter time-to-failure TF, as one extrapolates from high-field accelerated TDDB conditions to lower-field use conditions. This makes the E-Model the more conservative model. In terms of relative rank of conservatism: E-Model is the most conservative, followed by $\sqrt{E}$-Model, then the V-Model and finally the 1/E -Model.

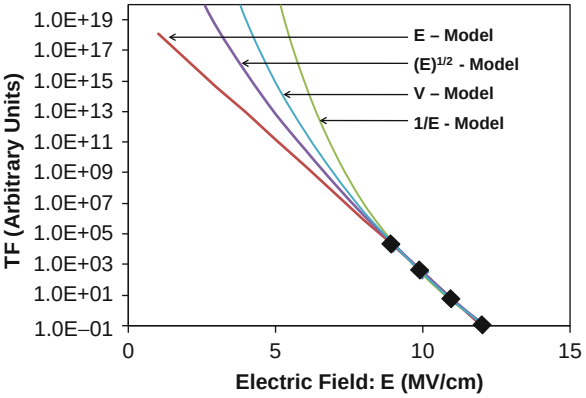

Fig. 11.25 Shown are the four models best fittings to the same set of accelerated TDDB data. All the models tend to give a very good fitting to the four accelerated TDDB data points. However, their extrapolated results to lower electric fields are quite different. The E-Model gives the shortest time-to-failure when the results are extrapolated to lower electric fields. The 1/E-Model gives the longest time-to-failure at lower electric fields. One could describe the E-Model as being the most conservative and the 1/E-Model as being the most optimistic in their projections.

It should be noted that the *E*-Model TF, unlike 1/E and V-Models, does not go to infinity as the field *E* (or voltage) goes to zero. This is because the poly/oxide/silicon capacitor has been fabricated into a very highly-ordered structure which is metastable, as discussed in Chapter 8. Thus, we expect this metastable state will degrade with time, even when the electric field (or voltage) is zero. Therefore, the electric field simply serves to accelerate this natural degradation process. When the electric field goes to zero, the natural degradation/diffusional-processes still exist which will degrade the dielectric quality and will eventually cause failure, even though it may take hundreds or thousands of years in the absence of electric field.

Example Problem 11.7

In a high-reliability application, capacitors were made of a silica-based dielectric of thickness 90 Å. During accelerated testing at 9 V, the dielectrics started to fail in 5 sec at 105°C. How long would the capacitors be expected to last at 5 V?

Solution

Since this is a high-reliability application, we will use a conservative TDDB model like the E-Model. In the E-Model, the field acceleration parameter γ is given by:

$$\gamma(T) = \frac{p_{eff}}{K_B T} \cong \frac{13e\overset{\circ}{A}}{(8.62 \times 10^{-5} eV/K)(105 + 273)K} \bullet \left(\frac{10^{-8} cm}{1\overset{\circ}{A}}\right)$$

$$= 4.0 \times 10^{-6} cm/V = 4.0\, cm/MV.$$

The acceleration factor for TDDB (using E-Model) becomes:

$$AF = \frac{(TF)_{5-Volts}}{(TF)_{9-volts}} = \exp\left[\gamma \bullet \left(\frac{9\,V}{t_{ox}} - \frac{5\,V}{t_{ox}}\right)\right]$$

$$= \exp\left[(4 \times 10^{-6} cm/V) \bullet \left(\frac{9\,V}{90 \times 10^{-8} cm} - \frac{5\,V}{90 \times 10^{-8} cm}\right)\right]$$

$$= 5.26 \times 10^{7}.$$

Therefore, one would expect that the capacitors would last at 105°C for:

$$(TF)_{5-Volts} = AF \bullet (TF)_{9-volts} = (5.26 \times 10^{7}) \bullet (5\,\text{sec}) = 2.63 \times 10^{8}\,\text{sec}$$

$$= (2.63 \times 10^{8}\,\text{sec}) \bullet \left(\frac{1hr}{3600\,\text{sec}}\right)\left(\frac{1\,yr}{8760hr}\right)$$

$$= 8.3\,yrs.$$

Example Problem 11.8

For the capacitors in Example Problem 11.7, what is the maximum design voltage which should be used for these capacitors, if one wants them to last at least 15 years at 105°C?

Solution

The caps lasted 5 sec at 9 V, but we need them to last a minimum of 15 yrs. Thus, we need an acceleration factor of at least:

$$(AF)_{needed} = \left(\frac{15\,yr}{5\,\text{sec}}\right) \bullet \left(\frac{3600\,\text{sec}}{1hr}\right) \bullet \left(\frac{8760hr}{1\,yr}\right) = 9.46 \times 10^7.$$

However, the acceleration factor is also given by:

$$AF = \frac{(TF)_{V-design}}{(TF)_{9-volts}} = \exp\left[\gamma \bullet \left(\frac{9\,V}{t_{ox}} - \frac{V_{design}}{t_{ox}}\right)\right],$$

Solving for V_{design} one obtains:

$$\begin{aligned} V_{design} &= 9\,V - \frac{t_{ox}}{\gamma}\ln(AF) \\ &= 9\,V - \frac{90 \times 10^{-8} cm}{4 \times 10^{-6} cm/V}\ln(9.46 \times 10^7) \\ &= 4.87\,V. \end{aligned}$$

Therefore, to last at least 15 yrs at 105°C, the maximum design voltage for this 90 Å silica-based dielectric is $\leq$ 4.87V.

11.5.6 Complementary Electric-Field and Current-Based Models

There have been several attempts to include both field-induced degradation and current-induced degradation into a single TDDB model with some degree of success. These modeling efforts permit both field-induced and current-induced dielectric degradation mechanisms to occur simultaneously, in parallel fashion, during the TDDB testing. If it is assumed that the root cause of TDDB is bond-breakage/trap-creation, then let us look at the bond-breakage rate equation,

$$\frac{dN}{dt} = -kN(t), \tag{11.28}$$

where N is the number of Si-O bonds in the region of interest and k is the bond-breakage rate constant. Separating variables in the above equation and integrating, one obtains:

$$\int_{N_o}^{N_{crit}} \frac{dN}{N} = -k \int_0^{TF} dt, \tag{11.29}$$

giving,

$$TF = \frac{\ln(1/f_{crit})}{k}, \tag{11.30}$$

where $f_{crit} = (N/N_o)_{crit}$ is the critical fraction of bonds that must be broken to produce failure. It is believed that only a relatively few of the total number of bonds must be broken to cause TDDB, thus f_{crit} is expected to be only slightly less than one.

Now let us assume that the total reaction rate constant k is the sum of two independent bond breakage mechanisms: $k = k_1 + k_2$. The total reaction rate becomes:

$$\begin{aligned} k = k_1 + k_2 &= \ln(1/f_{crit}) \left[\frac{1}{(TF)_1} + \frac{1}{(TF)_2} \right] \\ &= \ln(1/f_{crit}) \left[\frac{(TF)_1 + (TF)_2}{(TF)_1 (TF)_1} \right]. \end{aligned} \tag{11.31}$$

Combining Eqs. (11.30) and (11.31), one obtains:

$$TF = \frac{(TF)_1 (TF)_2}{(TF)_1 + (TF)_2}\,. \tag{11.32}$$

The above TF equation is valid for degradation mechanisms that are acting independently, but acting concurrently. One can see that if $(TF)_1$ is much greater than $(TF)_2$, then the time-to-failure TF is completely dominated by $(TF)_2$, and vice versa.

As for TDDB, let us assume that above E=10 MV/cm the current-based 1/E-Model physics (hole-catalyzed bond breakage mechanism) could be dominating the TDDB physics. Below E=10MV/cm, where anode hole-injection is relatively small, the field-based E-Model physics (thermal breakage of field-stretched bonds) could be dominating. Thus, a single time-to-failure equation (combining the physics of both the E-Model and 1/E-Model) would take the form:

$$TF = \frac{(TF)_{E-Model} (TF)_{1/E-Model}}{(TF)_{E-Model} \;+\; (TF)_{1/E-Model}}. \tag{11.33}$$

Shown in Fig. 11.26 is a single time-to-failure TF model, when both the field-based E-Model and the current-based 1/E-Model are combined into a single model.

Current-induced hole capture could serve to catalyze the bond breakage process,[43] thus playing an important role in TDDB. Hole capture can lead to a very strong Si-O bond suddenly becoming a much weaker bond. This weakened bond is now amenable to field enhanced thermal breakage. Also, a hydrogen-release model has been proposed to better explain the power-law *V*-Model (with an exponent of $n > 40$) used for time-to-failure. Both the hole-injection and the hydrogen-release models are expected to show a polarity dependence which is widely reported for hyper-thin(<4.0 nm) gate oxides. Also, the adverse effects of hydrogen on TDDB have been studied.

[43] Remember that a hole is simply a missing bonding electron. Hole capture thus eliminates one of the two electrons in the S-O bond. Therefore, hole capture serves to weaken the bond. Furthermore, the hole (if hot) can also bring energy to the bond to help in the bond-breakage process.

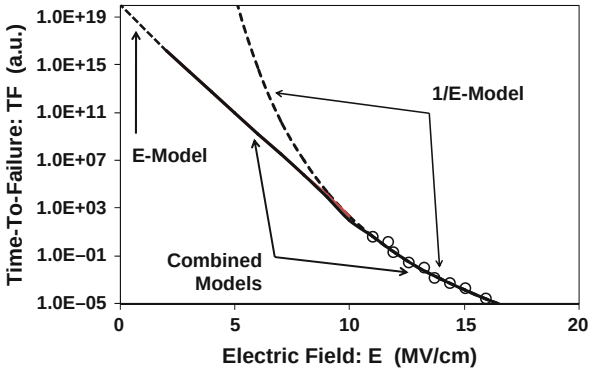

Fig. 11.26 E and 1/E Models are combined into a single time-to-failure model. It is believed that current–induced degradation may dominate at very high fields ($E > 10MV/cm$) while field-induced degradation may dominate at lower fields ($E < 10MV/cm$).

In summary, there has been great disagreement in the technical community as to the dominant degradation mechanism for low-field TDDB in SiO_2 thin films, i.e., is the major degradation mechanism related to current or field? Certainly hole capture and hydrogen release are relevant mechanisms and must be folded into any TDDB discussion. While the E-Model has been widely used and has been quite successful in describing low-field TDDB data for thick films > 4.0 nm, however, for very thin oxides (< 4.0 nm) the direct-tunneling current (ballistic transport) can be very high in these films and could mean that the degradation mechanism in hyper-thin oxide films is more controlled by current than field. In any case, as illustrated in Fig. 11.25, the E-Model is generally accepted as being the most conservative of the TDDB Models. The next most conservative model would be a complementary combination of the TDDB models, using the approach that was described by Eq. (11.32 and 11.33) and as illustrated in Fig. 11.26.

Also, TDDB should not be considered just a MOSFET gate-oxide or capacitor-oxide issue. The issue of TDDB has also been raised for interconnects (metallization plus surrounding/supporting dielectrics) with the introduction of low-k dielectrics.

TDDB data for interconnect dielectrics is normally taken using *comb-comb* or *comb-serpent* type test structures as illustrated in Fig. 11.27. While silica-based low-k dielectric materials enable significant performance gains at the interconnect level in terms of circuit delay reduction, they also possess substantially inferior electrical properties relative to gate-oxide dielectric quality in terms of leakage and breakdown strength.

Presently, minimum intra-metal spacing between adjacent interconnect stripes is approaching the physical dimensions of gate oxides (<100 nm) used a couple of decades ago. Hence, a discussion of which TDDB model to use is also pertinent to low-k dielectrics as well. Oxide-based low-k dielectrics have been shown to have inferior breakdown strength and significantly wider failure distributions under constant voltage stress. This is attributed to the presence of pre-existing defects in the

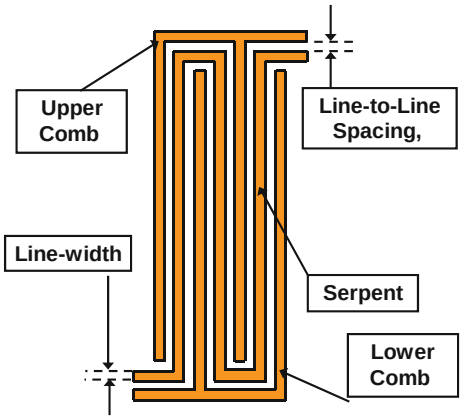

Fig. 11.27 Typical interconnect-dielectric test structure is illustrated. Shown is a comb-serpent type test structure with minimum pitch (minimum line-width plus minimum space). A simple breakdown strength measurement, or TDDB data, can be an indication of interconnect dielectric goodness.

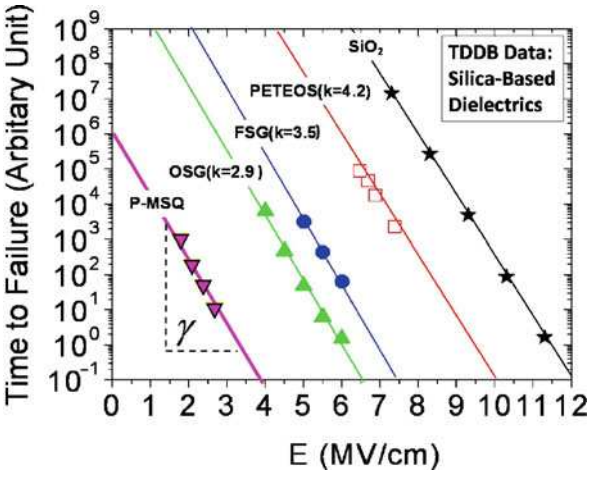

Fig. 11.28 Time-dependent dielectric breakdown (TDDB) data for various silica-based dielectrics at 105°C. The lower-k materials MSQ (k=2.3), OSG [SiCOH(k=2.9]), and FSG [SiOF(k=3.6)] generally have lower breakdown strength and time to failure. However, all of these silica based materials have a very similar E-Model field acceleration parameter of $\gamma \approx 4\ cm/MV$ (or a $p_{eff} \approx 13\ e$Å).

low-k dielectrics that scale roughly with the degree of porosity present within the low-k. Yet, as illustrated in Fig. 11.28, these low-k TDDB results indicate that the field acceleration parameter γ is similar for all of these silica-based materials: a field acceleration parameter of γ ~4 cm/MV at 105°C (giving an effective dipole moment p_{eff} ~13 eÅ).

A *pore* in the context of low-k porosity is defined as a localized region in the dielectric of low-polarizability. In this pore region weak bonds can exist and these can serve as charge traps. Percolation theory, along with the assumption of preexisting electrically active defects that scale with the degree of porosity, has been used to explain both the degraded breakdown strength and wider failure distributions with low-k dielectrics. Thus, the TDDB of the low-k materials should be assessed when using these low-k materials in an advanced integration scheme. Also, the contact to gate-edge spacing is presently only a few hundred Angstroms, similar to gate oxide thickness just a couple of decades ago. Thus, gate-to-contact TDDB should be considered.

11.6 Mobile-Ions/Surface-Inversion

Alkaline-metal elements such as Li, Na, and K can sometimes be found in the semiconductor processing materials. In SiO_2, these ions are very mobile under the presence of modest electric fields (~0.5 MV/cm) and temperatures (100°C). An accumulation of the drifted ions at the Si/SiO_2 interface (see Fig. 11.29) can cause surface inversion and can lead to increased leakage for isolation-type devices in silicon and eventual device failure.

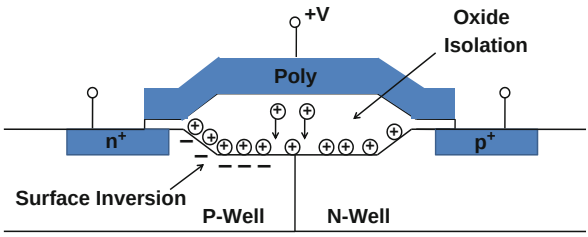

Fig. 11.29 If any mobile ions are in the dielectric, they can drift in the oxide isolation due to the presence of an electric field. Such mobile-ion drift can cause surface inversion in the P-well region. Surface inversion can result in a leakage-path creation from N-well to the adjacent n+ moat.

Sodium and potassium (and perhaps lithium) are the usual mobile-ion suspects, simply because of their high mobility and their relative abundance in some materials. Under bias, they can drift from the poly (anode) to the silicon substrate (cathode). A buildup of positive ions at the Si/SiO_2 interface can invert the surface and severely degrade the oxide isolation. Ionic drift in SiO_2 gate dielectric can also cause premature TDDB. In the case of EPROMs[44]/EEPROMs[45]/Flash-Memories[46], mobile-ion accumulation around the negatively-charged floating poly-gate can lead to data-retention fails.

Devices showing inversion-induced leakage failures can often recover during an unbiased high temperature bake. The bake causes a redistribution of the mobile ions from the accumulated Si/SiO_2 interface (or away from the floating poly in the case of an EPROM-like devices) and can bring about device recovery.

Since the mobile-ion flux is impacted by both electric field and temperature, the time-to-failure (TF) is usually described by

$$TF = A_o \, J_{ion}^{-1} \, Exp\left(\frac{Q}{K_B T}\right), \tag{11.34}$$

[44]EPROM is an erasable programmable read-only memory.

[45]EEPROM is an electrically erasable programmable read-only memory.

[46]Flash Memories are block-erasable EEPROMs.

where:

$$J_{ion} = \left\langle \left(\frac{D_o}{K_B T} \right) \rho \left[eE(t) \right] - D_o \frac{\partial \rho(x,t)}{\partial x} \right\rangle, \tag{11.35}$$

and where J_{ion} is the time-averaged flux of mobile ions. The first term on the right-hand side of Eq. (11.35) is the drift component, with E the externally applied electric field, D_o=diffusion coefficient and ρ=density of mobile ions. The second term is the *back-diffusion* component, and the brackets < > represent the time-averaged value of the time-dependent quantities enclosed. Note that if the field is turned off and the device is baked (an unbiased bake), the mobile ions will diffuse away from the interface and the device can recover. This is generally referred to as a bake-recovery failure mechanism. The activation energy Q depends upon the IC medium through which the ions must diffuse. For Na diffusion through silica-based dielectrics, device-failures tend to have an activation energy range from 0.75 to 1.8 eV, with 1.0 eV being typically used in modeling.

It is interesting to note that Cu-ions can be mobile in silica-based dielectrics, thus free Cu-ions under electrical bias are also a concern for interconnects. The loss of barrier integrity or the presence of Cu-related corrosion defects will lead to substantially degraded back-end dielectric reliability performance. Since many interfaces exist with Cu interconnect technology, relatively fast diffusion pathways always seemed to be available for any free Cu-ions. Since such defects are difficult to observe under use conditions, their statistical presence must be determined using accelerated test conditions and rapid tests such as ramped-breakdown testing.[47] Usually, Cu-ion drift under an electric-field is more of an interconnect TDDB issue than a surface inversion issue.

In summary, the activation energy for ion diffusion depends on: the diffusing species, medium through which the mobile ions diffuse, and the concentration of the ions. If the mobile-ion concentration is relatively low, and if deep interfacial traps exist, then one may see interfacial deep-traps that dominate with higher activation energy (∼1.8 eV) for Na+ diffusion noted. However, if the concentration of Na+ is relatively high, such that all deep interfacial traps are filled, leaving residual mobile Na+ ions to freely diffuse, then one may see lower activation energy (Q ∼0.75 eV).

11.7 Hot-Carrier Injection (HCI)

Channel *hot-carrier injection* (HCI) describes the phenomena by which electrons (or holes) can gain sufficient kinetic energy, as they are accelerated along the

[47] Ramped-to-breakdown testing was extensively discussed in Chapter 10. The ramp-to-breakdown test can be a very important test for interconnect dielectric reliability. Both intrinsic issues (low-k integrity) and extrinsic issues (metal/dielectric defects) can be found in a ramp-to-breakdown test at elevated temperature.

channel of a MOSFET (see Fig. 11.30), such that they can be injected over either the 3.1 eV barrier (for electrons) or 4.7 eV barrier (for holes) that exists at the Si/SiO_2 interface. The channel electrons, as they are accelerated from source to drain can acquire the needed energy for injection into the SiO_2, especially those *lucky electrons*[48] located near the *tail of the Boltzmann distribution*. These lucky electrons (or hot carriers)[49] are redirected toward the gate oxide as a result of impact ionization near the drain end of the MOSFET device where the channel electric field is the greatest. HCI serves to produce damage at the interface (interface-state generation).

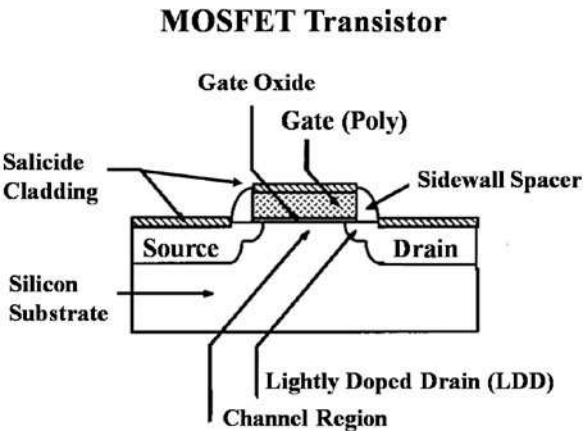

Fig. 11.30 Carriers traveling along N-MOSFET channel are accelerated from source to drain. These accelerated electrons reach kinetic energies well above their normal thermal energy $[(3/2)K_BT]$ and, as such, are referred to as hot carriers. Hot carriers can produce impact ionization near the drain end (where the electric field along the channel is greatest) causing some of the carriers to be redirected toward the gate oxide. These redirected (and energetic) electrons can interact with the normal bonding at the Si/SiO_2 interface and produce damage (create new interface states or fill existing ones). Interface-state generation usually results in device degradation (changes in critically important device parameters, e.g., V_t, gm, I_{drive}, etc.).

Interface-state generation and charge trapping by this HCI mechanism can result in transistor parameter degradation. This is an important degradation mechanism, especially for advanced technologies where the channel electric fields (which accelerate the carriers) have increased faster than the reductions in operating voltage. Thus, HCI can be an important MOSFET degradation mechanism. Since the MOSFET is a field-effect device, the interface between the silicon substrate and the SiO_2 gate dielectric is critically important. Usually device instabilities come about due to degradation (bond-breakage) at this interface. For this reason, a closer look at this interface is illustrated in Fig. 11.31.

[48] Lucky electron means that it obtains the maximum possible kinetic energy.

[49] These energetic electrons are referred to as *hot*, because their kinetic energy is greater than the average thermal energy $(3/2)K_BT$.

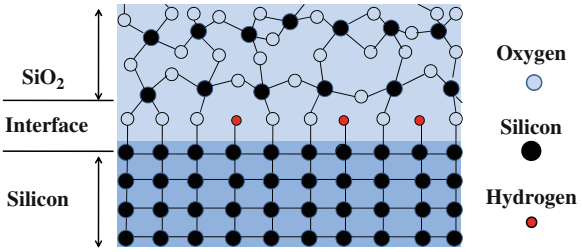

Fig. 11.31 Interface between the silicon substrate and the SiO_2 gate dielectric is illustrated. Silicon atoms in the silicon-substrate are four-fold bonded in a crystalline lattice. The SiO_2 layer is amorphous with the silicon four-fold bonded to neighboring oxygen (in a tetrahedral arrangement). The oxygen at the corners of each tetrahedron are two-fold bonded to neighboring silicon. Due to lattice mismatch at the interface, not all silicon bonds will be satisfied (creating dangling silicon bonds). Hydrogen is usually introduced during MOSFET fabrication, to chemically tie-up/terminate these dangling bonds and prevent them from being electrically active.

Silicon atoms in the silicon substrate are four-fold bonded in a crystalline lattice. The SiO_2 layer is amorphous with the silicon four-fold bonded to the neighboring oxygen (in a tetrahedral arrangement). The oxygen at the corners of each tetrahedron is two-fold bonded to neighboring silicon atoms. Due to the mismatch in lattice structure at the interface, not all silicon bonds will be satisfied (creating a silicon dangling bond). Hydrogen is usually introduced during MOSFET fabrication, in order to chemically tie-up/terminate these dangling bonds and to prevent them from being electrically active. The impact of Si-O and Si-H bond breakage, and its impact on time-dependent dielectric breakdown (TDDB) was discussed in Section 11.5 In this section and the next, we will focus on the impact that bond breakage at the Si/SiO_2 interface can have on MOSFET device stability.

Initially, after SiO_2 growth, there are likely to be at least some broken bonds, or at least some very weak Si-O bonds, in the bulk of the SiO_2 and at the Si/SiO_2 interface. Depending on the location of the *Fermi Level (Chemical Potential)*, these *dangling bonds*[50] can serve as electron traps, hole traps or remain neutral. If these dangling bonds thus charge during operation, then the MOSFET operational parameters can degrade. Interface stability can be extremely important for reliable MOSFET operation. If device operation serves to break the Si-H bonds at the interface, then the exposed Si-dangling bond may charge and degrade MOSFET operational parameters. Thus, the interface must remain relatively stable for the MOSFET device to be stable.

As discussed in Chapter 2 (Section 2.2), device-parameter degradation (induced by HCI) can be described by

$$\Delta P = B_o t^m. \tag{11.25}$$

[50]Normally, each Si-O bond has two electrons in it which are being shared. If the bond is broken (thus forming a dangling bond), depending on the *chemical potential (Fermi-level)*, a dangling bond can be neutral (retains a single electron), can become negative with the trapping of a second electron, or can give up its single electron (hole trap) and become positively charged.

where:

P is the parameter of interest (V_t, gm, I_{dsat}, etc.),
t is the time,
B_o is a material/device dependent parameter, and m is the power-law exponent for the time dependence.

As illustrated in Fig. 11.32 for N-channel MOSFETs, when the hot electron undergoes impact ionization near the drain-end of the device, holes are produced during the impact collision event which can be collected as substrate current I_{sub}. While it is gate current that produces the transistor damage, the substrate-current measurement is generally easier. Therefore, even though the substrate current is a *pseudo stress*, it is a good *proxy* for the actual stress (gate current).

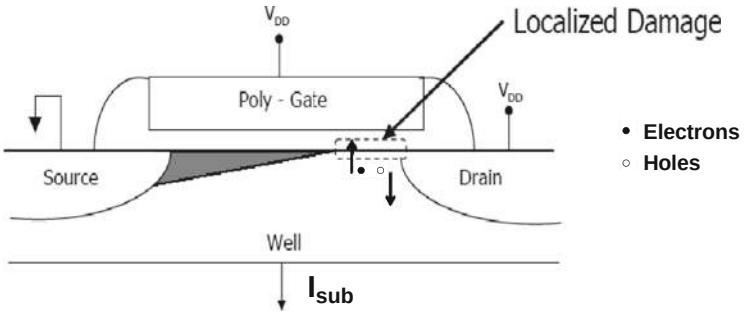

Fig. 11.32 As electrons are accelerated from source to drain, impact ionization at the drain end of the MOSFET can produce electron-hole pairs. Some of these energetic electrons will be re-directed toward the Si/SiO_2 interface. These energetic electrons are capable of producing interface damage in a localized region near the drain end. The holes (since they are majority carriers) are easily collected as substrate current. The substrate current is an indirect indicator of the HCI induced damage.

The peak I_{sub} current thus becomes an easy-to-measure indicator of the material/device stress that will be occurring during the channel hot carrier testing. The time-to-failure expression that is generally used for N-channel transistors is

$$TF = A_o \left(\frac{I_{sub}}{w}\right)^{-n} Exp\left(\frac{Q}{K_B T}\right), \tag{11.37}$$

where:

I_{sub} is the *peak substrate current*[51] during stressing,

[51] The gate voltage (Vgs) conditions must be determined that produce the maximum substrate current, for a fixed drain-to-source voltage Vds. For an n-type MOSFET, this could be Vgs = (1/2) Vds for n-type MOSFETs with longer channel lengths (>0.25um) but could be Vgs=Vds for devices with shorter channel lengths. In any case, the voltage conditions which produce the maximum substrate current must be established for the full range of expected device operation.

w is the width of the transistor,
n is the power-law exponent, approximately equal to 3, and
Q is the activation energy and is approximately −0.25 eV to +0.25 eV depending on channel length.
A_o is a device dependent parameter, which will vary from device to device and will produce a distribution of times-to-failure.

The peak substrate current I_{sub} has been divided by the transistor width w in an effort to make I_{sub}/w a *true stress* (a stress that is roughly independent of the device width, as discussed in Section 8.4.1). The activation energy for HCI is small, and can be positive or negative depending on channel length. The positive values for activation energy are generally observed only for gate lengths < 0.25 μm.

Example Problem 11.9

To better understand the hot carrier injection lifetime of an n-type MOSFET, a device was stressed for 1 hr at 7.5 volts and a 10% reduction in drive current was recorded. It was also recorded that the peak substrate current was 30 times higher at 7.5 V versus the expected 5.0 V operation. How long would it take to see a 10% reduction in drive current at the expected operation of 5.0 V?

Solution

Using Eq. (11.37), the acceleration factor becomes:

$$AF = \left[\frac{(I_{sub})_{@7.5\,V}}{(I_{sub})_{@5.0\,V}}\right]^3 = \left[\frac{30}{1}\right]^3 = 2.7 \times 10^4.$$

Therefore, the time-to-fail at 5.0 V versus 7.5 V becomes:

$$\begin{aligned} TF_{@5.0\,V} &= AF \bullet TF_{@7.5\,V} \\ &= (2.7 \times 10^4) \bullet 1hr \\ &= 2.7 \times 10^4 hr \left(\frac{1\,yr}{8760hr}\right) \\ &= 3.1 yrs. \end{aligned}$$

Historically, HCI for P-channel devices has been of lesser concern. This is generally true because of lower hole-mobility and the increase in barrier height for hole-injection. For P-channel devices, sometimes the gate current I_{gate} is the better indicator of the actual stress on the device. Thus, for P-channel devices the time-to-failure equation for HCI is usually written

$$TF = A_o \left(\frac{I_{gate}}{w}\right)^{-n} Exp\left(\frac{Q}{K_B T}\right), \tag{11.38}$$

where:

I_{gate} is the peak gate current during stressing,
w is the width of the transistor,
n is the power-law exponent and is generally from 2 to 4, and
Q is the activation energy, generally from −0.25 eV to +0.25 eV.

In summary, HCI-induced transistor degradation seems to be satisfactorily modeled by using peak substrate-current I_{sub} for the N-channels and peak gate-current I_{gate} for the P-channels, at least for transistors at > 0.25 μm. The drive current for the N-channel device tends to reduce after HCI stressing (i.e., HCI stressing tends to produce charge trapping such that it serves to increase the effective channel length for the N-channel device). The P-channel drive current tends to increase after HCI stress (i.e., HCI stressing tends to produce charge trapping such that the degradation serves to effectively shorten the channel length for the P-channel devices) and the off-state leakage can increase significantly.

While HCI-induced transistor degradation measurements and modeling seem to be quite accurate, the extrapolation from transistor degradation to circuit-level degradation is often difficult and makes IC time-to-failure predictions difficult. First, one must consider the actual fraction-of-time (duty cycle) that a transistor in an IC actually experiences the maximum/peak substrate current (or maximum gate-current) conditions. For fast switching transistors this can be less than 10% of the time. Second, how much transistor degradation (5%, 10%, 20%, or?) can the circuit tolerate before some critical circuit parameter (speed, power, leakage, etc.) starts to shift?

For the reasons listed above, sometimes it is easier and more precise to simply take an empirical approach to establishing the HCI impact at the circuit level. In this empirical approach one takes a sampling of the ICs and puts the sample on operational life test at an elevated voltage level (higher than expected operating voltage). The circuit-level degradation can then be recorded as a function of stress time. Using the acceleration factor, which is easily extracted from the above models, one can then find out how the circuit will be expected to degrade during normal operation.

11.8 Negative-Bias Temperature Instability (NBTI)

For a MOSFET device, as illustrated in Fig. 11.30, the stability of the Si/SiO_2 interface is of great importance. If the Si-H bonds at this interface become broken during device operation, as shown in Fig. 11.33, then the device properties will degrade and device failure can eventually occur.

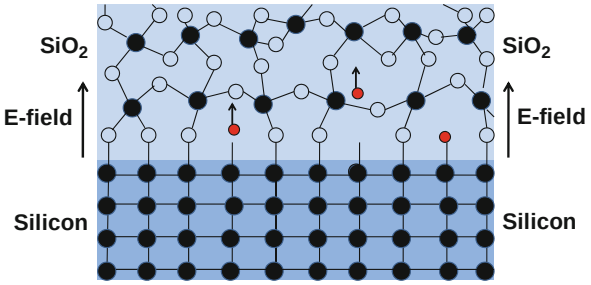

Fig. 11.33 Interface (Si/SiO_2) for a P-type MOSFET is illustrated. Since the P-type MOSFET operates with a negative gate voltage, the electric field in the SiO_2 layer is directed away from the interface. If a Si-H bond is broken during device operation, thus freeing an H^+ ion, the drift direction is away from the Si/SiO_2 interface.

In Fig. 11.33, the Si/SiO_2 interface is illustrated between the silicon substrate and the gate dielectric. Since the P-type MOSFET operates with a negative gate voltage, the electric field in the SiO_2 layer is directed away from the interface. If a Si-H bond is broken during device operation thus freeing an H+ ion, the drift direction is away from the Si/SiO_2 interface. This illustrates why negative-bias temperature instability for P-channel MOSFET is usually more of an issue than the sister problem of positive-bias temperature instability (PBTI) associated with an N-type MOSFET. However, PBTI can still be an issue when the dielectric is something other than SiO_2, e.g., high-k gate dielectrics.

The bond breakage mechanism is thought to be a result of hole capture by the Si-H bond during device operation. The degradation reaction is given by:

$$Si - H \quad + \quad (hole)^+ \quad \rightarrow \quad Si - \quad + \quad H^+, \tag{11.39}$$

where $Si - H$ represents a normal silicon-hydrogen bond, $Si -$ represents a silicon dangling bond, and H^+ represents a freed hydrogen ion (proton). Due to the electric field which is present, refer to Fig. 11.33, any hydrogen ions H^+ generated (due to the above reaction) will tend to drift away from the Si/SiO_2 interface and into the bulk of the SiO_2. Recall from Chapter 4, once the H+ ions are generated, one would expect the ions to drift away from the interface governed by the transport equation:

$$J(x,\, t) = \mu\rho(x,\, t)\,(|e|\,E) - D\frac{\partial\rho(x,\, t)}{\partial x}, \tag{11.40}$$

where $\rho(x, t)$ is the density of H^+ ions at a distance x from the interface at any time t, $|e|\,E$ is the force action on the H^+ ion, D is the diffusivity of the H^+ ion, and μ

is the mobility of the H^+ ion and is related to the diffusivity through the Einstein relation:

$$\mu = \frac{D}{K_B T} = \frac{D_o \exp\left(-\frac{Q}{K_B T}\right)}{K_B T}. \tag{11.41}$$

One can see from Eq. (11.40), as the H^+ ions tend to drift away from the interface due to the presence of the electric-field E, the concentration of H^+ ions in the SiO_2 starts to increase. As the concentration of H^+ ions grows in the SiO_2 dielectric, a *backflow* of H^+ ions (toward the interface) can be expected to develop. In fact, if the stress stops (electric field goes to zero), then the backflow of H^+ ions is expected to occur causing some device recovery to take place. Complete recovery does not generally take place because some of the H^+ ions may undergo a reduction reaction while in the SiO_2 gate dielectric.[52] Several reduction reactions are possible:

$$H^+ + e \rightarrow H, \tag{11.42a}$$

or

$$H^+ + H + e \rightarrow H_2, \tag{11.42b}$$

or

$$H^+ + H^+ + 2e \rightarrow H_2. \tag{11.42c}$$

The electrical impact of NBTI on p-MOSFET device characteristics is substantial: a shift can occur in the threshold voltage of the device and a decrease in hole mobility in the inversion channel. Both the V_t shift and mobility degradation lead to reduced current in the channel (I_{drive}) of the device and, as a consequence, degraded device performance. The threshold voltage V_t shift with time is observed to take the form:

$$\frac{\Delta V_t}{(V_t)_0} = B_o(E,T)(t)^m, \tag{11.43}$$

where $B_o(E,T)$ is a prefactor that is electric-field E and temperature T dependent. m is the power law exponent for the time t. Generally, m=0.15–0.35, with m=0.25 often observed.

Since the time-dependence exponent m is less than 1 then we know from Chapter 2 that the degradation with time will tend to saturate. Such degradation saturation is fully expected from the reaction-diffusion model illustrated in

[52] It is also possible that some of the H+ ions may be reduced and dispersed within the poly gate electrode and/or diffuse laterally from the gate region.

Fig. 11.33. Since the number of S-H bonds is finite, then the degradation rate due to Si-H bond breakage must reduce as the number of unbroken Si-H bonds dwindles with time.

Example Problem 11.10

During a NBTI stress test of a P-channel MOSFET, it was determined that the V_t shifted by 10% in 100 hrs. How long would it take the V_t to shift by 20%? Assume a time-dependence exponent of m=0.25.

Solution

Given the 10% degradation in 100 hrs, one can determine B_o for the set of stress conditions using Eq. (11.43):

$$0.1 = B_o(100\ hr)^{0.25},$$

giving: $B_o = 0.0316/(\text{hr})^{1/4}$. Solving Eq. (11.43) for time t, one obtains:

$$t = \left[\frac{1}{B_0}\left(\frac{\Delta V_t}{(V_t)_0}\right)\right]^{1/m},$$

giving

$$t = \left[\frac{1}{0.0316/(hr)^{1/4}}(0.2)\right]^4 = 1605 hrs.$$

Note that, because NBTI is a saturating degradation mechanism, it took only 100 hrs to reach a 10% degradation level for the device, but it took more than 1600 hrs to reach a 20% degradation level. The full plot is shown below.

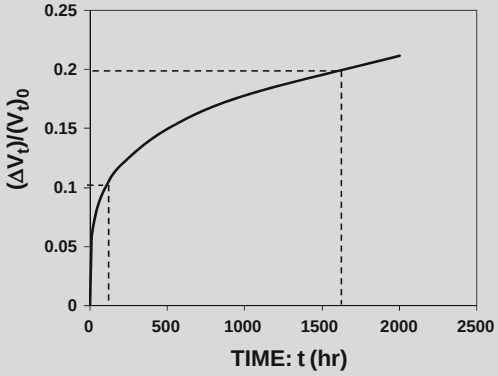

Fig. 11.34 NBTI degradation shows saturation effects for longer times. Time-to-degrade to 10% was 100 hrs while the time-to-degrade to 20% was over 1600 hrs.

The field E and temperature T dependence of the prefactor $B_o(E,T)$ takes the familiar form:

$$B_o(E,T) = C_o \exp\left[\gamma_{degradation} \bullet E\right] \exp\left[-\frac{Q_{degradation}}{K_B T}\right], \tag{11.44}$$

where C_o is proportional to the concentration of Si-H bonds at the Si/SiO_2 interface.

Time-to-failure TF for the device will occur at a time when the parameter degradation reaches some critical amount $[(\Delta V_t)/(V_t)_o]_{crit}$. Solving Eq. (11.43) for t = TF, one obtains

$$TF = \left[\frac{1}{B_0}\left(\frac{\Delta V_t}{(V_t)_0}\right)_{crit}\right]^{1/m}. \tag{11.45}$$

Using Eqs. (11.44 and 11.45), one obtains

$$TF = A_o \exp\left[-\gamma_{NBTI} \bullet E\right] \exp\left[\frac{Q_{NBTI}}{K_B T}\right], \tag{11.46}$$

where:

$$A_o = \left[\frac{1}{C_o}\left(\frac{\Delta V_t}{(V_t)_o}\right)_{crit}\right]^{1/m}, \tag{11.47}$$

$$\gamma_{NBTI} = \frac{\gamma_{degradation}}{m}, \tag{11.48}$$

and

$$Q_{NBTI} = \frac{Q_{degradation}}{m}. \tag{11.49}$$

One can see from Eq. (11.46) and Eq. (11.47) that the time-to-failure prefactor A_o is dependent on the amount of parameter degradation that can be tolerated and inversely dependent on the concentration C_o of Si-H bonds at the Si/SiO_2 interface. It is not surprising that as C_o goes to zero, the time-to-failure for the NBTI failure mechanism goes to infinity. One should also note that, just as Chapter 3 (Section 3.2) discussed, the time-to-failure kinetics (γ_{NBTI}, Q_{NBTI}) are not the same as the degradation kinetics ($\gamma_{degradation}, Q_{degradation}$).[53] Accelerated NBTI degradation data suggests that the time exponent for degradation is m=0.25 and the degradation kinetics are given by : ($\gamma_{degradation} = 0.8\, cm/MV$, $Q_{degradation} = 0.15\, eV$). Thus, the time-to-failure kinetics, as given by Eqs. (11.48 and 11.49), are expected to be four times greater or: ($\gamma_{NBTI} = 3.2\, cm/MV$, $Q_{NBTI} = 0.6\, eV$).

[53]Note that for the case m=0.25, the time-to-failure kinetics are four times greater than the degradation kinetics !

Example Problem 11.11

NBTI accelerated data was taken on a P-channel MOSFET device with a gate oxide thickness of $t_{ox} = 35Å$. At 3.0 V and 150°C, the time-to-failure (based on a 10% Vt shift) was recorded to be 1 hr. How long would a similar device be expected to last at the operating conditions of 1.8 V and 105°C? Assume an exponential field acceleration parameter: $\gamma_{NBTI} = 3.2\text{cm/MV}$.

Solution

Acceleration factor due to voltage:

$$\begin{aligned} AF_{voltage} &= \exp\left[\gamma_{NBTI} \bullet \left(\frac{V_{stress} - V_{op}}{t_{ox}}\right)\right] \\ &= \exp\left[(3.2 \times 10^{-6} cm/V) \bullet \left(\frac{3.0\,V - 1.8\,V}{35 \times 10^{-8} cm}\right)\right] \\ &= 5.82 \times 10^4. \end{aligned}$$

Acceleration factor due to temperature:

$$\begin{aligned} AF_{temp} &= \exp\left[\left(\frac{Q_{NBTI}}{K_B}\right)\left(\frac{1}{T_{op}} - \frac{1}{T_{stress}}\right)\right] \\ &= \exp\left[\left(\frac{0.6\,eV}{8.62 \times 10^{-5} eV/K}\right)\left(\frac{1}{(105+273)K} - \frac{1}{(150+273)K}\right)\right] \\ &= 7.10. \end{aligned}$$

Total acceleration factor:

$$AF = AF_{voltage} \bullet AF_{temp} = (5.82 \times 10^4) \bullet (7.10) = 4.13 \times 10^5.$$

Therefore, the expected time-to-failure at use conditions is:

$$\begin{aligned} &TF(1.8\,V, 105°C) = AF \bullet TF(3.0\,V, 150°C) \\ &= (4.13 \times 10^5) \bullet (1hr) \\ &= 4.13 \times 10^5 hr \left(\frac{1\,yr}{8760hr}\right) \\ &= 47yrs. \end{aligned}$$

Problems

1. Electromigration data was taken, for an Al-Cu alloy, using metal stripes much greater than the Blech length and with a width ~2x the average metal grain-size. At a current density of J = 2.5×10^6 A/cm^2 and temperature $T = 175°C$, the median time-to-failure was t_{50}=320 hrs with a logarithmic standard deviation of $\sigma = 0.5$. Assuming an activation energy of $Q = 0.8$ eV and a current density exponent of n=2, find the maximum design current density that can be used to have no more than 0.13% cumulative failures in 10 yrs at a metal temperature of 105°C.

   Answer: $J_{design} = 4.9 \times 10^5$A/cm^2

2. Electromigration data was taken, for dual-damascene Cu leads, using a via-fed Cu-stripe of minimum width and a length much longer than the Blech length. At a current density of 1.0×10^6 A/cm^2 and temperature T = 275°C, the median time-to-failure was t_{50}=31 hrs and with a logarithmic standard deviation of σ=0.4. Assuming an activation energy of $Q = 1.0$eV and a current density exponent of n=1, find the maximum design current density that can be used in order to have no more than 0.13% cumulative failures in 10yrs @ 105°C metal temp.

   Answer: $J_{design} = 1.5 \times 10^6$A/cm^2

3. In electromigration testing of an aluminum-alloy at 2×10^6A/cm^2 it was found that the time-to-failure was 2 times longer for 66um-long metal leads versus 132um-long metal leads. Determine the critical Blech constant $A_{Blech} = (J \bullet L)_{crit}$ for this Al-alloy metal system.

   Answer: $A_{Blech} = 6000$A/cm

4. In electromigration testing of copper at 1×10^6A/cm^2 it was found that the time-to-failure was 2 times longer for 30um-long metal leads versus 60um-long metal leads. Determine the critical Blech constant $A_{Blech} = (J \bullet L)_{crit}$ for this Cu-metal system.

   Answer: $A_{Blech} = 2000$A/cm

5. During stress migration testing of Cu interconnects it was found that a certain via would fail in 450 hrs when a chip was baked at 190°C. Assuming a power-law stress-migration exponent of n=3, activation energy for diffusion of Q =0.75 eV, and a stress free temperature of T_o =270°C:

   a) Find the time-to-failure at 105°C.
   b) What is the effective activation energy for the stress migration from 190°C versus 105°C?

   Answers: a) $TF_{@105C} = 3600$hrs b) $Q_{eff} = 0.37$ eV

6. During 85%RH and 85°C testing of plastic-packaged silicon chips, aluminum metallization failures due to corrosion started to occur at 750hrs of testing. Assuming an exponential humidity dependence of a=0.12/%RH and activation energy of 0.75 eV, find the expected time-to-failure at 40%RH and 50°C.

   Answer: TF = 264 yrs

7. The corrosion-free time window, for post chemical-mechanical polishing of Cu, was determined to be 3 hrs when the wafers are stored in 40%RH ambient at room temp. How long would the corrosion-free window be if the humidity is lowered to 30%RH? Assume an exponential humidity dependence with a=0.12/%RH.

   Answer: 10hrs

8. Thermal cycling of plastic-packaged silicon chips produced solder-ball failures after 500 cycles of −65°C/150°C. Assuming that the elastic range is negligibly small and that the temperature cycling exponent for the soft-solder metal is n=3, estimate the number of cycles-to-failure for temperature cycling from 0°C/85°C.

   Answer: 8100 cycles

9. Thermal cycling of plastic-packaged silicon chips produced crack propagation in the silicon substrate and caused a fractured-die failure mechanism after 500 cycles of −65°C/150°C. Assuming that time-zero cracks exist and that the temperature cycling exponent for hard/brittle silicon substrate is n=6, estimate the number of cycles-to-failure for temperature cycling from 0°C/85°C.

   Answer: 1.31×10^5 cycles

10. Time-dependent dielectric breakdown (TDDB) data was taken for capacitors at E=10MV/cm and a temperature of 105°C. The following Weibull results were obtained: t_{63}=200sec and β=1.4. Using an E-Model with $\gamma_{@105C}$=4.0 cm/MV:

    a) What is the expected time-to-failure, at 10MV/cm and 105°C, for 0.1% of the capacitors?
    b) What acceleration factor is needed to insure that no more than 0.1% of the capacitor will fail during 10 yrs of use at 105°C?
    c) What is the maximum allowed operational electric-field E_{op} to ensure that no more than 0.1% of the capacitors are expected to fail in 10 years of service at 105°C?

    Answers: a) $t_{0.1\%}$ = 1.44sec b) AF = 2.19×10^8 c) E_{op}=5.2MV/cm

11. Time-dependent dielectric breakdown (TDDB) data was taken for capacitors at E=10MV/cm and a temperature of 105°C. The following Weibull results were obtained: t_{63}=200sec and β=1.4. Using a 1/E - Model with $G_{@105C}$=303MV/cm:

a) What is the expected time-to-failure, at 10MV/cm and 105°C, for 0.1% of the capacitors?
b) What acceleration factor is needed to insure that no more than 0.1% of the capacitor will fail during 10 yrs of use at 105°C?
c) What is the maximum allowed operational electric field E_{op} to ensure that no more than 0.1% cap-fails will occur during 10 years at 105°C?

Answers: a) $t_{0.1\%} = 1.44$sec b) $AF = 2.19 \times 10^8$ c) E_{op}=6.12MV/cm

12. Linear ramp-to-breakdown testing at 105°C of a random collection of capacitors with a ramp rate of 1MV/cm/sec produced a breakdown distribution which could be described by a Weibull distribution with $t_{63} = 12$MV/cm and a Weibull slope of β=15.0. Using an E-Model, with $\gamma_{@105C}$=4.0 cm/MV, what is the expected fraction of capacitors that will fail in 10 yrs at 4 MV/cm at 105°C.

    Answer: 1.8%

13. Na ions are present in a group of MOSFET devices. If the devices start to fail in 400 hrs at 125°C and 5.0 V, what is the expected time-to-failure at 85°C and 3.3 V? Assume activation energy of 1.0 eV.

    Answer: 1.8 yrs

14. Minimum channel-length MOSFETS were hot-carrier injection (HCI) tested. The maximum substrate current was found to approximately double for each 0.5 V increase in operational voltage. If the time to failure was 1hr at 6.5 V, what is the expected time-to-failure at 4.0 V? Assume a time-to-failure power-law exponent of n=3 for the substrate current.

    Answer: 3.7yrs

15. MOSFETS were randomly selected and negative-bias temperature instability (NBTI) stress tested. The electric field in the gate oxide during stress was E_{stress}=8MV/cm and the stress temperature was T_{stress}=150°C. If the devices started to fail in 1 hr under NBTI stress, what would the time-to-failure be at E_{op}=5MV/cm and T_{op}=105°C? Assume an exponential model with γ_{NBTI} = 3.2 cm/MV and activation energy Q_{NBTI}=0.6 eV.

    Answer: 12yrs

References

Corrosion

Dunn, C. and J. McPherson: *Recent Observations on VLSI Bond Pad Corrosion Kinetics*, J. Electrochem. Soc., 661 (1988).

Flood, J.: *Reliability Aspects of Plastic Encapsulated Integrated Circuits*, IEEE International Reliability Physics Symposium Proceedings, 95 (1972).

Gunn, J., R. Camenga and S. Malik: *Rapid Assessment of the Humidity Dependence of IC Failure Modes by Use of Hast*, IEEE International Reliability Physics Symposium Proceedings, 66 (1983).

Koelmans, H.: *Metallization Corrosion in Silicon Devices by Moisture-Induced Electrolysis*, IEEE International Reliability Physics Symposium Proceedings, 168 (1974).

Lawrence, D.. and J. McPherson: *Corrosion Susceptibility of Al-Cu and Al-Cu-Si Films*, J. Electrochem. Soc., Vol. 137, 3879 (1990).

McPherson, J.: *VLSI Corrosion Models: A Comparison of Acceleration Factors,* Proceedings of Third Intern. Symp. on Corrosion and Reliability of Electronic Materials and Devices, Electrochem. Soc., Vol. 94–29, 270 (1994).

Paulson, W. and R. Kirk: *The Effects of Phosphorus-Doped Passivation Glass on the Corrosion of Aluminum*, IEEE International Reliability Physics Symposium Proceedings, 172 (1972).

Peck, D.: *The Design and Evaluation of Reliable Plastic-Encapsulated Semiconductor Devices*, IEEE International Reliability Physics Symposium Proceedings, 81 (1970).

Peck, D.: *A Comprehensive Model for Humidity Testing Correlation*, IEEE International Reliability Physics Symposium Proceedings, 44 (1986).

Schnable, A. and R. Keen: *Failure Mechanisms in Large-Scale Integrated Circuits*, IEEE International Reliability Physics Symposium Proceedings, 170 (1969).

Electromigration (EM)

Black, J.: *A Brief Survey of Some Recent Electromigration Results*, IEEE Trans. Electron Dev., ED-16, 338 (1969).

Blech, I. and H. Sello: *The Failure of Thin Aluminum Current-Carrying Strips on Oxidized Silicon*, Physics of Failures in Electronics Vol. 5, USAF-RADC Series, 496 (1966).

d-Heurle, F. and P. Ho, *Electromigration in Thin Films.* In: **Thin Films: Interdiffusion and Reactions**, John Wiley & Sons, 243 (1978).

Filippi, R., G. Biery and R. Wachnik: *The Electromigration Short-Length Effect in Ti-AlCu-Ti Metallization with Tungsten Plugs*, J. Appl. Phys., Vol. 78, 3756 (1995).

Graas, C., H. Le, J. McPherson and R. Havemann, *Electromigration Reliability Improvements of W-Plug vias by Titanium Layering*, IEEE International Reliability Physics Symposium Proceedings, 173 (1994).

Hau-Riege, S.: *Probabilistic Immortality of Cu Damascene Interconnects*, Journal of Applied Physics, 91(4), 2014 (2002).

Hau-Riege, C. A. P. Marathe, and V. Pham: *The Effect of Low-k ILD on the Electromigration Reliability of Cu Interconnects with Different Line Lengths*, 41st Annual IEEE International Reliability Physics Symposium Proceedings (IRPS), 173 (2003).

Hu, C. et al.: *Scaling Effect on Electromigration in On-Chip Cu Wiring*, IEEE International Interconnect Conference, 267 (1999).

Hu, C., et al.: *Effects of Overlayers on Electromigration Reliability Improvement for Cu/Low K Interconnects*, 42th Annual IEEE International Reliability Physics Symposium Proceedings (IRPS), 222 (2004).

Huntington, H. and A. Grone: *Current Induced Marker Motion in Gold Wires*, J. Phys. Chem. Solids, VOL. 20, 76 (1961).

Hussein, M. and J. He: *Materials Impact on Interconnect Process Technology and Reliability*, IEEE Transactions on Semiconductor Manufacturing, **18**(01), 69 (2005).

Lane, M., E. Liniger, and J. R. Lloyd: *Relationship between interfacial adhesion and electromigration in Cu metallization*, J. Appl. Phys., **93**(3), 1417 (2003).

Lee, K., X. Lu, E. T. Ogawa, H. Matsuhashi, and P. S. Ho: *Electromigration Study of Cu/low k Dual-damascene Interconnects*, 40th Annual IEEE International Reliability Physics Symposium Proceedings (IRPS), 322 (2002).

Lloyd, J.: *Electromigration in Thin Film Conductors*, Semicond. Sci. Technol. **12**, 1177 (1997).

Maiz, J.: *Characterization of Electromigration under Bidirectional and Pulsed Unidirectional Currents*, IEEE International Reliability Physics Symposium Proceedings, 220 (1989).

Martin, C. and J. McPherson: *Via Electromigration Performance of Ti/W/Al-Cu(2%) Multilayered Metallization*, VLSI Multilevel Interconnect Conference Proceedings, 168 (1989).

McPherson, J., H. Le and C. Graas: *Reliability Challenges for Deep Submicron Interconnects*, Microelectronics Reliability, Vol. 37, 1469 (1997).

Michael, N., C. Kim, P. Gillespie, and R. Augur: *Mechanism of Reliability Failure in Cu Interconnects with Ultra-Low Materials*, Applied Physics Letters, **83**(10), 1959 (2003).

Oates, A.: *Electromigration Failure Distribution of Contacts and Vias as a Function of Stress Conditions in Submicron IC Metallizations*, IEEE International Reliability Physics Symposium Proceedings, 164 (1996).

Ogawa, E., et al.: *Statistics of Electromigration Early Failures in Cu/Oxide Dual-Damascene Interconnects*, 39th Annual IEEE International Reliability Physics Symposium Proceedings (IRPS), 341(2001).

Ogawa, E., K.-D. Lee, V. A. Blaschke, and P. S. Ho: *Electromigration Reliability Issues in Dual-Damascene Cu Interconnections*, IEEE Transactions on Reliability, **51**(4), 403 (2002).

Ondrusek, J., C. Dunn and J. McPherson: *Kinetics of Contact Wearout for Silicided(TiSi2) and Nonsilicided Contacts*, IEEE International Reliability Physics Symposium Proceedings, 154 (1987).

Park, Y. Park, K.-D. Lee and W. R. Hunter, 43th Annual IEEE International Reliability Physics Symposium Proceedings (IRPS), 18 (2005).

Shatzkes, M. and J. R. Lloyd: *A Model for Conductor Failure Considering Concurrently with Electromigration Resulting in a Current Exponent of 2*, J. Appl. Physics, Vol. 59, 3890 (1986).

Steenwyk, S. and E. Kankowski: *Electromigration in Aluminum to Ta-Silicide Contacts*, IEEE International Reliability Physics Symposium Proceedings, 30 (1986).

Ting, L., J. May, W. Hunter and J. McPherson: *AC Electromigration Characterization and Modeling of Multilayered Interconnects*, IEEE International Reliability Physics Symposium Proceedings, 311 (1993).

Vaidya, S. et al.: *Electromigration Induced Shallow Junction Leakage with Al/Poly-Si Metallization*, J. Electrochem. Soc., Vol. 130, 496 (1983).

Vaidya, S., et al.: *Shallow Junction Cobalt Silicide Contacts with Enhanced Electromigration Resistance*, J. Appl. Phys. Vol. 55, 3514 (1984).

Hot Carrier Injection (HCI)

Aur, S., A. Chatterjee and T. Polgreen: *Hot Electron Reliability and ESD Latent Damage*, IEEE International Reliability Physics Symposium Proceedings, 15 (1988).

Fang, P., J.T. Yue, and D. Wollesen: *A Method to Project Hot-Carrier Induced Punch Through Voltage Reduction for Deep Submicron LDD PMOS FETs at Room and Elevated Temperatures*, IEEE International Reliability Physics Symposium Proceedings, 131 (1982).

LaRosa, G., et al.: *NBTI Channel Hot Carrier Efffects in PMOSFETS in Advanced CMOS Technologies*, IEEE International Reliability Physics Symposium Proceedings, 282 (1997).

Liu, Z., et al.: *Design Tools for Reliability Analysis, IEEE Design Tools for Reliability Analysis*, IEEE Design Automation Conference, pp. 182–185, (2006).

Lu, M., et al.: Hot *Carrier Degradation in Novel Strained Si n-MOSFETs*, IEEE International Reliability Physics Symposium Proceedings, pp. 18–21, (2004).

Ong, T., P. Ko and C. Hu: *Hot-Carrier Current Modeling and Device Degradation in Surface Channel PMOSFET*, IEEE Trans. on Electron Devices, ED-37, 1658 (1990).

Snyder, E., D. Cambell, S. Swanson and D. Pierce: *Novel Self-Stressing Test Structures for Realistic High-Frequency Reliability Characterization*, IEEE International Reliability Physics Symposium Proceedings**,** 57 (1993).

Takeda, E., R. Izawa, K. Umeda and R. Nagai: *AC Hot-Carrier Effects in Scaled MOS Devices*, IEEE International Reliability Physics Symposium Proceedings, 118 (1991).
Wang, W., et al.: *An Integrated Modeling Paradigm of Circuit Reliability for 65 nm CMOS Technology*, IEEE Custom Integrated Circuits Conference, pp. 511–514 (2007).
Wang-Ratkovic, J. et al.: *New Understanding of LDD CMOS Hot-Carrier Degradation and Device Lifetime at Cryogenic Temperatures*, IEEE International Reliability Physics Symposium Proceedings, 312 (1997).
Yue J.: *Reliability.* In: **ULSI Technology**, McGraw-Hill, 657 (1996).

Mobile-Ions/Surface-Inversion

Hefley, P. and J. McPherson: *The Impact of an External Sodium diffusion Source on the Reliability of MOS Circuitry*, IEEE International Reliability Physics Symposium Proceedings, 167 (1988).
Schnable, A.: *Failure Mechanisms in Microelectronic Devices*, Microelectronics and Reliability, (1988).
Snow, E., A.S. Grove, B.E. Deal, and C.T. Sah: *Ion Transport Phenomenon in Insulating Films*, J. Appl. Phys. Vol 36, 1664 (1965).
Snow, E. and B.E. Deal: *Polarization Phenomena and Other Properties of Phosphosilicate Glass Films on Silicon,* J. Electrochem. Soc., Vol 113, 263 (1966).
Stuart, D.: *Calculations of Activation Energy of Ionic Conductivity in Silica Glass by Classical Methods*, Journal of the American Ceramic Society, 573 (1954).

Negative-Bias Temperature Instability (NBTI)

Abadeer, W. and W. Ells: *Behavior of NBTI Under AC Dynamical Circuit Conditions*, IEEE International Reliability Physics Symp., pp. 17–22, (2003).
Alam, A., et. al.: *A Comprehensive Model of PMOS Negative Bias Temperature Degradation*, Microelectronics Reliability, pp. 71–81 (2005).
Chakravarthi, S. et al.: *A Comprehensive Framework for Predictive Modeling of Negative Bias Temperature Instability*, IEEE International Reliability Physics Symp. pp. 273–282,(2004).
Chen, G., et al.: *Dynamic NBTI of PMOS Transistors and Its Impact on Device Lifetime*, IEEE International Reliability Physics Symp. pp. 196–202, (2003).
Huard V. and M. Denais: *Hole Trapping Effect on Methodology for DC and AC Negative Bias Temperature Instability Measurements in pMOS transistors*, IEEE International Reliability Physics Symp. pp. 40–45 (2003).
Kimizuka, N., et al.,: *The Impact of Bias Temperature Instability for Direct-Tunneling in Ultra-thin Gate Oxide on MOSFET Scaling*, VLSI Symp. On Tech., pp. 73–74, (1999).
Krishnan, A., et al.: *NBTI Impact on Transistor and Circuit: Models, Mechanisms and Scaling Effects*, IEEE-IEDM, pp. 349–352, (2003).
Larosa, G., et al.,: *NBTI-Channel Hot Carrier Effects in Advanced Sub-Micron PFET Technologies*, IEEE Interational Reliability Physics Symp. Proceedings, pp. 282–286 (1997).
Mahaptra, S., et. al.: *Negative bias Temperature Instability in CMOS Devices,* Microelectronics *Reliability*, pp. 114–121 (2005).
Ogawa, S. and N. Shiono: *Generalized Diffusion-Reaction Model for the Low-Field Chaarge Buildup Instability at the Si-SiO2 Interface*, Physical Rev. B, p. 4218 (1995).
Rangan, S., et al.: *Universal Recovery Behavior of Negative Bias Temperature Instability*, IEEE-IEDM, pp. 341–344.(2003).
Reddy, V., et al.: *Impact of Negative Bias Temperature Instability on Digital Circuit Reliability,* pp. 248–254, (2002).

Schlunder, C. et al.: *Evaluation of MOSFET Reliability in Analog Applications*, IEEE, International Reliability Physics Symposium, pp. 5–10, (2003).
Stathis, J. and S. Zafar: *The Negative Bias Temperature Instability of MOS Devices: A Review*, Microelectronics Reliability, pp. 270–286 (2006).

Stress Migration/Stress-Induced Voiding

Edelstein, D., et al.: *Full Copper Wiring in a Sub-0.25 μm CMOS ULSI Technology*, IEEE International Electron Devices Meeting Technical Digest, 773 (1997).
Groothuis, S. and W. Schroen: *Stress Related Failures Causing Open Metallization*, IEEE International Reliability Physics Symposium Proceedings, 1 (1987).
Harper, J., et al.: *Mechanisms for Microstructure Evolution in Electroplated Copper Thin Films Near Room Temperature*, Journal of Applied Physics, 86(5), 2516 (1999).
Klema, J., R. Pyle and E. Domangue: *Reliability Implications of Nitrogen Contaminated during Deposition of Sputtered Aluminum/Silicon Metal Films*, IEEE International Reliability Physics Symposium Proceedings, 1 (1984).
McPherson, J. and C. Dunn: A *Model for Stress-Induced Metal Notching and Voiding in VLSI Al-Si Metallization*, J. Vac. Sci. Technology B, 1321 (1987).
McPherson, J.: *Accelerated Testing*. In: Electronic Materials Handbook, Volume 1 Packaging, ASM International Publishing, 887 (1989).
Ogawa, E., J. W. McPherson, J. A. Rosal, K. J. Dickerson, T. - C. Chiu, L. Y. Tsung, M. K. Jain, T. D. Bonifield, J. C. Ondrusek, and W. R. McKee: *Stress-Induced Voiding Under Vias Connected To Wide Cu Metal Leads*, 40th Annual IEEE International Reliability Physics Symposium Proceedings (IRPS), 312 (2002).
Paik, J., J.-K. Jung and Y.-C. Joo: *The Dielectric Material Dependence of Stress and Stress Relaxation on the Mechanism of Stress-Voiding of Cu Interconnects*, 43th Annual IEEE International Reliability Physics Symposium Proceedings (IRPS), 195 (2005).
Von Glasow, A., A. H. Fischer, M. Hierlemann, S. Penka, and F. Ungar: *Geometrical Aspects of Stress-Induced Voiding in Copper Interconnects*, Advanced Metallization Conference Proceedings (AMC), 161 (2002).
Yoshida, K., T. Fujimaki, K. Miyamoto, T. Honma, H. Kaneko, H. Nakazawa, and M. Morita: *Stress-Induced Voiding Phenomena for an actual CMOS LSI Interconnects*, IEEE International Electron Devices Meeting Technical Digest, 753 (2002).
Yue, J., W. Fusten and R. Taylor: Stress *Induced Voids in Aluminum Interconnects During IC Processing*, IEEE International Reliability Physics Symposium Proceedings, 126 (1985).
Yue, J.: *Reliability*. In: **ULSI Technology**, McGraw-Hill, 674 (1996).

Temperature-Cycling/Fatigue

Blish, R.: *Temperature Cycling and Thermal Shock Failure Rate Modeling*, IEEE International Reliability Physics Symposium Proceedings, 110 (1997).
Caruso, H. and A. Dasgupta: *A Fundamental Overview of Accelerated-Testing Analytical Models*, Proceedings of Annual Rel. and Maintainability Symposium, 389 (1998).
Coffin, L., Met. Eng. Q., Vol 3, 15 (1963).
Dieter, G.: **Mechanical Metallurgy**, McGraw-Hill, 467 (1976).
Dunn, C. and J. McPherson: *Temperature Cycling Acceleration Factors in VLSI Applications*, IEEE International Reliability Physics Symposium Proceedings, 252 (1990).
Manson, S.: **Thermal Stress and Low-Cycle Fatigue**, McGraw-Hill Book Co., New York, (1966).

Time-Dependent Dielectric Breakdown (TDDB)

Anolick, E. and G. Nelson: *Low-Field Time-Dependent Dielectric Integrity*, IEEE International Reliability Physics Symposium Proceedings, 8 (1979).

Berman, A.: *Time Zero Dielectric Reliability Test by a Ramp Method*, IEEE International Reliability Physics Symposium Proceedings, 204 (1981).

Boyko, K. and D. Gerlach: *Time Dependent Dielectric Breakdown of 210A Oxides*, IEEE International Reliability Physics Symposium Proceedings, 1 (1989).

Charparala, P., et al.: *Electric Field Dependent Dielectric Breakdown of Intrinsic SiO_2 Films Under Dynamic Stress*, IEEE International Reliability Physics Symposium Proceedings, 61 (1996).

Chen, I., S. Holland and C. Hu: *A Quantitative Physical Model for Time-dependent Breakdown*, IEEE International Reliability Physics Symposium Proceedings, 24 (1985).

Cheung, K.: *A Physics-Based, Unified Gate-Oxide Breakdown Model*, Technical Digest of Papers International Electron Devices Meeting, 719 (1999).

Crook, D.: *Method of Determining Reliability Screens for Time-Dependent Dielectric Breakdown*, IEEE International Reliability Physics Symposium Proceedings, 1 (1979).

Degraeve, R., et al.: *New Insights in the Relation Between Electron Trap Generation and the Statistical Properties of Oxide Breakdown*, IEEE Trans. Electron Devices 45, 904 (1998).

DiMaria, D. and J. Stasiak: *Trap Creation in Silicon Dioxide Produced by hot electrons*, J. Appl. Physics, Vol 65, 2342 (1989).

DiMaria, D., E. Cartier and D. Arnold: *Impact ionization, trap creation, degradation, and breakdown in silicon dioxide films on silicon*, J. Appl. Physics, Vol 73, 3367 (1993).

Eissa, M., D. A. Ramappa, E. Ogawa, N. Doke, E. M. Zielinski, C. L. Borst, G. Shinn, and A. J.McKerrow: *Post-Copper CMP Cleans Challenges for 90 nm Technology*, Advanced Metallization Conference Proceedings (AMC), 559 (2004).

Hu, C. and Q. Lu: *A Unified Gate Oxide Reliability Model*, IEEE International Reliability Physics Symposium Proceedings, 47 (1999).

Haase, G., E. T. Ogawa and J. W. McPherson: *Breakdown Characteristics of Interconnect Dielectrics*, 43th Annual IEEE International Reliability Physics Symposium Proceedings (IRPS), 466 (2005).

Kimura, M.: *Oxide Breakdown Mechanism and Quantum Physical Chemistry for Time-Dependent Dielectric Breakdown*, IEEE International Reliability Physics Symposium Proceedings, 190 (1997).

Lee, J., I. Chen and C. Hu: *Statistical Modeling of Silicon Dioxide Reliability*, IEEE International Reliability Physics Symposium Proceedings, 131 (1988).

McPherson, J. and D. Baglee: *Acceleration factors for Thin Gate Oxide Stressing*, IEEE International Reliability Physics Symposium Proceedings, 1 (1985).

McPherson, J. and H. Mogul: *Underlying Physics of the Thermochemical E-Model in Describing Low-Field Time-Dependent Dielectric Breakdown in SiO_2 Thin Films*, J. Appl. Phys., Vol. 84, 1513 (1998).

McPherson, J., R. Khamankar and A. Shanware: *Complementary Model for Intrinsic Time-Dependent Dielectric Breakdown in SiO_2 Dielectrics*, J. Appl. Physics, Vol. 88, 5351 (2000).

McPherson, J.: *Trends in the Ultimate Breakdown Strength of High Dielectric-Constant Materials*, IEEE Trans. On Elect. Devs., Vol. 50, 1771 (2003).

McPherson, J.: *Determination of the Nature of Molecular bonding in Silica from Time-Dependent Dielectric Breakdown Data*, J. Appl. Physics, Vol. 95, 8101 (2004).

Moazzami, R., J. Lee and C. Hu: *Temperature Acceleration of Time-Dependent Dielectric Breakdown*, IEEE Trans. Elect. Devices, Vol. 36, 2462 (1989).

Nicollian, P.: *Experimental Evidence for Voltage Driven Breakdown Models in Ultra-Thin Gate Oxides*, IEEE International Reliability Physics Symposium, 47 (1999).

Noguchi, J., N. Miura, M. Kubo, T. Tamaru, H. Yamaguchi, N. Hamada, K. Makabe, R. Tsuneda and K. Takeda: *Cu-Ion-Migration Phenomena and its Influence on TDDB Lifetime in Cu*

Metallization, 41st Annual IEEE International Reliability Physics Symposium Proceedings (IRPS), 287 (2003).

Ogawa, E., J. Kim and J. McPherson: *Leakage, Breakdown, and TDDB Characteristics of Porous Low-k Silica-Based Interconnect Dielectrics*, IEEE-IRPS Proceedings, 166 (2003).

Ogawa, E., J. Kim, G. S. Haase, H. C. Mogul, and J. W. McPherson: *Leakage, Breakdown, and TDDB Characteristics of Porous Low-K Silica-Based Interconnect Dielectrics*, 41st Annual IEEE International Reliability Physics Symposium Proceedings (IRPS), 166 (2003).

Pompl, T., et al.: *Change in Acceleration Behavior of Time-Dependent Dielectric Breakdown by the BEOL Process: Indications for Hydrogen Induced Transition in Dominant Degradation Mechanism*, IEEE International Reliability Physics Symposium, 388 (2005).

Schuegraph, K. and C. Hu: *Hole Injection Oxide Breakdown Model for Very Low Voltage Lifetime Extrapolations*, IEEE International Reliability Physics Symposium Proceedings, 7 (1993).

Suehle, J., et. al.: *Field and Temperature Acceleration of Time-Dependent Dielectric Breakdown in Intrinsic Thin SiO_2*, IEEE International Reliability Physics Symposium Proceedings, 120 (1994).

Suehle, J. and P. Chaparala: *Low Electric Field Breakdown of Thin SiO_2 Films Under Static and Dynamic Stress*, IEEE Trans. Elect. Devices, 801 (1997).

Sune, J., D. Jimenez, and E. Miranda: *Breakdown Modes and Breakdown Statistics of Ultrathin SiO_2 Gate Oxides*, J. High Speed Electronics and Systems, 11, 789 (2001).

Stathis, J and D. DiMaria: *Reliability Projection for Ultra-Thin Oxides at Low Voltage*, Technical Digest of Papers International Electron Devices Meeting, 167 (1998).

Swartz, G.: *Gate Oxide Integrity of NMOS Transistor Arrays*, IEEE Trans. on Electron Devices, Vol. ED-33, 1826 (1986).

Tsu, R., J. W. McPherson, and W. R. McKee: *Leakage and Breakdown Reliability Issues Associated with Low-k Dielectrics in a Dual-Damascene Cu Process*, 38th Annual IEEE International Reliability Physics Symposium Proceedings (IRPS), 348 (2000).

Wu, E. et. al.: *Experimental Evidence of TBD Power-Law for Voltage Dependence of Oxide Breakdown in Ultrathin Gate Oxides*, IEEE Trans. On Electron Devices, Vol. 49, 2244 (2002).

Wu, E., et. al.: *Polarity-Dependent Oxide Breakdown of NFET Devices for Ultra-Thin Gate Oxide*, IEEE International Reliability Physics Symposium, 60 (2002).

Chapter 12
Time-To-Failure Models for Selected Failure Mechanisms in Mechanical Engineering

The mechanical properties of materials are related to the fundamental bonding strengths of the constituent atoms in the solid and any bonding defects which might form. A molecular model is presented so that primary bond formation mechanisms (*ionic, covalent,* and *metallic*) can be better understood. How these bonds form and respond to mechanical stress/loading is very important for engineering applications. A discussion of elasticity, plasticity and bond breakage is presented. The theoretical strengths of most molecular bonds in a crystal are seldom realized because of crystalline defects limiting the ultimate strength of the materials. Important crystalline defects such as vacancies, dislocations, and grain boundaries are discussed. These crystalline defects can play critically important roles as time-to-failure models are developed for: creep, fatigue, crack propagation, thermal expansion mismatch, corrosion and stress-corrosion cracking.

12.1 Molecular Bonding in Materials

As emphasized in earlier chapters, mechanical device failures result from: materials degradation (generally causing a shift in some critical device parameter) and eventual device failure. Since the material's properties are ultimately related to the molecular bonding in the material and any bonding defects which might form, it is important to have a fundamental understanding of this bonding.

Figure 12.1 illustrates the bonding of two atoms. As the atoms are brought closer together (from a great distance away), an *attractive potential* develops tending to pull the atoms closer together. This attractive potential develops because of the transfer or sharing of the valence electrons of the interacting atoms. At very small distances ($r < r_0$), a strong *repulsive potential* develops between the two atoms because of atom-1 core electrons interacting with atom-2 core electrons due to the *Pauli Exclusion Principle*.[1]

[1] Classical description is — *two bodies cannot occupy the same space*.

J.W. McPherson, *Reliability Physics and Engineering*,
DOI 10.1007/978-1-4419-6348-2_12, © Springer Science+Business Media, LLC 2010

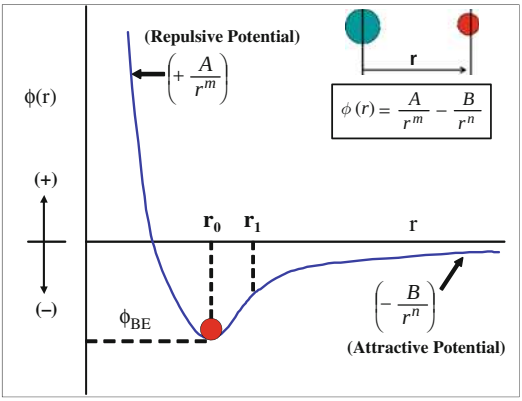

Fig. 12.1 Molecular bonding equilibrium develops due to the competition of the attractive and repulsive potential terms. Equilibrium bonding distance is $r = r_0$. The bonding energy is $-\phi_{BE}$.

The bonding potential in Fig. 12.1 is often approximated by using a Mie (or Mie-Grüneisen) Potential $\phi(r)$:

$$\phi(r) = \frac{A}{r^m} - \frac{B}{r^n} \quad (m > n). \tag{12.1}$$

The parameters A and B can be determined from equilibrium conditions at $r = r_0$ where the bonding energy is $-\phi_{BE}$ and the slope of the potential is zero:

$$\phi(r = r_0) = -\phi_{BE} \tag{12.2}$$

and

$$\left(\frac{\partial \phi}{\partial r}\right)_{r=r_0} = 0. \tag{12.3}$$

Thus, Eq. (12.1) becomes:

$$\phi(r) = \phi_{BE}\left(\frac{mn}{m-n}\right)\left[\frac{1}{m}\left(\frac{r_0}{r}\right)^m - \frac{1}{n}\left(\frac{r_0}{r}\right)^n\right]. \tag{12.4}$$

The repulsive exponent m is normally obtained from compressibility studies and is found to be generally in the range m=8–12. Some often used forms of this potential are: the Born-Landé potential (m=9, n=1) used for ionic bonding (transferring of valence electrons); the Harrison potential (m=9, n=2) used for covalent bonding (sharing of valence electrons); and the Lenard-Jones potential (m=12, n=6) used for dipolar bonding. Even for metallic bonding (sea of conduction electrons minimizing the repulsive nature of the host metal ions), the potential shown in Fig. 12.1 can still be useful.

The Pauling classification of ionic character of bonds is shown in Fig. 12.2.

Normally, any bond with an ionic character of $f^* = 0.6+/-0.1$ is considered to be strongly ionic/polar. Ionic bonds are of relatively longer range and are

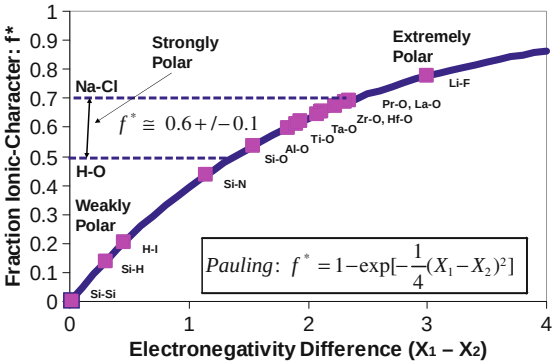

Fig. 12.2 Ionic character of bonds is shown using Pauling electronegativity. Bonds with f* values of greater than 0.5 are considered to be strongly polar.

non directional (no preferred direction). The valence electrons are transferred from an atom of low *electronegativity* to another atom of higher electronegativity. The atoms in a strongly ionic solid generally take a *close-pack* arrangement depending on the ionic radii of the bonding elements involved. Since ionic bonding is of longer range, the total bonding potential is due to nearest neighbors and beyond. The impact of the extended ionic bonding potential is often accounted for by the use of the *Madelung constant*[2] which comes from the summation of the contributions to the potential from both near and far neighbors.

Covalent bonds are generally highly directional because of quantum mechanical restrictions on the bonding to only along preferred directions. Covalent bonds are typically of shorter range (more localized). Shown in Fig. 12.3 is the longer-range nature of the ionic bond [(9,1) potential] versus the more covalent type bonds [(9,2) and (9,3) type bonds]. Covalent bonding generally leads to very hard and non-ductile materials such as diamond. Also, important semiconductors (silicon

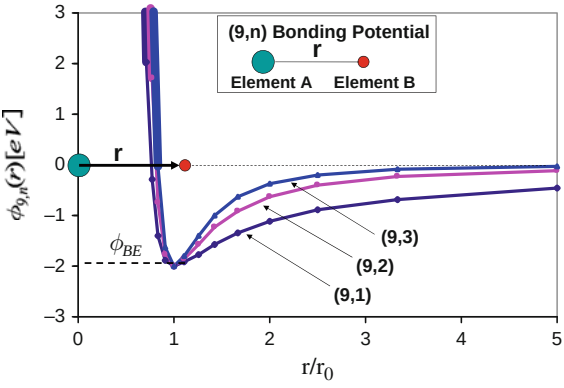

Fig. 12.3 The bonding potential (9,n) tends to show a more localized bonding nature when the value of n increases. Generally, n =1 is used for ionic bonds, n= 2 (or greater) for covalent bonds and n=6 is used for dipolar bonding.

[2]In order that ionic contributions are comprehended from both near and far, the potential for an ion-pair is often written as: $\varphi(r) = -\alpha e^2/r$, where α is the Madelung constant. In cubic crystalline structures, α=1 to 2.

and germanium) are due to covalent bonds. Normally these materials have higher modulus E and tend to be hard and can be brittle.

Metallic bonds (due to the relatively free-moving conduction electrons in a host metal-ion matrix) are less dependent on the exact positions of the host lattice metal ions. This type of bonding produces the ductile and malleable properties of metals. Large material deformation (yielding) is possible before material cracking or rupture occurs.

Secondary bonds (dipolar and hydrogen bonds) are generally much weaker than the primary bonds (ionic, covalent, and metallic). Since the secondary bonds are relatively weak, solid materials formed using these secondary bonds exclusively are characterized by relatively low melting points and relatively poor mechanical properties.

The bond energy $-\phi_{BE}$ is a critically important parameter because it represents the strength/stability of the bond. Very strong bonds can have values of bond energy on the order of several electron volts (eV) while very weak bonds generally have bonding energies of less than 1 eV. Shown in Table 12.1 are the single-bond energies for a few selected molecules. In this table, $U^{(e)}$ represents the electronic/covalent component to the bonding energy, $U^{(i)}$ represents the ionic component, and $U^{(t)}$represents the total bonding energy. In general, the stronger bonds have more ionic character and the bond energy can be several eV. The covalent bond energy is somewhat less, usually around a few eV. Dipolar and hydrogen bonding can result in relatively weaker bond energies (generally less than 1 eV). These bonds are relatively weak and that is the reason why water (dependent on secondary bonding) is a solid only below 0°C and it vaporizes easily at 100°C.

Table 12.1 Selected Single-Bond Energies (Pauling Approach).

Bond	Electronegativities ($X_A - X_B$)	$U^{(e)}$ (eV)	$U^{(i)}$ (eV)	$U^{(t)}$ (eV)	Ionic % of total bond energy (%)
O-O	3.5–3.5	1.4	0.0	1.4	0
F-F	4.0–4.0	1.6	0.0	1.6	0
N-N	3.0–3.0	1.7	0.0	1.7	0
Cl-Cl	3.0–3.0	2.5	0.0	2.5	0
H-H	2.1–2.1	4.5	0.0	4.5	0
Si-Si	1.8–1.8	1.8	0.0	1.8	0
H-Si	2.1–1.8	2.9	0.1	3.0	3
N-Si	3.0–1.8	1.8	1.9	3.7	51
Cl-Si	3.0–1.8	2.1	1.9	4.0	48
O-H	3.5–2.1	2.5	2.6	5.1	51
O-Si	3.5–1.8	1.6	3.8	5.4	70
F-Si	4.0–1.8	1.7	6.3	8.0	79

12.2 Origin of Mechanical Stresses in Materials

Let us now consider what happens when one applies an external force to the bond (load the bond), as shown in Fig. 12.4. One can see that the bond resists the external force by trying to create an equal, but opposite, internal force.

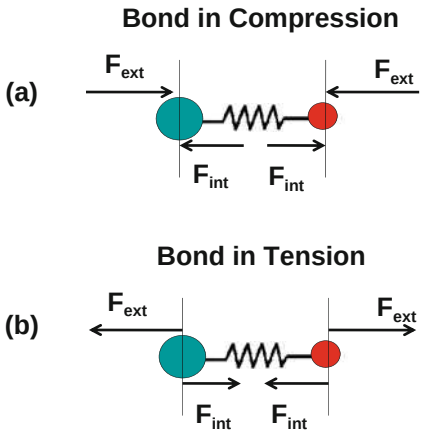

Fig. 12.4 Bonds are shown in states of compression and tension. External forces F_{ext} are shown as well as the internal resistive forces F_{int}.

In static equilibrium, the external forces must be equal and opposite to the internal forces and one can write:

$$F_{ext} = -F_{int}(r) = \left(\frac{\partial \phi}{\partial r}\right), \tag{12.5}$$

giving

$$F_{ext} = \phi_{BE}\left(\frac{mn}{m-n}\right)\left[-\frac{1}{r_0}\left(\frac{r_0}{r}\right)^{m+1} + \frac{1}{r_0}\left(\frac{r_0}{r}\right)^{n+1}\right]. \tag{12.6}$$

The general shape of the curve, for the external force F_{ext} versus atom separation r, is shown in Fig. 12.5.

The curve in Fig. 12.5 is very important because $dW = F_{ext}\ dr$ represents the incremental amount of work that is done by the external force on the bond (either stretching or compressing the bond). This incremental work serves to increase the energy of the bond (making the bond energy more positive) thus making the bond less stable and more susceptible to breakage. From Fig. 12.5, one can see what happens when we stretch or compress the bond beyond its elastic limit. The elastic region (*Hooke's Law* region) is a region where, once the external force is removed, the material returns back to its original unstressed position (thus no permanent changes to the bonding or to the materials).

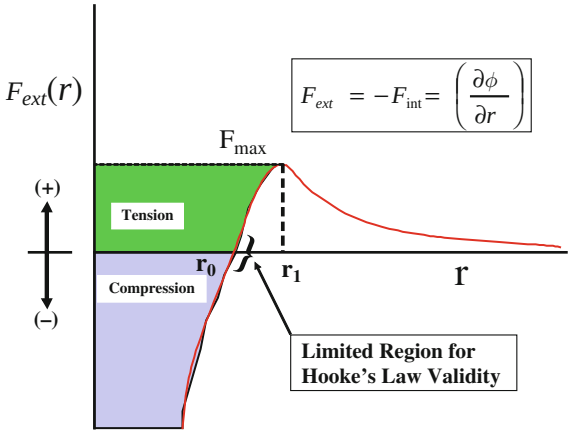

Fig. 12.5 External force F_{ext} versus bonding distance r.

12.3 Elastic Behavior of Materials

The elastic region for the bond can be characterized by a spring with *spring constant* (or *stiffness constant*) κ, as shown in Fig. 12.6. The value of κ can be determined from the molecular potential:

$$\kappa = \left(\frac{\partial^2 \phi}{\partial r^2}\right)_{r=r_0} = \phi_{BE}\left(\frac{mn}{r_0^2}\right). \tag{12.7}$$

The elastic behavior leads to a quadratic/harmonic potential energy of the form:

$$\phi(x) = -\int_0^x \vec{F} \bullet d\vec{x} = \kappa \int_0^x x dx = \frac{1}{2}\kappa\, x^2. \tag{12.8}$$

Note that the elastic energy goes as the square of the displacement (for small displacement) of the atoms from their equilibrium positions. Since this is a harmonic potential, once the atoms are displaced from their equilibrium positions and

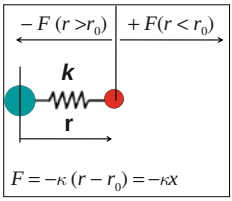

Fig. 12.6 In the region of Hooke's Law validity (elastic behavior), the force acting on the interacting atoms is directly proportional to the displacement of the atoms from their equilibrium positions. Hooke's law leads to a simple harmonic potential energy of the form: $\phi(x) = (1/2)\kappa\, x^2$, where $x = r - r_o$.

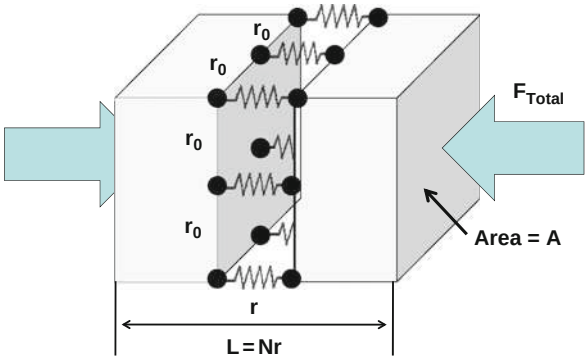

Fig. 12.7 Planar cross section illustrates the bonding/springs between nearest neighboring atoms along the length of the solid. Plane-to-plane bonding/springs are compressed by the applied stress. With N cross-sectional units along the length of the solid, then the length L of the solid is simply L=Nr. Only bonding/springs between planes are shown.

suddenly released, the atoms are expected to oscillate about their equilibrium positions until the elastic energy is dissipated.[3]

Let us now go from the microscopic level (atom level) to the macroscopic level (solid level) as shown in Fig. 12.7.

From Fig. 12.7, one can see that if the number of such bonds per unit area is η, then the stress needed to elastically displace the atoms from their equilibrium position is given by:

$$\sigma = \frac{F_{Total}}{A} = \frac{\eta \bullet A \bullet [\kappa(r - r_0]}{A} = \eta\ \kappa\ (r - r_0)\,. \tag{12.9}$$

But, since $\eta = 1\ bond/r_0^2$, then

$$\sigma = \frac{\kappa}{r_0}\left(\frac{r - r_0}{r_0}\right) = E\varepsilon, \tag{12.10}$$

where the modulus E is given by:

$$E = \frac{\kappa}{r_0} = \frac{(m \bullet n)\phi_{BE}}{r_0^3}. \tag{12.11}$$

[3]The classical oscillator will oscillate until all its energy is finally dissipated. The quantum oscillator, however, will dissipate its energy in quantum amounts $(n + 1/2)\hbar\omega$ until it finally reaches its ground state. In the ground state, the quantum oscillator will still have *zero-point energy* oscillation: $(1/2)\hbar\omega$.

Example Problem 12.1

Typical primary molecular single-bond energies are ~ 2 eV and typical equilibrium bond lengths are ~ 2Å. Estimate Young's modulus for: (a) (m=9, n=1) bonding potential, (b) (m=9, n=2) bonding potential and (c) (m=9, n=3) bonding potential.

Solution

Equation (12.11) gives:

$$E = \frac{(m \bullet n)\phi_{BE}}{r_0^3}.$$

(a) For (9,1) bonding one obtains:

$$E = \frac{(9 \bullet 1)2\,eV}{(2\mathring{A})^3} = 2.25\frac{eV}{(\mathring{A})^3} \bullet \left(\frac{1.6 \times 10^{-19} J}{1\,eV}\right) \bullet \left(\frac{1\mathring{A}}{10^{-10} m}\right)^3 \bullet \left(\frac{1Nm}{1\,J}\right) \bullet \left(\frac{1GPa}{10^9\,N/m^2}\right) = 360\ GPa.$$

This value of modulus is similar to modulus values reported for medium-strength steels, silicon nitride, titanium carbide, and tantalum carbide.

(b) For (9,2) bonding one obtains:

$$E = \frac{(9 \bullet 2)2eV}{(2\mathring{A})^3} = 720\ GPa.$$

This value of modulus is similar to very hard materials such as tungsten carbide.

(c) For (9,3) bonding one obtains:

$$E = \frac{(9 \bullet 3)2eV}{(2\mathring{A})^3} = 1080\ GPa.$$

This is similar to an extremely hard material such as diamond.

The *elastic energy density* in a macroscopic material can also be determined from the microscopic bonding. The elastic energy density (elastic energy per unit volume) is given by $u_{elastic}$:

$$u_{elastic} = \frac{Total\ Elastic\ Energy}{(Volume)_0} = \frac{\eta \bullet A \bullet \left[\frac{1}{2}\kappa(r - r_0)^2\right] \bullet N}{(Nr_0) \bullet A} \tag{12.12}$$

$$= \frac{1}{2}(\kappa \eta\ r_0)\left[\frac{N(r - r_0)}{Nr_0}\right]^2 = \frac{1}{2}\left(\frac{\kappa}{r_0}\right)\left[\frac{\Delta L}{L_0}\right]^2.$$

Therefore, the elastic energy density in a solid material is given by:

$$u_{elastic} = \frac{1}{2}E\varepsilon^2. \tag{12.13}$$

Example Problem 12.2

For many materials, the elastic region is fairly small (elastic behavior occurs for strains of about 1% or less) and the average bond distance is about 2Å. If the material's modulus is 350 GPa:

(a) Find the elastic energy density for a 1% strain.
(b) Find the elastic energy per atom for a 1% strain.

Solution

The elastic energy density is given by:

$$u_{elastic} = \frac{1}{2}E\varepsilon^2.$$

(a) The elastic energy density becomes:

$$u_{elastic} = \frac{1}{2}(350GPa)(0.01)^2 = 1.75 \times 10^{-2}GPa = 1.75 \times 10^7 \frac{N}{m^2}$$
$$= 1.75 \times 10^7 \frac{Nm}{m^3} \bullet \left(\frac{1J}{1Nm}\right) \bullet \left(\frac{1eV}{1.6 \times 10^{-19}J}\right) \bullet \left(\frac{1m}{100\,cm}\right)^3$$
$$= 1.09 \times 10^{20} \frac{eV}{cm^3}.$$

(b) Since the average bonding distance is 2 Å, the atom density becomes:

$$\frac{1atom}{(2\mathring{A})^3} \bullet \left(\frac{1\mathring{A}}{10^{-8}cm}\right)^3 = 1.25 \times 10^{23} \frac{atoms}{cm^3}.$$

Thus, the elastic energy per atom is:

$$\frac{elastic\ energy}{atom} = \frac{u_{elastic}}{\#atoms/volume} = \frac{1.09 \times 10^{20} eV/cm^3}{1.25 \times 10^{23} atom/cm^3}$$

$$= 8.72 \times 10^{-4} eV/atom$$

$$\cong 1 \times 10^{-3} \frac{eV}{atom}.$$

One should note that the elastic energy per atom is much, much smaller than the average single-bond strength (2 eV) per atom.

12.4 Inelastic/Plastic Behavior of Materials

When the bond is placed under the tensile load of an external force F_{ext}, one can see from Fig. 12.5 that the response of the bond to this load is linear only for very small displacements about r_0. When the displacement r is significantly greater than r_0, then the bond weakens, as indicated by the reduction in force F_{ext} needed to produce the next incremental displacement dr. Finally, as r is increased beyond r_1, the bond can no longer support the large fixed load F_{ext} and the bond will fail.

The value of r = r_1, which is an important bond parameter, can be found by using the fact that the external force F_{ext} is a maximum at $r = r_1$:

$$\left(\frac{\partial F}{\partial r}\right)_{r=r_1} = \left(\frac{\partial^2 \phi}{\partial r^2}\right)_{r=r_1} = 0. \tag{12.14}$$

This gives:

$$r_1 = \left(\frac{m+1}{n+1}\right)^{\frac{1}{m-n}} r_0. \tag{12.15}$$

With r_1 now determined, one can estimate the maximum tensile force that a bond can support:

$$(F_{ext})_{\max} = -(F_{int})_{r=r_1} = \left(\frac{\partial \phi}{\partial r}\right)_{r=r_1}, \tag{12.16}$$

giving,

$$(F_{ext})_{\max} = \left(\frac{\phi_{BE}}{r_0}\right) \eta(m,n), \tag{12.17}$$

Table 12.2 Important Bond-Modeling Parameters (Mie-Grüneisen Potential).

$\eta(m, n)$	m =12	m = 11	m = 10	m = 9	m = 8	m = 7	m = 6
n = 1	0.66	0.64	0.62	0.60	0.58	0.55	0.52
n = 2	1.19	1.15	1.12	1.07	1.03	0.97	0.91
n = 3	1.64	1.59	1.53	1.47	1.39	1.31	1.22
n = 4	2.03	1.96	1.89	1.80	1.71	1.60	1.48
n = 5	2.38	2.29	2.20	2.09	1.98	1.85	1.70
n = 6	2.69	2.59	2.47	2.35	2.21	2.06	
r_1/r_0	m = 12	m = 11	m = 10	m = 9	m = 8	m = 7	m = 6
n = 1	1.19	1.20	1.21	1.22	1.24	1.26	1.28
n = 2	1.16	1.17	1.18	1.19	1.20	1.22	1.24
n = 3	1.14	1.15	1.16	1.16	1.18	1.19	1.21
n = 4	1.13	1.13	1.14	1.15	1.16	1.17	1.18
n = 5	1.12	1.12	1.13	1.14	1.14	1.15	1.17
n = 6	1.11	1.11	1.12	1.13	1.13	1.14	

where,

$$\eta(m,n) = \left(\frac{mn}{m-n}\right)\left[\left(\frac{m+1}{n+1}\right)^{\frac{n+1}{n-m}} - \left(\frac{m+1}{n+1}\right)^{\frac{m+1}{n-m}}\right]. \tag{12.18}$$

In Table 12.2 are shown two key bonding coefficients/parameters for the Mie-Grüneisen potential. Because of their general usefulness and importance, the (m=9, n=1) and (m=9, n=2) potentials are highlighted. Note that the maximum strain $(r_1 - r_0)/r_0$ that the atoms can support before bond breakage occurs is generally $< 30\%$.

Example Problem 12.3

The bond energy for two elements was determined to be 2.5 eV with an equilibrium bond distance of 1.5Å. Assuming that the bond can be described by a (m=9, n=1) bonding potential,

(a) What is the maximum tensile force that the bond can support?
(b) What is the maximum bond displacement from equilibrium before the bond fails?
(c) If there are approximately 10^{15} such bonds per cm^2 in a cross-sectional area of the solid, then estimate the maximum tensile stress, in Giga-Pascals (GPa), that this material can withstand before it ruptures.

Solution

(a) Using Eq. (12.17) and Table 12.2, one obtains:

$$(F_{ext})_{\max} = \left(\frac{\phi_{BE}}{r_0}\right)\ \eta(9,1) = \left(\frac{2.5\,eV}{1.5\mathring{A}}\right)(0.60) = 1\ eV/\mathring{A}.$$

Conversion factors used:

$$1\left(\frac{eV}{\mathring{A}}\right)\left(\frac{1.602\times10^{-12}erg}{eV}\right)\left(\frac{1\mathring{A}}{10^{-8}cm}\right)\left(\frac{1dyne-cm}{erg}\right) = 1.602\times10^{-4}dynes.$$

(b) Table 12.2 tells us that the maximum displacement, before bond rupture occurs, is:

$$\frac{r_1}{r_0} = 1.22 \quad \Rightarrow \quad r_1 - r_0 = 0.22r_0 = 0.22(1.5\mathring{A}) = 0.33\mathring{A}.$$

Note that this represents a strain of:

$$\frac{r_1 - r_0}{r_0} = 22\%.$$

(c) Since it takes a force of 1.6×10^{-4} dynes to rupture a single bond and there are approximately 10^{15} such bonds per cm^2—then it represents a stress of:

$$(stress)_{\max} = \frac{(F_{ext})_{\max}}{bond}\left(\frac{10^{15}bonds}{cm^2}\right) = \left(\frac{1.6\times10^{-4}dynes}{bond}\right)\left(\frac{10^{15}bonds}{cm^2}\right)$$
$$= 1.6\times10^{11}\frac{dynes}{cm^2}.$$

Conversion to GPa becomes:

$$1.6\times10^{11}\frac{dynes}{cm^2}\left(\frac{0.1\,N/m^2}{1dyne/cm^2}\right)\left(\frac{1\,Pa}{1\,N/m^2}\right) = 1.6\times10^{10}Pa = 16GPa.$$

A tensile strength σ_{TS}=16GPa, calculated using our atomistic model, is significantly higher than the typical σ_{TS}=1–2GPa observed during testing of high strength steels. This is because, in real/macroscopic materials, crystalline defects (e.g., vacancies, dislocations, grain boundaries, etc.) exist in polycrystalline materials; these naturally occurring defects can dominate the onset of yielding and the ultimate tensile strength of the material. Dislocations can reduce the ultimate tensile strength of a material by at least an order of magnitude.

12.5 Important Defects Influencing Material Properties

There are three important metal defects that we will discuss: *vacancies, dislocations* and *grain boundaries*. These defects can dominate the electrical, mechanical, and electrochemical properties of the material. Understanding their roles in the materials can have important reliability implications.

12.5.1 Vacancies

A *vacancy* is illustrated in Fig. 12.8. The vacancy is simply a *vacant lattice site* in an otherwise normal matrix. As such, it is usually referred to as a *point defect*. Note that the vacancy might be thought of as a fundamental *unit of free space* in the normal lattice with a volume size of Ω. As discussed in Chapter 11 (see stress migration), the vacancy can move under the presence of stress gradients.[4] The force acting on a vacancy can be written:

$$\vec{F} = -\Omega \vec{\nabla} \sigma, \tag{12.19}$$

where $\vec{\nabla} \sigma$ is the stress gradient and it is a vector quantity. The negative sign in the previous equation is needed because vacancies tend to move from regions of relative tensile stress to regions of relative compressive stress. By *relative*, it is meant that vacancies may also move from regions of higher tensile stress to regions of

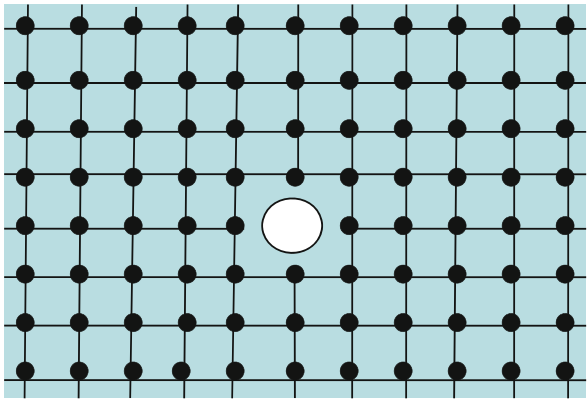

Fig. 12.8 A vacancy (vacant lattice site) is shown in an otherwise normal lattice. The vacancy represents a point defect in the lattice and it has an amount of free space Ω associated with it. Movement of such vacancies, due to stress gradients, and eventual flux divergencies can lead to vacancy-clustering (void-growth) and a weakening/degradation of the material.

[4]The stress gradient is given by: $\vec{\nabla} \sigma = \left[\hat{x} \frac{\partial}{\partial x} + \hat{y} \frac{\partial}{\partial y} + \hat{z} \frac{\partial}{\partial z} \right] \sigma(x, y, z)$.

lower tensile stress. Vacancy movement from regions of lower compressive stress to regions of higher compressive stress can also occur.[5]

A divergence in vacancy movement can lead to voiding. The reliability impact of vacancy movement was discussed under stress migration in Chapter 11. One should always keep in mind that atom flow is opposite to the direction of vacancy flow and can be an important stress-relief mechanism.

Example Problem 12.4

Assuming the *formation/creation energy* for a vacancy is $(\Delta H_o)_{formation} = 1.0$ eV, estimate the vacancy density in a single-crystal piece of Cu at 500°C.

Solution

The density of Cu atoms ρ_{atoms} is given by:

$$\rho_{atoms} = \frac{N_A \rho_{Cu}}{(Atom\ Mass)_{Cu}}$$

$$= \frac{(6.02 \times 10^{23} atoms/mole)(8.6\, g/cm^3)}{63.5\, g/mole}$$

$$= 8.2 \times 10^{22} atoms/cm^3.$$

The Boltzmann probability for vacancy formation gives:

$$\rho_{vacancies} = \rho_{atoms} \exp\left[-\frac{(\Delta H_o)_{formation}}{K_B T}\right].$$

With $(\Delta H_o)_{formation} = 1.0$eV and T = 500°C = 773K, the vacancy density becomes:

$$\rho_{vacancies} = 2.5 \times 10^{16}/\text{cm}^3.$$

12.5.2 Dislocations

An *edge dislocation* is illustrated in Fig. 12.9 and it is usually referred to as a linear defect (extending into and out of the plane of atoms shown). The edge dislocation is created when an extra partial plane of atoms is introduced into an otherwise normal lattice. These dislocations can move under shear stress. As the dislocations move

[5] Atom movement is opposite to vacancy movement. Atoms tend to move from relative compressive regions to relative tensile regions. Such atom movement tends to reduce both the relative compressive stress and the relative tensile stress. Atom (or vacancy) movement due to stress gradients is a stress-relief mechanism.

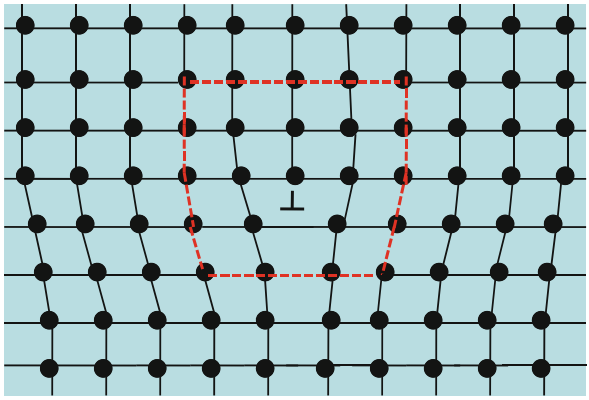

Fig. 12.9 Edge dislocation is illustrated. Note that the edge dislocation represents an extra partial plane of atoms (extending into and out of the plane shown) that has been introduced into an otherwise normal lattice.

under shear stress, they carry mass with them since the dislocation represents an extra partial plane of atoms. Thus, dislocation movement permits mass flow (creep) to occur at much lower values of stress than would be predicted for a defect-free lattice.

For the edge dislocation to move (and thus to carry mass with it), a shearing stress must be developed along a *slip plane* direction. Slip planes are high *specific-density*[6] planes such as (111) planes in a face-centered cubic lattice. Dislocations tend to move with relative ease along these slip planes under a shearing-type stress. Even though a tensile stress may be applied to a material, a shearing stress can also develop as illustrated in Fig. 12.10.

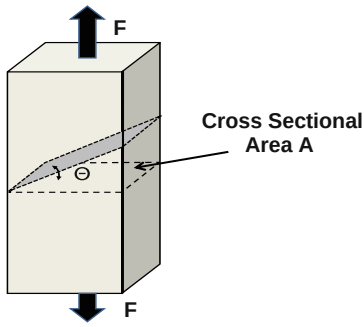

Fig. 12.10 The external force shown produces a tensile stress σ in the material but it also produces a shearing stress τ along the elevated plane as illustrated. The maximum value of the shearing stress occurs for θ=45°, giving a maximum shear stress of $\tau_{max} = \sigma/2$.

The external force shown in Fig. 12.10 serves to put the material in a tensile-stress condition given by: $\sigma = F/A$. However, the external force also serves to produce a shearing force of: $Fsin\theta$ acting over the heavily shaded area $A/cos\theta$. Thus, the shearing stress τ becomes:

$$\tau = \frac{F\sin(\theta)}{A/\cos(\theta)} = \sigma\sin(\theta)\cos(\theta). \tag{12.20}$$

[6] *Specific density* represents the number of atoms per unit area.

It can be easily shown that the maximum shear stress τ_{max} occurs for $\theta = 45°$, thus giving $\tau_{\max} = \sigma/2$.

As the edge dislocation moves along slip planes (illustrated in Fig. 12.11) under a shear stress, it carries this extra partial plane of atoms with it. Thus, dislocation movement under mechanical shear stress can serve as an important mass-flow mechanism—and important mechanism for creep. This leads to creep occurring at much lower values of mechanical stress than would be expected from a perfect lattice.[7] Dislocations can thus be thought of as carriers of mass, permitting material flow from one region to another and bringing about plastic deformation in the material. Strengthening mechanisms in metals, such as steel, are normally associated with reducing the relative ease of dislocation movement. For example, the addition of relatively small amounts of carbon to iron can serve to *pin* the dislocation movement and convert relatively weak iron into strong steel.

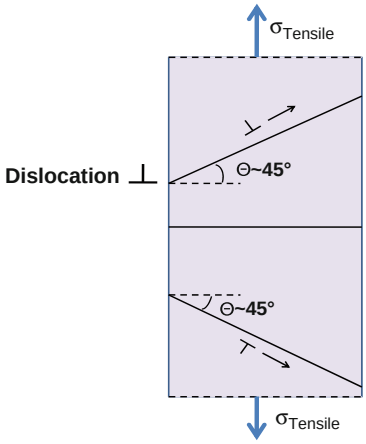

Fig. 12.11 Under tensile loading, the maximum shear stress will develop along planes at 45° to the tensile stress. Dislocations on a slip plane close to this direction can propagate due to the shearing stress. Dislocation movement results in a mass transfer bringing about plastic deformation within the material (creep).

Thus far, our analysis has been primarily confined to bond stability under tensile stress. What happens to the bond under compression? One can see from Fig. 12.5 that, under compression, the external force required to produce an incremental change in dr increases dramatically (below r_0) with no apparent bond breakage/rupture indicated in the figure. While it is generally true that solids are stronger under compressive stress, compressive materials will fail (via cracking, buckling, delamination, blistering, etc.). By putting the polycrystalline material under compression, dislocation movement is again possible, leading to a mass transfer (plastic deformation). One must remember — what gives the bond stability is its negative bond energy ($-\phi_{BE}$). The bond is no longer stable when the work ΔW done by the external force is greater than ϕ_{BE}. Therefore, all bond stability is lost when:

[7] Other dislocation types can exist, such as screws dislocations (not discussed here). These can also be important in the mass-flow/creep process.

$$\Delta W = \int_{r_o}^{r_{fracture}} F_{ext}\, dr \geq \phi_{BE}. \tag{12.21}$$

Similar to our use of tensile strength σ_{TS}, a crushing strength σ_{CS} can also be determined by loading the material under compression. For metals (or any material which can show plastic deformation) the tensile strength and crushing strength are roughly the same. However, for brittle materials such as ceramics, the crushing strength may be as much as 15x greater than the tensile strength. This is because the failure mechanism is quite different in ceramic materials under tension versus compression. Whereas, a single crack can dominate the failure mechanism (rapid crack propagation) under tension, numerous cracks tend to develop under compression and seem to mitigate the erratic/rapid propagation with a single crack. Whereas cracks tend to propagate perpendicular to the tensile stress axis, cracks tend to propagate parallel to the compressive-stress axis. Even if the time-zero crack formation is not parallel to the compressive-stress axis, it is likely to *twist out* of its initial orientation to an orientation parallel to the compressive stress axis. The fact that many cracks tend to form in brittle materials under compressive stress can be used to make fine powders from a much larger piece of the brittle material.

12.5.3 Grain Boundaries

Grain boundaries can often play extremely important roles in the reliability of a material. Many materials (especially metals/conductors) are polycrystalline. Polycrystalline is a term used in materials science to describe solid materials which consist of many tiny single-crystals, called *grains*, co-existing in the solid material. At the region between grains, the *grain boundary*, the two grains may be *poorly matched* in specific density (often referred to as *lattice mismatch*) and this can sometimes lead to weaker-bonded interfaces.

Figure 12.12 illustrates the specific density of atoms for two crystalline planes, (100) and (110), for the face-centered cubic crystalline structure. The number of enclosed atoms for both cases is the same: $1 + 4(1/4) = 2$ atoms for the (100) plane and $2(1/2) + 4(1/4) = 2$ atoms for the (110) plane. However, the areas are different. This causes the specific density for the (100) plane to be higher than the (110) plane. Thus, if these two planes were brought together to form a *grain boundary*, then there would be mismatch in specific densities of atoms (lattice mismatch).

Figure 12.13 illustrates the mismatch that can happen when two grains of different orientations and different specific densities are brought together for joining/bonding. For large specific-density differences at the g-b interface between the two grains, the two grains will be poorly matched resulting in a g-b interface with a relatively high density of dangling and/or stretched bonds. This causes the g-b free energy to increase, relative to the normal-bonding state, and this causes the g-b to become generally weaker and less stable than the grains. The g-bs with large mismatch introduce considerable free space into an otherwise normal lattice

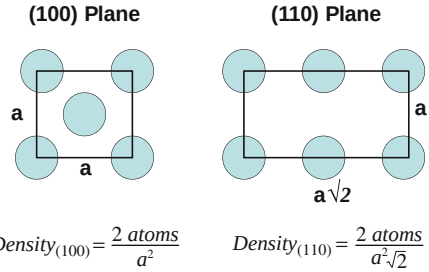

Fig. 12.12 Specific density of atoms is illustrated for (100) and (110) planes in the face-centered cubic crystalline structure. One can see that the specific density of atoms in the (100) plane is greater than in the (110) plane. Thus, if two such interfaces formed the bonding interface, a mismatch in specific density of atoms would occur. This mismatch can lead to dangling and/or severely bent bonds.

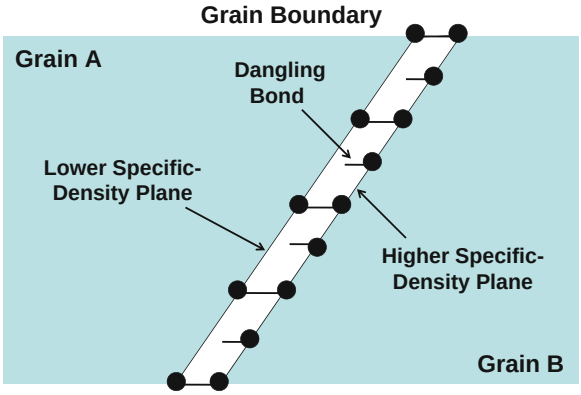

Fig. 12.13 When the two grains A and B are joined along the grain boundary (g-b) interface, a mismatch in specific density of atoms at the interface can result in a large number of dangling and/or stretched bonds along this g-b interface. This causes the g-b free energy to increase above the normal-bonding value and thus causes the g-b to become less stable. This means that g-bs can be prime locations for: enhanced crack propagation, higher corrosion activity, higher impurity precipitation, higher diffusion rates, etc.

and can thus serve as a site for impurity precipitation. Also, the g-bs can serve as prime locations for: crack formation, crack propagation, higher corrosion activity, and higher diffusion rates.

Since poorly matched grain boundaries have much higher free energy versus the better matched ones, then, during high temperature annealing, the grains with preferred orientations will tend to grow at the expense of some of the other grains. This grain growth, in order to minimize the number of high free-energy grain boundaries, will tend to minimize the total number of grain boundaries, i.e., the average grain size increases during annealing. Of course, the grain growth during high temperature annealing will also be subject to any mechanical stresses that might be present (or generated) in the material during the annealing process.

12.6 Fracture Strength of Materials

The facture strength (or toughness) of a material is generally found by recording the strain as the stress is increased (ramped) to failure. The *ramp-stress-to-failure/rupture* test[8] is an important mechanical test for several reasons: (1) it is a time-zero test of relatively short duration, (2) it is a relatively easy test to perform, and (3) it can be a strong indicator of the reliability of such materials/devices.[9] A major downside with *ramp-stress-to-failure* testing is that it is a destructive test. Thus, *ramp-stress-to-failure* testing can only be used on a sampling basis (for a few materials/devices which were randomly selected for the test). The reliability of the remaining population must be statistically inferred.

A *ramp-stress-to-failure/rupture* test is normally used to gather the indicated data that is illustrated in Fig. 12.14. As the stress increases from the zero-strain state, the stress depends linearly on the strain and this continues up to the yield point $\sigma_Y = E\varepsilon_Y$. Above the yield point, the stress depends on the strain in a more complicated fashion (a power-law):

$$\sigma = E\varepsilon \qquad (\varepsilon < \varepsilon_Y) \tag{12.22a}$$

and

$$\sigma = B_0\varepsilon^n \qquad (\varepsilon > \varepsilon_Y). \tag{12.22b}$$

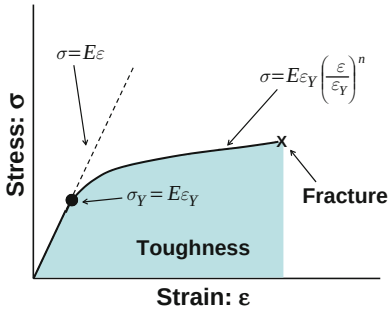

Fig. 12.14 The fracture/rupture strength is determined by ramping up the stress (at some specified rate) and monitoring the strain until fracture/rupture occurs. The toughness is the area under the curve.

By matching the two equations at ε_Y, one obtains:

$$\sigma = E\varepsilon \qquad (\varepsilon \leq \varepsilon_Y) \tag{12.23a}$$

and

[8] The ramp-to-failure/rupture test was described in detail in Chapter 10.

[9] The usefulness of *ramp-voltage-to-breakdown* test for capacitor dielectrics was highlighted in Chapter 11.

$$\sigma = E\varepsilon_Y \left(\frac{\varepsilon}{\varepsilon_Y}\right)^n \qquad (\varepsilon \geq \varepsilon_Y). \tag{12.23b}$$

Generally, n=0.1−0.5 is observed for many materials.

The material toughness is given by the area under the stress-stain (σ−ε) curve:

$$Toughness = \int_0^{\varepsilon_{fracture}} \sigma \, d\varepsilon = E\int_0^{\varepsilon_Y} \varepsilon \, d\varepsilon + E\varepsilon_Y \int_{\varepsilon_Y}^{\varepsilon_{fracture}} \left(\frac{\varepsilon}{\varepsilon_Y}\right)^n d\varepsilon. \tag{12.24}$$

Example Problem 12.5

The stress-strain curve for a material with modulus of E=600GPa was very similar to that shown in Fig. 12.14. If the elastic-strain region extends to a level of 1.5% and the fracture strain is 30%, then calculate the toughness for this material. Assume that the power-law model, which describes the stress versus strain relation in the plastic region, is given by n=0.25.

Solution

$$\begin{aligned}
Toughness &= \int_0^{\varepsilon_{fracture}} \sigma \, d\varepsilon = E\int_0^{\varepsilon_Y} \varepsilon \, d\varepsilon + E\varepsilon_Y \int_{\varepsilon_Y}^{\varepsilon_{fracture}} \left(\frac{\varepsilon}{\varepsilon_Y}\right)^n d\varepsilon \\
&= E\left[\frac{\varepsilon_y^2}{2}\right] + E\left(\varepsilon_y\right)^{1-n} \int_{\varepsilon_y}^{\varepsilon_{fracture}} \varepsilon^n d\varepsilon \\
&= E\left\{\left[\frac{\varepsilon_y^2}{2}\right] + \left(\varepsilon_y\right)^{1-n}\left[\frac{\left(\varepsilon_{fracture}\right)^{n+1} - \left(\varepsilon_y\right)^{n+1}}{n+1}\right]\right\} \\
&= 600GPa\left\{\frac{(0.015)^2}{2} + (0.015)^{0.75}\left[\frac{(0.30)^{1.25} - (0.015)^{1.25}}{1.25}\right]\right\} \\
&= 4.5GPa \\
&= 4.5GPa\left(\frac{10^9\, N/m^2}{1GPa}\right)\left(\frac{1\,J}{1Nm}\right)\left(\frac{1\,eV}{1.6\times 10^{-19}J}\right)\left(\frac{1m}{100\,cm}\right)^3 \\
&= 2.8\times 10^{22} eV/cm^3.
\end{aligned}$$

In Problem 1 of Chapter 4, it was shown that ~10^{23}atoms/cm^3 exist in most dense solids. Therefore, the toughness represents only a few tenths of eV/atom, significantly lower than the bond energy per atom. This is because of intrinsic lattice defects (vacancies, dislocations, grain boundaries, etc.) existing in the materials.

12.7 Stress Relief in Materials

From the discussions in this chapter, one should now clearly understand that the bonding energy of a solid material is negative and reaches its lowest value when the bonded atoms are in their equilibrium state (non-stretched or non-compressed state). Mechanically stressing the material, either by stretching or compressing the bonds, serves to raise the total energy of the material, making the material less stable and more prone to degradation and eventual failure. Therefore, materials will tend to look for ways of relaxing the mechanical stress σ (e.g., vacancy movement, dislocation movement, cracking, buckling, delamination, etc.). These are all important stress-relief mechanisms.

The time dependence of the stress relief, as illustrated in Fig. 12.15, generally takes the form:

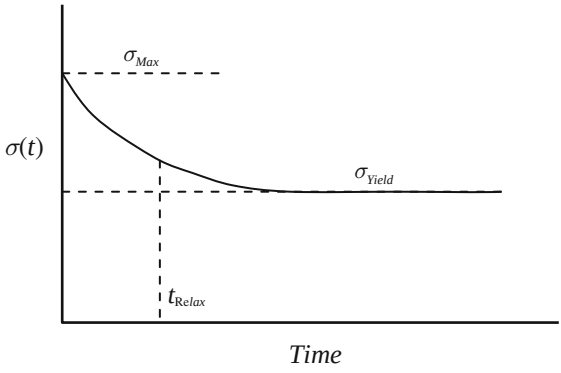

Fig. 12.15 General stress-relaxation curve is illustrated. Stress relaxation may take many forms: vacancy movement, dislocation movement, voiding, cracking, buckling, delamination, etc.

$$\frac{d\sigma}{dt} = -k\,(\sigma - \sigma_{Yield}), \tag{12.25}$$

where k is a stress-relaxation rate constant and σ_{yield} is the yield stress. Below the yield stress, it is assumed that little/no relaxation is possible and the material will show elastic behavior (no further degradation with time). Separation of variables and integration of Eq. (12.25),

$$\int_{\sigma_{Max}}^{\sigma} \frac{d\sigma}{(\sigma - \sigma_{Yield})} = -k \int_{0}^{t} dt, \tag{12.26}$$

gives:

$$\sigma(t) \;=\; \sigma_{Yield} \;+\; (\sigma_{Max} - \sigma_{Yield}) \exp(-kt)\,. \tag{12.27}$$

Solving Eq. (12.27) for the time-to-relax ($t = t_{Relax}$), one obtains:

$$t_{Relax} = -\left(\frac{1}{k}\right) \ln\left[\frac{\sigma(t = t_{Relax}) - \sigma_{yield}}{\sigma_{\max} - \sigma_{yield}}\right]. \tag{12.28}$$

The time for the stress $[\sigma(t = t_{Relax}) - \sigma_{yield}]$ to relax, to one-half of its original value $[\sigma_{\max} - \sigma_{yield}]$, is given by:

$$t_{Relax} = \frac{\ln(2)}{k}. \quad ^{10} \tag{12.29}$$

Stress relaxation can take on several materials-degradation forms: creep, voiding, cracking, delamination, blistering, buckling, etc. The stress relaxation process will continue until the mechanical stress level (originally above the yield strength of the material) relaxes to the yield strength of the material. The yield stress may be quite high and rather precisely defined for some materials (steel) but low and poorly defined for others (aluminum). For brittle materials, such as ceramics, crack formation and propagation may be the only effective stress-relief mechanism available.

12.8 Creep-Induced Failures

One of the more important failure mechanisms for mechanical systems is creep-induced failure. *Creep* can refer to an *increase in strain with time for a fixed load (constant stress)*.[11] However, creep can also refer to *stress relaxation for a fixed strain*. Either type of creep can produce material degradation as illustrated in Fig. 12.16 and eventual device failure in certain applications.

12.8.1 Creep Under Constant Load/Stress Conditions

Creep under a constant load (constant stress) is shown in Fig. 12.17. When the material is exposed to an applied stress σ, the time-zero strain that occurs is: $\varepsilon = (L - L_0)/L_o$. If the applied stress (which is assumed to be beyond the material's elastic-region/yield-point) is held constant, then strain will increase with time: $\varepsilon(t) = [L(t) - L_0]/L_o$.

[10] Recall from Chapter 8, one expects the relaxation-rate constant to be thermally activated: $k = k_o \exp\left[-Q/(K_B T)\right]$.

[11] The load/force is constant. The average stress is only approximately constant during testing due to some expected cross-sectional area changes.

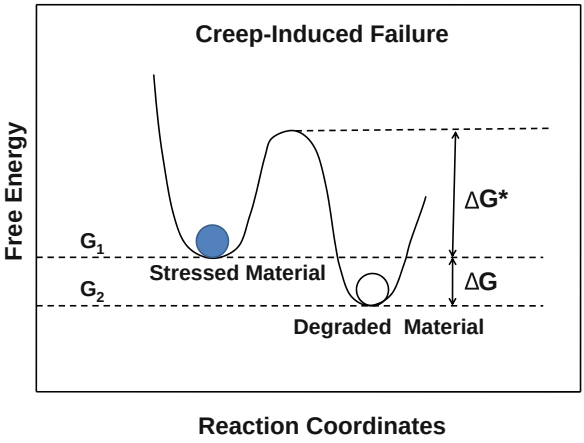

Fig. 12.16 When a mechanical stress is applied to a material, the material can become metastable with a driving force (ΔG) favoring the degraded state. However, the rate of the degradation (creep) is limited by the activation energy (ΔG^*) which is generally associated with dislocation movement along the slip planes.

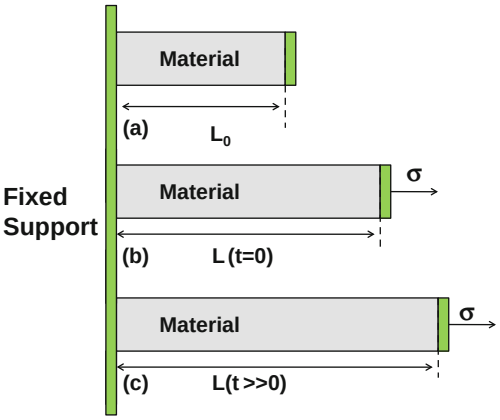

Fig. 12.17 Creep behavior under a fixed load (constant stress). (a) At time zero, the length of the material is L_0. (b) Immediately after a stress σ is applied, the strain is: $\varepsilon = (L - L_0)/L_0$. (c) If the applied stress σ (assumed to be above the materials yield-point) is held constant, then the strain $\varepsilon(t) = [L(t) - L_0]/L_0]$ will increase with time. Creep, under constant load, is usually referred to as an increase in strain with time for a fixed stress.

A typical creep curve is shown in Fig. 12.18. After an initial period of non-linear creep, the creep shows an extended period of linear behavior and then, eventually, a shorter period of rapid turn-up and material rupture. Also, one can see in Fig. 12.19 the creep rate depends on the stress level in the material and the temperature (creep is thermally activated). Generally, creep can be an issue for metals when the use temperature is above 40% of the melting temperature: $T_{creep} > 0.4\ T_{melt}$, where

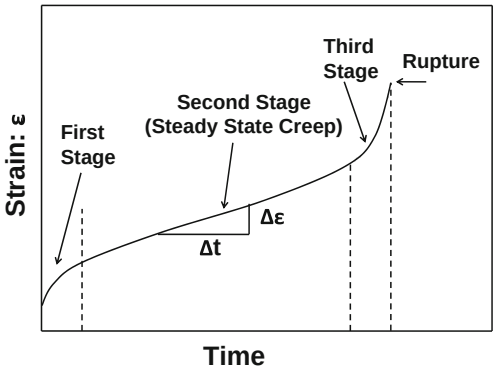

Fig. 12.18 Typical creep behavior for ductile materials is illustrated.

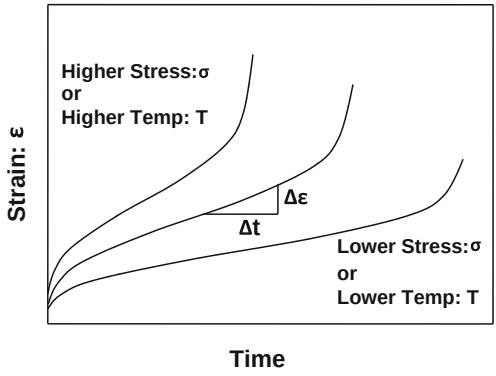

Fig. 12.19 Creep rate dε/dt increases with stress. Creep rate is also thermally activated.

temperatures must be expressed in Kelvin. For example, aluminum melts at 660°C (933 K). Therefore, creep in Al could become an issue for $T_{creep} > 0.4(933K) = 373K = 100°C$.[12]

In the linear creep region (steady-state creep region), the creep as a function of time is given by:

$$\varepsilon(t) = \varepsilon_0 + \left(\frac{d\varepsilon}{dt}\right) t. \tag{12.30}$$

From the previous equation, one can see that the creep rate (dε/dt) is of primary/fundamental importance and becomes the focus of our attention. The creep can continue until a time-to-failure is reached. Time-to-failure (TF) will occur when the total creep becomes too large for specified tolerances (or the material fractures/ruptures) at t = TF, giving:

[12]Recall, from Chapter 11, that the stress-migration/creep bakes for aluminum were generally done at temperatures above 100°C.

$$TF = \left[\frac{\varepsilon(t = TF) - \varepsilon_0}{(d\varepsilon/dt)}\right]. \tag{12.31}$$

One can see from the previous equation that the time-to-failure is directly proportional to the amount of creep that can be tolerated and with a simple inverse-dependence on creep rate (since the creep rate is constant in the linear creep region).

For the information shown in Fig. 12.19, one can see that the creep rate (dϵ/dt) depends on both the level of stress and the temperature (thermally activated). Thus, the creep rate can be written:

$$\frac{d\varepsilon}{dt} = B_0(\sigma - \sigma_{yield})^n \exp\left(-\frac{Q}{K_B T}\right). \tag{12.32}$$

Since the creep rate (degradation rate) for constant stress σ takes the above form, then the time-to-failure equation can be easily extracted:

$$\int_0^{\varepsilon_{crit}} d\varepsilon = \left[B_0(\sigma - \sigma_{yield})^n \exp\left(-\frac{Q}{K_B T}\right)\right] \int_0^{TF} dt, \tag{12.33}$$

giving,

$$TF = A_o(\sigma - \sigma_{yield})^{-n} \exp\left(\frac{Q}{K_B T}\right). \tag{12.34}$$

Note that the kinetics (*n, Q*) for creep rate *dε/dt* and time-to-failure *TF* are the same, except for a change of sign. This is because the creep is assumed to increase linearly with time (creep rate is constant). As before, A_o is a material/process-dependent coefficient that depends on the total amount of creep that can be tolerated. A_o can vary from device to device and generally results in a lognormal or Weibull distribution of times-to-failure. Often, the time-to-failure stress dependence is described by n=1–3 for relative soft/weak materials (e.g., Pb-alloy solders and viscous glasses), n=3–6 for strong metals (e.g., mild steels and many inter-metallic formations) and n=6–9 for very strong/brittle materials (e.g., hardened steels and ceramics).

One should be cautioned against taking creep-rate data under very high-stress/high-temperature test conditions and then extrapolating to very low-stress/low-temperature operational conditions using the same kinetic values (n,Q). Generally, when creep testing above $T > 0.5T_{melt}$ one my observe different values for n and activation energy Q than when creep testing at temperatures $T < 0.5T_{melt}$. One needs to ensure that the extrapolations from stress to use conditions are not too optimistic. This caution is emphasized in Example Problem 12.6.

Example Problem 12.6

Creep-rate (dϵ/dt) data was collected for a given metal alloy and the results are shown in the following test matrix. The tensile stress and temperature conditions during testing are indicated in the table. For this particular metal alloy, the yield strength is very low (relative to the stress conditions used) and therefore can be neglected.

Table 12.3 Creep-Rate (dϵ/dt) Data For A Metal Alloy.

	Temperature		
Stress	400°C	450°C	500°C
1.0 MPa	0.001/hr	0.01/hr	0.1/hr
1.5 MPa	–	0.05/hr	–
2.0 MPa	–	0.16/hr	–

(a) Determine the activation energy Q and the stress dependence exponent n that produce the best fitting for the accelerated data for this metal alloy.
(b) Construct the time-to-failure equation for this metal alloy.
(c) Construct the acceleration factor equation for this metal alloy.
(d) If a mechanical component (made of this metal alloy) fails in 2 hrs at a tensile stress level of 1.9MPa and a temperature of 380°C, how long would the component be expected to last at 1.25MPa and a temperature of 310°C?
(e) How long would the component be expected to last at a tensile stress level of 0.5MPa and a temperature of 250°C?

Solution

The creep rate equation is given by:

$$\frac{d\varepsilon}{dt} = B_o(\sigma)^n \exp\left(-\frac{Q}{K_B T}\right).$$

Taking the natural logarithm of both sides of the equation yields:

$$Ln(d\varepsilon/dt) = Ln(B_o) \quad + \quad nLn(\sigma) \quad - \quad \frac{Q}{K_B T}.$$

Thus, the activation energy for the creep is given by,

$$Q = -K_B \left(\frac{\partial Ln(d\varepsilon/dt)}{\partial(1/T)}\right)_{\sigma=constant},$$

and the creep exponent n is given by:

$$n = \left(\frac{\partial Ln(d\varepsilon/dt)}{\partial Ln(\sigma)}\right)_{T=constant} = \left(\frac{\partial Log(d\varepsilon/dt)}{\partial Log(\sigma)}\right)_{T=constant}.$$

(a) The plot of Ln(dε/dt) versus (1/T) is shown in Fig. 12.20 for the constant stress condition of 1MPa. [Reminder: one must always convert the temperature from degrees centigrade (^{0}C) to Kelvin (K).]

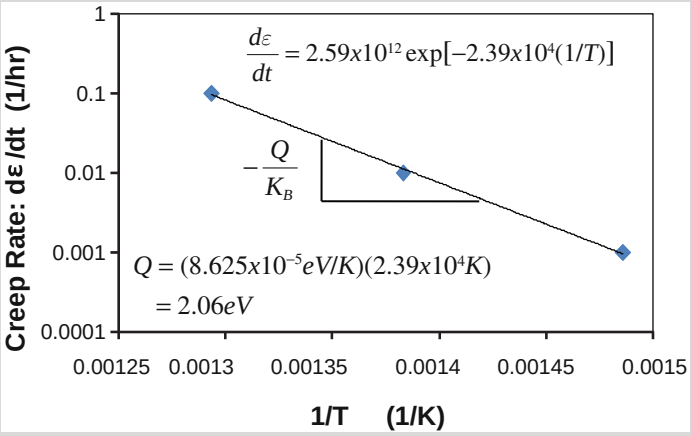

Fig. 12.20 Semi-log plot of creep rate (dε/dt) versus 1/T is shown.

From the slope of the previous plot, one obtains:

$$Q = -K_B\left(\frac{\partial Ln(d\varepsilon/dt)}{\partial(1/T)}\right)_{\sigma=constant} = 2.06eV.$$

The log-log plot of creep rate ($d\varepsilon/dt$) versus stress (σ) is shown in Fig. 12.21 for the constant temperature condition of 450^{0}C=723 K.

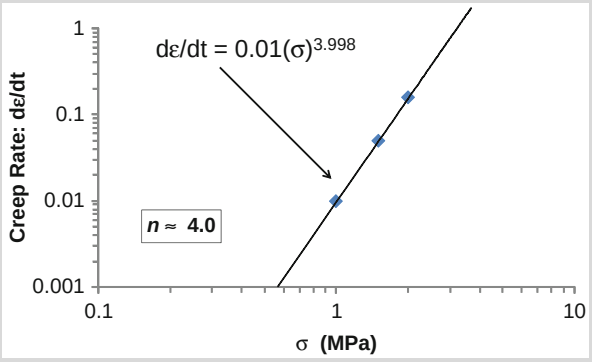

Fig. 12.21 Log-Log plot of creep rate (dε/dt) versus stress (σ) is shown.

From the previous plot one obtains the creep power-law exponent n:

$$n = \left(\frac{\partial Ln(d\varepsilon/dt)}{\partial Ln(\sigma)}\right)_{T=constant} = \left(\frac{\partial Log(d\varepsilon/dt)}{\partial Log(\sigma)}\right)_{T=constant} \cong 4.0.$$

(b) The time-to-failure equation for this metal alloy is given by:

$$TF = A_o(\sigma)^{-4} \exp\left(\frac{2.06\,eV}{K_B T}\right).$$

(c) The acceleration factor for this metal alloy use conditions is:

$$AF = \frac{(TF)_1}{(TF)_2} = \left(\frac{\sigma_2}{\sigma_1}\right)^4 \exp\left[\frac{2.06\,eV}{K_B}\left(\frac{1}{T_1} - \frac{1}{T_2}\right)\right].$$

(d) The acceleration factor becomes:

$$AF = \left(\frac{1.9\,MPa}{1.25\,MPa}\right)^4 \exp\left[\frac{2.06\,eV}{8.62 \times 10^{-5}\frac{eV}{K}}\left(\frac{1}{(310+273)K} - \frac{1}{(380+273)K}\right)\right]$$
$$= (5.34)(81.0) = 432.5\ .$$

The time to failure becomes:

$$TF_{1.25\,MPa,\,310^oC} = AF \bullet TF_{1.9\,MPa,380^oC} = (432.5) \bullet (2hrs) = 865hrs.$$

(e) Note that the proposed use conditions (0.5MPa, 250°C) are well below the regions where accelerated data was actually taken (see the previous table).

Optimistic approach: assume that the kinetics (n=4, $Q_{creep} = 2.06$eV) are valid throughout the full range of stresses and temperatures, giving:

$$AF = \left(\frac{1.9\,MPa}{0.5\,MPa}\right)^4 \exp\left[\frac{2.06\,eV}{8.62 \times 10^{-5}\frac{eV}{K}}\left(\frac{1}{(250+273)K} - \frac{1}{(380+273)K}\right)\right]$$
$$= (208.5)(8926.6) = 1.86 \times 10^6.$$

The time-to-failure becomes:

$$TF_{0.1\,MPa,\,200^oC} = AF \bullet TF_{1.9\,MPa,380^oC} = (1.86 \times 10^6) \bullet (2hrs) = 3.72 \times 10^6 hrs$$
$$= 3.72 \times 10^6 hr\left(\frac{1\,yr}{8760hr}\right) = 425yrs.$$

Conservative approach: assume that the kinetics (n=4, Q_{creep} = 2.06eV) are valid over the region where actual data is available and then use more conservative kinetic values (n=2 and Q_{creep} = 1.0eV) below this region.

$$AF = \left(\frac{1.9\,MPa}{1.0\,MPa}\right)^4 \bullet \left(\frac{1.0\,MPa}{0.5\,MPa}\right)^2$$

$$\bullet \exp\left[\frac{2.06\,eV}{8.62\times10^{-5}\frac{eV}{K}}\left(\frac{1}{(300+273)K}-\frac{1}{(380+273)K}\right)\right]$$

$$\bullet \exp\left[\frac{1.0\,eV}{8.62\times10^{-5}\frac{eV}{K}}\left(\frac{1}{(250+273)K}-\frac{1}{(300+273)K}\right)\right]$$

$$= (13.03) \bullet (4) \bullet (165.6) \bullet (6.93) = 5.98\times10^4.$$

Using this more conservative approach, the time-to-failure becomes:

$$TF_{0.5\,MPa,250^oC} = AF \bullet TF_{1.9\,MPa,380^oC} = (5.98\times10^4) \bullet (2hrs) = 1.20\times10^5 hrs$$
$$=1.2\times10^5 hrs\left(\frac{1\,yr}{8760hrs}\right) = 13.7yrs.$$

Example Problem 12.7

Shown in Fig. 12.22 is a mechanical rotor that must rotate continuously at 2500 revolutions per minute (rpm). A heavy mass (0.5 kg) is attached to the end of an aluminum connecting rod (10 cm long, cross sectional-area 1 cm^2). The mass of the connecting rod is negligible compared to the heavy mass on the end. The designer is worried that the tensile stress in the small diameter connecting rod (during 2500 rpm operation) may be excessive and creep will eventually cause the large mass to come into contact with the cylindrical walls causing the component to freeze up (fail). To test his hypothesis, the engineer decided to use accelerated testing and subjected the component to accelerated operation at 8000 rpm for an extended period of time. The component failed in 18hrs, because of creep, i.e., the large revolving mass started to rub the cylindrical wall ($\Delta r = \Delta x$) after 18 hrs under these accelerated conditions.

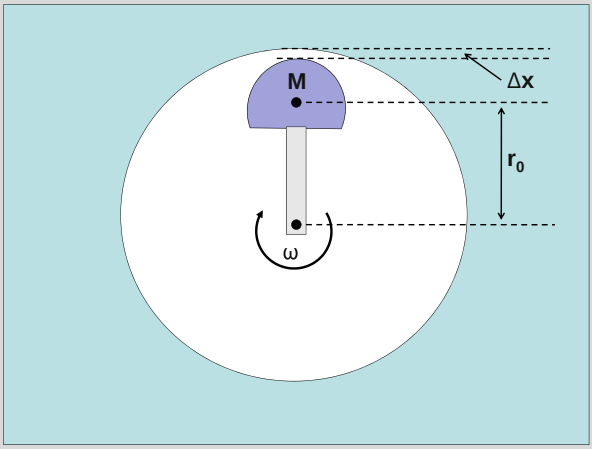

Fig. 12.22 Mechanical rotor is designed to rotate at an angular speed of ω. The rotor consists of a heavy mass M that is constrained to rotate by a light Al-alloy connecting rod. The tolerance Δx is the free space between the mass and the cylinder walls. If significant creep with time occurs in the aluminum rod, the mass will make contact with the cylinder walls and the rotor will fail (freeze up).

Assume the following material properties for the aluminum-alloy connecting rod: tensile strength $\sigma_{TS} = 0.6$ GPa, modulus E = 75 GPa, a negligible yield point, and a stress dependence power-law exponent of n=4.

a) Find the stress in the aluminum component during 8000 rpm accelerated operation.
b) Find the stress in the aluminum component for the expected normal 2500 rpm operation.
c) Given that the aluminum component lasted 18hrs at 8000 rpm, how long would the component last during normal operation at 2500 rpm?

Solution

a) Due to circular motion, tensile stress is constant in the aluminum-alloy rod and is given by:

$$\sigma_{T,8000\,rpm} = \frac{F_r}{A} = \frac{Mr\omega^2}{1\,cm^2}$$

$$= \frac{(0.5\,kg)(0.1m)[2\pi(8000\,rpm)(1\,\text{min}/60\,\text{sec})]^2}{1\,cm^2}\left(\frac{100\,cm}{1m}\right)^2$$

$$= 0.351 \times 10^9\,N/m^2 = 0.351GPa.$$

With no yield point, creep is expected at 8000 rpm.

b) At 2500 rpm, the tensile stress would be:

$$\sigma_{T,2500\,rpm} = \left(\frac{\omega_{use}}{\omega_{accelerated}}\right)^2 \sigma_{T,8000\,rpm} = \left(\frac{2500}{8000}\right)^2 (0.351GPa)$$
$$= 0.034GPa.$$

c) The acceleration factor is:

$$AF = \frac{TF_{@2500\,rpm}}{TF_{@8000\,rpm}} = \left(\frac{\sigma_{T,8000\,rpm}}{\sigma_{T,2500\,rpm}}\right)^4 = \left(\frac{\omega^2_{@8000\,rpm}}{\omega^2_{@2500\,rpm}}\right)^4$$
$$= \left(\frac{8000}{2500}\right)^8 = 1.1 \times 10^4.$$

Therefore, for 2500 rpm operation, then one would expect the component to last:

$$TF_{@2500\,rpm} \geq AF \bullet TF_{@8000\,rpm} = (1.1 \times 10^4)(18hrs) = 198,000hrs$$
$$= 198,000hrs\left(\frac{1\,yr}{8760hr}\right) = 22.6\ yrs.$$

Note that the AF depends on the 8th power of the angular speed. Hopefully, one can start to better understand why mechanical components in an engine tend to fail much, much faster under engine race conditions (8000+ rpm) versus normal auto driving conditions (2500 rpm).

12.8.2 Creep Under Constant Strain Conditions

Creep under a constant strain is shown in Fig. 12.23. When the material is exposed to an applied stress σ (assumed to be above the material's yield point), the time-zero strain that occurs is: $\varepsilon = (L - L_0)/L_o$.

If the *strain is held constant* and the stress is monitored with time, then the stress $\sigma(t)$ will relax with time—the forced per unit area needed to hold the fixed strain in the material will reduce with time. General features of stress relaxation were discussed earlier, see Fig. 12.15, but we would like to take a closer look at stress relaxation under the condition of constant strain.

The total strain can be written in terms of the elastic (recoverable) part plus the plastic (permanent deformation) part:

$$\varepsilon_{total} = \varepsilon_{elastic} + \varepsilon_{plastic}. \tag{12.35}$$

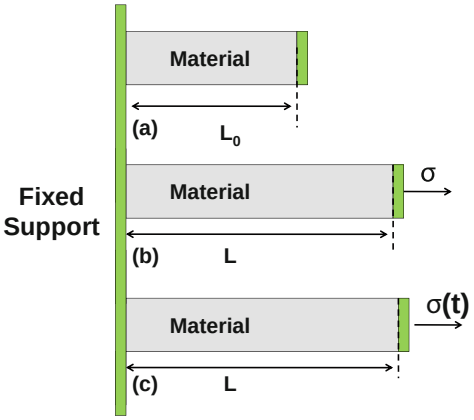

Fig. 12.23 Illustration of creep under a fixed strain. (a) At time zero, the length of the material is L_0. (b) Immediately after a stress σ is applied, the strain is: $\varepsilon = (L - L_0)/L_0$. (c) If the strain is held constant, then the stress σ(t) will be a function of time. Creep at constant strain is referred to as stress relaxation. The time dependence of the stress relaxation is expected to be similar to that shown in Fig. 12.15.

For stress relaxation, where the total strain remains constant, then

$$\frac{d\varepsilon_{total}}{dt} = 0 \quad \Rightarrow \quad \frac{d\varepsilon_{plastic}}{dt} = -\frac{d\varepsilon_{elastic}}{dt} = -\frac{1}{E}\frac{d\sigma}{dt}. \tag{12.36}$$

Creep occurs because of plastic deformation, therefore:

$$\frac{d\varepsilon_{plastic}}{dt} = A_0(\sigma - \sigma_{yield})^n \exp\left(\frac{-Q}{K_B T}\right). \tag{12.37}$$

For constant strain, one can use Eq. (12.35) to write:

$$\frac{d\varepsilon_{plastic}}{dt} = -\frac{d\varepsilon_{elastic}}{dt} = -\frac{1}{E}\frac{d\sigma}{dt} = B_0(\sigma - \sigma_{yield})^n. \tag{12.38}$$

Separating variables in Eq. (12.38) and integrating, one obtains:

$$\int_{\sigma_{\max}}^{\sigma} \frac{d\sigma}{(\sigma - \sigma_{yield})^n} = -B_0 E \int_0^t dt. \tag{12.39}$$

For n=1, the previous equation reduces to Eq. (12.27):

$$\sigma(t) - \sigma_{yield} = (\sigma_{\max} - \sigma_{yield}) \exp[-kt], \tag{12.40}$$

where k is the relaxation rate constant, $k = B_0 E$. If we define time-to-failure (TF) as the stress level at which $[\sigma(t = TF) - \sigma_{yield}]$ becomes some fraction f of $[\sigma_{max} - \sigma_{yield}]$, then:

$$\begin{aligned} TF &= -\tfrac{1}{k}\ln(f) \\ &= -\tfrac{\ln(f)}{k_o}\exp\left(\tfrac{Q}{K_B T}\right), \end{aligned} \tag{12.41}$$

where we have used the expectation from Chapter 8 that the relaxation rate constant will be thermally activated and given by,

$$k = k_o \exp\left[-\frac{Q}{K_B T}\right]. \tag{12.42}$$

For values of n≠1, one obtains from Eq. (12.39):

$$\frac{1}{[\sigma(t) - \sigma_{yield}]^{n-1}} - \frac{1}{[\sigma_{\max} - \sigma_{yield}]^{n-1}} = (n-1)\,kt. \tag{12.43}$$

Again, if one defines time-to-failure (TF) as $[\sigma(t = TF) - \sigma_{yield}] = f[\sigma_{max} - \sigma_{yield}]$, then:

$$\begin{aligned} TF &= \frac{1}{k(n-1)[\sigma_{\max} - \sigma_{yield}]^{n-1}}\left[\frac{1 - f^{n-1}}{f^{n-1}}\right] \\ &= \frac{1}{k_o(n-1)[\sigma_{\max} - \sigma_{yield}]^{n-1}}\left[\frac{1 - f^{n-1}}{f^{n-1}}\right]\exp\left(\frac{Q}{K_B T}\right) \\ &= A_0\left(\sigma_{\max} - \sigma_{yield}\right)^{-(n-1)}\exp\left(\frac{Q}{K_B T}\right). \end{aligned} \tag{12.44}$$

At first glance, stress relaxation might be thought to be a good thing— *lower stress is good, right*? *No, not always*. Many fasteners (e.g., nuts and bolts) may rely on very high stress levels to properly *clamp things into place*. This is why one generally wants to *snug up* a nut on a bolt during the assembly of mechanical components so that the nut and bolt will serve as an adequate clamp for the components (so that they will be held tightly in place). In a critically important clamping application, one does not want the stress in the materials to relax. This is illustrated in Example Problem 12.8.

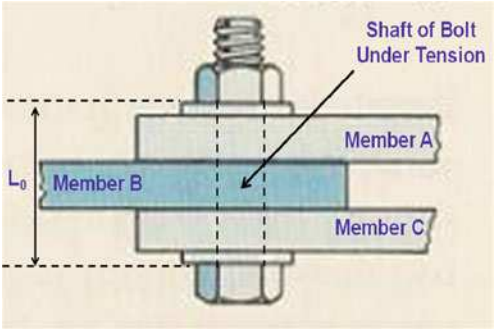

Fig. 12.24 Nut and bolt are used to clamp three members of a multi-component system. As the nut is tightened (to create an effective clamp) the bolt shaft comes under a state of tension while members A, B, and C are compressed.

Example Problem 12.8

Three mechanical components are fastened/clamped using a nut and bolt as illustrated in Fig. 12.24. During the initial stage of tightening of the nut, free space is simply being eliminated between the nut and the various members as shown. Once the free space is eliminated, then the tensile stress rises rapidly in the bolt shaft with each turn of the nut. Due to the pitch of the threads on the bolt, during each turn of the nut (after free space elimination), the length of unstressed bolt region (above the nut) increases by 0.4% for each complete turn of the nut. The properties of the mild steel used in bolt and nut fabrication are: modulus E= 200 GPa, tensile yield strength σ_Y= 0.2 GPa, tensile strength σ_{TS} = 0.5 GPa, and a power-law creep exponent of n=4. To make sure that the members are properly clamped, the nut is tightened to a tensile level of 0.4 GPa in the bolt and the level of stress must stay above 0.25 GPa for adequate clamping.

a) Immediately after the free space elimination between nut and members, estimate the tensile stress in the bolt with each additional ¼ turn of the nut.
b) If we assume that most of the stress relaxation occurs within the shaft of the bolt, as opposed to the other materials, then if the stress in the bolt relaxes from 0.4 GPa to 0.35 GPa in 1 year, how long will it take for the stress to relax to 0.25 GPa?

Solution

(a) Assume that the bolt is initially in the elastic region. Since a single turn of the nut produces a strain of 0.004 in the bolt, then the ¼ turn will produce a strain of 0.001. The tensile stress σ in the bolt associated with this level of strain (ε = 0.001) is:

$$\sigma = E\varepsilon = (200GPa)(0.001) = 0.2GPa.$$

(b) First we must determine the relaxation rate constant *k*. Assuming a creep power-law exponent of n = 4, one obtains:

$$k = \frac{1}{3t}\left[\frac{1}{\sigma(t)^3} - \frac{1}{\sigma_{\max}^3}\right]$$
$$= \frac{1}{3(1\,yr)}\left[\frac{1}{(0.35GPa)^3} - \frac{1}{(0.4GPa)^3}\right]$$
$$= \frac{2.57}{(GPa)^3\,yr}.$$

Thus, the time-to-relax to a value of 0.25GPa becomes:

$$t = \frac{1}{3\,k}\left[\frac{1}{\sigma(t)^3} - \frac{1}{\sigma_{\max}^3}\right]$$
$$= \frac{1}{3\left(\frac{2.57}{(GPa)^3\,yr}\right)}\left[\frac{1}{(0.25GPa)^3} - \frac{1}{(0.4GPa)^3}\right]$$
$$= 6.3\,yr.$$

Let us now turn our attention to what is happening to the metal inside the shaft of the bolt. As the tensile stress in the shaft of the bolt relaxes, the bolt loses some of its clamping effectiveness. This stress relaxation necessitates a continual tightening of the nut to maintain proper clamping. Let us suppose that every six months the nut must be turned one-quarter of a turn in order to return the shaft of the bolt back to its original tensile stress level (which restores its original clamping effectiveness). With each complete turn, the nut (due to the pitch of the threads on the bolt/nut) results in 0.4% of the mass (originally in the shaft) now being above the top of the nut. Since the mass of the bolt above the top of the nut is virtually in a stress-free state then, effectively, 0.4% of the metal in the shaft of the bolt will transfer/flow from the high stress shaft region of the bolt to a lower stress region above the nut every two years. Since this is a mass-conserving process, then the density of the metal in the shaft must be reducing with time (due to the flux divergence effect discussed in Chapter 4). This reduction in density of the metal in the shaft with time normally results in void formations along grain boundaries which are roughly perpendicular to the axis of the shaft, as illustrated in Fig. 12.25.

The previous example (voiding in the shaft of a bolt under tension) serves to illustrate a very important point: atoms will flow from regions of higher stress to regions of lower stress so as to reduce the stress-level in the material. However, this material flow, and resulting flux divergences (as discussed in Chapter 4), can produce void formations in the material. The mass flow and voiding at temperatures well below the melting temperature, tend to occur along grain boundaries finally resulting in failure with time.

12.9 Crack-Induced Failures

Crack-induced failures can be particularly important because it is difficult to fabricate mechanical devices without at least some micro-cracks developing during fabrication. Once a crack has developed, the crack may tend to propagate under loading with *crack propagation* eventually leading to device failure.

At first thought, the introduction of a small crack would seem to be insignificant. For example, suppose that one introduces a small thin crack of radius a in a

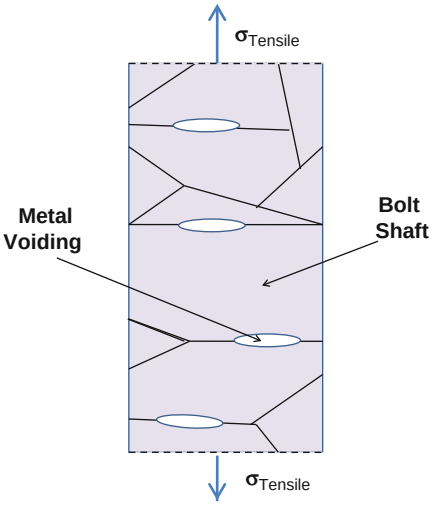

Fig. 12.25 For confined metals under tension, stress relaxation can result in void formations along grain boundaries.

cylindrical rod of radius R. Further assume that the crack is perpendicular to the length of the rod which is the tensile-stress axis. Thus, the impact on the average tensile stress would be:

$$\sigma_T = \frac{F}{\pi R^2 - \pi a^2} = \frac{(\sigma_T)_o}{1 - \left(\frac{a}{R}\right)^2}. \tag{12.45}$$

Thus, the impact of a small crack on the average tensile stress would seem to be very small if $a << R$. However, Eq. (12.45) is not valid for reliability assessments of materials with cracks. To emphasize this, suppose that the initial tensile $(\sigma_T)_o$ is well below the yield strength of the material. With the introduction of a small crack, it is unlikely that the small crack (a<<R) introduction will cause the average tensile stress σ_T to increase above the yield strength of the material. Thus, one might come to the erroneous conclusion that the small crack should have little/no impact on the reliability of the cylindrical rod. Our initial reliability assessment of the reliability impact of the crack is flawed (pardon the pun) because it ignores the *stress raisers/risers* at crack tips.

12.9.1 Stress Raisers/Risers At Crack Tips

Eq. (12.45) is not the proper reliability analysis for a crack. While it does comprehend a small rise in average tensile stress in the rod with crack introduction, this equation does not comprehend the large *stress raiser/riser*[13] that can occur at the

[13]Historically, these localized stresses at crack tips have been referred to as either *stress raisers* or *stress risers.* The terms will be used interchangeably.

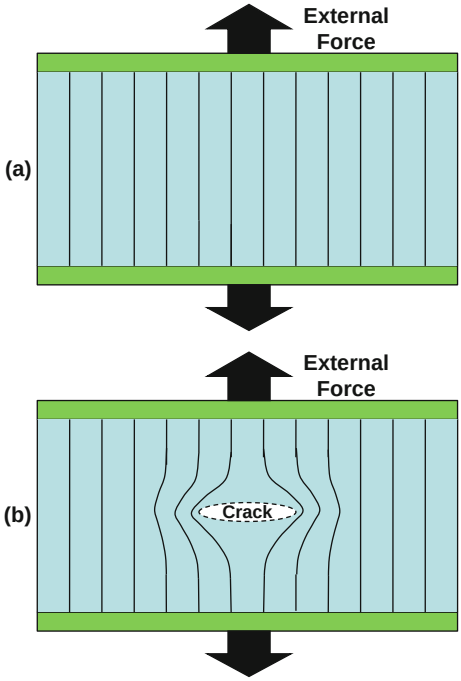

Fig. 12.26 (a) Lines of force are uniform and parallel initially, producing a uniform stress of σ=Force/Area. (b) The introduction of the crack causes the lines of force to become non-uniform and non-parallel (producing a crowding of force lines at the crack tip). The higher density of force lines at the crack tip produces a stress riser (much higher stress level than the uniform stress level σ) and this may induce additional crack growth.

tips of the crack. This is illustrated in Fig. 12.26, where we look more closely at what happens to the lines of force when a crack is introduced.

The lines of force before and after a horizontal crack introduction are shown in Fig. 12.26. Before the introduction of the crack, the lines of force are parallel and uniform, producing a uniform tensile stress σ *(=F/Area)* as illustrated in Fig. 12.26a. However, after crack introduction, the lines of force are no longer uniform and parallel as illustrated in Fig. 12.26b.

The higher density of lines of force at the tips of the crack produces a *stress raiser* (increase in stress) at the crack tips and a non-uniform stress in the material. At some distance away from the crack, the lines of force again will become uniform and parallel. The stress raiser, however, serves to bring the tip of the crack to a stress level which may exceed the yield stress of the material and thus produces continued plastic deformation/damage in the material.

Figure 12.27 illustrates a more microscopic (molecular level) view of things. One can see that the bonds are broken at the site of the crack which tends to increase the bonding energy. Above the crack, however, the bonds are more relaxed (reducing the strain energy). Near the crack tip, the bonds are severely strained (raising the bond energy). This region is often referred to as the *plastic* region.

Griffith has shown that for brittle materials with an elliptical crack of length 2a (major diameter) and width 2b (minor diameter) as shown in Fig. 12.27, the stress raiser σ_{raiser} at the tip of the crack is given by:

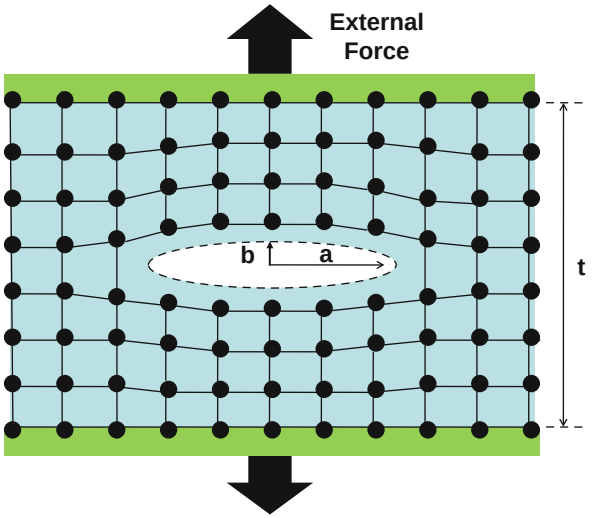

Fig. 12.27 Molecular bonds are shown broken for the elliptical crack of major diameter 2a and minor diameter 2b. The strain energy, above and below the crack, has been partially relieved. Bonds near the crack tip are severely strained (plastic region). Regions well beyond the crack tip are in the normal tensile-stressed state.

$$\sigma_{raiser} = \sigma_o \left[1 + 2\left(\frac{a}{b}\right)\right], \tag{12.46}$$

where σ_o is the uniform stress before crack introduction. A useful term is the *stress concentration factor K* given by:

$$K = \frac{\sigma_{raiser}}{\sigma_o} = 1 + 2\left(\frac{a}{b}\right). \tag{12.47}$$

Example Problem 12.9

A cylindrical rod has yield strength of 600MPa and it is tensile loaded with an average stress of 400MPa. If an elliptical crack is introduced with major axis 2*a* and minor axis 2*b,* such that the ratio is given by *a/b*=4, estimate the stress raiser at the tip of the crack and comment on its reliability impact.

Solution

$$\begin{aligned}\sigma_{raiser} &= \sigma_o \left[1 + 2\left(\frac{a}{b}\right)\right] \\ &= 400\,MPa[1 + 2(4)] \\ &= 3.6GPa.\end{aligned}$$

Note that the stress at the crack tip (3.6GPa) is well above the yield strength (0.6GPa) of the material and plastic-deformation/damage is expected at the crack tip; thus, crack propagation is likely. Even for the most forgiving crack (a spherically shaped crack with a=b), the stress-riser is still three times the nominal/average-stress.

12.9.2 Strain-Energy Release Rate

Figure 12.28 illustrates a material which is uniformly tensile stressed by the fixed external force. If a thin horizontal crack develops, as illustrated in Fig. 12.28, then some of the tensile strain energy stored in the material will be reduced/released, both above and below the crack. If the horizontal crack propagates further, then even more strain energy stored in the material will be released. The fundamental question is, of course, will the *strain energy released* with crack growth be more than offset by the rise in potential energy due to the bond breakage which occurs as the crack propagates? If the answer is yes, then crack propagation is expected to continue and will eventually lead to device failure.

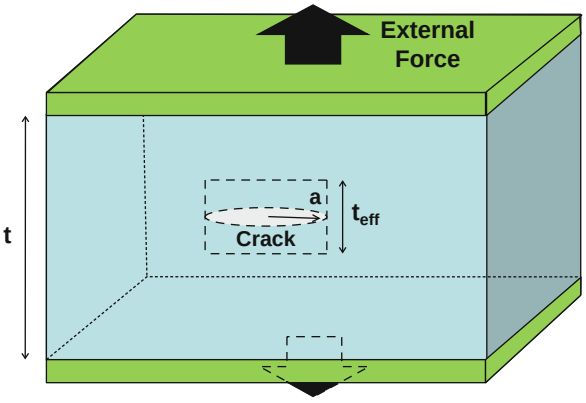

Fig. 12.28 The external force is acting to put the material in a uniform tensile state. The strain energy stored in this film can be released/reduced by crack formation and growth.

While the analysis presented here may be oversimplified, it is instructive to consider how much strain energy would be released when the thin circular crack shown in Fig. 12.28 grows in size. We first consider brittle materials (where the strain energy stored is in terms of elastic energy) and then generalize the results to comprehend plastic materials.

The impact on the molecular bonding due to crack formation/growth is illustrated in Fig. 12.27. Note that the crack (of length $2a$) allows the material above and below the crack to relax to a more unstressed state, thus reducing the strain energy in the material. However, the bonds in the material region near the cracked tip are highly strained. Well beyond the crack tip, the material is in the normal tensile-stress state.

The *strain energy density* (energy per unit volume) stored in a brittle crack-free material of modulus E is given by:

$$u_{elastic} = \frac{1}{2}E\varepsilon^2 = \frac{1}{2}\left(\frac{\sigma^2}{E}\right). \tag{12.48}$$

While an oversimplification, let us assume that a thin crack develops and propagates horizontally in a *circular pattern,* as indicated in Fig. 12.28. To further simplify the analysis presented, let us assume that the strain energy immediately

above and below the crack area is released/relaxed for some effective thickness t_{eff}. Therefore, the strain energy that is released when a thin circular crack develops in a brittle material and propagates horizontally is:

$$U_{released} = u_{elastic} \bullet (Volume)_{eff} = \frac{1}{2}\left(\frac{\sigma^2}{E}\right)\left(\pi a^2 t_{eff}\right).^{14} \tag{12.49}$$

In analyzing crack growth problems, the *strain-energy release rate G* is of great importance. *G* represents the energy released (when a crack of radius *a* increases to *a*+*da*). For a circular crack growing horizontally, as illustrated in Fig. 12.28, G can be determined from Eq. (12.49) and is given by:

$$G = \frac{1}{t_{eff}}\left(\frac{dU_{released}}{da}\right) = \pi a\left(\frac{\sigma^2}{E}\right). \tag{12.50}$$

While Eq. (12.50) for *G* was produced here, under some oversimplified assumptions, Griffth has shown that this equation for *G* is generally valid for brittle materials. It is interesting to note that *G*, as normally defined by Eq. (12.50), represents a rate only in the sense that $dU_{released}/da$ represents the *strain energy released for an incremental change in crack size da*. Given the previous energy balance discussion—the strain energy released must be greater than or equal to the bonding energy increase associated with the crack size growth—then this energy requirement can be restated, for the crack size to grow at a rapid rate:

$$G \geq G_{critical}. \tag{12.51}$$

12.9.3 Fast Fracture/Rupture

G_{crit} has been measured for many materials by introducing a crack (actually a half-crack) in the side of the material to a known depth *a* and then recording the level of average stress in the material which causes rapid/catastrophic fracture. G_{crit} is determined by combining Eqs. (12.50) and (12.51), giving:

$$\sigma_{fracture}\sqrt{\pi a} = \sqrt{EG_{crit}}. \tag{12.52}$$

Typical measured values of G_{crit} for several material types are shown in Table 12.4.

Let us make sure that we clearly understand the implications of Eq. (12.52). The right-hand side of this equation is in terms of measured material parameters only and is a constant. The left-hand side is a product of the average stress σ in the material

[14]The elastic energy $U_{elastic}$ of the material reduces with crack propagation, thus we have defined $\Delta U_{released}$ such that it is always positive, i.e., $\Delta U_{released} = -\Delta U_{elastic}$.

Table 12.4 Representative Values for G_{crit} and K_{crit}.

Material	G_{crit} (kJ/ m^2)	K_{crit} (MN/ $m^{3/2}$)
Dutile Metals: Cu, Ni, Al, Ag	100–1000	100–350
Steel	10–100	50–150
Al-Alloys	10–30	20–50
Strong Polymers, Cast Iron	1–10	1–15
Granite, Silicon Nitride	0.1–1.0	2–5
Beryllium, Silicon Carbide, Alumina, Glass	0.01–0.1	1–3
Ice	0.003	0.2

and the root of π times the half-crack size a; if this product is equal to or greater than the right side of the equation, then rapid/catastrophic fracture is expected.

Also shown in Table 12.4 are the related *stress concentration factors K_{crit} (also called fracture toughness)*, where K_{crit} is given by:

$$K_{crit} = \sigma_{fracture}\sqrt{\pi a} = \sqrt{EG_{crit}}. \tag{12.53}$$

One should note that since the units of G are in energy/area, then the energy release rate G can be thought of as the energy required for the creation of two new surfaces 2Γ, where Γ is the specific energy (surface energy per unit area). Thus, with G=2Γ, Eq. (12.50) can be rewritten as:

$$\sigma_{fracture} = \sqrt{\frac{E2\Gamma}{\pi a}}. \tag{12.54}$$

While the previous equations were developed under the brittle material assumption (no plastic deformation), in most ductile materials crack propagation involves more energy considerations than simply new surfaces creation — around each crack an extensive plastic region exists, as illustrated in Fig. 12.27. Yielding in metals occurs at the ends of the crack thus increasing the toughness of the material, as indicated in Table 12.4. Generally, ductile metals show much greater toughness (higher G_{crit} and K_{crit}). Brittle materials such as glass show little toughness.

Irwin has shown that the plastic region associated with the crack simply serves to increase the specific surface energy and thus produces an effective specific surface energy Γ_{eff} which can be written:

$$\Gamma_{eff} = \Gamma_{surface} + \Gamma_{plastic}. \tag{12.55}$$

Thus, the Griffith criterion can still be used even for ductile materials:

$$G_{crit} = \pi a\left(\frac{\sigma_{rupture}^2}{E}\right). \tag{12.56}$$

The rupture stress $\sigma_{rupture}$ is used here for ductile materials since fracture stress $\sigma_{fracture}$ is usually reserved for brittle materials. Therefore, one can write for both brittle and ductile materials:

$$\sigma_{rupture} = \sqrt{\frac{EG_{crit}}{\pi a}} = \sqrt{\frac{2E\Gamma_{eff}}{\pi a}} = \frac{K_{crit}}{\sqrt{\pi a}}. \tag{12.57}$$

Again, we remind ourselves — when the right-hand side of Eq. (12.57) is equal to the nominal/average stress in the material, then we expect rapid crack propagation and catastrophic rupture.[15] The nominal/average stress level in the material at which this occurs is referred to as the rupture stress σ_{rupture}. One can see that the larger the crack size a, the lower the average stress level in the material needed to produce rapid rupture. Also, perhaps it is helpful to remember a common-experience example. When striking a piece of wood parallel to the wood fibers with an axe, the piece of wood will show fast rupture/splitting when a combination of stress level and indentation/crack-size produced by the axe reaches a critical level.

12.10 Fatigue-Induced Failures

During the discussion of crack propagation, it was emphasized that rapid crack propagation resulting in rapid/catastrophic failure was expected when:

$$K = K_{crit} = \sigma_{rupture}\sqrt{\pi a} = \sqrt{EG_{crit}}. \tag{12.58}$$

This does not mean, however, that the material will not fail with time when $K < K_{\text{crit}}$. The material will fail with time, and the time-to-failure will depend on the level of stress.

One mechanism that can produce time-dependent failure is fatigue. For example, crack formation often occurs in a metal sign/light pole at its welded connection to its supporting base plate as illustrated in Fig. 12.29. As the pole sways, in a gusting wind, one side of the metal pole at its supporting base-plate connection will come under tension while the opposite side will come under compression. The stress state and the magnitude of these stresses will continually change with a changing wind. Also, the tensile and compressive states in the pole will be reversed with a reversal of wind direction.

Fatigue failure can result in cycles-to-failure problems. The subject of fatigue can be so important that it is discussed separately in this text. Fatigue can arise

[15] Note that when the crack size a goes to zero, the apparent rupture stress goes to infinity. However, in these situations, where the right-hand side of the equation becomes extremely large, the rupture stress will be limited by the normal crack-free rupture mechanisms and σ_{rupture} will assume the crack-free rupture strength.

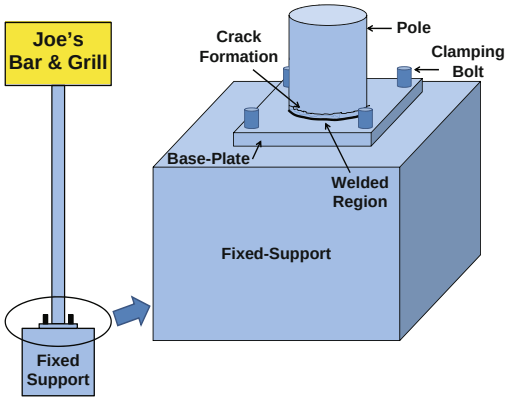

Fig. 12.29 Cracks can develop just above the welded connection of a sign/light pole to its base plate. Gusting-wind conditions and/or changes in wind direction can result in a cyclical stress in the metal. Cyclical stress can cause the cracks to grow, eventually leading to failure. Also note that the cracks tend to form in the heat affected region (the region in the pole just above the welded region).

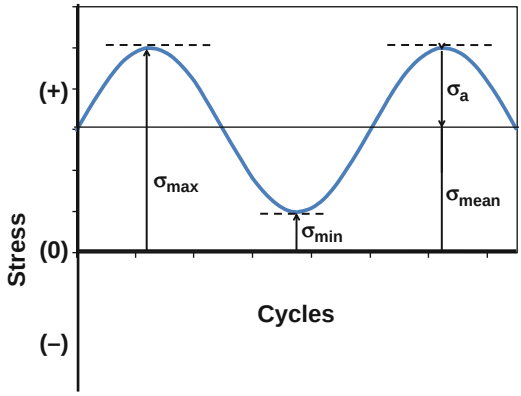

Fig 12.30 Cyclical stress is shown. Key parameters for the cyclical stress are: maximum stress level (σ_{max}) and minimum stress level (σ_{min}) that define the stress range ($\Delta\sigma$), mean stress level (σ_{mean}), and stress amplitude (σ_a).

when a material is continually put under cyclical stress conditions as illustrated in Fig. 12.30.
Useful stress parameters for describing cyclical stress are:

$$\Delta\sigma = \sigma_{max} - \sigma_{min}\,, \quad \sigma_{mean} = \frac{\sigma_{max} + \sigma_{min}}{2}, \quad \sigma_a = \frac{\sigma_{max} - \sigma_{min}}{2}, \tag{12.59}$$

where $\Delta\sigma$ is the stress range, σ_{mean} is the mean stress, and σ_a is the amplitude of stress relative to the mean.

We will first consider cyclical stressing where one has alternating equal amounts of tensile and compressive stress, i.e., $\sigma_{mean} = 0$, and then generalize to $\sigma_{mean} \neq 0$ conditions. Also, rather than discussing time-to-failure (TF), it is more useful to discuss cycles-to-failure (CTF) for fatigue related failures.

12.10.1 Fatigue for Materials (No Pre-Existing Cracks)

Shown in Fig. 12.31 is a typical stress-strain (σ–ϵ) curve for a material. In the elastic region, it is assumed that no damage is occurring during cycling. In the plastic region, each stress cycle will induce a certain amount of plastic deformation (damage/degradation) to the material. The degradation will continue with each cycle until the material fails.

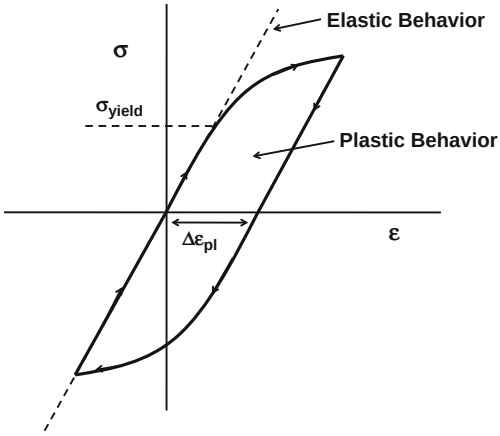

Fig. 12.31 Stress(σ)–Strain(ε) curve for one cycle of cyclical stress with $\sigma_{mean} = 0$. Material damage/degradation can be expected during plastic deformation. The amount of strain in the plastic region is represented by $\Delta\varepsilon_{pl}$.

12.10.2 Low-Cycle Fatigue

Since the damage to the material during each cycle depends on the amount of plastic deformation $\Delta\varepsilon_{pl}$, then a power-law model for the CTF would seem to be reasonable:

$$CTF = B_0(\Delta\varepsilon_{pl})^{-n} \text{ (low-cycle fatigue).} \tag{12.60}$$

The previous equation is referred to as the Coffin-Manson Model and it is generally valid for low-cycle fatigue (where CTF is generally $< 10^4$ cycles) due to large plastic strain $\Delta\varepsilon_{pl}$ during the cycling. The values of n generally range from n=1–3 for ductile metals, 3–6 for hard materials, and 6–9 for brittle materials. One can see in Fig. 12.32, with a mean stress offset ($\sigma_{mean} > 0$), that even greater plastic strain $(\Delta\varepsilon_{pl})_1$ occurs during each cycle thus shorter CTF can be expected:

$$CTF = B_0(\Delta\varepsilon_{pl})_1^{-n} \text{ (low-cycle fatigue).} \tag{12.61}$$

The stress offset serves to increase the amount of plastic deformation [$(\Delta\varepsilon_{pl})_1$ greater than $(\Delta\varepsilon_{pl})_0$] during each cycle thus reducing the number of cycles-to-failure.

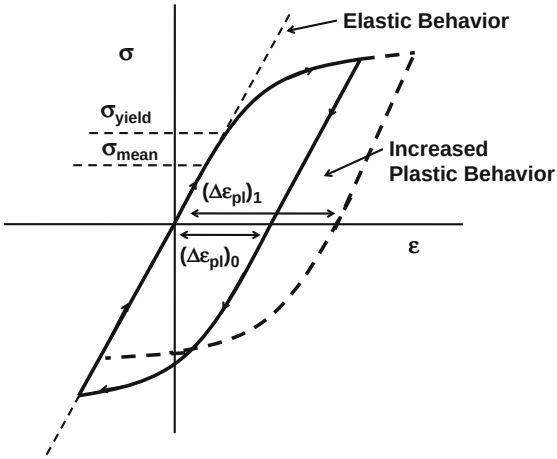

Fig. 12.32 Stress(σ)–Strain(ε) curves. Solid curve represents a cycle with $\sigma_{mean} = 0$. Dashed curve represents a cycle with $\sigma_{mean} > 0$. For a constant $\Delta\sigma$ range, greater material damage/degradation can be expected with $\sigma_{mean} > 0$ during plastic deformation due to the fact that $(\Delta\varepsilon_{pl})_1 > (\Delta\varepsilon_{pl})_0$.

12.10.3 High-Cycle Fatigue

An alternative equation (power-law expression using the stress range $\Delta\sigma$ rather than the plastic strain) is generally used for high-cycle ($> 10^4$ cycles) fatigue:

$$CTF = B_0(\Delta\sigma - \Delta\sigma_{elastic})^{-m} \text{ (high-cycle fatigue)}, \tag{12.62}$$

where the total stress range is $\Delta\sigma$ and $\Delta\sigma_{\text{elastic}}$ is the portion of the total stress range that is in the elastic region (thus producing no damage). The previous equation is generally referred to as Basquin's Law. This equation is used for cyclic stresses, where the stress range is given by $\Delta\sigma$ and zero mean stress ($\sigma_{\text{mean}} = 0$). If, however, $\sigma_{\text{mean}} \neq 0$ (e.g., offset in the tensile-stress direction), then a Goodman-like relation can be developed for the effective stress range $(\Delta\sigma)_{\text{eff}}$:

$$(\Delta\sigma)_{eff} = \frac{\Delta\sigma}{1 - (\sigma_{mean}/\sigma_{TS})}. \tag{12.63}$$

Note that with a mean stress offset of σ_{mean} (if it is a significant fraction of the tensile strength σ_{TS}) it serves to increase the effective cyclical stress range $\Delta\sigma_{\text{eff}}$. An increase in the effective stress range, according to Eq. 12.62, reduces the number of cycles-to-failure CTF.

An example of a mean stress offset is illustrated in Fig. 12.33. In Fig. 12.33(a), a metal pole is shown supporting a sign. During gusting-wind conditions, a cyclical stress will be generated in the pole, with the maximum bending moment occurring where the metal pole is welded to its base plate. Shown in Fig. (12.33b) is a similar situation of a pole supporting a sign; except in this case, a cantilever attachment of a stoplight to the pole also exists. This cantilevered attachment of the stoplight to the pole will serve to put the left side of the pole, at its base plate connection, in a state of mean tension and the opposite side in a state of mean compression. Now, with

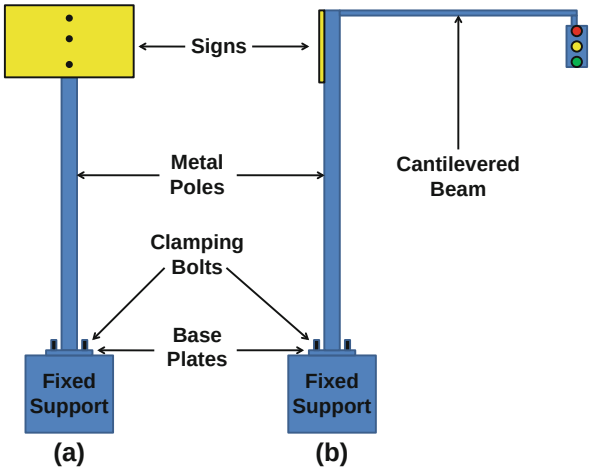

Fig. 12.33 Shown in (a) is metal pole supporting a sign. Also shown are the bolts used to clamp the base plate to the fixed support. Shown in (b) is a similar configuration except that a cantilevered beam is also attached to the pole behind the sign. On the cantilevered beam hangs a stoplight which serves to produce an added moment (additional mean stress) at the base plate.

gusting wind conditions, the left side of the pole will have cyclical stress about a mean tensile stress. With a mean tensile stress in the pole, the effective stress range $(\Delta\sigma)_{eff}$ given by Eq. 12.63 will now be larger than the actual stress range $(\Delta\sigma)$ and each cycle will now produce more damage.

On can see from Eq. (12.63) that as the mean stress σ_{mean} increases (relative to the tensile strength σ_{TS} of the material), then the effective stress range $(\Delta\sigma)_{\text{eff}}$ increases and a shorter number of cycles-to-failure (CTF) is expected, given by:

$$CTF = B_0 \left[\frac{\Delta\sigma}{1 - (\sigma_{mean}/\sigma_{TS})} - \Delta\sigma_{elastic} \right]^{-m}. \tag{12.64}$$

Example Problem 12.10

A metal pole experiences a cyclic stress at the base-plate connection due to the swaying of the pole. During a half cycle, one side of the metal pole at the base plate will come under tension while the opposite side comes under compression, then the roles of tension /compression are reversed during the next half cycle. In addition, if the pole also supports an overhanging structure such as the stoplight shown in Fig. 12.33, then an additional mean stress offset of $\sigma_{\text{mean}} = 190\text{MPa}$ will occur. To make sure that the pole will last the required time, accelerated data was taken on poles (without an overhanging structure) where a cyclical stress was applied to the poles whereby the metal at the base plate came under a continuous cyclical stress range of -600MPa to $+600\text{MPa}$ with a mean tensile stress of zero. The poles failed at the base plate connection after 10,000 cycles. Assuming a power-law exponent of n=4 for the cycling,

a metal tensile strength of 800MPa and no defined elastic range (due to cracks or other issues):

a) Estimate the number of cycles-to-failure CTF that would be expected if the normal-use stress range is between −200MPa to + 200MPa and there is no overhanging structure.
b) Estimate the number of cycles-to-failure CTF that would be expected if the normal-use stress range is between −200MPa and + 200MPa and there is an overhanging structure that produces mean tensile offset of σ_{mean}=190MPa.

Solution

a) Expected acceleration factor for the cycling:

$$AF = \left[\frac{(\Delta\sigma)_{stress})}{(\Delta\sigma)_{operation})}\right]^{n} = \left[\frac{[600-(-600)]MPa}{[200-(-200)]MPa}\right]^{4} = [3]^{4} = 81.$$

Therefore:

$$(CTF)_{operation} = AF \bullet (CTF)_{stress} = 81(10,000 cycles) = 810,000 cycles.$$

b) The overhang which serves to produce a mean stress in the pole also serves to increase the effective stress range under use conditions:

$$(\Delta\sigma)_{eff} = \frac{\Delta\sigma}{1-\frac{\sigma_{mean}}{\sigma_{TS}}} = \frac{[200-(-200)]MPa}{1-\frac{190\,MPa}{800\,MPa}} = 525\,MPa.$$

The acceleration factor now becomes:

$$AF = \left[\frac{(\Delta\sigma)_{stress})}{(\Delta\sigma)_{effective})}\right]^{n} = \left[\frac{[600-(-600)]MPa}{525\,MPa}\right]^{4} = [2.286]^{4} = 27.$$

Therefore:

$$(CTF)_{op} = AF \bullet (CTF)_{stress} = 27(10,000 cycles) = 270,000 cycles.$$

12.10.4 Fatigue for Materials (With Pre-Existing Cracks)

A material with a pre-existing crack is stressed with a sinusoidal stress as shown in Fig. 12.34. The stress concentration factor K for a crack was previously defined for a constant tensile stress load σ. ΔK values are useful for cyclical stress:

$$\Delta K \;=\; K_{high} - K_{low} \;=\; (\sigma_{high} - \sigma_{low})\sqrt{\pi a} \;=\; \Delta\sigma\sqrt{\pi a}. \tag{12.65}$$

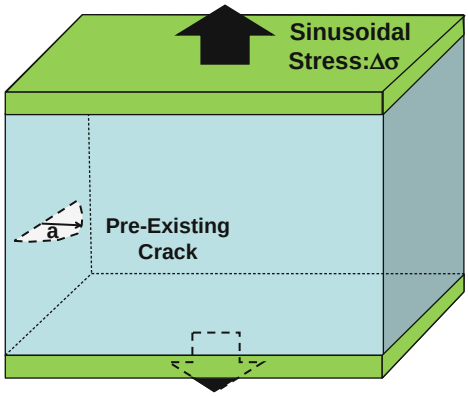

Fig. 12.34 Sinusoidal stress is applied to a material with a pre-existing crack.

The crack growth *da* per cycle *dN* can be written:

$$\frac{da}{dN} = C_0(\Delta K)^m = F_0(\Delta\sigma)^m\,(a)^{m/2}\,. \tag{12.66}$$

Separating variables and integrating, gives:

$$\int_0^{CTF} dN = \left[\frac{1}{F_0}\int_{a_0}^{a_{fail}} \frac{da}{a^{m/2}}\right](\Delta\sigma)^{-m}. \tag{12.67}$$

The above equation reduces simply to a power-law dependence:

$$CTF = A_0\,[\Delta\sigma]^{-m}\,. \tag{12.68}$$

No elastic range $\Delta\sigma_{\text{elastic}}$ appears in Eq. (12.68) because it assumes that the stress riser at crack tips reduces the elastic range to zero. As previously discussed, for cyclical stressing when $\sigma_{\text{mean}} \neq 0$, then

$$CTF = A_0\left[\frac{\Delta\sigma}{1-(\sigma_{mean}/\sigma_{TS})}\right]^{-m}. \tag{12.69}$$

One can see that the functional form for CTF in Eqs. (12.62) and (12.63) [for materials without cracks] is very similar in form to that for materials with cracks, Eqs. (12.68) and (12.69). However, there is no assumed elastic range $\Delta\sigma_{elastic}$ when the crack is present and the prefactors ($A_o$and B_o) are quite different. In general, for materials with cracks, A_o is much less than B_o. Also, the cracks (which may vary greatly in number and size from device to device) generally drive a wider spread in the CTF data. This serves to produce a larger logarithmic standard deviation (in the case of the lognormal distribution) or a smaller Weibull slope (in the case of the Weibull distribution).

Example Problem 12.11

Suppose that a certain batch of poles (described in Example Problem 12.10) has cracks (at time-zero) just above the welded region at the base plate. Rather than failing at 10,000 cycles under accelerated cyclical stress, they now fail in 1000 cycles.

a) Estimate the number of cycles-to-failure CTF that would be expected if the normal-use stress range is between −200MPa to + 200MPa (without an overhanging structure).
b) Estimate the number of cycles-to-failure CTF that would be expected if the normal-use stress range is between −200MPa and + 200MPa and with an overhanging structure that produces mean offset of σ_{mean} = 190MPa.

Solution

One would expect that the cracks will impact the prefactor in the CTF Eq. (12.78) but the acceleration factors are expected to be similar. Thus,

a) $(CTF)_{operation} = AF \bullet (CTF)_{stress} = 81(1,000 cycles) = 81,000 cycles.$
b) $(CTF)_{op} = AF \bullet (CTF)_{stress} = 27(1,000 cycles) = 27,000 cycles.$

12.11 Adhesion Failures

Adhesion failures are associated with the *debonding* of materials. Similar to all the other failure mechanisms discussed, adhesion failures are driven by a free energy difference between the bonded and debonded materials.

Consider two materials that are bonded at an interface, as shown in Fig. 12.35. Let us compare the stress energy in the films (which is positive) to the interfacial bonding energy (which is negative). The stress energy would be lower if the two materials would delaminate but the interfacial energy would be higher due to the broken bonds. These are the two competing energy mechanisms that serve to hold the two materials together.

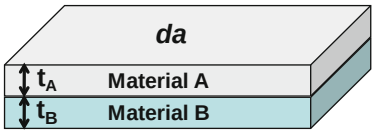

Fig. 12.35 Two materials, A and B, are bonded together. If there are stresses in the two materials (due to Material A interacting with Material B, and visa versa) then there will be a driving force for the two materials to delaminate. A driving force for delamination, over some interfacial area da, will exist if the stress-energy reduction in A and B is greater than the increase in bonding energy associated with the formation of the delaminated region da.

The elastic stress-energy density u in the two materials can be written:

$$u_{elastic} = u_A + u_B = \frac{1}{2}\left(\frac{1}{E_A}\right)\sigma_A^2 + \frac{1}{2}\left(\frac{1}{E_B}\right)\sigma_B^2. \tag{12.70}$$

If the two materials A and B delaminate, two new surfaces will be created, one with a specific energy density[16] Γ_A and the other Γ_B. Thus, the total specific energy density associated with the formation of the two new surfaces is given by: $\Gamma_{total} = \Gamma_A + \Gamma_B$.

Therefore, the free energy driving force for the materials to delaminate is: the stress energy reduction in some differential area *da* must be greater than the increase in bonding energy associated with the creation of the two new surfaces at the interface:

$$\left[\frac{1}{2}\left(\frac{1}{E_A}\right)\sigma_A^2\right](t_A da) + \left[\frac{1}{2}\left(\frac{1}{E_B}\right)\sigma_B^2\right](t_B da) \geq [\Gamma_A + \Gamma_B]da. \tag{12.71}$$

This reduces simply to:

$$\frac{1}{2}\left(\frac{t_A}{E_A}\right)\sigma_A^2 + \frac{1}{2}\left(\frac{t_B}{E_B}\right)\sigma_B^2 \geq \Gamma_A + \Gamma_B. \tag{12.72}$$

While the focus of this section is on adhesion, there is a similarity with crack propagation previously discussed. For a crack to propagate, the strain energy released within the materials or along their interfaces must be greater than the increase in specific energy density associated with the newly created surfaces/interfaces during the crack growth.[17] For delamination to continue, the strain energy release rate by delamination must be greater than the specific energy increase associated with the two new surfaces.

[16] Recall that specific energy density is the energy per unit area.

[17] Historically, this has been referred to as Griffith's equation which was developed for brittle materials. More recently, Irwin is usually credited for developing the failure in terms of a *strain energy release rate G* [(Eq. (12.56)], which incorporates both elastic and plastic deformations when new surfaces or interfaces are formed.

12.12 Thermal-Expansion Induced Failures

Solid materials tend to expand when heated. The reason for this is the asymmetrical bonding potential between the atoms forming the solid (as illustrated in Fig. 12.1). The thermal expansion of materials, in itself, is not a reliability issue. The thermal expansion simply redefines a new equilibrium position. However, if the material is constrained in any way, while it is trying to expand thermally, then large thermomechanical stresses can develop in the materials. It is these large thermomechanical stresses that can cause material degradation and eventual failure of the device.

12.12.1 Thermal Expansion

The molecular bonding model shown in Fig. 12.1 permits one to discuss what happens to the equilibrium bonding positions as the temperature is increased. The asymmetrical potential associated with molecular bonding is illustrated in Fig. 12.36.

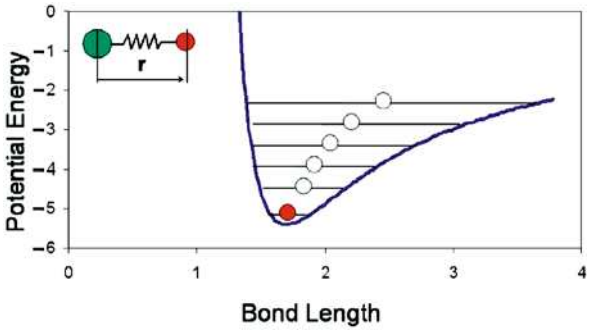

Fig. 12.36 Increase in temperature serves to increase the probability that higher vibrational quantum states will be occupied. Due to the asymmetrical bonding potential, the higher quantum states will have an increase in mean bond length.

Quantum mechanics permits only certain allowed vibrational states to exist. Increasing the temperature (thermal energy) serves to make the population of the higher vibrational states more probable. However, the mean position for the vibrating atom tends to increase with higher vibrational-state population. Therefore, the mean bond length tends to increase with temperature.

Since the change in bond length Δr with temperature is generally small compared with the original bond length r_0, a Taylor expansion normally suffices:

$$r(T) \cong r(T_0) + \left(\frac{\partial r}{\partial T}\right)_{T=T_0} (T - T_0). \tag{12.73}$$

Eq. (12.73) can be rewritten simply as:

$$\frac{\Delta r}{r_0} = \alpha \Delta T, \tag{12.74}$$

where α is the linear thermal expansion coefficient defined as:

$$\alpha = \frac{1}{r_0}\left(\frac{\partial r}{\partial T}\right)_{T=T_0}.^{18} \tag{12.75}$$

The translation from microscopic (molecular) dimensions r to macroscopic length L (solid) dimensions is straightforward. If the length of the solid material is L, then L must be given by the number of elemental units N times the elemental distance r, then one can write:

$$\frac{\Delta L}{L_0} = \frac{L(T) - L(T_0)}{L(T_0)} = \frac{N\,[r_0 + \Delta r] - N r_0}{N r_0} = \frac{\Delta r}{r_0}. \tag{12.76}$$

Therefore:

$$\alpha = \frac{1}{r_0}\left(\frac{\partial r}{\partial T}\right)_{T=T_0} = \frac{1}{L_0}\left(\frac{\partial L}{\partial T}\right)_{T=T_0}. \tag{12.77}$$

Since the linear strain ϵ is given by $\Delta L/L_0$ (or equivalently $\Delta r/r_0$), then the thermal expansion strain, from Eq. (12.74), is given by:

$$\varepsilon = \alpha\ \Delta T. \tag{12.78}$$

12.12.2 Constrained Thermal-Expansion

If a material is constrained such that it cannot move during temperature changes, then a thermomechanical stress σ develops in the material given by:

$$\sigma = E\varepsilon = \alpha\ E\ \Delta T, \tag{12.79}$$

where E is Young's modulus. Using Eq. (4.13a) from Chapter 4, then time-to-failure due to a constrained thermo-mechanical stress is expected to take the form:

$$TF = A_0(\sigma)^{-n} \exp\left(\frac{Q}{K_B T}\right) = B_0(T - T_0)^{-n} \exp\left(\frac{Q}{K_B T}\right) \quad (for\ T > T_0) \tag{12.80a}$$

or

$$TF = A_0(\sigma)^{-n} \exp\left(\frac{Q}{K_B T}\right) = B_0(T_0 - T)^{-n} \exp\left(\frac{Q}{K_B T}\right) \quad (for\ T < T_0). \tag{12.80b}$$

[18] Linear coefficients of thermal expansion are listed for several material types (in units of $10^{-6}/^{\circ}C$): $\alpha_{polymers} \cong 50$, $\alpha_{metals} \cong 10$, $\alpha_{ceramics} \cong 2$, $\alpha_{glass} \cong 0.5$.

In the previous equation, T_0 is assumed to be the temperature at which zero stress exists in the material. As one goes to a temperature above or below T_0, a thermomechanical stress develops in the material. The thermomechanical stress can bring about material degradation and possible failure due to creep, especially at elevated temperatures. The impact of this thermomechanical stress on the time-to-failure is expected to be thermally activated (activation energy = Q). However, the effective/observed activation energy will be complicated by the fact that the prefactor in the above equation is also temperature dependent. This was discussed in detail for stress migration in Chapter 11.

12.12.3 Thermal-Expansion Mismatch

Seldom is there only a single material used in a device. Different materials are often joined/bonded together to form the device. If these materials have significantly different thermal expansion coefficients, then large thermal-expansion mismatch stresses can be generated during thermal cycling. These thermomechanical stresses can induce failures because of: creep, fatigue, cracking, buckling and/or delamination.

Shown in Fig. 12.37 are two materials, *A* and *B*, which are constrained to move together during thermal expansion due to the adhesion forces existing at the interface of materials *A* and *B*. If the two materials were joined at temperature T_0, and if material *A* is assumed to have a greater thermal expansion coefficient than *B*, then an increase in temperature above T_0 will result in A being under a state of compression and B under tension.

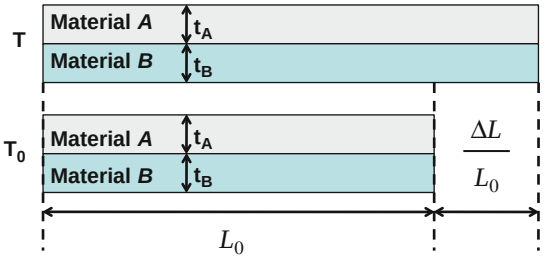

Fig. 12.37 Two materials are constrained by interfacial adhesion to move together during thermal expansion from T_0 to T. If the thermal expansion coefficient for A is greater than B, then constrained thermal expansion above T_0 results in A being in compression and B in tension.

The strain in material *A* is given by:

$$\varepsilon_A = \frac{\Delta L}{L_0} - \alpha_A \Delta T, \tag{12.81}$$

and, likewise, the strain in B is given by

$$\varepsilon_B = \frac{\Delta L}{L_0} - \alpha_B \Delta T. \tag{12.82}$$

Since the two materials are constrained to move together during the thermal expansion, then Newton's third law tells us that the force of Material A acting on B must be equal and opposite to B acting on A:

$$\begin{aligned} & F_A = -F_B \\ & \Rightarrow \sigma_A(t_A \bullet Width) = -\sigma_B(t_B \bullet Width) \\ & \Rightarrow (E_A \varepsilon_A) t_A = -(E_B \varepsilon_B) t_B \\ & \Rightarrow \varepsilon_A = -\left(\frac{E_B}{E_A}\right)\left(\frac{t_B}{t_A}\right)\varepsilon_B \,, \end{aligned} \tag{12.83}$$

where E is the modulus for each material and t is the thickness of each material. Solving Eqs. (12.81–12.83) for σ_A and σ_B, one obtains:

$$\sigma_A = E_A \varepsilon_A = \frac{E_A(\alpha_B - \alpha_A)\Delta T}{1 + \left(\frac{E_A}{E_B}\right)\left(\frac{t_A}{t_B}\right)}, \tag{12.84}$$

and

$$\sigma_B = E_B \varepsilon_B = \frac{E_B(\alpha_A - \alpha_B)\Delta T}{1 + \left(\frac{E_B}{E_A}\right)\left(\frac{t_B}{t_A}\right)}. \tag{12.85}$$

Note that when $\alpha_A > \alpha_B$, material A will be under compression and material B will be under tension.

It is instructive to look at the strain ratio ($\varepsilon_A/\varepsilon_B$), stress ratio ($\sigma_A/\sigma_B$) and the stress energy density ratio (u_A/u_B) for thermal expansion mismatch:

Strain Ratio:

$$\frac{\varepsilon_A}{\varepsilon_B} = -\left(\frac{E_B}{E_A}\right)\left(\frac{t_B}{t_A}\right) \tag{12.86}$$

Stress Ratio:

$$\frac{\sigma_A}{\sigma_B} = -\left(\frac{t_B}{t_A}\right) \tag{12.87}$$

Energy Density Ratio:

$$\frac{u_A}{u_B} = \frac{\frac{1}{2}E_A\varepsilon_A^2}{\frac{1}{2}E_B\varepsilon_B^2} = \frac{E_B}{E_A}\left(\frac{t_B}{t_A}\right)^2. \tag{12.88}$$

Note that if the material thicknesses are equal, $t_A = t_B$, then Eq. (12.86) shows that most of the strain will be in the lower modulus material. Furthermore, Eq. (12.88) indicates that most of the energy density will be in the lower modulus material.

12.12.4 Thin Films on Thick Substrates

It is well known that thin layers (thin films) on thick materials (thick substrates) are prone to delamination, cracking, buckling, or blistering Eqs. (12.86), (12.87) and (12.88) can be used to understand why this is the case. Assuming that the modulus for *A* is similar to that for *B*; when the substrate (material *B*) is very thick compared to material *A*, then most of the strain, stress, and energy density is in thin film *A*. If the adhesion strength of materials *A* and *B* is relatively good, then tensile-stressed films can crack (Fig. 12.38) to relieve the strain energy. Compressive films can buckle (Fig. 12.39) in order to release the strain energy—this is why a thermal expansion gap in concrete is often used. If the adhesion strength of *A* and *B* is relatively poor, then delamination/blistering can occur (Fig. 12.40) in order to release the strain energy.

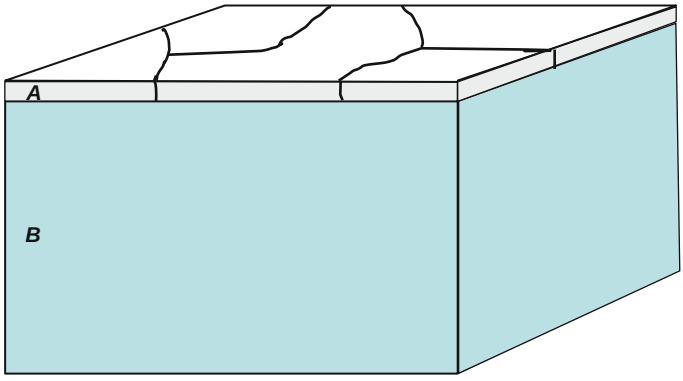

Fig. 12.38 Cracking can occur when material A is under tensile stress. Cohesive cracking is a stress/strain-energy release mechanism when the adhesion of A and B is strong. Delamination of layer A from layer B can occur if the adhesion of A to B is relatively weak.

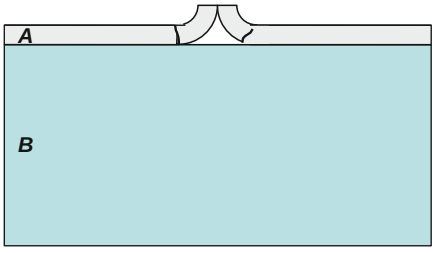

Fig. 12.39 Shown is the buckling which can occur when material A is under compressive stress. Buckling can be a compressive stress-relief/strain-energy release mechanism when the adhesion of layer A to layer B is strong.

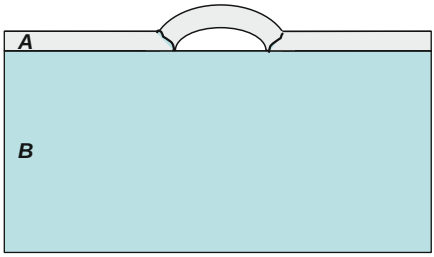

Fig. 12.40 Shown is the blistering which can occur when material A is under compressive stress. Blistering is a compressive stress-relief/strain-energy release mechanism when the adhesion of layers A and B is relatively weak.

In addition to thermomechanical stress in thin films, intrinsic stresses can also be very important. Intrinsic stresses can develop during fabrication of the material and these stresses are not related to thermal-expansion mismatch. An example of intrinsic stress is the stress which can develop in thin metal-oxide layers which are thermally grown at a fixed temperature on relatively thick metal substrates. If the volume of the metal oxide is much larger than the volume of the metal consumed, then a large compressive stress will develop in the metal-oxide layer during growth. Likewise, if the volume of the metal oxide is much less than the volume of the metal consumed, then a large tensile stress will develop in the metal-oxide layer during growth. These intrinsic stresses are developed during thin-film fabrication (metal-oxide growth) and, as such, are built into the film during fabrication. As these metal-oxide films are then lowered from their fabrication/growth temperature, then the thermal expansion mismatch can add to or reduce the mechanical stress in these thin films.

Example Problem 12.12

A metal component in a certain application will be thermal cycled from room temperature to an oxidizing ambient of 250°C. To prevent oxidation of the metal at the high temperatures, a thin ceramic coating is used on the metal component. The concern is that cracks will develop in the ceramic layer during thermal cycling thus exposing the metal to oxidation. To accelerate the cracking, the components were thermal cycled from room temperature to 700°C. If cracks start to develop in the ceramic layer after 100 thermal cycles from room temperature to 700°C, how many crack-free cycles would be expected from room temperature to 250°C? Assume that the ceramic material is hard/brittle with a temperature exponent of at least n = 7.

Solution

$$AF \geq \left[\frac{(\Delta T)_{stress}}{(\Delta T)_{operation}}\right]^{n} = \left[\frac{(700-25)^{o}C}{(250-25)^{o}C}\right]^{7} = (3)^{7} = 2187.$$

Therefore:

$$(CTF)_{operation} \geq AF \bullet (CTF)_{stress} = 2187(100 cycles) = 218,700 cycles.$$

12.13 Corrosion-Induced Failures

There is a strong driving force (large free energy difference) for metals to oxidize/corrode as illustrated in Fig. 12.41. This is why, in nature, one can easily find metal oxides (ores) but it is very difficult to find the element in its pure-metallic form. The only exception to this is gold (which generally does not oxidize) and it can found in nature in the metallic state. However, generally, metals are found in nature as metal oxides.

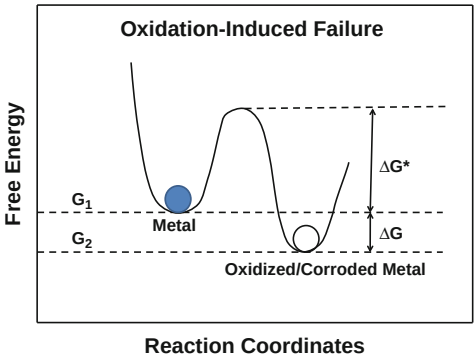

Fig. 12.41 Strong driving force (large ΔG) exists for metal oxidation. The activation energy (ΔG^*) tends to limit the corrosion rate.

In order to obtain metal in a pure metallic form, a significant energy input is required to separate the metal from its oxide/ore. Once in the metallic form, tremendous amounts of money (tens of $billions each year) are spent for corrosion prevention and replacement of corroded parts.

An example of corrosion failure is shown Fig. 12.42 where a U-type support clamp has totally corroded away at the point of maximum bending.

Fig. 12.42 Corrosion failure of a U-type metal support clamp. The metal at the bottom of the support clamp has corroded away. One should note that the corrosion rate was greatest in the regions where the metal was severely bent.

12.13.1 Dry Oxidation

Table 12.5 shows the very strong driving force ($\Delta G_{\text{Formation}}$) for a metal atom to combine with O_2 to form a metal oxide. The more negative the formation energy, the stronger the driving force for the metal atom to oxidize. However, the activation energy which limits the oxidation rate depends on the ability of the metal ions and/or oxygen ions to diffuse through M_xO_y oxide layer formed, as well as the ability of the electrons to conduct through this oxide layer. Key features of the oxidation process are shown in Fig. 12.43.

The process of oxidation generally converts metals into insulators. Normally this is thought to have negative consequences; but, in at least one very important case (oxidation of silicon), this oxide formation permits one to build metal/oxide/silicon field-effect transistors (MOSFETs) which were instrumental in driving the > $250B/yr semiconductor industry in 2008. It is very difficult to

Table 12.5 Free Energy For Metal-Oxide (MxOy) Formation.

Metal	Oxidation State	M_xO_y	ΔG [kJ/ (Mole of O_2)]	ΔG [eV/ (O_2 molecule)]
Be	$Be \rightarrow Be^{2+} + 2e$	BeO	−1182	−12.27
Al	$Al \rightarrow Al^{3+} + 3e$	Al_2O_3	−1045	−10.85
Ti	$Ti \rightarrow Ti^{2+} + 2e$	TiO	−1000	−10.38
Si	$Si \rightarrow Si^{4+} + 4e$	SiO_2	−848	−8.80
Ta	$Ta \rightarrow Ta^{5+} + 5e$	Ta_2O_5	−764	−7.93
Cr	$Cr \rightarrow Cr^{3+} + 3e$	Cr_2O_3	−757	−7.86
Zn	$Zn \rightarrow Zn^{2+} + 2e$	ZnO	−636	−6.60
W	$W \rightarrow W^{6+} + 6e$	WO_3	−510	−5.29
Fe	$Fe \rightarrow Fe^{2+} + 2e$	FeO	−508	−5.27
Sn	$Sn \rightarrow Sn^{2+} + 2e$	SnO	−500	−5.19
Ni	$Ni \rightarrow Ni^{2+} + 2e$	NiO	−439	−4.56
Cu	$Cu \rightarrow Cu^{2+} + 2e$	CuO	−254	−2.64
Pt	$Pt \rightarrow Pt^{4+} + 4e$	PtO_2	−160	−1.66
Ag	$Ag \rightarrow Ag^{+} + e$	Ag_2O	−5	−0.05
Au	$Au \rightarrow Au^{3+} + 3e$	Au_2O_3	80	0.83

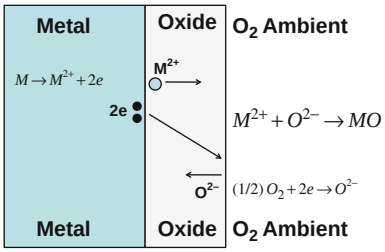

Fig. 12.43 Dry metal corrosion (oxidation in an O_2 containing gas ambient at high temperatures) results in an metal-oxide (M_xO_y) formation on the surface of the metal. The quality of this oxide layer generally controls the oxidation reaction rate by limiting M-ion and/or O-ion diffusion. Also shown are the freed electrons (from the metal ion) that must be able to conduct through this oxide layer in order for the oxidation process to continue.

imagine life without computers, laptops, smart phones, iPods, iPads, implantable medical devices, etc. In addition, copper oxide tends to be superconducting at low temperatures.

There are at least three oxidation models often used to describe the rate of oxidation: linear growth rate, parabolic growth rate, and logarithmic growth rate. Often, the initial growth rate for a period of time t_0 will be erratic until some minimum oxide thickness x_0 (at least a few monolayers) is reached. Then above the initial thickness and time conditions (x_0,t_0), the growth rate is relatively well behaved and generally described by one of the three models given below.

12.13.1.1 Linear Oxide-Growth Region

In the linear growth region, one assumes that the oxide thickness x grows at a constant rate k_1 which is temperature dependent:

$$\frac{dx}{dt} = k_1, \tag{12.89}$$

where,

$$k_1 = k_{10} \exp\left(-\frac{Q}{K_B T}\right). \tag{12.90}$$

Separating the variables, in Eq. (12.89), and integrating from the initial conditions (x_o,t_o) to the conditions (x,t), one obtains:

$$x = x_0 + k_1(t - t_0). \tag{12.91}$$

Assuming that time-to-failure (t=TF) for a device occurs when the oxide thickness increases to some critical level $(\Delta x)_{crit} = (x_{crit} - x_0)$, then TF is given by:

$$TF = t_0 \quad + \quad \frac{(\Delta x)_{crit}}{k_{10}} \exp\left(\frac{Q}{K_B T}\right) = t_0 + A_{10} \exp\left(\frac{Q}{K_B T}\right). \tag{12.92}$$

Normally, TF >> t_0 and t_0 is often ignored.

Some metals such as iron tend to show poor resistance to oxidation because the oxide layer cracks and/or delaminates during oxidation. Oxide damage will tend to occur when the volume of the metal oxide M_xO_y is much different from the volume of the consumed metal M. If the metal oxide M_xO_y volume is less than the volume of the metal M consumed, then the oxide layer will be in a severe state of tension and a strong driving force for oxide cracking will exist. If the metal oxide M_xO_y volume is much greater than the metal M consumed, then the oxide layer will be under severe state of compression and oxide layer delamination (blistering or buckling) can be anticipated. Shown in Fig. 12.44 is a pure piece of Cu after it has been exposed to dry oxidation at 250C. Note that the damage that occurs in the Cu_xO_y layer is because of intrinsic stresses developed during oxide growth.

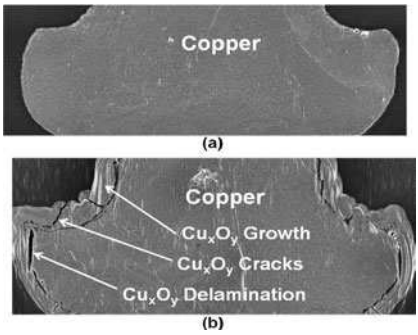

Fig. 12.44 Dry oxidation of pure copper. (a) Copper at time-zero. (b) After 250°C storage in an oxygen-containing ambient. Cu_xO_y layer shows evidence of cracking and delamination.

12.13.1.2 Parabolic Oxide-Growth Region

In the parabolic oxide-growth region, one assumes that the growth rate is inversely proportional to the oxide thickness and directly proportional to the reaction rate constant k_2 which is temperature dependent:

$$\frac{dx}{dt} = \frac{k_2}{x}, \tag{12.93}$$

where

$$k_2 = k_{20} \exp\left(-\frac{Q}{K_B T}\right). \tag{12.94}$$

Separating variables, in Eq. (12.93), and integrating:

$$\int_{x_0}^{x} x dx = k_2 \int_{to}^{t} dt, \tag{12.95}$$

then one obtains

$$x^2 = x_o^2 + 2k_2(t - t_0). \tag{12.96}$$

Note that for $t >> t_0$ and $x >> x_0$, then one obtains the standard diffusion relation:

$$x = \sqrt{Dt}, \tag{12.97}$$

where,

$$D(T) = 2k_2(T) = 2k_{20} \exp\left(-\frac{Q}{K_B T}\right) = D_0 \exp\left(-\frac{Q}{K_B T}\right). \tag{12.98}$$

Assuming that t=TF, when the oxide thickness reaches some critical value x_{crit}, then

$$TF = t_0 + \left(\frac{x_{crit}^2 - x_0^2}{2k_{20}}\right) \exp\left(\frac{Q}{K_B T}\right) = t_0 + A_{20} \exp\left(\frac{Q}{K_B T}\right). \tag{12.99}$$

Often, $TF >> t_0$ and t_0 is ignored.

Example Problem 12.13

The critically important integrated circuit (IC) industry is based on the ability to grow a self-passivating oxide layer on silicon. During parabolic oxide growth at high temperatures, it was found that SiO_2 grew to an oxide thickness of 100Å in one hour. How long would it take for SiO_2 oxide to grow to 200Å?

Solution

For a parabolic growth rate, and assuming that the time-zero oxide thickness on the silicon is negligible, one obtains:

$$x^2 = kt$$

$$\Rightarrow k = \frac{x^2}{t} = \frac{(100\,\overset{o}{A})^2}{1hr} = \frac{10000\,\overset{o}{A^2}}{1hr} = 1 \times 10^4 \frac{\overset{o}{A^2}}{hr}.$$

Therefore, the total time required to grow the oxide layer to 200Å is:

$$t = \frac{x^2}{k} = \frac{(200\,\overset{o}{A})^2}{1 \times 10^4 \frac{\overset{o}{A^2}}{hr}} = 4hrs.$$

Example Problem 12.14

In the previous example problem, it took 4 hrs to grow 200Å of SiO_2 on silicon at 950°C. How long would it take to grow the 200Å of SiO_2 at 1000°C? Assume the activation energy for the growth rate is Q=2.0 eV.

Solution

The reaction rate constant k at 1000°C is expected to take the form:

$$k(T) = k_o \exp\left[-\frac{Q}{K_B}\left(\frac{1}{T} - \frac{1}{T_o}\right)\right]$$

$$= 1.0 \times 10^4 \frac{\overset{o}{A^2}}{hr} \exp\left[-\frac{2.0\,eV}{8.62 \times 10^{-5} eV/K}\left(\frac{1}{(1000+273)K} - \frac{1}{(950+273)K}\right)\right]$$

$$= 2.1 \times 10^4 \frac{\overset{o}{A^2}}{hr}.$$

Therefore, the time at 1000°C to grow 200Å of SiO_2 would be:

$$t = \frac{x^2}{k} = \frac{(200\,\overset{o}{A})^2}{2.1 \times 10^4 \frac{\overset{o}{A^2}}{hr}} = 1.9 hrs.$$

12.13.1.3 Logarithmic Oxide-Growth Region

In the logarithmic oxide-growth region, one assumes that the growth rate saturates with time. Thus, the growth rate is assumed to be inversely proportional to the growth time t and directly proportional to the reaction rate constant k_3, which is temperature dependent:

$$\frac{dx}{dt} = \frac{k_3}{t + t_0}, \tag{12.100}$$

where

$$k_3 = k_{30} \exp\left(-\frac{Q}{K_B T}\right). \tag{12.101}$$

Separating variables in Eq. (12.100) and integrating, one obtains:

$$\int_{x_0}^{x} dx = k_3 \int_{t_0}^{t} \frac{dt}{t + t_0}, \tag{12.102}$$

giving,

$$x = x_0 + k_3 \ln\left(\frac{t + t_0}{2t_0}\right), \tag{12.103}$$

where,

$$k_3 = k_{30} \exp\left(-\frac{Q}{K_B T}\right). \tag{12.104}$$

Setting t=TF, when $x = x_{crit}$, then the time-to-failure equation becomes:

$$TF = t_0 \left\{ 2 \exp \left[A_{30} \exp \left(\frac{Q}{K_B T} \right) \right] - 1 \right\}, \tag{12.105}$$

where,

$$A_{30} = \frac{x_{crit} - x_0}{k_{30}}. \tag{12.106}$$

Another way of writing Eq. (12.105), for easier parameter extraction/determination, is

$$\ln \left[\frac{TF + t_0}{2t_0} \right] = A_{30} \exp \left(\frac{Q}{K_B T} \right), \tag{12.107}$$

where it is assumed t_0 is not equal to zero.

12.13.2 Wet Corrosion

Wet corrosion (or electrolytic corrosion) is significantly different from dry corrosion in that metal hydroxides $M(OH)_n$tend to form during wet oxidation (in aerated water) at relatively low temperatures, whereas metal oxides (M_xO_y) tend to form during dry oxidation at relatively high temperatures.

The formation of metal hydroxides during wet corrosion is a critically important difference—whereas metal oxides generally do not dissolve easily in water, metal hydroxides can dissolve relatively easily in water and thereby constantly exposing fresh metal for continued oxidation. While metal dry oxidation is normally an issue only at elevated temperatures, wet corrosion may occur easily at room temperature.

The critical features of wet corrosion are illustrated in Fig. 12.45. For wet corrosion to occur, one needs the four key elements of an *electrolytic cell* to exist: an *anode* (where oxidation can occur), a *cathode* (where reduction can occur), a *conductor* (for electrons to flow) and an *electrolyte* (for the ions to flow).

With no protective oxide formation, which could serve to limit the corrosion rate, the corrosion rate is generally expressed as a linear corrosion rate with:

$$TF = A_0 \exp \left(\frac{Q}{K_B T} \right). \tag{12.108}$$

The prefactor A_0 can be a strong function of the concentration of any corrosive contaminants (e.g., chlorine or fluorine) in the water and a function of the acidity (pH level) of the water.

12.13.2.1 Galvanic Series

When dissimilar metals are connected electrically, three elements of the corrosion cell are assured: *anode*, *cathode* and *conductor*. Usually impure water (e.g., sea

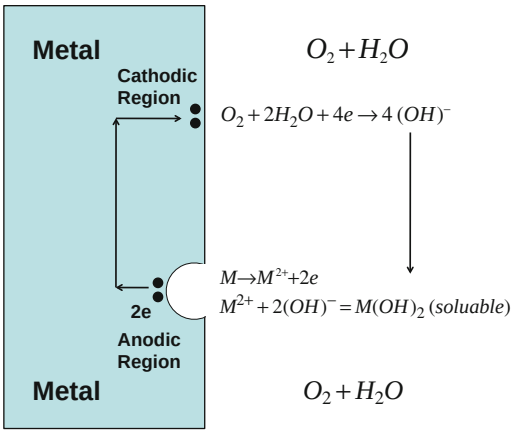

Fig. 12.45 Metal wet-corrosion (corrosion in aerated water) results in an metal-hydroxide [$M_x(OH)_y$] formation on the surface of the metal. Metal hydroxides can dissolve in water, thus exposing fresh metal for continued corrosion. Certain regions in the metal can become anodic, relative to other locations, depending on mechanical stress differences, grain size differences, impurity concentration differences, impressed potentials, etc.

water) or water vapor, with chloride or fluoride contaminants, can provide the fourth key element (*electrolyte*) for the corrosion cell to work. The connection of two dissimilar materials can be described as a *Galvanic couple*. The corrosion potential of the couple is described by the potential difference between the two elements forming the couple. The standard electrode potentials (relative to the hydrogen electrode) of several elements are shown in Table 12.6.

For a Galvanic couple, under standard conditions (1-atmosphere, 1- molar solution, 25°C) the driving force is the free energy difference per ion ΔG, given by:

$$\Delta G = (ze)\Delta V_o, \tag{12.109}$$

where z is the ionic charge state and e is the electron charge. A Galvanic couple composed of Fe and Cu can potentially produce a large free energy reduction per oxidized Fe-ion:

$$\Delta G = (2e)[-0.44 - (+0.34)] = -1.56eV. \tag{12.110}$$

This is a very strong driving potential for corrosion to occur. The corrosion rate (thickness x of Fe impacted per unit time t) is given by:

$$\frac{dx}{dt} = \frac{(Mole)_{wt}}{\rho}\left(\frac{\Im}{zF}\right), \tag{12.111}$$

where $(Mole)_{wt}$ is the molecular weight of Fe, ρ is the density of iron, z (=2) is the charge transferred during Fe oxidation, F is Faraday's constant (96,500

Table 12.6 Standard Electrode Potentials.

Metal	Oxidation State	Standard Electrode Potential: V_o [Volts]	
Mg	$Mg^{2+} + 2e$	−2.36	More Anodic
Al	$Al^{3+} + 3e$	−1.66	↑
Zn	$Zn^{2+} + 2e$	−0.76	
Cr	$Cr^{3+} + 3e$	−0.74	
Fe	$Fe^{2+} + 2e$	−0.44	
Cd	$Cd^{2+} + 2e$	−0.40	
Co	$Co^{2+} + 2e$	−0.28	
Ni	$Ni^{2+} + 2e$	−0.25	
Sn	$Sn^{2+} + 2e$	−0.14	
Pb	$Pb^{2+} + 2e$	−0.13	
H_2	$2H^{+} + 2e$	0.00	Reference Electrode
Cu	$Cu^{2+} + 2e$	0.34	
Ag	$Ag^{+} + e$	0.80	
Pd	$Pd^{2+} + 2e$	0.99	
Pt	$Pt^{2+} + 2e$	1.20	↓
Au	$Au^{3+} + 3e$	1.50	More Cathodic

Coulomb/Mole), and $\Im$ is the current density (current per unit corroded area). In general, one can write the previous equation as:

$$\frac{dx}{dt} = A_o \, \Im(t). \tag{12.112}$$

One can see that the corrosion rate (metal thickness corroded per unit time) is dependent on the *corrosion current density* $\Im$. For a constant corrosion current, the corrosion rate may be much faster in a small area and thus can form a *corrosion pit*. Also, time-to-failure equations can be extracted, as done in sections (12.13.1.1–12.13.1.3), when the current density $\Im(t)$ is specified as a function of time:

$$\int_0^x dx = A_o \int_0^{TF} \Im(t) dt. \tag{12.113}$$

12.13.2.2 Humidity-Induced Oxidation/Reduction

Many examples of corrosion cannot be described simply as either dry oxidation or wet oxidation. For many cases of corrosion, the process can be described more accurately as *humidity-induced oxidation/reduction*. When a metal atom oxidizes, gives up its conduction electrons at the anode region of the metal, the metal ion must

be able to diffuse away from the corroded region for the corrosion process to continue; otherwise, the local electric potential will increase thus offsetting the chemical potential for oxidation. An example of humidity-induced oxidation/reduction is shown in Fig. 12.46 for an integrated circuit (IC) during chip fabrication.

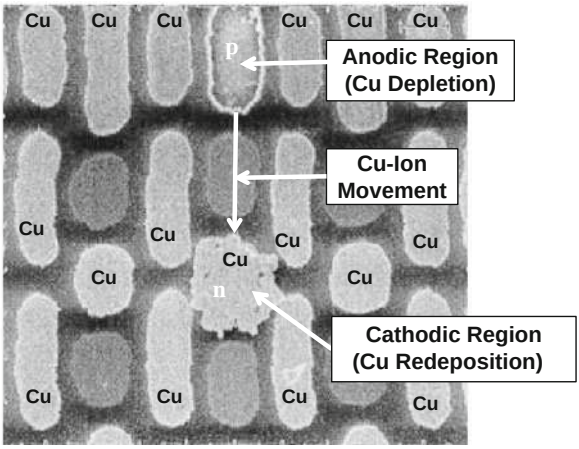

Fig. 12.46 Under light exposure, a photovoltaic-induced voltage of ~0.7 volts is created because of a p/n junction in the silicon (to which the metal is connected). Due to this impressed potential, and with the presence of humidity, the Cu will oxidize in the anode contact region ($Cu \rightarrow Cu^{2+} + 2e$) and then the Cu ions will migrate to the cathode contact region for reduction and redeposition ($Cu^{2+} + 2e \rightarrow Cu$). The Cu-ion mobility along the oxide free surface (and thus the Cu oxidation/reduction rate) is very sensitive to the % relative humidity (%RH).

As discussed in Chapter 11 (corrosion of integrated circuits), the mobility on an oxide surface increases exponentially with humidity (from 20 to 80%) and exponentially with temperature. Thus the time-to-failure equation for metal corrosion under humid conditions can be written as:

$$TF = A_0 \exp\left[-a \bullet (\%RH) + \frac{Q}{K_B T}\right], \tag{12.114}$$

where a and Q are the corrosion time-to-failure kinetics.

The coefficient A_0 in Eq. (12.114) can be a strong function of any corrosive contamination (e.g., chlorides or fluorides) present on the surface of the metal. Chlorides and fluorides are particularly important because they tend to reduce the metal-oxide layer which is trying to serve as a self-protection layer.

Example Problem 12.15

During IC processing, Cu oxidation of the type shown in Fig. 12.46 can occur while exposed Cu surface is waiting for dielectric-barrier/passivation deposition. To minimize such occurrences of exposed-Cu oxidation, the processing

time window is normally kept short. If the normal/safe processing window is 4hrs at 45% relative humidity, how much longer would the processing window be at 35%RH? Assume an exponential humidity dependence with parameter a=0.12/%RH.

Solution

The acceleration factor becomes:

$$\begin{aligned} AF &= \exp\left[a\left(\%RH_1 - \%RH_2\right)\right] \\ &= \exp\left[\frac{0.12}{\%RH}\left(45\%RH - 35\%RH\right)\right] \\ &= 3.32. \end{aligned}$$

Therefore, the time window at 35%RH becomes:

$$\begin{aligned} Time_{@35\%RH} &= AF \bullet Time_{@45\%RH} \\ &= 3.32(4hrs) \\ &= 13.3hrs. \end{aligned}$$

12.13.3 Impact of Stress on Corrosion Rates

Mechanical stress can have a strong impact on the rate of corrosion. Regions of relatively-high tensile stress will generally corrode more rapidly. This is illustrated in Fig. 12.47. The upper convex curvature of a bent piece of metal is under tension while the lower surface is under compression. This mechanical stress reduces the normal bonding energy of the atoms thus making oxidation/corrosion of the atoms more likely to occur.

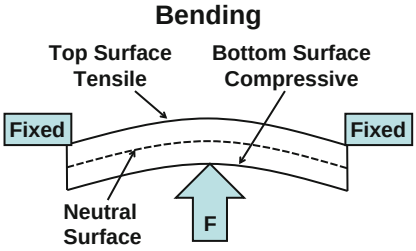

Fig. 12.47 Simple bending, as shown, produces a top surface under tension and a bottom surface under compression. The neutral stress region is also shown. The corrosion rate will be the greatest on the top surface where the tensile stress is the greatest. This is because the tensile stress serves to stretch the bonds, making the existing bonds less stable and more prone to oxidation.

For humidity-driven corrosion of metals, regions of higher stress generally have higher corrosion rates. As we have done many times in previous chapters, let us try to describe the corrosion rate constant (dependence on mechanical stress σ in the metal) as a power-law:

$$k(\sigma, \%RH, T) = k_o(\%RH, T)(1 + b\sigma^m). \tag{12.115}$$

One will note in Eq. (12.115) that, even when the mechanical stress σ in the material goes to zero, the metal-oxidation rate constant simply reverts to its k_o value. This is because metals are expected to oxidize even in a stress-free state. However, with the addition of mechanical stress in the metal, the corrosion rate constant is expected to increase. From the corrosion rate constant, Eq. (12.115), one can now extract the time-to-failure equation:

$$TF(\sigma, \%RH, T) = A_o(1 + a_o\sigma^m)^{-1} \exp\left(-a \bullet (\%RH) + \frac{Q}{K_B T}\right). \tag{12.116}$$

If the piece of metal in Fig. 12.47 is plastically deformed, such that a bend is still evident after the stress is removed, then the bent region will corrode faster. This is illustrated in Fig. 12.48 where a chain-link fence is shown. Note that the highest corrosion rate occurs at the bends where the plastic deformation is the greatest. This is the region where the bonds have been stretched the greatest making them less stable and more prone to oxidation.

For permanent bends (as shown in the chain-link fence in Fig. 12.48) the amount of plastic deformation in the metal will be assumed to be proportional to the radius

Fig. 12.48 Higher stress regions (and more plastic deformation) occur at the crossover bending points of this chain-link fence. Note the enhanced corrosion rates at these crossover/bent-wire locations. Also note that for each bend, the top surface (in tension) generally shows more corrosion than does the underneath surface (in compression).

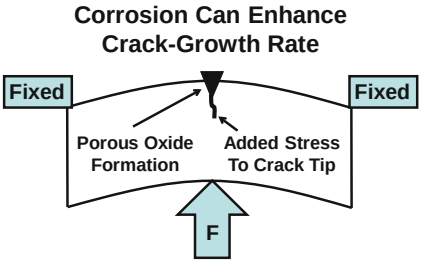

Fig. 12.49 Corrosion tends to occur along existing grain boundaries and/or cracks, especially in tensile stress regions. If the oxide volume is larger than the metal consumed, then the metal-oxide formation can act like a wedge thus causing the crack tip to come under additional stress and thus accelerating the crack propagation. Assuming that the metal oxide formed is rather porous, then the growth of the metaloxide along the crack will continue and this will continue to exacerbate the normal crack growth rate process. Similar oxidation processes can also accelerate fatigue.

of curvature R for the bend, producing a time-to-failure equation which can be written as:

$$TF(\sigma, R, T) = A_o \left[1 + c_o \left(\frac{1}{R}\right)^m\right]^{-1} \exp\left[-a \bullet (\%RH) + \frac{Q}{K_B T}\right]. \qquad (12.117)$$

Corrosion can also enhance the *crack growth rate* in stressed materials. As noted earlier, the volume of the oxide can be much greater than the metal consumed thus creating additional stress at the site of the crack. If a porous oxide formation is assumed, such that the corrosion can continue, then the oxide formed will increase the mechanical stress at the crack tip and will tend to accelerate crack growth. This is illustrated in Fig. 12.49.

Problems

1. Two atoms are bonded and the bonding potential can be described by the (9,1) bonding potential, with an equilibrium bond energy 3.0 eV and equilibrium bonding distance of 2.0Å. Calculate the value of the spring/stiffness constant for small relative displacements of the two atoms.

   Answer: 6.75 eV/(Å)^2 = 108 N/m

2. The bond energy for two atoms is 2.2 eV and the equilibrium bond distance is 1.9Å. Assuming that the bond can be described by a (9,2) bonding potential:

   a) What is the maximum tensile force that the bond can support?
   b) What is the maximum bond extension, from equilibrium bonding distance, before the bond fails?

   Answers: a) 1.24 eV/Å = 1.98 × 10^{-4}dynes b) 0.36Å

3. If the Young's modulus for a solid material is E = 500GPa, what is the estimated single-bond energy for two atoms in the solid? Assume that the bonding can be described by the (9,2) potential with an equilibrium bonding distance for the two atoms of 2Å.

   Answer: 222 GPa(Å)^3 = 1.4eV

4. If the Young's modulus of a solid material is E = 250 GPa, estimate the elastic energy density in the material when the material is tensile strained by 1%($\varepsilon = \Delta L/L_o = 0.01$).

   Answer: 1.25×10^{-2} GPa = 7.81×10^{19}eV/cm^3

5. The stress-strain curve for a material with modulus of E=400GPa is very similar to that shown in Fig. 12.14. If the elastic region extends to 1% strain and the fracture strain is 22%, then calculate the toughness of this material. Assume that the power-law model, which describes the stress versus strain relation in the plastic region, is given by n=0.3.

   Answer: 1.7 GPa = 1.1×10^{22}eV/cm^3

6. Using the vacancy density results from Example Problem 12.4, show that the flux J of vacancies, described by Eq. (4.10), has an activation energy of $Q = (Q)_{\text{formation}} + (Q)_{\text{diffusion}}$.

7. Creep can occur in metals due to dislocation movement along slip planes due to shear stress. If a pure tensile stress σ_T is applied, as illustrated in Fig. 12.10, then a shearing stress τ is generated: $\tau = \sigma \sin(\theta)\cos(\theta)$. Show that the maximum shear stress occurs at $\theta = 45°$.

8. Creep, under constant tensile-stress conditions, can be an important failure mechanism for gas turbines due to high angular speeds and high temperatures during operation. To make sure that the turbine blades can withstand the expected creep, a random selection of turbines was stressed to failure by using an angular speed of 2x the expected operation conditions and at a temperature of 800°C versus the expected operating temperature of 600°C. The turbines started to fail after one week under these accelerated conditions. How long would the turbine blades be expected to last (due to creep) at the expected operational conditions? Assume a creep exponent of at least n=4, an activation energy of at least 1.2 eV, and all stresses are well above the yield strength of the material.

   Answer: 96 yrs

9. Creep, under constant strain, can be an important failure mechanism for clamps/fasteners. To make sure that a clamp is reliable at 200°C, accelerated data was taken for clamps tightened to 2x their normal stress level while stored at 300°C. The clamps lose their effectiveness after one week under these accelerated conditions. Find the time-to-failure for the clamps under the operational conditions at 200°C. Assume a creep exponent of at least n=4, an activation

energy of at least 1.2 eV and that all stresses are well above the yield point of the material.

Answer: 26 yrs

10. Time-zero cracks are found on the outside of a stainless steel storage vessel. If the depth of the cracks is 20 mm, determine if fast facture is expected as the vessel is pressurized to a level such that 400MPa of tensile stress exists in the metal. Assume that the stress concentration factor for the stainless steel is $K_{crit} = 75(MN/m^{3/2})$.

    Answer: Yes, since 400MPa $> \sigma_{rupture} = 299$MPa, fast rupture is expected as the vessel is being pressurized.

11. Aluminum-alloy rods were randomly selected and ramped-to-rupture at the intended use temperature with a linear ramp rate of tensile stress of 50MPa/day. The breakdown distribution was described by a Weibull distribution with $(\sigma_{rupture})_{63} = 600$MPa and a Weibull slope of β=6. Assuming that the tensile stress during normal operation is $\sigma_{op} = 100$MPa, a time-to-failure power-law with a stress exponent of n=6, and that the aluminum-alloy has no well defined yield point:

    a) What fraction of the Al-alloy rods will fail immediately (<0.3 day) when loaded with a tensile stress of 100MPa?
    b) What fraction of the Al-alloy rods will fail after 10 years with a 100MPa loading?

    Answers: a) 0.0021% b) 7%

12. In a certain batch of the aluminum-alloy rods, described in problem 9, some of the rods were found to have small cracks. While the characteristic rupture strength $(\sigma_{rupture})_{63} = 600$MPa showed little/no change, the Weibull slope β degraded to 4. Assuming that the tensile stress during normal operation is $\sigma_{op} = 100$MPa and a time-to-failure power-law with a stress exponent of n=6 for the aluminum-alloy:

    a) What fraction of the metal rods will fail immediately (<0.3 day) when loaded with a tensile stress of 100MPa?
    b) What fraction of the metal rods will fail after 10 years with a 100MPa loading?

    Answers: a) 0.08% b) 16%

13. Steel rods were selected for a high-temperature and high tensile-stress application. During a ramp-testing determination of the rupture strength of steel, at the intended application temperature of 600°C and with a ramp rate of 200MPa/day, the following data was obtained: $(\sigma_{rupture})_{63} = 1600$MPa. The yield strength of the steel is 600MPa and the intended application is 700MPa. Assuming a time-to-failure power-law with a stress exponent of n=6:

a) What fraction of the metal rods will fail immediately (<0.5 day) when loaded with a tensile stress of 700MPa?
b) What fraction of the metal rods will fail after 10 years with a 700MPa loading?

Answers: a) 0.03% b) 0.8%

14. On a certain batch of steel rods described in Problem 13, small cracks were discovered on some of the rods. While the characteristic Weibull strength $(\sigma_{rupture})_{63} = 1600$MPa was virtually unchanged, the Weibull slope degraded to β=6. The yield strength of the steel is 600MPa and the intended application is 700MPa. Assuming a time-to-failure power-law with a stress exponent of n=6:

a) What fraction of the metal rods will fail immediately when loaded with a tensile stress of 700MPa?
b) What fraction of the metal rods will fail after 10 years with a 700MPa loading?

Answers: a) 0.7% b) 5.3%

15. Metal poles, that are intended to support signs, undergo continual cyclical stressing at the base plate due to changing wind conditions. To better understand their reliability, such poles were randomly selected for cyclical stress testing. Under an accelerating cyclical stress of $\Delta\sigma = 800$MPa, the poles started to crack at the base plate after 5000 cycles. How many cycles are the poles expected to last at the effective operating condition of $\Delta\sigma = 200$MPa?

Answer: 1.28×10^6 cycles.

16. The poles described in Problem 15 will be used to support an extended sign which puts a mean stress tensile stress of 200MPa in addition to cyclical stress of $\Delta\sigma = 200$ MPa. Assuming that the tensile strength in these poles is $\sigma_{TS} = 800$MPa, calculate the expected number of cycles to failure.

Answer: 4.0×10^5 cycles

17. A metal rod has a thermal expansion coefficient of $\alpha = 24 \times 10^{-6}/°C$ and a modulus of E=70GPa.

a) If the metal rod is free to expand from 25°C to 300°C, what fractional change in rod length would be expected?
b) If the rod is fully constrained (cannot move), how much thermal stress would be generated in the rod?

Answers: a) 0.66% b) 462MPa

18. A metal component, in a certain application, will be thermal cycled from room temp to an oxidizing ambient of 300°C. To prevent oxidation of the metal at the high temperatures, a thin ceramic coating is used on the metal component. The concern is that cracks will develop in the ceramic layer during thermal cycling thus exposing the metal to oxidation. To accelerate the cracking, the components were thermal cycled from room temperature to 600°C. If cracks start to

develop in the ceramic layer after 500 thermal cycles, how many crack-free cycles would one expect from room temp to 300°C? Assume that the ceramic material is hard/brittle with a temperature-cycling power-law exponent of n = 9.

Answer: 382,000 cycles

19. If left unprotected, how much faster will a scratch in the paint of your new car oxidize at 80% versus 40% relative humidity. Assume an exponential model with parameter: $a = 0.12/\%\text{RH}$.

Answer: 122 times faster

References

Materials Science

Ashby, M. and D. Jones: **Engineering Materials, 2nd Edition**, Butterworth/Heinemann Publishers, (1980).

Ashby, M. and D. Jones: **Engineering Materials 1**, Elsevier Publishing, (2005).

Askeland, D.: **The Science and Engineering of Materials, 3rd Edition,** PWS Publishing Company, (1994).

Barrett, C., W. Nix and A. Tetelman: **The Principles of Engineering Materials**, Prentice Hall, (1973).

Callister, W.: **Materials Science and Engineering an Introduction**, John Wiley and Sons, (2003).

Jastrzebski Z.: **The Nature and Properties of Engineering Materials, 2nd Edition**, John Wiley and Sons, (1976).

Keyser, C.: **Materials Science in Engineering, 3rd Edition**, Charles E. Merril Publishing, (1980).

Ralls, K., T. Courtney, and J. Wulff: **Introduction to Materials Science and Engineering**, John Wiley and Sons, (1976).

Ruoff, A.: **Introduction to Materials Science**, Prentice-Hall, (1972).

Tu, K., J. Mayer, and L. Feldman: **Electronic Thin Film Science For Electrical Engineers and Materials Science**, Macmillan Publishing Company, (1992).

Mechanics of Materials

Bedford, A. and K. Liechti: **Mechanics of Materials**, Prentice Hall, (2000).

Eisenberg, M.: **Introduction to the Mechanics of Solids**, Addison-Wesley Publishing, (1980).

Gere, J.: **Mechanics of Materials, 5th Edition**, Brooks/Cole Publishing, (2001).

Fracture Mechanics

Anderson, T.: **Fracture Mechanics**, 2nd Edition, CRC Press, (1995).

Dunn, C. and J. McPherson: *Temperature Cycling Acceleration Factors for Aluminum Metallization Failure in VLSI Applications*, IEEE International Reliability Physics Symposium, 252 (1990).

Griffith, A.: *The Phenomena of Rupture and Flow in Solids*, Philosophical Transactions, Series A, Vol. 221, pp. 163–198, (1920).

Hertzberg, R.: **Fracture Mechanics and Engineering Materials**, John Wiley and Sons, (1996).

Irwin, G.: *Fracture Dynamics,* Fracturing of Metals, American Society for Metals, Cleveland, pp. 147–166, (1948).

Stokes, R. and D. Evans: **Fundamentals of Interfacial Engineering**, Wiley-VCH, (1997).

Physical Chemistry

Atkins, P.: **Physical Chemistry, 5th Edition**, W.H Freeman and Company, New York, (1994).
Engel, T. and P. Reid: **Physical Chemistry**, Pearson & Benjamin Cummings, (2006).
McPherson, J.: *Determination of the Nature of Molecular Bonding in Silica from Time-Dependent Dielectric Breakdown Data,* J. Appl. Physics, **95**, 8101 (2004).
Pauling, L.:**The Nature of the Chemical Bond, 3rd Edition**, Cornel University Press, (1960).
Silbey, R. and R. Alberty: **Physical Chemistry, 3rd Edition**, John Wiley and Sons (2001).

Solid State Physics

Ashcroft, N. and David Mermin: **Solid State Physics**, Harcourt Brace College Publishers, (1976).
Blakemore, J.: **Solid State Physics, 2nd Edition**, Cambridge University Press, (1985).
Kittel, C.: **Introduction to Solid State Physics, 7th Edition**, John Wiley and Sons, (1996).
McPherson, J.: *Underlying Physics of the Thermochemical E-Model in Describing Low-Field Time-Dependent Dielectric Breakdown in SiO_2* Thin Films, J. Appl. Physics, **84**, 1513 (1998).
Turton, R.: **The Physics of Solids**, Oxford University Press, (2000).

Quantum Mechanics

Atkins, P. and R. Friedman: **Molecular Quantum Mechanics, 3rd Edition**, Oxford University Press, (1997).
Dirac, P.: **The Principles of Quantum Mechanics, 4th Edition**, Oxford Science Publications, (1958).
Griffiths, D.: **Introduction to Quantum Mechanics**, Prentice Hall, (1995).
Harrison, W.: **Applied Quantum Mechanics**, World Scientific Publishing, (2000).
McPherson, J.: *Quantum Mechanical Treatment of Si-O Bond Breakage in Silica Under Time-Dependent Dielectric Breakdown*, IEEE International Reliability Physics Symposium, 209 (2007).
Robinett, R.: **Quantum Mechanics, 2nd Edition**, Oxford University Press, (2006).
Shift, L.: **Quantum Mechanics**, McGraw-Hill Book Company, (1949).

Semiconductors and Dielectrics

Dumin, D.: **Oxide Reliability, A Summary of Silicon Oxide Wearout, Breakdown, and Reliability**, World Scientific, (2002).
Grove, A.: **Physics and Technology of Semiconductor Devices**, John Wiley and Sons, (1967).
Matare, H.: **Defect Electronics in Semiconductors**, Wiley-Interscience, (1971).
Streetman, B. and S. Banerjee: **Solid State Electronic Devices, 5th Edition**, Prentice Hall, (2000).
Sze, S.: **Physics of Semiconductor Devices**, 2nd Edition, John Wiley and Sons, (1981).
Sze, S.: **Semiconductor Devices: Physics and Technology, 2nd Edition**, John Wiley and Sons, (2002).

Thermodynamics and Statistical Mechanics

Desloge, E.: **Statistical Physics**, Holt, Riehart and Winston, (1966).
Haase, R.: **Thermodynamics of Irreversible Processes**, Dover Publications, (1969).
Kittel, C. and H. Kroemer: **Thermal Physics, 2nd Edition**, W.H. Freeman and Co., (1980).
Schrodinger, E.: **Statistical Thermodynamics**, Dover Publications, (1952).

Chapter 13
Conversion of Dynamical Stresses into Effective Static Values

The time-to-failure models which were developed in the previous chapters assume that the stress remains constant with time until the material fails. Even when we discussed fatigue (a failure mechanism caused by a cyclical stress), it was assumed that the stress range $\Delta\sigma$ remained constant with time. However, seldom is the applied stress constant with time, as illustrated in Fig. 13.1. In integrated circuits, the currents and fields are continually changing during operation and generally depend on the frequency of operation. In mechanical devices, the mechanical stress usually varies with time (the mechanical stress in a metal light pole changes with wind direction and with wind speed while the mechanical stress in the shaft of a rotor changes with the number of rpm). Therefore, a question naturally arises: *how does one convert dynamical stresses (time-dependent stresses) $\xi(t)$ into an effective static form $\xi_{effective}$ so that all of the previously developed time-to-failure models can be used*? This chapter presents a methodology for that conversion.

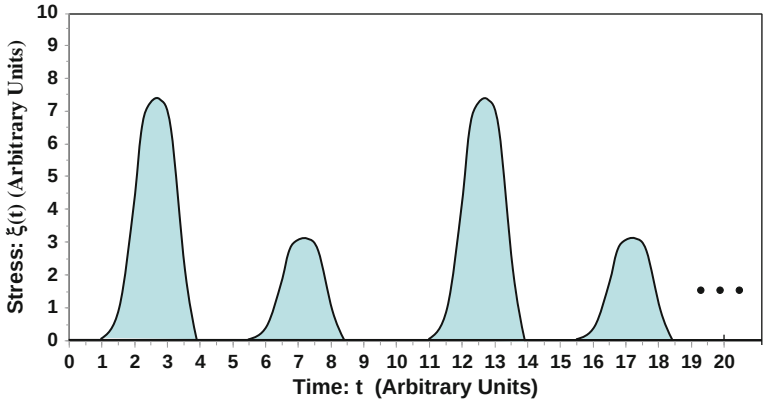

Fig. 13.1 Example of a dynamical (time-dependent) stress is illustrated. It will be assumed that the stress amplitudes are sufficiently low that they only accelerate the normal physics-of-failure — they do not change the normal physics-of-failure.

J.W. McPherson, *Reliability Physics and Engineering*,
DOI 10.1007/978-1-4419-6348-2_13, © Springer Science+Business Media, LLC 2010

13.1 Effective Static-Stress Equivalent Values

Figure 13.2 illustrates a dynamical (time-dependent) stress $\xi(t)$. Also shown is an effective static-stress equivalent $\xi_{effective}$. We want to determine $\xi_{effective}$ such that it will produce an equivalent amount of material/device degradation and thus the same time-to-failure as the dynamical stress $\xi(t)$.

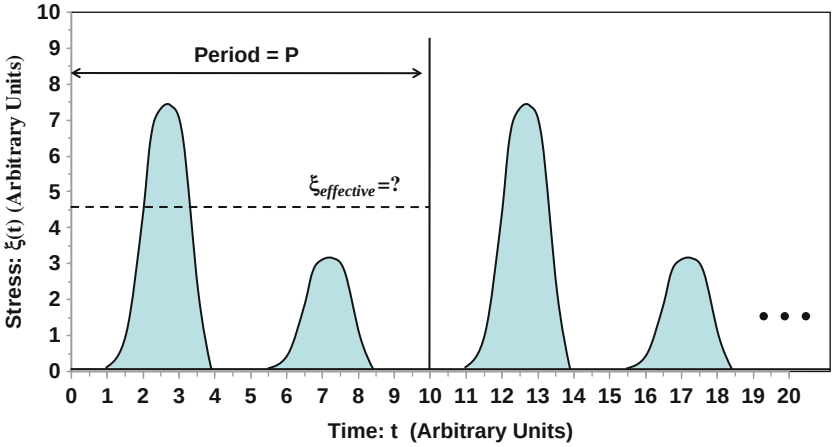

Fig. 13.2 Dynamical (time-dependent) stress $\xi(t)$ is shown. $\xi_{effective}$ represents the effective static-stress level that would produce the same amount of material/device degradation and same time-to-failure as would the dynamical stress $\xi(t)$. If the dynamical stress is also periodic, as shown, then only the first period is needed in the $\xi_{effective}$ determination.

One would expect that when $\xi(t) > \xi_{effective}$, then the actual degradation rate for the material/device during this time interval will be decelerated relative to degradation rate at $\xi_{effective}$. However, when $\xi(t) < \xi_{effective}$, the actual degradation rate for the material/device during this time interval will be *decelerated* relative to degradation rate at $\xi_{effective}$.

The time is either accelerated or decelerated, depending on whether the actual stress level $\xi(t)$ is above or below the constant $\xi_{effective}$ value. If one compares an increment of time dt' under constant stress $\xi_{effective}$ with an increment of time dt under actual accelerated/decelerated conditions, then the following equation must hold:

$$dt' = AF_{\xi(t),\,\xi_{effective}}\, dt. \tag{13.1}$$

If one integrates both sides of the above equation from t=0 to t=TF, then one obtains:

$$TF = \int_0^{TF} AF_{\xi(t),\,\xi_{effective}}\, dt. \tag{13.2}$$

Thus, the *compliance equation for dynamical stresses* that ensures the material/device degradation caused by the effective static-stress $\xi_{effective}$ is identical to the degradation caused by the time-varying stress $\xi(t)$ is given by:

$$\frac{1}{TF}\int_0^{TF} AF_{\xi(t),\,\xi_{effective}}\,dt = 1. \tag{13.3}$$

If the dynamical stress is periodic, with a period P (as indicated in Fig. 13.2), then we only need to determine $\xi_{effective}$ over one period (since it will be the same for all other periods). The *compliance equation for periodic dynamical stresses* becomes:

$$\frac{1}{P}\int_0^{P} AF_{\xi(t),\,\xi_{effective}}\,dt = 1. \tag{13.4}$$

As we will see in the remaining sections of this chapter, the compliance equations permit us to determine $\xi_{effective}$ for arbitrary dynamical conditions.

13.2 Effective Static-Stress Equivalent Values When Using Power-Law TF Models

The acceleration factor for the power-law TF model is given by:

$$AF_{\xi(t),\,\xi_{effective}} = \left(\frac{\xi(t) - \xi_{yield}}{\xi_{effective} - \xi_{yield}}\right)^n. \tag{13.5}$$

Substituting the above equation into Eq. (13.4) and solving for $\xi_{effective}$, one obtains $\xi_{effective}$ when using the power-law TF model:

$$\xi_{effective} - \xi_{yield} = \left[\frac{1}{P}\int_0^{P}\left[\xi(t) - \xi_{yield}\right]^n dt\right]^{1/n}. \tag{13.6}$$

In Eq. (13.6) it will be understood that only when $\xi(t) > \xi_{yield}$ does damage occur, thus only the values of $\xi(t) > \xi_{yield}$ should be included in the integral.[1]

[1]Recall from Chapter 12, if a yield stress truly exists, then when the applied stress is below the yield stress no material degradation is expected.

Example Problem 13.1

Assuming a power-law time-to-failure model with n=4 and a negligibly small yield stress, find the static effective stress $\xi_{effective}$ for the dynamic stress $\xi(t)$ shown in Fig. 13.2.

Solution

If the exact functional form of the stress $\xi(t)$ is known, then $\xi_{effective}$ can be determined from:

$$\xi_{effective} = \left[\frac{1}{P} \int_0^P \xi^4(t)\, dt \right]^{1/4} .$$

Usually the exact functional form of the stress ξ(t) is not known (as the case here) and has to be approximated. One can use numerical integration to find the area under the curve. However, a much simpler and often-used approach is to simply approximate the area under each lobe of the curve using the peak/maximum value for height and for the width: use the full-width at half-maximum (fwhm). This is the conservative approach that we have used here and is shown in Fig. 13.3.

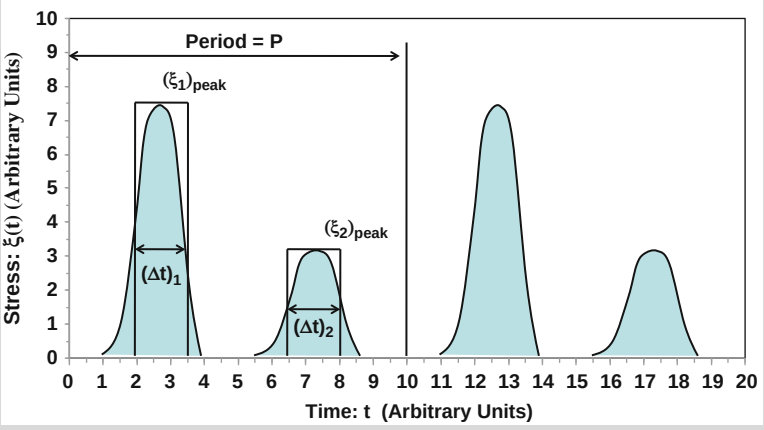

Fig. 13.3 For dynamical stresses which are roughly Gaussian in shape, the full width at half-max/peak (fwhm) approach is often used to approximate the area under each lobe[2].

[2]If the pulse is purely Gaussian, with standard deviation σ, then fwhm $= 2.355\sigma$.

With n=4 and the yield stress equal to zero, one obtains:

$$\begin{aligned}\xi_{effective} &= \left[\frac{1}{P}\int_0^P \xi^4(t)dt\right]^{1/4} \\ &\cong \left\{\frac{1}{P}\left[\sum_i (\xi^4_{peak})_i(\Delta t)_i\right]\right\}^{1/4} \\ &= \left\{\frac{1}{10}\left[(7.5)^4(1.5)+(3.2)^4(1.5)\right]\right\}^{1/4} \\ &= 4.7\ (\textit{arbitrary units})\end{aligned}$$

In summary, with a power law exponent of n = 4, one would expect a constant stress of $\xi_{\text{effective}} = 4.7$ (arbitrary units) to produce the same amount of degradation to the material/device as would the dynamical stress ξ(t) and, therefore, produce an equivalent time-to-failure. Usually, the fwhm method is a conservative approach to handling the reliability impact of pulses.

13.3 Effective Static-Stress Equivalent Values When Using Exponential TF Models

The acceleration factor for the exponential TF model is given by:

$$AF_{\xi(t),\,\xi_{effective}} = \exp\left\{\ \gamma\ \left[\xi(t) - \xi_{effective}\right]\ \right\}. \tag{13.7}$$

Substituting the above equation into Eq. (13.4) and solving for $\xi_{\text{effective}}$, one obtains $\xi_{effective}$ for the exponential TF model:

$$\xi_{effective} = \frac{1}{\gamma}\ \ln\left\{\frac{1}{P}\int_0^P \exp[\ \gamma\xi(t)]\ dt\ \right\}. \tag{13.8}$$

Example Problem 13.2

Assuming an exponential time-to-failure model with γ=2 (in units of reciprocal stress), find the effective static stress $\xi_{\text{effective}}$ for the dynamic stress ξ(t) shown in Fig. 13.3.

Solution

Using an exponential time-to-failure model with $\gamma = 2$ (in units of reciprocal stress), along with Eq. (13.8) and Figure 13.3, one can write:

$$\xi_{effective} = \frac{1}{\gamma} \ln \left\{ \frac{1}{P} \int_0^P \exp\left[\gamma\, \xi(t)\right] dt \right\}$$

$$\cong \frac{1}{\gamma} \ln \left\{ \frac{1}{P} \sum_i (\Delta t)_i \exp\left[\gamma\, (\xi_{peak})_i\right] \right\}$$

$$= \frac{1}{2} \ln \left\{ \frac{1}{10} \left[(1.5)\exp[2(7.5)] + (1.5)\exp[2(3.2)]\right] \right\}$$

$$= 6.6.$$

In summary, with an exponential time-to-failure model and with $\gamma = 2$ (in units of reciprocal stress), we would expect a constant stress of $\xi_{\text{effective}} = 6.6$ (arbitrary units) to produce the same amount of material/device degradation and time-to-failure as would the dynamic stress $\xi(t)$.

13.4 Conversion of a Dynamical Stress Pulse into a Rectangular Pulse Stress Equivalent

It would be very useful if one could somehow convert a rather complicated dynamical stress pulse, over some time interval t_a *to* t_b, into a rectangular pulse effective stress which would produce an equivalent amount of material/device degradation over this same time interval t_a *to* t_b. This is illustrated in Fig. 13.4.

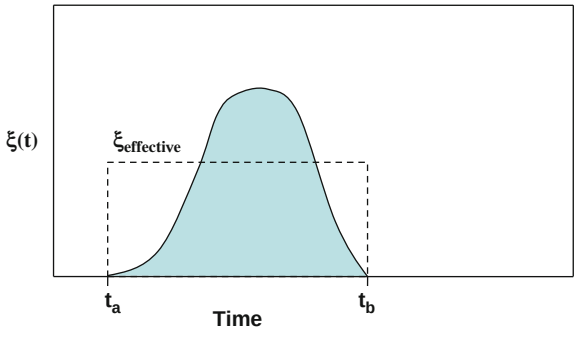

Fig. 13.4 A single dynamical stress pulse $\xi(t)$ is shown over the time interval t_a to t_b. $\xi_{effective}$ represents the effective rectangular pulse, over the same time interval, and is expected to produce an equivalent amount of degradation to the material/device.

The *compliance equation* for dynamical stresses can again aid us in developing the effective rectangular pulse stress equivalent of a single dynamical pulse. Since the amount of degradation to the material/device must be equivalent over the region a to b, then we can restate the compliance equation for the conversion of a dynamic pulse into the rectangular pulse stress equivalent

$$\frac{1}{(t_b - t_a)} \int_{t_a}^{t_b} AF_{\xi(t),\, \xi_{effective}}\, dt = 1. \tag{13.9}$$

13.4.1 Effective Rectangular Pulse Stress-Equivalent Values for Power-Law TF Models

Since the acceleration factor for the power-law TF model is given by:

$$AF_{\xi(t),\, \xi_{effective}} = \left(\frac{\xi(t) - \xi_{yield}}{\xi_{effective} - \xi_{yield}} \right)^n, \tag{13.10}$$

the *compliance equation* yields the effective rectangular pulse stress-equivalent value $\xi_{effective}$ for the power-law exponential model:

$$\xi_{effective} - \xi_{yield} = \left[\frac{1}{(t_b - t_a)} \int_{t_a}^{t_b} \left[\xi(t) - \xi_{yield} \right]^n dt \right]^{1/n}. \tag{13.11}$$

In Eq. (13.11) it will be understood that damage only occurs when $\xi(t) > \xi_{yield}$. Thus, only the values of $\xi(t) > \xi_{yield}$ should be included in the integral.

13.4.2 Effective Rectangular Pulse Stress-Equivalent Values for Exponential TF Models

Since the acceleration factor for the exponential TF model is given by:

$$AF_{\xi(t),\, \xi_{effective}} = \exp\left\{ \gamma \left[\xi(t) - \xi_{effective} \right] \right\}, \tag{13.12}$$

the *compliance equation* yields the effective rectangular pulse stress-equivalent value $\xi_{effective}$ for the exponential TF model

$$\xi_{effective} = \frac{1}{\gamma} \ln \left\{ \frac{1}{t_b - t_a} \int_{t_a}^{t_b} \exp[\, \gamma \xi(t)]\, dt \right\}. \tag{13.13}$$

13.4.3 Numerical Integration

Since the determination of the rectangular pulse stress equivalents of dynamical pulses [Eqs. (13.11) and (13.13)] generally requires the integration of rather complicated functions, a numerical method of integration is suggested.

The *Composite Trapezoidal and Simpson's Rule* numerical method of integration is illustrated in Fig. (13.5). The method begins by segmenting the total area into m sub-intervals (of equal spacing) Δt. The height of each rectangular area is given by $[f(t_i) + f(t_{i-1})]/2$. Summing the areas of m such rectangles gives:

$$\int_a^b f(t)\,dt \;\cong\; \Delta t \sum_{i=1}^{m} \left[\frac{f(t_i)+f(t_{i-1})}{2}\right] = \Delta t \sum_{i=1}^{m} f_i, \tag{13.14}$$

where

$$\Delta t = \frac{t_b - t_a}{m} \quad \textit{and} \quad f_i = \left[\frac{f(t_i)+f(t_{i-1})}{2}\right]. \tag{13.15}$$

This method of numerical integration is illustrated in Fig. 13.5.

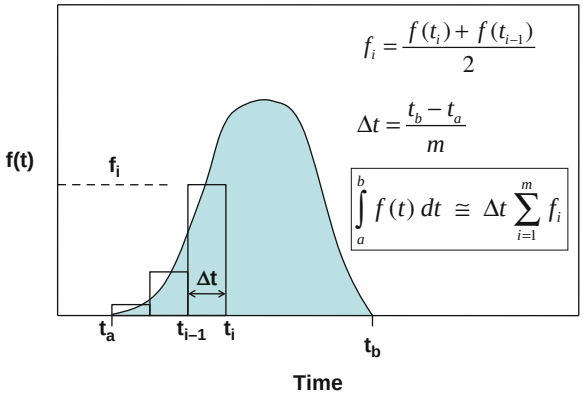

Fig. 13.5 Numerical integration method is illustrated using the Composite Trapezoidal and Simpson's Rule.

Thus, $\xi_{effective}$ for a rectangular pulse equivalent of a dynamical pulse, using the power-law TF model, becomes:

$$\begin{aligned} \xi_{effective} - \xi_{yield} &= \left[\frac{1}{(t_b - t_a)} \int_{t_a}^{t_b} \left[\xi(t) - \xi_{yield}\right]^n dt\right]^{1/n} \\ &\cong \left[\frac{\Delta t}{t_b - t_a} \sum_{i=1}^{m} \left(\xi^n\right)_i\right]^{1/n}, \end{aligned} \tag{13.16}$$

where

$$(\xi^n)_i = \frac{\left[\xi(t_i) - \xi_{yield}\right]^n + \left[\xi(t_{i-1}) - \xi_{yield}\right]^n}{2}. \tag{13.17}$$

It is understood that damage only occurs when the stress level ξ(t) is greater than ξ_{yield}. Therefore, only values $\xi(t) > \xi_{yield}$ should be included in the integral/summations.

$\xi_{effective}$ for a rectangular pulse stress equivalent of a dynamical pulse, using the exponential model becomes:

$$\begin{aligned} \xi_{effective} &= \frac{1}{\gamma} \ln\left\{\frac{1}{t_b - t_a}\int_{t_a}^{t_b} \exp\left[\gamma\xi(t)\right]dt\right\} \\ &\cong \frac{1}{\gamma}\ln\left\{\frac{\Delta t}{t_b - t_a}\sum_{i=1}^{m}\left[\exp(\gamma\xi)\right]_i\right\}, \end{aligned} \tag{13.18}$$

where

$$\left[\exp(\gamma\xi)\right]_i = \frac{\exp\left[\gamma\xi(t_i)\right] + \exp\left[\gamma\xi(t_{i-1})\right]}{2}. \tag{13.19}$$

Example Problem 13.3

Shown in Fig. 13.6 is a dynamic stress pulse given by:

$$\xi(t) = 6\sin[\pi(t/5)] \quad \text{(arbitrary units)}.$$

Using numerical integration, divide the pulse area into m=20 area segments of equal width Δt=0.25 and determine the effective rectangular pulse equivalent $\xi_{effective}$ for the dynamical pulse assuming:

(a) power-law model with n=4 and negligibly small yield stress, and
(b) exponential model with γ=2 (in units of reciprocal stress).

Solution

(a) For the power-law model (with n=4 and ξ_{yield}=0) we have:

$$\begin{aligned} \xi_{effective} &= \left[\frac{1}{(t_b - t_a)}\int_{t_a}^{t_b}\xi^n(t)\,dt\right]^{1/n} \\ &\cong \left[\frac{\Delta t}{t_b - t_a}\sum_{i=1}^{m}\left(\xi^n\right)_i\right]^{1/n} = \left[\frac{0.25}{5-0}\sum_{i=1}^{20}\left(\xi^4\right)_i\right]^{1/4}. \end{aligned}$$

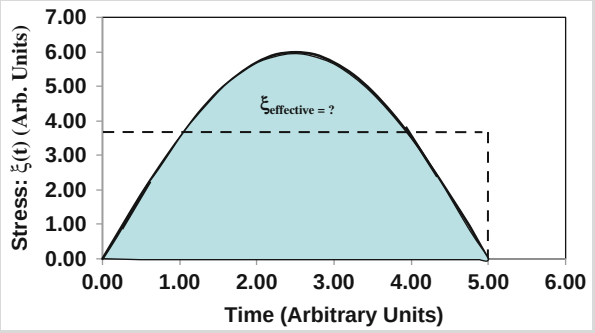

Fig. 13.6 A single pulse of waveform $\xi(t) = 6\sin[\pi(t/5)]$ is shown. $\xi_{\text{effective}}$ is an effective rectangular pulse for this dynamical pulse.

The details of the numerical integration are shown in the following spreadsheet. In summary, using a power-law TF model with n=4, we obtain an effective rectangular pulse value of $\xi_{\text{effective}} = 4.70$ (arbitrary units).

$$\xi(t) = 6\sin\left[\pi\ (t/5)\right]$$
$$t_b - t_a = 5$$
$$m = 20$$
$$\Delta t = (t_b - t_a)/m = 0.25$$
$$n = 4$$

t	ξ(t)	$\xi(t)^4$	$\frac{\Delta t}{t_b - t_a}\left[\frac{\xi^n(t_i) + \xi^n(t_{i-1})}{2}\right]$
0.00	0.00	0.00	
0.25	0.94	0.78	0.02
0.50	1.85	11.82	0.31
0.75	2.72	55.05	1.67
1.00	3.53	154.70	5.24
1.25	4.24	324.00	11.97
1.50	4.85	555.19	21.98
1.75	5.35	816.83	34.30
2.00	5.71	1060.31	46.93
2.25	5.93	1233.35	57.34
2.50	6.00	1296.00	63.23
2.75	5.93	1233.34	63.23
3.00	5.71	1060.30	57.34
3.25	5.35	816.82	46.93
3.50	4.85	555.17	34.30
3.75	4.24	323.99	21.98
4.00	3.53	154.69	11.97

(continued)

t	ξ(t)	$\xi(t)^4$	$\frac{\Delta t}{t_b - t_a}\left[\frac{\xi^n(t_i) + \xi^n(t_{i-1})}{2}\right]$
4.25	2.72	55.05	5.24
4.50	1.85	11.82	1.67
4.75	0.94	0.78	0.31
5.00	0.00	0.00	0.02
			Sum = 486.00
		$\xi_{\text{effective}} = (\text{Sum})^{(1/4)}$	= 4.70

(b) For the exponential model with $\gamma = 2$ (reciprocal stress units):

$$\xi_{effective} = \frac{1}{\gamma} \ln\left\{\frac{1}{t_b - t_a}\int_{t_a}^{t_b} \exp[\gamma\xi(t)]\,dt\right\}$$
$$\cong \frac{1}{\gamma}\ln\left\{\frac{\Delta t}{t_b - t_a}\sum_{i=1}^{m}\left[\exp(\gamma\xi)\right]_i\right\}$$
$$= \frac{1}{2}\ln\left\{\frac{0.25}{5-0}\sum_{i=1}^{20}\left[\exp(\gamma\xi)\right]_i\right\}.$$

The numerical integration is shown in the spreadsheet below.

$\xi(t) = 6\sin[\pi(t/5)]$
$t_b - t_a = 5$
$m = 20$
$\Delta t = (t_b - t_a)/m = 0.25$
$\gamma = 2$

t	ξ(t)	$\exp[(\gamma\ \xi\ (t))]$	$\frac{\Delta t}{t_b - t_a}\left[\frac{\exp[\gamma\xi(t_i)] + \exp[\gamma\xi(t_{i-1})]}{2}\right]$
0.00	0.00	1.00	
0.25	0.94	6.54	0.19
0.50	1.85	40.78	1.18
0.75	2.72	232.27	6.83
1.00	3.53	1156.83	34.73

(continued)

t	$\xi(t)$	$\exp\left[(\gamma\,\xi(t))\right]$	$\frac{\Delta t}{t_b - t_a}\left[\frac{\exp\left[\gamma\xi\,(t_i)\right] + \exp\left[\gamma\xi\,(t_{i-1})\right]}{2}\right]$
1.25	4.24	4843.04	150.00
1.50	4.85	16452.28	532.38
1.75	5.35	44006.49	1511.47
2.00	5.71	90462.36	3361.72
2.25	5.93	140402.18	5771.61
2.50	6.00	162754.79	7578.92
2.75	5.93	140400.24	7578.88
3.00	5.71	90459.89	5771.50
3.25	5.35	44004.72	3361.62
3.50	4.85	16451.43	1511.40
3.75	4.24	4842.73	532.35
4.00	3.53	1156.75	149.99
4.25	2.72	232.25	34.72
4.50	1.85	40.78	6.83
4.75	0.94	6.53	1.18
5.00	0.00	1.00	0.19
			Sum = 37897.69
		$\xi_{\text{effective}} = (1/\gamma)\ln(\text{Sum})$	= 5.27

In summary, for the exponential model with $\gamma = 2$ (reciprocal stress units), $\xi_{\text{effective}} = 5.27$ (arbitrary units).

13.5 Effective Static-Temperature Equivalents

Similar to stress, the temperature T of the material/device is not usually constant during device operation. For example, a computer generally runs hotter (higher power dissipation) during *heavy number crunching* (many computations per sec) versus the *sleep mode* (a period of relative inactivity). An electrical power transformer (from your local utility company) generally runs hotter in the summer months versus the winter months since the transformer is continuously exposed to the ambient weather conditions. Engine components are obviously much hotter when the engine is running.

Thus, for reliability estimations, it would be very useful to have an effective static-temperature $T_{\text{effective}}$ (as illustrated in Fig. 13.7) which produces an equivalent amount of material/device degradation [versus the dynamical temperature T(t)].

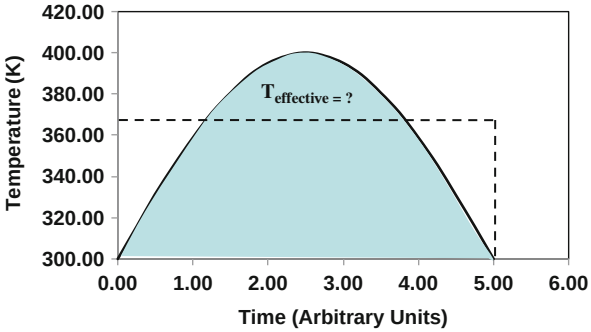

Fig. 13.7 The temperature of a device is seldom constant. The effective static temperature $T_{effective}$ is of great reliability importance.

One can use the compliance equation to determine $T_{effective}$ over any interval t_a to t_b:

$$\frac{1}{(t_b - t_a)} \int_{t_a}^{t_b} AF_{T(t),\, T_{effective}}\, dt = 1, \tag{13.20}$$

where

$$AF_{T(t),\, T_{effective}} = \exp\left[\frac{Q}{K_B}\left(\frac{1}{T_{effective}} - \frac{1}{T(t)}\right)\right]. \tag{13.21}$$

Using Eq. (13.21) and solving Eq. (13.20) for $T_{effective}$, one obtains:

$$\begin{aligned} T_{effective} &= \frac{-(Q/K_B)}{\ln\left\{\dfrac{1}{t_b - t_a}\displaystyle\int_{t_a}^{t_b} \exp\left[-\frac{Q}{K_B T(t)}\right] dt\right\}} \\ &\cong \frac{-(Q/K_B)}{\ln\left\{\dfrac{\Delta t}{t_b - t_a}\displaystyle\sum_{i=1}^{m}\left[\exp\left(-\frac{Q}{K_B T}\right)\right]_i\right\}}, \end{aligned} \tag{13.22}$$

where

$$\left[\exp\left(-\frac{Q}{K_B T}\right)\right]_i = \frac{\exp\left(-\dfrac{Q}{K_B T_i}\right) + \exp\left(-\dfrac{Q}{K_B T_{i-1}}\right)}{2}. \tag{13.23}$$

Example Problem 13.4

The time dependence of the temperature shown in Fig. 13.7 is given by:

$$T(t) = 300\,K + 100\,K \sin\left(\frac{\pi}{5}t\right).$$

Assuming an activation energy of Q = 1.0 eV, determine the effective static temperature over the time interval from 0 to 5.

Solution

Using the equation,

$$T_{effective} \cong \frac{-(Q/K_B)}{\ln\left\{\frac{\Delta t}{t_b - t_a}\sum_{i=1}^{m}\left[\exp\left(-\frac{Q}{K_B T}\right)\right]_i\right\}}$$

the numerical integration is shown in the following spreadsheet.

$T(t) = 300 + 100\sin[\pi(t/5)]$

$t_b - t_a = 5$

$m = 20$

$\Delta t = (t_b - t_a)/m = 0.25$

$Q = 1\,ev$

$K_B = 8.625 \times 10^{-5}\,eV/K$

t	T(t)	$\exp\left[-\frac{Q}{K_B T}\right]$	$\frac{\Delta t}{t_b - t_a}\left[\frac{\exp\left[-\frac{Q}{K_B T_i}\right] + \exp\left[-\frac{Q}{K_B T_{i-1}}\right]}{2}\right]$
0.00	300.00	1.64E−17	
0.25	315.64	1.12E−16	3.20E−18
0.50	330.90	6.07E−16	1.80E−17
0.75	345.40	2.64E−15	8.12E−17
1.00	358.78	9.24E−15	2.97E−16
1.25	370.71	2.61E−14	8.84E−16
1.50	380.90	6.03E−14	2.16E−15
1.75	389.10	1.15E−13	4.37E−15
2.00	395.11	1.80E−13	7.37E−15
2.25	398.77	2.36E−13	1.04E−14
2.50	400.00	2.58E−13	1.24E−14
2.75	398.77	2.36E−13	1.24E−14
3.00	395.11	1.80E−13	1.04E−14

(continued)

t	T(t)	$\exp\left[-\frac{Q}{K_B T}\right]$	$\frac{\Delta t}{t_b - t_a}\left[\frac{\exp\left[-\frac{Q}{K_B T_i}\right] + \exp\left[-\frac{Q}{K_B T_{i-1}}\right]}{2}\right]$
3.25	389.10	1.15E−13	7.37E−15
3.50	380.90	6.03E−14	4.37E−15
3.75	370.71	2.61E−14	2.16E−15
4.00	358.78	9.23E−15	8.84E−16
4.25	345.40	2.64E−15	2.97E−16
4.50	330.90	6.07E−16	8.12E−17
4.75	315.64	1.12E−16	1.80E−17
5.00	300.00	1.64E−17	3.20E−18
		Sum = 7.59E–14	
		$T_{effective} = -(Q/K_B)/[\ln(Sum)] = 383.79$	

In summary, the effective static temperature is $T_{effective} = 384\ K = 111°C$.

13.6 Mission Profiles

A mission (or use) profile is a succinct description of the intended use conditions for the device throughout its lifetime. It is very important, especially during the design and materials selection phase of a new device, that the mission profile is fully comprehended. Now that we have learned how to convert dynamic stresses into effective static stress equivalents, these can be used for a succinct description of the mission profile expected for the device.

The mission profile describes the expected use conditions for the device during its entire lifetime. An example of a mission profile is shown below in Table 13.1. The expected lifetime for the device is 10 years (120 Months).

Table 13.1 Mission Profile For A Device.

Stress: ξ (Arbitrary Units)	Time (Months)	Duty Cycle
ξ_1	1	0.008
ξ_2	7	0.058
ξ_3	12	0.100
ξ_4	70	0.583
ξ_5	24	0.200
ξ_6	6	0.050
	Sum = 120	1.000

If a power-law time-to-failure model is used, then the effective constant-stress value $\xi_{\text{effective}}$ for the entire mission profile becomes:

$$\begin{aligned}(\xi)_{effective} - \xi_{yield} &= \left[\frac{1}{TF}\int_0^{TF}\left[\xi(t) - \xi_{yield}\right]^n \, dt\right]^{1/n} \\ &\cong \left[\frac{1}{TF}\sum_i (\Delta t)_i \left[\xi_i - \xi_{yield}\right]^n\right]^{1/n} \\ &= \left[\sum_i (dyc)_i \left[\xi_i - \xi_{yield}\right]^n\right]^{1/n},\end{aligned} \tag{13.24}$$

where the duty cycle is given by:

$$(dyc)_i = \frac{(\Delta t)_i}{TF}. \tag{13.25}$$

The duty cycle (dyc) is simply the fraction of time that the stated stress is active during the expected 10 years (120 months) of use. It is understood in Eq. (13.24) that damage only occurs when the stress level ξ(t) is greater than ξ_{yield}. Thus, only values $\xi(t) > \xi_{\text{yield}}$ should be included in the integral/summations.

If an exponential TF model is used, then the effective constant-stress value $\xi_{\text{effective}}$ for the entire mission becomes:

$$\begin{aligned}E_{effective} &= \frac{1}{\gamma}\ln\left\{\frac{1}{TF}\int_0^{TF}\exp\left[\gamma\xi(t)\right] \, dt\right\} \\ &\cong \frac{1}{\gamma}\ln\left\{\sum_i (dyc)_i \exp\left[\gamma\xi_i\right]\right\}.\end{aligned} \tag{13.26}$$

Similarly, a mission profile can be described for the expected use temperature and is shown in Table 13.2. The expected lifetime for the device is 10 years.

Table 13.2 Mission Profile For Device.

Temp (°C)	Time (Months)	Duty Cycle
180	1	0.008
150	7	0.058
125	12	0.100
95	70	0.583
75	24	0.200
25	6	0.050
	Sum = 120	1.000

The effective constant-temperature equivalent T_{eff} for the full 10 years (120 months) of device use can be easily determined in terms of the temperature T_i for each time interval and its duty cycle $(dyc)_i$:

$$T_{effective} = \frac{-(Q/K_B)}{\ln\left\{\frac{1}{TF}\int_{t_a}^{t_b}\exp\left[-\frac{Q}{K_B T(t)}\right]dt\right\}} \cong \frac{-(Q/K_B)}{\ln\left\{\sum_{i=1}^{m}(dyc)_i \exp\left(-\frac{Q}{K_B T_i}\right)\right\}}. \tag{13.27}$$

Example Problem 13.5

For the mission profile shown in Table 13.2, find the effective static-temperature equivalent for the expected 10 years of use. Assume an activation energy of 1 eV.

Solution

Using Eq. (13.27):

$$T_{effective} = \frac{-(Q/K_B)}{\ln\left\{\sum_{i=1}^{m}(dyc)_i \exp\left(-\frac{Q}{K_B T_i}\right)\right\}}.$$

The following spreadsheet was used to determine $T_{effective}$.

$Q = 1\,eV$

$K_B = 8.62E{-}5\,eV/K$

Temp (°C)	Temp (K)	Time (Months)	Duty Cycle (dyc)	$(dyc)_i\left[\exp\left(-\frac{Q}{K_B T_i}\right)\right]$
180	453	1	0.00833	6.29394E−14
150	423	7	0.05833	7.16528E−14
125	398	12	0.10000	2.1936E−14
95	368	70	0.58333	1.18879E−14
75	348	24	0.20000	6.65869E−16
25	298	6	0.05000	6.19719E−19
	Sum = 120		1.00000	1.69083E−13

$T_{eff} = -(Q/K_B)/LN(Sum) = 394.2\,K$
$= 121.2\,°C$

With an activation energy of $Q = 1\,eV$, the effective static temperature T_{eff} for this mission profile is $T_{eff} = 121°C$.

Example Problem 13.6

The voltage dropped across a 70Å thick SiO_2 capacitor dielectric is shown below for one period. Assuming that the operating temperature is 105°C and that the field acceleration can be estimated by:

$$\gamma = \frac{p_{eff}}{K_B T} \cong \frac{13e\overset{o}{A}}{K_B T} = \frac{13 \times 10^{-8} e(cm)}{(8.635 \times 10^{-5} eV/K)(105 + 273)K}$$

$$= 4.0\, cm/MV = 4.0 \times 10^{-6} cm/V,$$

find the effective voltage V_{eff} for the time-dependent dielectric breakdown (TDDB) failure mechanism.

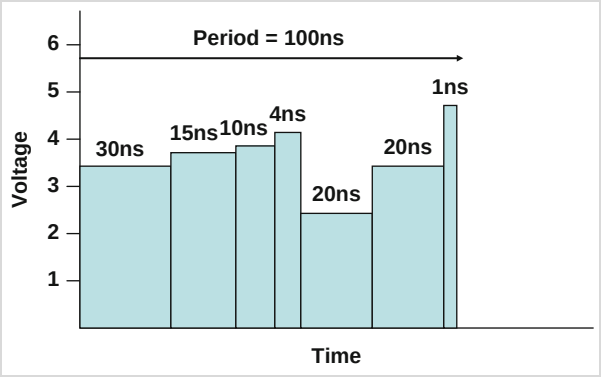

Solution

The stress ξ in this example problem, which produces time-dependent dielectric breakdown (TDDB), is electric field E. From Equation (13.26) one can write:

$$E_{effective} \cong \frac{1}{\gamma} \ln \left\{ \sum_i (dyc)_i \exp[\gamma \xi_i] \right\}.$$

Since $E = V/t_{ox}$, where t_{ox} is the thickness of the dielectric, then one can write the effective voltage for TDDB as:

$$V_{effective} = \frac{t_{ox}}{\gamma} \ln \left\{ \sum_i (dyc)_i \exp\left[(\gamma/t_{ox}) V_i\right] \right\}.$$

$V_{effective}$ determination is shown in the following spreadsheet.

$t_{ox} = 7.00E{-}07$ cm

$\gamma = 4.00E{-}06$ cm/V

Voltage (V)	Duty Cycle	$(dyc)_i \exp[(\gamma/t_{ox})V_i]$
3.3	3.00e−01	4.64E+07
3.6	1.50E−01	1.29E+08
3.9	1.00E−01	4.77E+08
4.1	4.00E−02	5.98E+08
2.5	2.00E−01	3.20E+05
3.6	2.00E−01	1.72E+08
4.8	1.00E−02	8.17E+09
		Sum = 9.59E+09

$$V_{effective} = (t_{ox}/\gamma)\ln(\text{Sum}) = 4.02 \text{ volts}$$

In summary, the mission profile for this dielectric is equivalent to an effective constant voltage of $V_{effective} = 4.02V$ for time-dependent dielectric breakdown (TDDB).

Example Problem 13.7

The mission profile is shown below for a conductor.

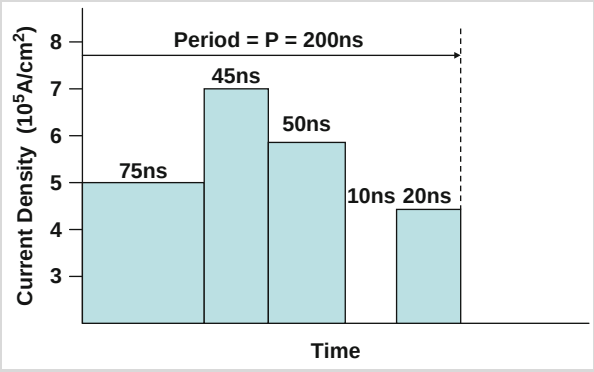

Fig. 13.8 Mission profile for current densities in a conductor over one period P.

Because the current density is rather high, one would like to find the effective current density for electromigration(EM)-induced failure. Since EM-induced failure is impacted by the average current density, find the average current density J_{ave} for the EM mission profile shown above.

Solution

The average current density can be easily determined using Eq. (13.24) with $n = 1$:

$$J_{effective} - J_{crit} = \sum_i (dyc)_i \, [J_i - J_{crit}].$$

Assuming that J_{crit} is negligibly small for the conductor length, the following spreadsheet was used to calculate $J_{effecitve} = J_{ave}$.

Current Density (A/cm^2)	(duty cycle)$_i$	(dyc)$_i$[J]$_i$
5.00E+05	3.75E–01	1.88E+05
7.00E+05	2.25E−01	1.58E+05
5.80E+05	2.50E−01	1.45E+05
0.00E+00	5.00E−02	0.00E+00
4.70E+05	1.00E−01	4.70E+04
		Sum = 5.37E+05
		$J_{effective} = J_{ave}$ = Sum = 5.37E+05 A/cm^2

In summary, for electromigration-induced failures, the effective current density $J_{effective}$ is simply the average current density J_{ave}. However, the assumption here is — the constituent current densities, in the mission profile, are each of sufficiently low value that significant Joule heating (self heating) is not an issue for the conductor, i.e., the conductor temperature remains constant. If this is not the case, then the conductor temperature will have to be taken into account and the effective temperature T_{eff} will have to be calculated, as in example problem 13.5. When $J_{effective} = J_{ave}$ is obtained, the time-to-failure TF goes as TF$\sim (J_{ave})^{-2}$ for aluminum-alloys and as TF $\sim (J_{ave})^{-1}$ for copper.

Example Problem 13.8

The mission profile, for fatigue considerations, is shown below. Find the effective stress range $(\Delta\sigma)_{effective}$ for the mission profile. Assume a stress-range exponent of n=4 and $(\Delta\sigma)_{yield} = 400$MPa.

Stress Range: $\Delta\sigma$ (MPa)	$(\text{duty cycle})_i$
200	0.10
400	0.25
700	0.36
900	0.23
1200	0.05
1400	0.01

Solution

The effective stress range $(\Delta\sigma)_{\text{effective}}$ can be determined from Eq. (13.24) with n=4 and $(\Delta\sigma)_{\text{yield}} = 400\text{MPa}$:

$$(\Delta\sigma)_{effective} - (\Delta\sigma)_{yield} \cong \left[\sum_i (dyc)_i \left[(\Delta\sigma)_i - (\Delta\sigma)_{yield}\right]^4\right]^{1/4}.$$

Recall that no damage is occurring when the stress range is less than $(\Delta\sigma)_{\text{yield}}$; thus, only the stress range above $(\Delta\sigma)_{\text{yield}}$ is used in the following spreadsheet for the effective stress range $(\Delta\sigma)_{\text{eff}}$ calculation.

Stress Range: $\Delta\sigma$ (MPa)	Stress Range Above Yield: $(\Delta\sigma)_i - (\Delta\sigma)_{\text{yield}}$ (MPa)	$(\text{duty cycle})_i$	$(\text{dyc})_i \left[(\Delta\sigma)_i - (\Delta\sigma)_{\text{yield}}\right]^n$
200	0.00	0.10	0
400	0.00	0.25	0
700	300.00	0.36	2.92E+09
900	500.00	0.23	1.44E+10
1200	800.00	0.05	2.05E+10
1400	1000.00	0.01	1.00E+10
			Sum = 4.78E+10
		$(\Delta\sigma)_{\text{effective}} - (\Delta\sigma)_{\text{yield}} = [\text{Sum}]^{1/4} = 468\,\text{MPa}$	

In summary, for the mission profile shown, the effective stress range is $(\Delta\sigma)_{\text{effective}} - (\Delta\sigma)_{\text{yield}} = 468\text{MPa}$ or $(\Delta\sigma)_{\text{effective}} = 868\text{MPa}$.

13.7 Avoidance of Resonant Frequencies

There is a strong caution that we must discuss before this chapter ends. Nearly every component/system has certain natural or resonant frequencies that must be avoided. If the applied time-dependent stress $\xi(t)$ is periodic, with a frequency close to a system's natural/resonant frequency, then unexpectedly large-amplitude oscillations can occur. This is true for both mechanical systems and circuits. If the applied stress is near a natural resonance for the system, then what might have been initially thought to be a rather benign stress level, may actually cause severe damage to the system.

One has probably heard stories about the large amplitude oscillations that can occur when a dog simply trots across a suspension bridge. Certainly, most of us have experienced something similar when a dog simply trots across a wooden floor in our house. The entire room may tend to shake as the dog trots across the floor. Even though the energy input per step associated with the dog's movement is rather small, an oscillator (close to its natural frequency) is very effective in absorbing the input energy. Thus, the amplitude of the oscillation tends to grow rapidly as the dog trots.

The equations developed in this chapter assume that the applied dynamical stress $\xi(t)$ is not close to a natural frequency for the device/system. Remember — because of resonance, a soprano can shatter a wine glass with simply the voice!

Problems

1. The electric field E in a capacitor dielectric is expected to operate at 4MV/cm during a period of 16 ns. However, during this period, a sharp rise/pulse in the electric field (rising from 4 MV/cm to 8 MV/cm) occurs between 4 and 7 ns. Using the full-width-at-half-maximum approach for the pulse, calculate the effective constant electric field for the 16 ns period shown. Assume an exponential field acceleration parameter of $\gamma = 4.0$cm/MV.

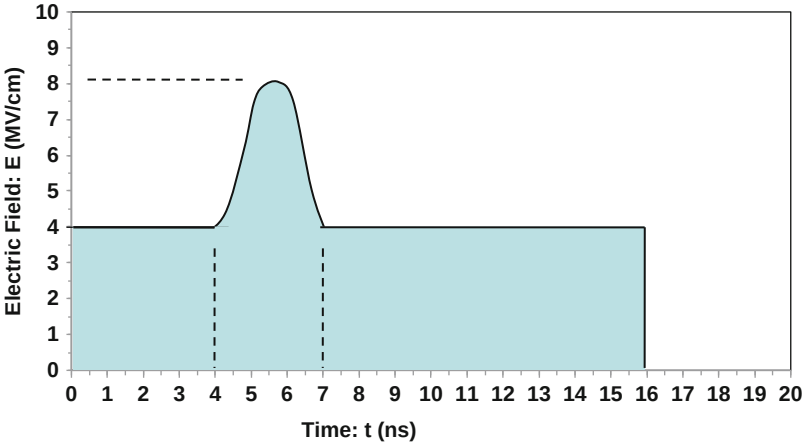

Answer: $E_{effective} = 7.48$ MV/cm

2. A mechanical component experiences a time-dependent tensile-stress waveform given by:

$$\sigma(t) = \frac{1.863 \times 10^{-5}}{(hr)^9}(t)^9 \exp\left[-\left(\frac{t}{8}\right)^{10}\right].$$

The shape of the waveform is shown below.

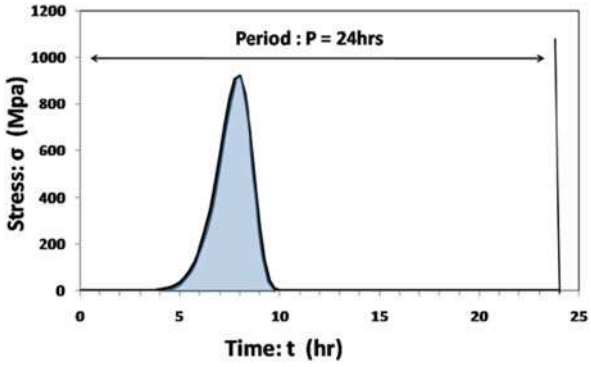

Assuming a creep power-law exponent of n = 4:

a) Find the effective rectangular pulse over the time interval from 4 hrs to 10 hrs.
b) Assuming the period is 24 hrs, what is the effective constant value of the stress over this period?

Answer: a) 599 MPa b) 424 MPa

3. For wind turbine use, the energy contained in the wind is a critically important parameter. The energy contained in the wind is proportional to the square of the wind speed. For Dallas, Texas, the following mean wind speeds were reported by month:

Month	# Days	Wind Speed: S (mph)	$(\text{duty cycle})_i$
Jan	31	11.0	0.085
Feb	28	11.7	0.077
Mar	31	12.6	0.085
Apr	30	12.4	0.082
May	31	11.1	0.085
Jun	30	10.6	0.082
Jul	31	9.8	0.085
Aug	31	8.9	0.085
Sep	30	9.3	0.082
Oct	31	9.7	0.085
Nov	30	10.7	0.082
Dec	31	10.8	0.085

a) Find the mean value for the wind speed S for the entire year.
b) Given the energy in the wind goes as the square of the wind speed, find the constant $(S)_{\text{effective}}$ for turbine use during the entire year.

Answers:

a) Mean Speed = 10.7 mph
b) $(S)_{\text{effective}} = 10.8$ mph

4. The mission profile is shown below for a mechanical component. Assuming that the mechanical component is a metal that has no yield point and a power-law of n=4 for creep, find the effective constant stress $\sigma_{\text{effective}}$ for the full 10 years (120 Months) of service.

Stress Level: σ (MPa)	Time (Months)	$(\text{duty cycle})_i$
0	1	0.008
100	2	0.017
200	4	0.033
300	6	0.050
400	18	0.150
500	35	0.292
600	25	0.208
700	15	0.125
800	9	0.075
900	4	0.033
1000	1	0.008
	Total = 120	1.000

Answer: $\sigma_{\text{effective}} = 612$ MPa

5. Using the mission profile for the metal component in Problem 4, what would be the effective constant-stress value $\sigma_{effective}$ for the full 10 years (120 months) of service if the metal component has a power-law stress exponent of n=4 for creep and has a yield strength of 400 MPa?

   Answer: $\sigma_{effective} - \sigma_{yield} = 283$ MPa or $\sigma_{effective} = 683$ MPa

6. Using the mission profile for the metal component in Problem 4, what would be the effective constant-stress value $\sigma_{effective}$ for the full 10 years (120 months) of service if a power-law exponent of n=6 for creep is assumed and no defined yield strength?

   Answer: $\sigma_{effective} = 650$ MPa

7. Using the mission profile for the metal component in Problem 4, what would be the effective constant-stress value $\sigma_{effective}$ for the full 10 years (120 months) of service if a power-law exponent of n=6 for creep is assumed and a yield strength of 400 MPa?

   Answer: $\sigma_{effective} - \sigma_{yield} = 331$ MPa or $\sigma_{effective} = 731$ MPa

8. Electromigration is a concern for a certain conductor. The current densities in the conductor are shown below. What is the average current density?

Current Density: J (A/cm^2)	$(\text{duty cycle})_i$
5.00E+05	0.4
7.00+05	0.3
9.00E05	0.2
1.20E+06	0.1

   Answer: $(J)_{average} = 7.1 \times 10^5$ A/cm^2

9. The mission profile for a component, with fatigue concerns, is shown below. Assuming a power-law exponent of n=4 and no elastic range, find the effective constant value for the stress range $(\Delta\sigma)_{effective}$.

Stress Range: $\Delta\sigma$ (MPa)	$(\text{duty cycle})_i$
300	0.10
400	0.25
500	0.36
600	0.23
700	0.05
800	0.01

   Answer: $(\Delta\sigma)_{effective} = 524$ MPa

10. A silica-based capacitor dielectric of thickness 45Å will see the following voltages during operation. What is the effective constant voltage V_{eff} for TDDB? Assume an exponential field acceleration parameter of $\gamma = 4.0$ cm/MV.

Voltage (V)	$(\text{duty dycle})_i$
2.5	3.00E−01
2.8	1.50E−01
3.1	1.00E−01
3.4	4.00E−02
3.7	2.00E−01
4.0	2.00E−01
4.3	1.00E−02

Answer: $V_{effective} = 3.9V$

11. The thermal profile for a device is shown below. Assuming an activation energy of 0.7 eV, what is the effective constant-temperature $T_{effective}$?

Temp (°C)	Temp (K)	Time (Months)	Duty Cycle (dyc)
180	453	1	0.00833
150	423	7	0.05833
125	398	12	0.10000
95	368	70	0.58333
75	348	24	0.20000
25	298	6	0.05

Answer: $T_{effective} = 112°C$

Chapter 14
Increasing the Reliability of Device/Product Designs

Design engineers are continually asked reliability questions such as: (1) *how long is your newly designed device/product expected to last and (2) how can you make cost-effective design changes to improve the reliability robustness of the device?* Often the designer will attempt to answer these questions by stating a *safety factor* χ which was used for a design:

$$\xi_{design} = \xi_{strength}/\chi. \tag{14.1}$$

The safety factor, however, is only a qualitative indicator of the reliability margin of the designed device. It states that the designer tried to stay below the expected material's strength distribution by some safety factor χ. For example, the designer may have used a safety factor of $\chi = 2$. While this tends to give some degree of reliability assurance, the fundamental reliability question still remains: *how long is the device/product expected to last*, i.e., is the safety factor large enough or is it too large? If the safety factor χ is too small, then a reliability problem may occur with time (a very costly mistake). If the safety factor is too large, then the device/product may be over-designed (a very costly mistake). The previous chapters of this book emphasized that with accelerated testing data (this data may already exist in the literature) and using the modeled acceleration factors (which have been presented in this text for many of the potential failure mechanisms), one can answer the question: *how long is your newly designed device/product expected to last?*

As one can surely appreciate, the design engineer is always working in a tight space where *device reliability* is one constraint and *cost of the device* is another, the proverbial *rock and a hard place* for the designer. Because of higher materials costs and/or higher device-performance demands, the designer is usually forced to design more aggressively (less conservative with respect to reliability) and must be able to answer the question: *how long is the newly designed device/product expected to last?* If the time-to-failure answer is millions of years, then it is likely a costly over-design issue. If the time-to-failure answer is only one year, it could be a costly reliability issue. In this chapter design areas are emphasized where a relatively small design improvement could have a large impact on device reliability.

J.W. McPherson, *Reliability Physics and Engineering*,
DOI 10.1007/978-1-4419-6348-2_14, © Springer Science+Business Media, LLC 2010

14.1 Reliability Enhancement Factor

Many time-to-failure models have been presented in this text and these can be used to define a very useful expression, the *reliability enhancement factor* (*REF)*:

$$REF = \frac{TF_{improved-design}}{TF_{design}}. \tag{14.2}$$

The *REF* should be > 1 for an improvement in reliability.[1] If *REF* < 1, the improved-design actually has reduced reliability (perhaps the changes were made for improved performance reasons, not for improved reliability reasons) and it tells the designer how much reduction in reliability/lifetime can be expected.

Several examples are shown in this chapter for improving the reliability of designs from both electrical and mechanical considerations. Since many device designs (electro-mechanical devices) have both electrical and mechanical aspects to the product reliability, inclusion of design examples from both electrical and mechanical engineering into this single chapter may be of significant value for all engineers. One will find that Eq. (14.2) is very helpful when one looks for design areas where a small design change can have a large impact on device reliability. The *REF* can be used to quickly estimate the impact on device reliability/lifetime when changes are made to the design.

14.2 *Electromigration* Design Considerations

Electromigration(EM)-induced voiding in conductors (electron wind forcing the metal ions to drift) generally occurs under high current densities J and at elevated temperatures T. The design reliability enhancement factor *REF* for *EM* can be written:

$$\begin{aligned} REF &= \left(\frac{J_{design} - J_{crit}}{J_{improved-design} - J_{crit}}\right)^{n_{EM}} \exp\left[\frac{Q_{EM}}{K_B}\left(\frac{1}{T_{improved-design}} - \frac{1}{T_{design}}\right)\right] \\ &= \left[\frac{\left(\frac{I}{wt}\right)_{design} - J_{crit}}{\left(\frac{I}{wt}\right)_{design-improved} - J_{crit}}\right]^{n_{EM}} \exp\left[\frac{Q_{EM}}{K_B}\left(\frac{1}{T_{improved-design}} - \frac{1}{T_{design}}\right)\right], \end{aligned} \tag{14.3}$$

where $n_{EM} = 2$ and $Q_{\mathrm{EM}} = 0.75\mathrm{eV}$ are often used for aluminum-alloys, $n_{EM} = 1$ and $Q_{\mathrm{EM}} = 1.0\mathrm{eV}$ are often used for copper, and I is the current in the conductor of width w and thickness t. J_{crit} is usually negligible except for very short leads (< 100 μm). Changes in these design parameters can have a significant impact on *REF*. The *REF* value tells the designer how much longer the device/product will last if one uses the *improved-design* parameters. One can see that, for long leads

[1] A REF=2 means that the improved design should last 2 times longer than the original design, a REF=3 means the improved design should last 3 times longer than the original design, etc.

with Al-alloy metallization, reducing the design current density by 50% can produce a REF = 4. This means that the expected lifetime increases by a factor of 4 (or a 300% improvement in lifetime).

The improved-design temperature $T_{improved\text{-}design}$ is usually achieved through lowering the device operating temperature. This is normally achieved by designing for lower device operating-power (reduced self-heating effects) and/or by improved heat dissipation. The improved heat dissipation can be achieved through the design use of more thermally conductive materials (e.g., Cu, SiC, Si, diamond, etc.), heat-sinks, air foils to improve convection heat losses, fans to improve air flow for better convection heat losses, or circulating fluids to improve heat losses (similar to circulating coolants in combustion engines) Assuming an activation energy of Q∼1 eV, a rough rule of thumb is: *for each 10°C drop in device operating temperature, the device will last ∼2 times longer.*

14.3 *TDDB* Design Considerations

Time-dependent dielectric breakdown (*TDDB*) occurs when a dielectric is operated at elevated electric fields *E* and at elevated temperatures *T*. If one uses a conservative *TDDB* model, such as the *E*-Model, the *REF* for *TDDB* can be written:

$$\begin{aligned} REF &= \exp\left[\gamma_{TDDB} \bullet (E_{design} - E_{improved-design})\right] \exp\left[\frac{Q_{TDDB}}{K_B}\left(\frac{1}{T_{improved-design}} - \frac{1}{T_{design}}\right)\right] \\ &= \exp\left[\gamma_{TDDB} \bullet \left(\frac{V_{design} - V_{improved-design}}{t_{ox}}\right)\right] \exp\left[\frac{Q_{TDDB}}{K_B}\left(\frac{1}{T_{improved-design}} - \frac{1}{T_{design}}\right)\right]. \end{aligned} \tag{14.4}$$

The value of γ_{TDDB} is temperature and dielectric-type dependent. For silica-based dielectrics (which are critically important for ICs), γ is often approximated by: $\gamma_{TDDB}(T) = p_{eff}/(K_B T)$, where $p_{eff} = 13eÅ$. Thus, at 105°C(378 K), $\gamma_{TDDB} = 4.0 \times 10^{-6}$ cm/V. The electric field *E* (which is the voltage V drop in the dielectric divided by the dielectric thickness t_{ox}) generally plays a greater role in *TDDB* than does temperature. One can see that for a 1 MV/cm reduction in electric-field E, at a temperature of 105°C, the dielectric lifetime due to TDDB will increase by at least 55 times. One can also see that even small changes in voltages are important when the gate oxide thickness t_{ox} is very thin. More optimistic models such as the 1/*E* – Model or *V*-Model (for hyper-thin gate dielectrics $t_{ox} < 40Å$) have also been used. While the activation energy for TDDB is usually complicated by the fact that it is field dependent, an effective activation energy of $Q_{TDDB} = 0.3 - 0.6$ eV is often used for silica-based dielectrics.

14.4 *NBTI* Design Considerations

Negative-bias temperature instability (*NBTI*) is a threshold voltage instability which occurs in p-channel MOSFET devices in CMOS IC technologies. Under device

operation (presence of electric field E in the gate oxide) and at elevated temperatures T, the metastable Si-H bonds (at the gate oxide/silicon interface) can start to break with the H-ions drifting away from this interface. This bond-breakage mechanism results in an increase in *threshold voltage* for the *p-channel device* and results in a corresponding reduction in p-channel *drive-current*. *NBTI* can result in failure for some CMOS circuits. The *REF* for *NBTI* can be written:

$$REF = \exp\left[\gamma_{NBTI} \bullet (E_{design} - E_{improved-design})\right] \exp\left[\frac{Q_{NBTI}}{K_B}\left(\frac{1}{T_{improved-design}} - \frac{1}{T_{design}}\right)\right]$$
$$= \exp\left[\gamma_{NBTI} \bullet \left(\frac{V_{design} - V_{improved-design}}{t_{ox}}\right)\right] \exp\left[\frac{Q_{NBTI}}{K_B}\left(\frac{1}{T_{improved-design}} - \frac{1}{T_{design}}\right)\right], \tag{14.5}$$

where t_{ox} is the gate oxide thickness. It is normally best practice to use your own empirically determined values for γ and Q. However, if you don't have access to such accelerated data, sometimes the following values are used: $\gamma_{NBTI} = 3.2$cm/MV and $Q_{NBTI} = 0.6$eV. Remember, one can always use more conservative values (lower values for γ and Q). Note that for a 40 Å gate dielectric, a reduction in gate voltage of only 0.1 V will produce a REF=2.23 (a 2.23x improvement in NBTI lifetime).

14.5 *HCI* Design Considerations

Hot carrier injection (HCI) is generally an instability issue for n-channel devices in CMOS IC technologies. Due to electrons being accelerated laterally from source to drain in n-channel MOSFET devices, scattering will cause some of these *hot electron*s to be redirected vertically into the gate oxide, thereby causing damage generally at the gate-oxide/silicon interface. This interface damage tends to produce an increase in threshold voltage with a corresponding reduction in the drive current for n-channel devices. This type of device degradation may eventually result in circuit failure. The *REF* for the *HCI*-induced failure mechanism can be written:

$$REF = \exp\left[\alpha_{HCI} \bullet \left(\frac{1}{V_{improved-design}} - \frac{1}{V_{design}}\right)\right] \exp\left[\frac{Q_{HCI}}{K_B}\left(\frac{1}{T_{improved-design}} - \frac{1}{T_{design}}\right)\right]$$
$$= \exp\left[\beta_{HCI} \bullet \left(1 - \frac{V_{improved-design}}{V_{design}}\right)\right] \exp\left[\frac{Q_{HCI}}{K_B}\left(\frac{1}{T_{improved-design}} - \frac{1}{T_{design}}\right)\right] \quad . \tag{14.6}$$

It is normally best practice to use empirically determined values for β_{HCI} and Q_{HCI} for your own devices. However, if you don't have access to such accelerated data, sometimes the following values are useful: $\beta_{HCI} \approx 30$ and Q_{HCI} is very small (sometimes positive, sometimes negative) and generally the activation energy is in the range: $-0.30\text{eV} < Q_{HCI} < 0.30\text{eV}$). Remember, one can always use more

conservative values (lower values for β_{HCI} and Q_{HCI}). The voltage V in Eq. (14.6) is the voltage drop from source gate edge to drain gate edge because this is the voltage drop that is accelerating the electrons. This may be a consideration for drain and/or source extended devices. Note that a 10% reduction in voltage may produce a REF=20 (a 20x improvement in HCI lifetime).

14.6 *Surface Inversion* Design Considerations

MOSFET devices (especially threshold-dependent oxide-isolation devices) can suffer from *surface inversion* if mobile ions, such as Li+, Na^+ and K^+ are accidentally incorporated in the silica-based dielectrics. The ions may drift under normal device operation. Accumulation of these drifted mobile ions at the silica/silicon interface can cause Si surface-inversion resulting in an unwanted leakage increase for oxide-isolation devices. The *REF* for surface inversion due to mobile ions can be written:

$$REF = \left(\frac{E_{design}}{E_{improved-design}}\right) \exp\left[\frac{Q_{Mobile-Ions}}{K_B}\left(\frac{1}{T_{improved-design}} - \frac{1}{T_{design}}\right)\right]$$
$$= \left[\frac{(V/tox)_{design}}{(V/tox)_{improved-design}}\right] \exp\left[\frac{Q_{Mobile-Ions}}{K_B}\left(\frac{1}{T_{improved-design}} - \frac{1}{T_{design}}\right)\right]. \tag{14.7}$$

For mobile ion induced surface inversion, voltage is of relatively weak importance because it is a *drift mechanism.* Therefore, the burden of preventing mobile-ion reliability issues usually falls on manufacturing. The mobile-ion issues are usually resolved by material purity improvements and/or the use of layers which getter the mobile ions or serve as diffusion barriers. The activation energy for mobile ion induced failures is generally high, with $Q_{Mobile\text{-}Ions} = 1.0$ eV often used.

14.7 *Creep* Design Considerations

Creep induced failures can be very important in mechanical components. The *REF* for creep can be written:

$$REF = \left(\frac{\sigma_{design} - \sigma_{yield}}{\sigma_{improved-design} - \sigma_{yield}}\right)^{n_{creep}} \exp\left[\frac{Q_{creep}}{K_B}\left(\frac{1}{T_{improved-design}} - \frac{1}{T_{design}}\right)\right], \tag{14.8}$$

where σ is the mechanical stress in the material.[2] Note that if the improved-design stress $\sigma_{improved-design}$ can be brought very close to the yield strength, then the *REF*

[2]Recall that the stress-level σ_{design} must be greater than the yield-strength σ_{yield} for creep to occur.

goes to infinity. This means that, in theory, an infinite improvement in lifetime can be achieved and the device should never fail! However, as we have cautioned several times in this text, if even small cracks exist in the material, stress risers can develop at crack tips. These stress risers can serve to increase the local stress levels at crack tips (originally below the yield point without crack) to levels that easily exceed the yield point and degradation may occur. Thus, one should always question: *does a yield stress really exist in the materials being used?*

If the designer does not have creep data for the component materials being used in the design, then the following values can sometimes be useful: for soft metals (such as solder), $n_{creep}= 3$ is often used; for strong metals, such as mild steels, $n_{creep}= 5$ is often used;[3] and, for very strong metals, $n_{creep}= 7$ is sometimes used. Since creep is usually a more severe problem at temperatures $> 0.5T_{melt}$, then the creep activation energy Q_{creep} is usually close to the lattice-diffusion/bulk activation energy $Q_{lattice\text{-}diffusion}$ (1–4 eV).

The *REF*, Eq. (14.8), can be very helpful because the designer only needs to know the equations for the maximum stress in the material for a given loading. Fortunately, these equations may already exist and are often found in *Strength of Materials, Solid Mechanics, Fracture Mechanics,* and *Materials Science* textbooks. Several examples of creep will follow.

14.7.1 Creep in Rotors

Creep can be very important for mechanical components (rotors) that have to rotate with high angular speed ω. The REF equation for a simple rotor (rotating mass attached to a light connecting rod) becomes:

$$REF = \left(\frac{\left(\frac{Mr\omega^2}{A}\right)_{design} - \sigma_{yield}}{\left(\frac{Mr\omega^2}{A}\right)_{improved-design} - \sigma_{yield}} \right)^{n_{creep}} \exp\left[\frac{Q_{creep}}{K_B} \left(\frac{1}{T_{improved-design}} - \frac{1}{T_{design}} \right) \right]. \tag{14.9}$$

Creep exponent data can usually be found in the literature for a given material. If such empirical data is unavailable to you, for strong metal alloys, the kinetic values are sometimes used: $n_{creep} =4$ (likely a conservative value) and $Q_{creep}=1$ eV (likely a conservative value). One can see that for mechanical designs where creep in rotors can be an issue, the designer can dramatically improve reliability robustness by: reducing the angular velocity ω of the rotor, reducing the effective radius r of the rotor, reducing the mass M at the end of the rotor, and by increasing the cross-sectional area A of the connecting rod. Assuming that the yield stress is negligibly small and a creep exponent of $n_{creep}=4$, the REF goes as the 8^{th} power of angular

[3]The value of $n_{creep}=5$ is used so often in creep analysis that it is generally referred to as the literature as the *five-power-law* for creep behavior.

speed ω and as the 4th power for the connecting arm length r, mass M of rotor, and cross sectional area A of the connecting rod. Note that a 20% reduction in angular speed can produce a REF = 6, or a 500% increase in lifetime.

14.7.2 Creep in Pressurized Vessels

Creep can be a very important degradation mechanism for *thin-walled vessels* that are continually pressurized and then evacuated. The *REF* for creep can be written for a spherical thin-walled vessel:

$$REF = \left(\frac{\left(\frac{\mathrm{Pr}}{2t}\right)_{design} - \sigma_{yield}}{\left(\frac{\mathrm{Pr}}{2t}\right)_{improved-design} - \sigma_{yield}} \right)^{n_{creep}} \exp\left[\frac{Q_{creep}}{K_B} \left(\frac{1}{T_{improved-design}} - \frac{1}{T_{design}} \right) \right]. \tag{14.10}$$

P is the pressure difference of the gas inside versus outside of the vessel, r is the radius of the spherical vessel, t is the thickness of the vessel wall and it is assumed that $t << r$. Assuming that the yield stress is negligibly small and has a creep exponent of $n_{creep} = 4$ (likely a conservative value), then the *REF* goes as the 4th power of the gas pressure P, vessel radius r and vessel thickness t. Note that a 20% increase in the thickness of the vessel can increase the REF to 2, or a 100% increase in the expected lifetime. Also, as a caution, this analysis assumes that the gas in the vessel does not chemically react with or diffuse into the vessel material, thus possibly changing the material properties during the lifetime of the product. Finally, creep is strongly temperature dependent. A conservative value for the activation energy is Q_{creep} =1.0 eV.

14.7.3 Creep in a Leaf Springs

Creep can be a very important degradation mechanism in *leaf springs* when the beam is loaded. A simple leaf spring (illustrated in Fig. 14.1) is a rectangular beam

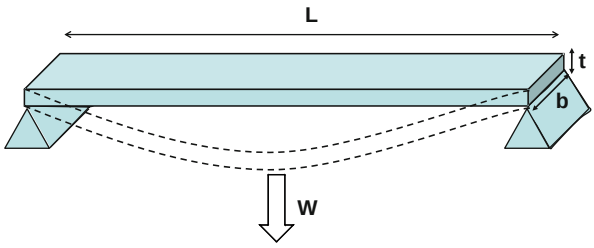

Fig. 14.1 Leaf spring (bending beam) is shown.

of length *L,* width *b* and thickness *t*. The leaf spring is supported at both ends and must carry a weight *W*.

One can write the REF for creep in a leaf spring as:

$$REF = \left(\frac{\left(\frac{3WL}{2bt^2}\right)_{design} - \sigma_{yield}}{\left(\frac{3WL}{2bt^2}\right)_{improved-design} - \sigma_{yield}} \right)^{n_{creep}} \exp\left[\frac{Q_{creep}}{K_B} \left(\frac{1}{T_{improved-design}} - \frac{1}{T_{design}} \right) \right]. \tag{14.11}$$

Assuming that the yield stress is negligible and the beam is made of a material that is hard/strong with a creep exponent of $n_{creep} = 4$ (likely conservative), then the REF for this simple leaf spring goes as at least the 8th power of the thickness of the beam while the other beam design dimensions go as the 4th power. Therefore, if the designer goes with an improved design and increases the beam thickness by 20%, then REF=4.3, or a 330% increase in lifetime. Also, creep is thermally activated with Q_{creep}=1.0 eV (likely conservative value).

14.7.4 Stress Relaxation in Clamps/Fasteners

Stress relaxation can induce failures for critically important clamping applications. The *REF* equation, for the stress relaxation (due to creep with an exponent of *n*) in a clamp/fastener, can be written:

$$REF = \left(\frac{(\sigma_{\max})_{design} - \sigma_{yield}}{(\sigma_{\max})_{improved-design} - \sigma_{yield}} \right)^{n_{creep}-1} \exp\left[\frac{Q_{creep}}{K_B} \left(\frac{1}{T_{improved-design}} - \frac{1}{T_{design}} \right) \right]. \tag{14.12}$$

Assuming that a minimum clamping force F must be maintained for adequate bolt and nut type clamping and that all stress relief occurs in the shaft of the bolt, then the REF for stress relaxation that is occurring in the shaft of the bolt of radius r is given by:

$$REF = \left(\frac{\left(\frac{F}{\pi r^2}\right)_{design} - \sigma_{yield}}{\left(\frac{F}{\pi r^2}\right)_{improved-design} - \sigma_{yield}} \right)^{n_{creep}-1} \exp\left[\frac{Q_{creep}}{K_B} \left(\frac{1}{T_{improved-design}} - \frac{1}{T_{design}} \right) \right]. \tag{14.13}$$

Assuming negligible yield strength and that the shaft of the bolt is made of material that is reasonably hard/strong with a creep exponent of n_{creep}=4 (likely conservative), then one can see that the REF for stress relief goes as the 6th power of the radius of the shaft of the bolt. Note that a 20% increase in the bolt-shaft radius can result in a REF=3, or a 200% increase in lifetime. Also, creep is strongly temperature dependent with $Q_{creep} = 1.0$ eV (likely a conservative value).

14.8 *Fatigue* Design Considerations

Fatigue can be a very important reliability issue for devices which undergo a cyclical stress. This can be an important failure mechanism for storage vessels that are continually pressurized and then evacuated; it can be an important failure mechanism for ICs that undergo continual power-up and power-down cycles; it can be an important failure mechanism for turbine blades that experience continual starting and stopping; it can be an important failure mechanism for light poles that must respond to continual changes in the wind speed and direction; etc. The REF equation due to cyclical stress can be written as:

$$REF = \left[\frac{(\Delta\sigma)_{design} - (\Delta\sigma)_{elastic}}{(\Delta\sigma)_{improved-design} - (\Delta\sigma)_{elastic}} \right]^{n_{fatigue}}, \tag{14.14}$$

where $\Delta\sigma$ is the total stress range and $(\Delta\sigma)_{\text{elastic}}$ is the part of the total stress range that is considered to be in the elastic region (where no degradation is expected). Note that the stress range $(\Delta\sigma)_{\text{elastic}}$ is analogous to the yield stress.

14.8.1 Fatigue in Storage Vessels

Fatigue can be an important failure mechanism for a vessel that is continually pressured with a gas and then evacuated. The REF equation due to fatigue can be written as:

$$\begin{aligned} REF &= \left[\frac{(\Delta\sigma)_{design} - (\Delta\sigma)_{elastic}}{(\Delta\sigma)_{improved-design} - (\Delta\sigma)_{elastic}} \right]^{n_{fatigue}} \\ &= \left[\frac{\left(\frac{\Delta\sigma}{1-(\sigma_{mean}/\sigma_{TS})} \right)_{design} - (\Delta\sigma)_{elastic}}{\left(\frac{\Delta\sigma}{1-(\sigma_{mean}/\sigma_{TS})} \right)_{improved-design} - (\Delta\sigma)_{elastic}} \right]^{n_{fatigue}}. \end{aligned} \tag{14.15}$$

For a spherical vessel that is continually pressured to $P_{\max}$ then evacuated to $P_{\min}$, the stress range is given by:

$$\Delta\sigma = \frac{(P_{\max} - P_{\min})r}{2t} \quad \text{and} \quad \sigma_{mean} = \frac{(P_{\max} - P_{\min})r}{4t}. \tag{14.16}$$

σ_{TS} is the tensile stress of the material used to make the spherical vessel. Assuming that the yield stress is negligible (because of cracks or other issues) and that the vessel is made of hard/strong metals, then $n_{fatigue} = 4$ (likely conservative) can be used. From a design standpoint, one can see that fatigue can be minimized by keeping the pressure difference $(P_{max} - P_{min})$ as small as possible, keeping the

radius r of the spherical vessel as small as possible, and selecting materials with high tensile strength σ_{TS}.

14.8.2 Fatigue in Integrated Circuits (ICs)

Each time that an IC is powered up and then down, the device undergoes cyclical stress due to the thermal expansion mismatch in the materials used for IC fabrication. Since these are thermomechanical stresses, the *REF* equation for thermal cycling is often written as:

$$REF = \left[\frac{\alpha_{ij}[(\Delta T) - (\Delta T)_{elastic}]_{design}}{\alpha'_{ij}[(\Delta T) - (\Delta T)_{elastic}]_{\ improved-design}} \right]^{n_{fatigue}}, \tag{14.17}$$

where ΔT is the full thermal-cycling range and α_{ij} represents the thermal expansion mismatches for the materials of interest. $(\Delta T)_{\text{elastic}}$ represents the part of the total temperature range that is expected to be in the elastic range. Anything that can be done to minimize the thermal expansion mismatch of the materials and/or the temperature cycling range will improve *REF*. An exponent of $n_{\text{fatigue}}=4$ is often used for fatigue in ICs. If solder is the material failing, then perhaps $n_{\text{fatigue}}=2$ is more appropriate.

Problems

1. An IC designer worried about electromigration decides to increase the metal width of an aluminum-alloy conductor by 20%. Assuming J_{crit} is negligibly small, how much of an increase in lifetime can the designer expect?

   Answer: REF = 1.44 (or a 44% increase in lifetime)

2. If the conductor in Problem 1 is copper, how much lifetime improvement can be expected with an increase in conductor width by 20%?

   Answer: REF = 1.2 (or a 20% increase in lifetime)

3. If the temperature of the Al-alloy conductor in Problem 1 could be reduced from 105°C to 95°C by using a heat sink, how much longer would the conductor be expected to last?

   Answer: REF = 1.87 (or a 87% increase in lifetime)

4. If the temperature of the copper conductor in Problem 2 could be reduced from 105°C to 95°C by using a heat sink, how much longer would the conductor be expected to last?

   Answer: REF = 2.30 (or a 130% increase in lifetime)

5. A 45 Å gate oxide MOSFET operates in inversion with a gate voltage of 2.7 V. How much would the time-dependent dielectric breakdown (TDDB) lifetime increase if gate voltage is reduced to 2.5 V?

   Answer: REF = 5.92 (or a 492% increase in lifetime)

6. If the transistor described in Problem 5 is a p-channel MOSFET, how much would the negative-bias temperature instability (NBTI) lifetime increase if the gate voltage is reduced from 2.7 to 2.5 V?

   Answer: REF = 4.15 (or a 315% increase in lifetime)

7. If the transistor described in Problem 5 is a n-channel MOSFET, how much would the hot-carrier injection (HCI) lifetime increase if the device operating voltage is reduced from 2.7 V to 2.5 V?

   Answer: REF = 9.23 (or a 823% increase in lifetime)

8. Assuming that a rotor's arm is made of a strong metal and that the operational stress in the rotor's arm is much greater than the materials yield point, what is the expected increase in creep lifetime if the length of the rotor's arm r is reduced by 20%?

   Answer: REF = 2.44 (or 144% increase in lifetime)

9. Assuming that a thin-walled spherical storage vessel is made of a strong metal and that the operational stress is much greater than the materials yield point, what is the expected increase in creep lifetime if the thickness of the wall is increased by 30%?

   Answer: REF = 2.86 (or 186% increase in lifetime)

10. Assuming that a leaf spring is made of a strong metal and that the operational stress is much greater than the materials yield point, what is the expected increase in creep lifetime if the thickness of the spring is increased by 30%?

    Answer: REF = 8.16 (or 716% increase in lifetime)

11. Assuming that a nut and bolt type clamp is made of a strong metal and that the operational stress in the shaft of the bolt is much greater than the materials yield point, what is the expected increase in stress-relaxation lifetime if the radius of shaft is increased by 30%?

    Answer: REF = 4.83 (or 383% increase in lifetime)

12. Assuming that a thin-walled spherical storage vessel is made of a strong metal and that the operational stress is much greater than the materials yield point, what is the expected increase in fatigue lifetime if the allowed pressure range is decreased by 20%?

    Answer: REF = 2.44 (or 144% increase in lifetime)

13. Assuming that the elastic range is negligibly small and that a fatigue exponent of n=4 can be used for a plastic molded integrated circuit, what is the expected increase in IC thermal-cycling lifetime if the operational thermal range is decreased by 20%?

    Answer: REF = 2.44 (or 144% increase in lifetime)

Index

J.W. McPherson, *Reliability Physics and Engineering*,
DOI 10.1007/978-1-4419-6348-2,